



Assessing the Sustainability of Iron-Bearing
Clay Mineral Redox Reactions for Application in
Engineered Systems

Harry Brooksbank

A thesis submitted to Newcastle University in partial fulfilment of the requirements for
the degree of Doctor of Philosophy within the School of Engineering

Declaration

I hereby declare that the work presented in this thesis has not been submitted for any other degree or professional qualification, and that it is the result of my own independent work.

Harry Brooksbank

11/03/2022

Date

Abstract

Iron is abundant in natural sediments, and the Fe(II)-Fe(III) redox couple is crucial in the cycling of nutrients and for the environmental fate of contaminants. Clay minerals contain structural Fe thought to be resistant to reductive dissolution, and which after reduction, can reductively degrade a range of organic compounds. In the natural environment, clay mineral Fe can be reduced via different pathways, most importantly direct reduction by micro-organisms and interactions with dissolved reductants such as Fe(II). Although sediments and soils are likely to experience natural fluctuations in redox chemistry over time, most research has focused on exploring clay mineral redox reactivity upon initial Fe reduction, disregarding how multiple reduction-oxidation cycles might impact the long-term efficacy of Fe-bearing clay minerals. This project investigated how reduction-oxidation cycling via various reduction pathways impacts the structure and reactivity of Fe-bearing clay minerals. Reduction pathways included dithionite, Fe(II)_{aq}, and electron shuttles (as bioreduction proxy), and hydrogen peroxide as oxidant. Effects of redox cycling on mineral structure were monitored with techniques including Mössbauer spectroscopy, scanning electron microscopy and X-ray diffraction analysis. Redox reactivity was assessed by measuring the reductive transformation of probe compound and model contaminant, 3-chloronitrobenzene. Results showed that redox cycling using dithionite did not affect reactivity, but caused structural alterations at high reduction extents. Using electron-shuttles as reductants was largely sustainable, with negligible impact on structure and reactivity. Using aqueous Fe(II) as reductant led to irreversible structural changes, formation of secondary minerals, and significant increases to system reactivity.

Acknowledgements

The work produced and presented in this thesis is the culmination of four and half years of my life, during which time I faced many ups and downs including a global pandemic. I am very proud of what I have achieved, and I would like to personally thank a few individuals who have helped sculpt this period of my life in Newcastle.

First, a colossal thank you to supervisors Dr. Anke Neumann and Dr Neil Grey who have been outstanding role models throughout this project. In particular, I am incredibly grateful to have had the opportunity to work with Anke. No one could ask for a better supervisor than Anke, and there's nothing that she could have to improve. She has consistently been an excellent mentor, manager, and even friend, and I cannot speak highly enough about her. To quote one of her colleagues: "The problem with Anke is she makes us all look bad". Thank you for all your help and guidance across these last few years, your work has made my PhD experience a very positive one.

Secondly, I am very grateful for four years of unwavering love and belief from my partner Venetia. She has been there for me every step of the way, and has selflessly provided support in more ways that I can count. Having met her when we were cheerleaders, she has certainly continued that role beyond her position on the squad. It is with her help that I have got to this point, and I am forever grateful and indebted to her kindness. She was also an excellent housemate throughout a year of COVID lockdowns. Thank you.

I am thankful to all the members of the Neumann research group, past and present. To my predecessors Kath and Jim, they helped teach me the skills I have today. To Shaikha who worked with me on her MSc research project. And finally, a huge thankyou to Maggie, who has patiently helped me in many a painful HF digestion and with XRD analysis. Maggie was a fantastic addition to the team, and a great friend.

Finally I would like to say a huge thankyou to EPSRC for funding this project and allowing me to conduct this research. Thankyou to the Clay Minerals Society, the Clay Minerals Group, and the Mineral Physics Group who have awarded me in various ways. Finally a big thankyou to all my family who supported me, and have tolerated 4.5 years of perpetual studentship. Thankyou all for allowing me to complete this project.

Table of contents

Declaration	i
Abstract	ii
Acknowledgements	iii
Table of contents	iv
List of figures	viii
List of tables	x
Chapter 1: Introduction	11
Chapter 2: Literature review	14
2.1 Introduction to clay mineralogy, and electron transfer processes of clay mineral structural Fe	14
2.2 A comparison of different reduction pathways to achieve structural Fe(II) in clay minerals	18
2.2.1 Effects on clay minerals due to chemical reduction by dithionite	18
2.2.2 Microbial clay mineral Fe reduction, and electron shuttling compounds	20
2.2.3 Biologically-mediated, abiotic reduction with aqueous Fe(II)	23
2.3 Understanding structural impacts of redox cycling Fe-bearing clay minerals, and extent of reversibility	24
2.3.1 Irreversible structural alterations caused by clay mineral reduction	24
2.3.2 Degrees of irreversibility	26
2.3.3 Introduction to Mössbauer spectroscopy.....	28
2.4 Effects of redox cycling on clay mineral reactivity towards environmental contaminants	30
2.4.1 Introduction to nitroaromatic compounds as contaminants	32
2.5 Environmental implications of evaluating the effects of multiple reduction- oxidation cycles on the structure and reactivity of Fe-bearing clay minerals.....	34

2.6	Aims and Objectives	37
Chapter 3: Effects of chemically-induced reduction-oxidation cycling on the structure and reactivity of nontronite		
38		
3.1	Introduction.....	38
3.2	Methods	39
3.2.1	Mineral Preparation	39
3.2.2	Mineral Fe reduction and oxidation.....	40
3.2.3	Nitroaromatic compound transformation experiments.....	41
3.2.4	Organic contaminant quantification	42
3.2.5	Data evaluation and kinetic modelling	43
3.2.6	Elemental analysis.....	45
3.2.7	Morphological analysis (particle size and SEM / EDX).....	45
3.2.8	Mössbauer analysis	46
3.2.9	Contributions	46
3.3	Results and discussion	47
3.3.1	Dithionite-reduced kinetics.....	47
3.3.2	Effects of redox cycling on clay mineral morphology and size	52
3.3.3	Effects of redox cycling on clay mineral structure and Fe speciation.....	57
3.3.4	Connecting structural changes and observable clay mineral Fe redox reactivity towards contaminants (Environmental Impact/Conclusions)	72
3.4	Supporting information	73
Chapter 4: Effects of Fe redox cycling by electron shuttles on the reactivity and structure of clay minerals		
82		
4.1	Introduction.....	82
4.2	Methods	83
4.2.1	Mineral preparation	83
4.2.2	Electrochemical reduction of anthraquinone-2,6-disulfonate	84

Assessing the sustainability of Fe-bearing clay mineral redox reactions

Acknowledgements and contents

4.2.3	Reduction-oxidation cycling of NAu-1	86
4.2.4	Kinetic batch experiments	87
4.2.5	Particle size analysis	88
4.2.6	Mössbauer Spectrometry	88
4.2.7	Fe analysis	88
4.2.8	Contributions	89
4.3	Results and Discussion	89
4.3.1	Clay mineral Fe reduction with AH ₂ DS.....	89
4.3.2	Contaminant transformation kinetics of AQDS-reduced NAu-1.....	91
4.3.3	Impacts of reduction-oxidation cycling with AH ₂ DS and H ₂ O ₂ on clay mineral structure	96
4.3.4	Is AH ₂ DS a feasible and appropriate surrogate for biological reduction of clay mineral Fe?	106
4.4	Supporting information	110
Chapter 5: Effects of redox cycling via biologically-mediated, abiotic reduction – impact on clay mineral structure and secondary precipitates		116
5.1	Introduction.....	116
5.2	Methods	117
5.2.1	Reduction-oxidation cycling of NAu-1 with aqueous Fe(II)	117
5.2.2	Transformation of contaminant 3-chloronitrobenzene and reaction kinetics experiments	118
5.2.3	Mössbauer analysis with Fe isotopes	123
5.2.4	Contributions	125
5.3	Results and Discussion	125
5.3.1	Contaminant transformation with Fe(II)-reduced NAu-1.....	125
5.3.2	Analysis of contaminant degradation kinetics.....	128

Assessing the sustainability of Fe-bearing clay mineral redox reactions

Acknowledgements and contents

5.3.3	Characterisation of Fe species, and impacts of Fe(II) redox cycling on mineralogy	135
5.3.4	Relating structure to reaction kinetics.....	165
5.3.5	Conclusions / summary	170
5.3.6	Supporting information.....	171
Chapter 6: Synthesis and Conclusions		177
6.1	Introduction.....	177
6.1.1	Assessment of dithionite reduction as proxy for reduction in natural sediments	178
6.1.2	Effects of Fe redox cycling by electron shuttles on the reactivity and structure of clay minerals, and suitability as proxy for microbial reduction	180
6.2	Effects of redox cycling via biologically-mediated, abiotic reduction – impact on clay mineral structure and the role of secondary precipitates	181
6.3	Environmental impacts on the suitability of clay minerals as sustainable materials for remediation of land contamination	183
References		185

List of figures

2.1 3D illustration of smectite mineral structure.....	15
2.2 Diagram of Fe redox cycle.....	17
2.3 Illustration of “pseudo-random” electron transfer.....	19
2.4 Illustration of “edge-inwards” electron transfer.....	22
2.5 Illustration of trioctahedral configuration.....	25
2.6 Mössbauer hyperfine parameters.....	29
2.7 Transformation pathway of 3-chloronitrobenzene.....	33
3.1 Transformation of 3-chloronitrobenzene with dithionite-reduced N Au-1.....	47
3.2 Dithionite-reduced N Au-1 kinetic parameters.....	50
3.3 Particle size analysis for dithionite-reduced N Au-1.....	53
3.4 EDX measured intensity data.....	56
3.5 Mössbauer spectra of dithionite-reduced N Au-1 at 77 k temperature.....	59
3.6 Mössbauer spectra of dithionite-reduced N Au-1 at 4 K temperature.....	64
3.7 Spectra of reoxidised samples at 13 K and 4 K.....	68
SI 3.1 Precision and accuracy measurements for HPLC method	73
SI 3.2 Gradient of eluent in HPLC method.....	74
SI 3.3 All contaminant transformation data for dith.-reduced N Au-1.....	75
SI 3.4 SEM images for dith.-reduced N Au-1.....	76
SI 3.5 Spectrum without asymmetry and 20% dith.-reduced re-re-reoxidised	77
SI 3.6 SEM images with EDX overlay.....	78
4.1 Diagram of electrochemical cell setup.....	84
4.2 AQDS vs AH ₂ DS UV-Vis spectra.....	85
4.3 UV spectra of AH ₂ DS before and after N Au-1 reduction.....	91
4.4 Transformation of 3-chloronitrobenzene with AH ₂ DS-reduced N Au-1.....	92
4.5 AH ₂ DS-reduced N Au-1 kinetic parameters.....	94
4.6 Particle size analysis for AH ₂ DS-reduced N Au-1.....	98
4.7 Mössbauer spectra of AH ₂ DS-reduced N Au-1 at 77 K and 4 K.....	99

Thesis title

List of figures

4.8 Mössbauer spectra of AH ₂ DS-reduced, reoxidised N Au-1 at 77 K and 4 K.....	104
4.9 Dithionite vs AH ₂ DS reoxidised Mössbauer spectra.....	105
SI 4.1 Image of electrochemical cell setup.....	110
SI 4.2 Transformation of UV spectra from AQDS to AH ₂ DS.....	111
SI 4.3 Image of native N Au-1 vs AH ₂ DS-reduced N Au-1.....	112
SI 4.4 All contaminant transformation data for AH ₂ DS-reduced N Au-1.....	113
SI 4.5 Mössbauer spectrum of 9% dith.-reduce N Au-1 at 4 K.....	114
5.1 Transformation of 3-chloronitrobenzene with Fe(II)-reduced N Au-1.....	126
5.2 Fe(II)-reduced N Au-1 kinetic parameters.....	129
5.3 Diagram of labelling protocol for isotope experiments.....	136
5.4 Mössbauer spectra of both reduced + reoxidised clay minerals at 77 K.....	137
5.5 Mössbauer spectra of both reduced + reoxidised clay minerals at 4 K.....	140
5.6 Relative percentages of Fe speciation in clay mineral.....	146
5.7 XRD spectra of native and reoxidised N Au-1 samples.....	147
5.8 Mössbauer spectra of both reduced + reoxidised precipitates at 77 K.....	150
5.9 Mössbauer spectra of both reduced + reoxidised precipitates at 4 K.....	158
SI 5.1 All contaminant transformation data for Fe(II)-reduced N Au-1.....	171
SI 5.2 Image of native vs reoxidised N Au-1 samples	172
SI 5.3 XRD spectrum of reoxidised sample with corresponding peaks.....	172
SI 5.4 XRD spectrum of Fe(II)-reduced N Au-1 vs native.....	173

List of tables

3.1 Mössbauer hyperfine parameters for dithionite-reduced N _{Au} -1 at 77 K.....	61
3.2 HF digestion and phenanthroline assay data.....	62
3.3 Mössbauer hyperfine parameters for dithionite-reduce N _{Au} -1 at 4 K.....	66
SI 3.1 ICP-OES data and dissolved species.....	79
SI 3.2 All kinetic parameters for contaminant transformation.....	80
SI 3.3 Mössbauer hyperfine parameters reoxidised N _{Au} -1.....	81
4.1 Mössbauer hyperfine parameters for AH ₂ DS-reduced N _{Au} -1 at 77 and 4 K.....	102
SI 4.1 Electron balance data.....	115
5.1 Aqueous solution phenanthroline analysis data.....	131
5.2 Mössbauer hyperfine parameters of clay mineral at 77 K.....	138
SI 5.1 Mössbauer hyperfine parameters of clay mineral at 4 K.....	174
SI 5.2 Mössbauer hyperfine parameters of precipitates at 77 K.....	175
SI 5.3 Mössbauer hyperfine parameters of precipitates at 4 K.....	176

Chapter 1: Introduction

Contaminated land is an internationally significant issue that poses a severe threat to populations and natural resources (Panagos et al. 2013). Unsustainable commercial activity and industrial malpractice have produced a plethora of contaminated sites across the planet, with high concentrations of harmful substances polluting land and water resources. In Europe alone, a report by the European Environment Agency (EEA) suggests there could be up to 2.5 million contaminated soil sites within their jurisdiction (EEA 2014). Hazardous contaminants such as heavy metals, radioactive waste products, and organic contaminants such as petrochemicals, chlorinated solvents, and nitroaromatics can infiltrate and persist in soil and water (Haderlein and Schwarzenbach 1995, Fruchter 2002, Lewis et al. 2004, Hashim et al. 2011, Yu et al. 2015). The toxicity and carcinogenicity of these compounds make land contamination a significant threat to human health, and cause substantial damage to local ecosystems (Chapman 2000, Dayan and Paine 2001, Hou and Al-Tabbaa 2014). Environmental protection and the remediation of contaminated sites is a growing priority for governments and international organizations (Brombal et al. 2015, Rizzo et al. 2016) to protect the health and welfare of local populations. Indeed, protection and prevention against land and water contamination is crucial to the success of multiple United Nations Sustainable Development Goals including promoting good health, clean water and benefiting life on land.

However, contaminated land and groundwater sites can be difficult and costly to fix, and organisations are more frequently investigating remediation techniques that are both effective and environmentally sustainable (Barth et al. 1994, Rizzo et al. 2016, Hou et al. 2020). Iron (Fe) minerals have shown significant promise as potentially sustainable *in-situ* and *ex-situ* remediation techniques for contaminated land and water resources (Cundy et al. 2008, Braunschweig et al. 2013, Fu et al. 2014). Iron is abundant in soils and sediments, and Fe minerals can be easily sourced or produced. Fe minerals are useful for contaminant control due to their sorptive properties, and the variable oxidation state of Fe as a transition metal allows for useful reductive and oxidative capabilities (Cundy et al. 2008). Fe typically exists as two possible valence states in natural systems; firstly as the more soluble Fe(II) in its reduced state, and

secondly as Fe(III) in its oxidised state which tends to precipitate as a solid (Cundy et al. 2008). The Fe(II)/Fe(III) redox couple plays a major role in the biology, mineralogy, and chemistry of the environment (Huang et al. 2021, Kappler et al. 2021). As an electron acceptor, Fe(III) can facilitate a means of respiration for microbes in anoxic systems (Roden et al. 2012, Melton et al. 2014). As an electron donor, Fe(II) can control the cycling of vital nutrients, as well as transform or degrade multiple environmental contaminants in the subsurface (Hofstetter et al. 2006, Yu and Kuzyakov 2021). However, the variable oxidation state can also make Fe a difficult material to utilise sustainably. When valency of solid Fe is altered to Fe(II) (by microbial activity for instance), minerals such as Fe-oxides can be dissolved into solution (Dong et al. 2003). The fluctuation of solubility can make Fe highly mobile, and when unchecked and in high concentrations Fe can itself become an environmental contaminant (Burke and Banwart 2002).

Clay minerals could provide one potential solution to this issue. Fe can be incorporated into the structure of clay minerals (Sposito et al. 1999), offering similar reductive / oxidative capacity but with reduced risk of mineral dissolution and leaching. Considering the prevalence and abundance of Fe-bearing clay minerals (Newman 1984, Stucki 1988), their potential as a naturally occurring, sustainable engineering material could prove highly valuable. Clay minerals in both natural and engineering systems may face large and frequent changes to Fe oxidation state. For instance, the redox state of the subsurface can incur dramatic shifts due to factors such as porewater chemistry variations and microbial ecology (Meng et al. 2021, Calabrese and Porporato 2019). Understanding whether clay minerals can persist through such chemical changes, can help determine the extent to which they can be used sustainably and renewably.

To achieve this, this project has investigated how multiple cycles of reduction and oxidation affect both the structure of Fe-bearing clay minerals, and their potential to reductively transform contaminants. Fe-bearing clay minerals can be reduced through several potential reduction pathways, and this research investigated three different pathways, including those relevant in the environment.

The research results are presented in the following chapters:

Chapter 2: provides a literature review of the current state of knowledge and research into this field, and highlights the gaps in literature on the impacts of redox cycling of Fe-bearing clay minerals.

Chapter 3: assesses how chemical reduction (using dithionite as the electron donor) to both high and low extents of structural Fe reduction (Fe(II)/Fe(total)) impacts the structure and reactivity of Fe-rich smectite clay minerals.

Chapter 4: investigates how redox-cycling of clay minerals via electron-shuttling organic compounds impacts structure and reactivity. Electron-shuttles are typically utilised and exuded by microbes, and this chapter aims to assess whether these compounds can act as suitable abiotic substitutes for microbial reduction.

Chapter 5: examines the interaction and electron-transfer between aqueous Fe(II) and clay mineral structural Fe. This chapter investigates how the interplay between the two pools of Fe affects overall observable reactivity towards contaminants. A specific focus of this chapter is the assessment of the formation of secondary Fe minerals during the process.

Finally, the project will conclude with an assessment of the different effects across all three reduction pathways investigated. We will discuss the environmental implications and attempt to determine whether Fe-rich clay minerals can be considered sustainable materials for application in engineered or natural systems.

Chapter 2: Literature review

2.1 Introduction to clay mineralogy, and electron transfer processes of clay mineral structural Fe

Clay minerals are a group of crystalline, aluminosilicate minerals found ubiquitously in the environment and natural sediments. Clay minerals are classed as phyllosilicates due to their structure of layered sheets consisting of silica tetrahedra and metal octahedra (commonly aluminium). Phyllosilicates can be classed as either 1:1 or 2:1 silicate structure dependant on the ratio of tetrahedral to octahedral sheets. Clay minerals classed as 1:1 (e.g. kaolinite) have one octahedral sheet for every tetrahedral sheet (TO). Whereas, 2:1 type clay minerals (such as illite and smectites) are composed of one octahedral sheet between two tetrahedra (TOT) (Bergaya and Lagaly 2006). Figure 2.1 shows a typical structure for 2:1 clay minerals.

Although clay minerals are generally classed as alluminosilicates, metal cations such as Mg or Fe can be incorporated into the octahedral sheet of the crystal structure. Isomorphic substitutions can create a net negative charge of the clay structure. The negative charge is balanced by exchangeable cations located in the interlayer space. The interchangeability of clay mineral components provides the mineral several interactive properties including adsorption, the ability to exchange cations with the environment, and in smectites the capacity to swell with hydration (Sposito et al. 1999). Combined with a large surface area, these properties make clay minerals a crucial component in many natural processes, determining the fate of key nutrients, trace metals, and contaminants in soils and sediments (Kome et al. 2019). The same properties make clay minerals a highly useful and valued material for numerous industrial sectors. Clay minerals have wide-reaching application across a plethora of industries, ranging from pharmaceuticals, battery components, construction, cosmetics, paints, as well as playing key roles in oil and gas production and environmental engineering (Murray 1991, Sandi et al. 2003, Bergaya and Lagaly 2006, Silva-Valenzuela et al. 2019).

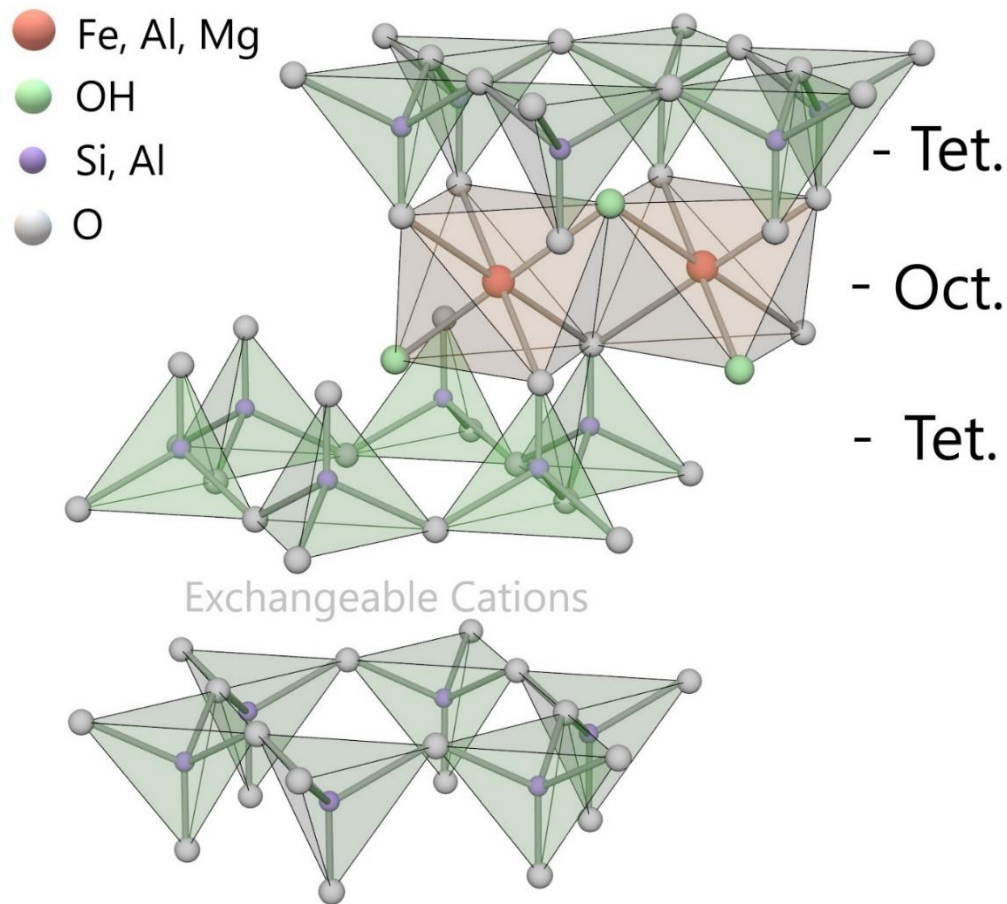


Figure 2.1: 3-Dimensional representation of a 2:1 smectite clay mineral structure. The tetrahedral silica sheet is noted by "Tet." and the octahedral sheet is denoted by "Oct.". Adapted and re-drawn from Grim (1962)

Iron (Fe) is one cation that can be isomorphically substituted into the octahedral sheet. As Fe is the fourth most abundant mineral in the Earth's surface, clay mineral octahedral incorporation of Fe is common and a large proportion of crustal Fe is held in phyllosilicates (Kostka et al. 2002, Stucki et al. 2006, Neumann et al. 2008). The weight percentage (wt%) of clay mineral structural Fe can vary widely between samples and different minerals. The smectite nontronite for instance can possess an octahedral sheet almost entirely comprised of Fe (Keeling et al. 2000). Additionally, in some cases Fe can be incorporated into the tetrahedral sheet (Gates et al. 2002).

While many minerals can incorporate Fe into their structure, clay mineral-bound Fe poses many advantages over other naturally-occurring Fe minerals. The most notable advantage being a potential resistance to dissolution. The prevailing chemistry of soils and porewaters influence the oxidation state of environmental Fe, and reduction

potential (Eh) and pH can vary widely in natural systems (Husson et al. 2016). Low pH values, and more negative Eh values lead to more reducing environments, while increased pH and more positive Eh lead to more oxidising environments. The boundary determining whether Fe presents as Fe(II) or Fe(III) can be found around circumneutral Eh and pH values (Beverkog and Puigdomenech 1996). Fe(II) is typically more soluble, whereas Fe(III) is typically insoluble, which means that fluctuations in soil and redox chemistry can severely impact solubility of mineral Fe (Cundy et al. 2008). Unlike, many naturally-occurring Fe minerals such as Fe-oxides and oxyhydroxides, clay mineral Fe are thought to participate in a variety of electron transfer reactions without dissolution of the mineral structure under reducing conditions (Neumann et al. 2008). The resistance to dissolution under reducing conditions makes clay minerals a more sustainable material, and may allow for the Fe(II)/Fe(III) redox couple to be utilised renewably in natural environments (Fialips et al. 2002).

Clay mineral structural Fe can be reduced by electron transfer via multiple different pathways. Firstly, chemical reduction can occur by reaction with reductive compounds such as hydrazine, sodium sulphide, or commonly dithionite (Rozenon and Heller-Kallai 1976a, 1976b, Stucki et al. 1984b). Secondly, structural Fe can be used as an electron acceptor for anaerobic respiration by metal-reducing microbes, such as the genera *Shewanella* and *Geobacter* (Kostka et al. 1996, 1999, Dong et al. 2003, 2009, Melton et al. 2014). Clay minerals can also be reduced by electron transfer from aqueous Fe(II) released into aqueous phase due to the reductive dissolution of other Fe minerals (Schaeffer et al. 2011, Neumann et al. 2013). This has been described as biologically-mediated abiotic reduction, as the electron transfer is from an abiotic source but is driven by biological activity.

Once in a reduced state, clay mineral structural Fe(II) can subsequently be used to reductively alter a variety of environmental contaminants, such as radionuclides, chlorinated solvents, heavy metals, nitrates, as well as nitroaromatics (Hofstetter et al. 2006, Neumann et al. 2009, Yang et al. 2012, Zhao et al. 2015, Tsarev et al. 2016). Figure 2.2 illustrates the reduction-oxidation process of clay mineral structural Fe, from reduction pathway through to contaminant transformation.

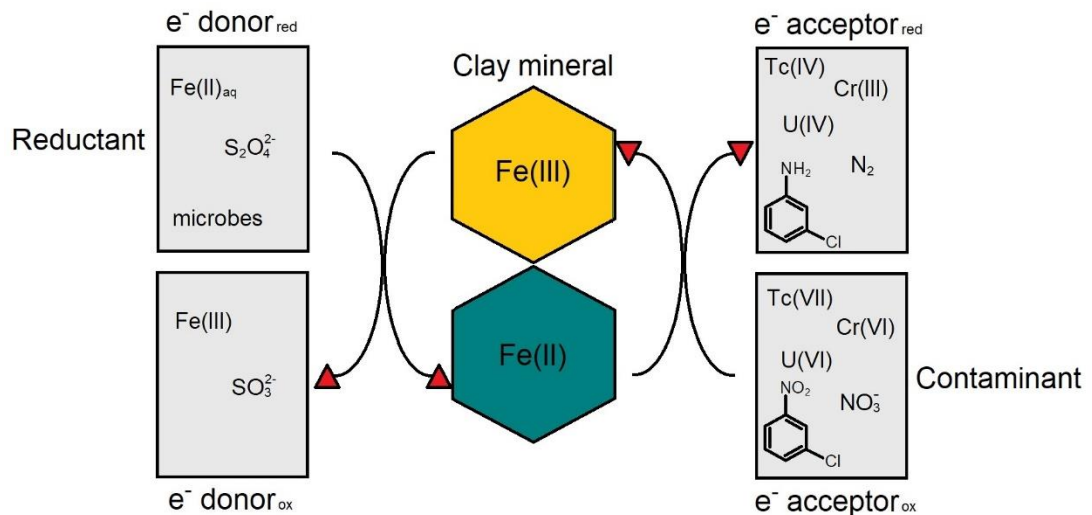


Figure 2.2: Diagram illustrates the redox cycling behaviour of clay mineral structural (octahedral) Fe. Structural Fe(III) (yellow hexagon) is reduced by electron donors / reducing agent, to structural Fe(II) (blue hexagon). Contaminants are reduced by electron transfer from clay mineral structural Fe(II), and transformed to products. Reduction of environmental contaminants oxidises the structural Fe(II) back to Fe(III). Figure adapted from Neumann et al. in Tratnyek (2011)

Changes in the oxidation state of clay mineral structural Fe can affect several physicochemical properties including ion exchange and fixation capacity, surface hydration, and mineral swelling (Stucki et al. 1977, 1984a, 1987, 2000, 2002, Gates et al. 1993, Kostka et al. 1999, Gorski et al. 2012). Unlike many other Fe minerals, clay minerals are thought to be more resistant to reductive dissolution. The ability to donate and accept electrons without incurring reductive dissolution makes Fe-bearing clay minerals a potentially renewable source of environmental reduction equivalents (Komadel 1990, 1995, Ernstsens et al. 1998, Fialips et al. 2002). Consequently, Fe-bearing clay minerals could be valuable materials for sustainable transformation of environmental contaminants *in-situ*. However, there is also evidence to suggest that subjecting clay minerals to multiple cycles of reduction and oxidation can incur irreversible alterations (e.g. Ribeiro et al. 2009, Yang et al. 2012, Gorski et al. 2012, 2013). The extent to which redox cycling of clay mineral structural Fe can be conducted sustainably has not yet been sufficiently understood. Chemical reduction, microbial reduction, and reduction via aqueous Fe(II) (biologically-mediated, abiotic reduction) have all produced conflicting results indicating each produces different effects on the clay mineral (e.g. Ribeiro et al. 2009, Yang et al. 2012, Zhao et al. 2015, Tsarev et al. 2016). There is a significant knowledge gap on exactly how effects of redox cycling by each reduction pathway impacts the clay mineral, and the implications of these effects on the resulting clay minerals Fe(II) reactivity.

Hence, this literature review will highlight:

- Impact of redox cycling on clay mineral structure, and observed differences between reduction pathway
- Extent of reversibility of clay mineral structural changes during redox cycling
- Impact of structural changes during redox cycling on the reactivity of clay mineral Fe(II) towards environmental contaminants

2.2 A comparison of different reduction pathways to achieve structural Fe(II) in clay minerals

2.2.1 Effects on clay minerals due to chemical reduction by dithionite

There are multiple methods to chemically reduce clay mineral structural Fe, and research has achieved reduction using several different reductive compounds including sodium sulfide and hydrazine (Rozenson and Heller-Kallai 1976a, 1976b). However, dithionite reduction conducted in a citrate-bicarbonate buffer is by far the most effective method (Stucki et al. 1984b). In unbuffered solutions, dithionite-reduction can cause major shifts in pH, and ultimately has been thought to cause significant release of structural Fe from the clay mineral (Rozensen and Heller-Kallai 1976, Stucki et al. 1984b). Unlike other methods, dithionite-reduction can achieve up to 100% reduction of structural Fe(III) to Fe(II). Although dithionite and hydrazine have a similar electrode reduction potential, dithionite is a far more effective reductant due to the way in which it reduces structural Fe. The molecule separates into two sulfoxylate free radicals, which greatly increase its electron activity and improve reducing capacity (Stucki et al. 2002). An additional benefit of dithionite is that it is also the easiest to remove from solution (Stucki et al. 1984b).

Dithionite-reduction of structural Fe has been described to occur via electron transfer through the clay mineral basal planes. For Fe-rich clay minerals such as nontronite with high octahedral Fe content, electron transfer follows a “pseudo-random with nearest neighbour exclusion” pattern of reduction (Lear and Stucki 1987, Ribeiro et al. 2009). For partially reduced minerals, this means that octahedral Fe(II) is randomly distributed across the octahedral layer, separated by neighbouring Fe(III) domains. No

Fe(II)-O-Fe(II) pairs will form until all Fe(II)-O-Fe(III) pairs have been filled (Lear and Stucki 1987), as illustrated in Figure 2.3A.

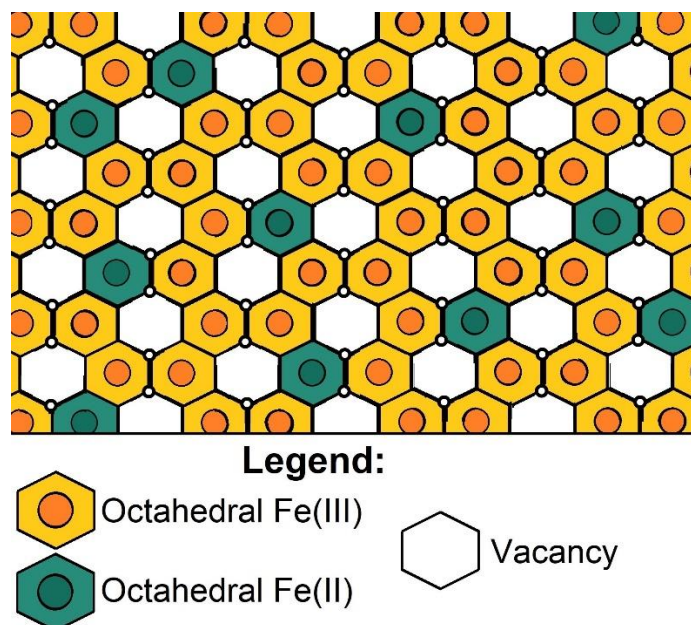


Figure 2.3: Diagram A demonstrates the “pseudo-random” pattern of Fe(II) octahedra site occupancy within Fe-rich clay mineral octahedral sheets, produced after partial reduction by dithionite. Orange hexagons represent Fe(III), green hexagons represent Fe(II), white hexagons represent octahedral vacancies. Illustration adapted from Ribeiro et al. (2009), and Stucki et al. (2011)

Evidence for this mechanism of electron transfer has been provided by results from multiple studies, including results gathered through Mössbauer, ultraviolet (UV) and infrared (IR) absorption spectroscopy (e.g. Lee et al. 2006, Ribeiro et al. 2009). The Fe(II)-O-Fe(III) pairs formed by partial reduction enable intervalence electron transfer between the neighbouring atoms. This mobile electron transferring between the two Fe atoms absorbs light at 730 nm and causes a visible change in the colour of clay minerals. UV adsorption spectroscopy for partially dithionite reduced clay minerals showed that adsorption at 730 nm wavelength was highest around 40% clay mineral Fe reduction extent. This value coincides with where the maximum number of Fe(II)-O-Fe(III) pairs would be produced (Komadel et al. 1990). Ribeiro et al (2009) used Mössbauer spectroscopy to examine clay mineral structural Fe after partial reduction with dithionite, and results suggested that Fe(II) entities were not distinctly separate from Fe(III). This combined evidence supports the hypothesis of reduction following a pseudo-random electron transfer mechanism.

While dithionite does not typically occur naturally in the environment, using dithionite to achieve a low extent of clay mineral Fe reduction could be an effective surrogate for

chemical reduction caused by fluctuating porewater chemistry. Clay minerals in natural systems will inevitably face changing redox conditions due to fluctuations in porewater chemistry (e.g. Parsons et al. 2017, Winkler et al. 2018, Meng et al. 2021), and this might impact the capacity of land and sediments to naturally attenuate contamination. Previous research has also discussed the possibility of injecting the compound *in-situ* to artificially manipulate the subsurface redox state for contaminant control (Nzengung et al. 2001, Fruchter et al. 2002, Szecsody et al. 2004). Indeed, dithionite-reduction of contaminated soils has been shown to be successful in remediating pollutants when tested on small to intermediate laboratory scale (e.g. Istok et al. 1999, Boparai et al. 2008). Using dithionite-reduction to achieve different extents of clay mineral Fe(II) has produced different results (e.g. Ribeiro et al. 2009, Stucki et al. 2011, Gorski et al. 2013). It is unclear whether dithionite-reduction to low and high structural Fe(II) extents will produce different outcomes for sustainable re-use, and for reactivity towards contaminants.

Research so far has not adequately determined whether clay mineral Fe can be used sustainably in the face of multiple chemical reduction-oxidation cycles. Does the structure of the clay mineral persist, and is the reactivity towards environmental contaminants impacted by successive redox cycles?

2.2.2 Microbial clay mineral Fe reduction, and electron shuttling compounds

Microbes are found abundantly in crustal sediments, and mainly drive the redox state of soils, sediments, and other natural systems. There are a wide range of bacteria that utilise mineral Fe in the subsurface for respiration and metabolic processes. Some bacterial species oxidise dissolved Fe(II) as a means to allow denitrification or anoxygenic photosynthesis, producing solid Fe-oxyhydroxides in the process (Miot et al. 2009). There are also several Fe(III)-reducing bacteria that rely on mineral Fe as an electron acceptor to allow anaerobic respiration, notable examples include *Shewanella*, and *Geobacter* (Kostka et al. 1996, Coates et al. 1996). Some species such as *Geobacter metallireducens*, have been shown to demonstrate both Fe(III) reduction, or Fe(II) oxidation dependant on the prevailing conditions of the sediment (Weber et al. 2006, Coby et al. 2011).

Metal-reducing bacteria employ a wide range of methods to transfer electrons to mineral Fe (Weber et al. 2006). Electron transfer can be achieved through direct contact, via conductive nano-wires or pili, by producing Fe-chelating agents to solubilise Fe(III), or finally via electron shuttling organic compounds (Melton et al. 2014). Microbes can utilise natural organic compounds such as humic substances or fulvic acids, or may secrete electron-shuttling compounds like flavins, or quinones e.g. anthraquinone-2,6-disulfonate (AQDS) (Lovley et al. 1996, Stucki et al. 2006, Liu et al. 2013, Piepenbrock and Kappler 2013, Melton et al. 2014, Zuo et al. 2020).

While it has been demonstrated that Fe-reducing bacteria use clay mineral structural Fe(III) as a means of anaerobic respiration (Stucki et al. 1987), studies indicate that the effects of bacterial reduction of clay minerals differ from those observed for chemical reduction. Firstly, multiple studies have demonstrated microbial reduction cannot access all structural Fe in Fe-rich smectites. For Fe-rich clay minerals, microbial reduction typically achieves a maximum of between 10-40% Fe(II)/Fe_{Tot} dependant on the chosen mineral, contact time, and the presence or absence of electron shuttling compounds (e.g. Lee et al. 2006, Jaisi et al. 2007a, Ribeiro et al. 2009, Yang et al. 2012, Zhao et al. 2015, Shi et al. 2021). There are a number of proposed explanations for this limit in achievable reduction extent, including: (1) energetic / thermodynamic limitations of the system (Jaisi et al. 2007a, Luan et al. 2014), (2) inhibition by secondary reaction products, or by surface-sorbed Fe released from the mineral due to reduction (Kostka et al. 1996, Jaisi et al. 2007a, Zhao et al. 2015), and (3) an inherent maximum of bio-reducible Fe in the mineral structure (Shi et al. 2016). However, when microbial reduction is conducted in the presence of electron-shuttling compounds such as AQDS, the extent of structural Fe(II) reduction is significantly increased (e.g. Dong et al. 2003, 2009, Jaisi et al. 2007a).

Studies have inferred that microbial reduction of structural Fe follows a different mechanism of electron transfer than that observed using dithionite. Mössbauer spectroscopy results measuring microbially-reduced smectites indicate that Fe(II) and Fe(III) octahedra are separated into two distinct domains (Ribeiro et al. 2009). It has thus been hypothesised that electron transfer from microbial reduction is believed to

occur as a moving front of Fe(II) from the edge Fe sites towards the interior (Komadel et al. 2006), as illustrated in Figure 2.4.

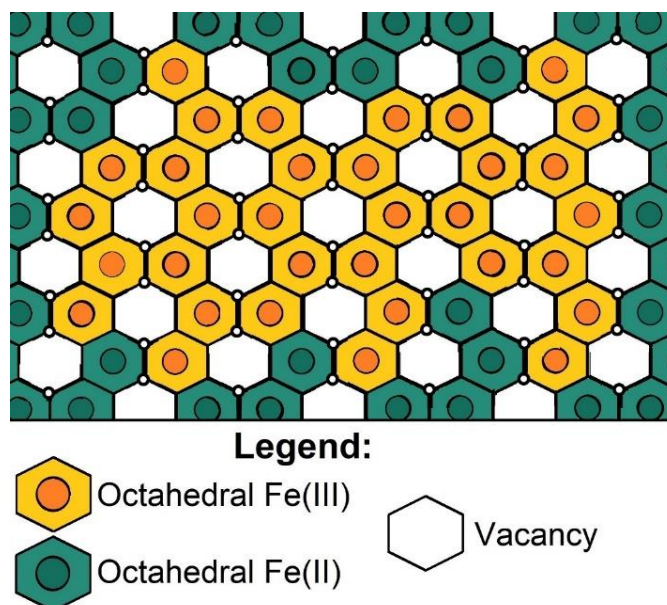


Figure 2.4: Diagram illustrating the “edge-inwards” electron transfer mechanism of microbial reduction. Orange hexagons represent Fe(III), green hexagons represent Fe(II), white hexagons represent octahedral vacancies. Illustration adapted from Komadel et al. (2006), Ribeiro et al. (2009).

Electron-shuttling compounds such as AQDS can increase the accessibility of structural Fe to microbes by allowing electron transfer over greater distances out of reach to the microbe. By increasing the quantities of Fe accessible to microbial reduction, electron shuttles can facilitate a large fraction of mineral bioreduction (Lovley et al. 1996, Dong et al. 2003, Melton et al. 2014). While some bacteria utilise organic compounds present in solution, others can produce their own electron-shuttling compounds for reduction of mineral Fe from a distance (e.g. Lovley et al. 1996, 1998, Melton et al. 2014). The mechanism by which electron shuttles react with clay minerals is currently uncertain, with some studies suggesting it follows the edge-inwards path of microbes (e.g. Ribeiro et al. 2009), and others suggesting it follows a pseudo-random pattern as with dithionite (Zhao et al. 2015). Studies have demonstrated that isolated electron shuttles (in the absence of microbes) can effectively reduce clay minerals (Luan et al. 2014). However, so far studies have only examined a single reduction and have not determined if this reduction pathway is sustainably repeatable.

By using electron-shuttling compounds in their reduced state as the electron donor, it may be possible to imitate bacterial reduction without the presence of living

organisms. The effects of microbial redox cycling on clay minerals in the absence of microbes is yet to be understood. This project will investigate the effects of redox cycling with electron-shuttles and will attempt to determine whether they are an appropriate surrogate for microbial reduction in the absence of living organisms.

2.2.3 Biologically-mediated, abiotic reduction with aqueous Fe(II)

The fluctuations in subsurface redox state are thought to be a result of primarily microbial activity (Stucki et al. 1987, Kostka et al. 1996, Lee et al. 2006). The microbial ecology of soils and sediments can utilise Fe-bearing minerals as electron acceptors, allowing a means for anaerobic respiration. Microbial reduction of naturally forming Fe minerals such as Fe-oxides and -oxyhydroxides leads to mineral dissolution (Dong et al. 2003), and subsequently can result in an increased concentration of aqueous Fe(II) in solution (Zachara et al. 2002). Recently, electron transfer from aqueous Fe(II) to clay mineral structural Fe(III) has been demonstrated (Schaefer et al. 2011, Neuman et al. 2013). The interfacial electron transfer from the aqueous phase to the solid clay mineral is a form of *biologically-mediated*, abiotic reduction.

Studies have demonstrated that electron transfer from aqueous Fe(II) to both Fe-rich, and Fe-poor clay mineral structural Fe can proceed via either the basal plane, or by edge-sites (Neumann et al. 2013, Latta et al. 2017). The process is highly pH-dependant, with Fe(II) sorbing primarily to the basal plane at low pH values (i.e. below pH 6), and dramatic increases in edge-site sorption at pH values at 7.5 and above. The extents of clay mineral structural Fe(II) achievable by reduction via aqueous Fe(II) can range between 5-20% of the total mineral Fe, dependant on the clay minerals used (Schaefer et al. 2011, Neumann et al. 2013, Jones et al. 2017, Entwistle 2021). It is unknown exactly how this mechanism of electron transfer impacts the clay mineral structure and Fe speciation, or whether the impacts resemble those of dithionite or microbial reduction. Isotope tracer experiments have also demonstrated that interactions between structural Fe and aqueous Fe(II) results in significant atom exchange between the clay mineral and the aqueous phase (Neumann et al. 2015).

In natural systems Fe minerals are abundant, and over time clay minerals will have frequent interactions with aqueous Fe(II). While several notable phenomena have been observed, a comprehensive understanding of the interactions between aqueous

Fe(II) and clay minerals in natural systems is yet to be produced. Furthermore, studies so far have only examined a single reduction, and it is currently unknown whether repeated reduction via this pathway significantly will significantly alter the clay mineral. This project aims to understand how multiple cycles of reduction via aqueous Fe(II) and oxidation affects the structure and reactivity of Fe-bearing clay minerals, and whether this impacts their reactivity towards environmental contaminants.

Additionally, the partial oxidation of aqueous Fe(II) and the interaction with clay minerals can cause the formation of secondary Fe precipitate minerals (Schaefer et al. 2011, Soltermann et al. 2014, Tsarev et al. 2016). In some cases, the secondary minerals have been described to be mixed-valent species such as green rusts (e.g. Jones et al. 2017), and previous work has indicated that the minerals may be highly reactive in contaminant transformation (Rothwell 2018, Entwistle et al. 2019). The nature and identity of the secondary minerals varies with pH and aqueous Fe(II) concentration, and so far the minerals have not been conclusively characterised (Entwistle 2021). Research so far has examined the formation of secondary Fe minerals as a result of a single Fe(II)-reduction, however no work has been done to understand how these secondary minerals are altered as the reduction is successively repeated. This project will also further investigate the nature of these secondary minerals and their role in contaminant transformation in the presence of Fe smectite. Furthermore, the project will attempt to understand how these secondary minerals are altered through multiple cycles of fluctuating redox conditions.

2.3 Understanding structural impacts of redox cycling Fe-bearing clay minerals, and extent of reversibility

2.3.1 Irreversible structural alterations caused by clay mineral reduction

Reduction of structural Fe has been shown to cause irreversible alterations to the clay mineral structure, observable across a variety of different analyses. If the clay mineral is irreversibly altered by reduction-oxidation cycling, this could impact the longevity and sustainability of the mineral as an engineering material.

At low clay mineral Fe reduction extent, predominantly cation uptake balances the increased negative excess charge of the clay mineral, whereas proton uptake increases with increasing structural Fe(II) concentrations in order to compensate for the

increasingly negative charge (Stucki and Roth 1977, Stucki et al. 1984a, Drits and Manceau 2000). This protonation occurs at hydroxyl groups, which can subsequently become expelled from the clay mineral structure (Drits and Manceau 2000). High reduction extents (typically only achievable with dithionite) can cause major structural rearrangements of the octahedral layer. Infrared spectrometry revealed that octahedral Fe transitioned from dioctahedral to trioctahedral coordination after reduction (Manceau et al. 2000a, 2000b, Lee et al. 2006). Also X-Ray Diffraction (XRD) and Extended X-ray Absorption Fine Structure (EXAFS) analyses showed that octahedral Fe migrated from *cis*- to *trans*- octahedral domains, leaving behind structural voids in the octahedral layer (Manceau et al. 2000a, 2000b), as illustrated in Figure 2.5. The shift to trioctahedral domains and the formation of voids occur simultaneously with dehydroxylation.

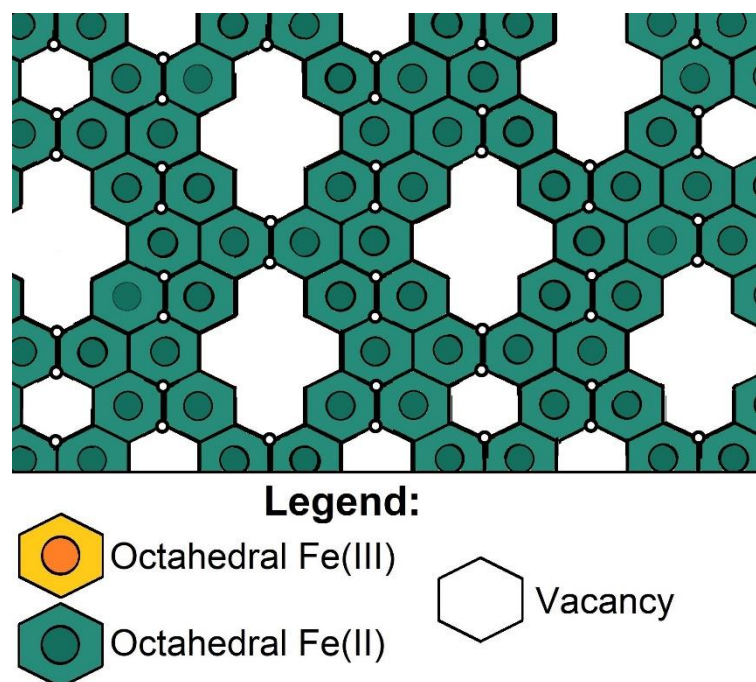


Figure 2.5: Diagram illustrating the rearrangement of structural Fe from dioctahedral to trioctahedral configuration due to reduction, and the corresponding formation of structural voids. Adapted from Manceau et al. 2000b, and Ribeiro et al. 2009

Research has also investigated the impact of microbial redox cycling on Fe-rich clay minerals, and have observed different structural impacts to those of dithionite-reduction. Some papers have indicated that microbial reduction leads to major alterations of the clay mineral, including complete transformation of smectites to illite (e.g. Kim et al. 2004, Dong et al. 2009). Illitization could cause the irreversible loss of

some clay mineral properties such as swelling capacity (Stucki and Kostka 2006). Multiple papers have described significant dissolution of smaller, less crystalline mineral particles due to microbial reduction (Yang et al. 2012, Zhao et al. 2015, Shi et al. 2021).

However, it is unclear whether these effects are truly a result of microbial *electron transfer*, or rather the unintended results caused by the sum of all microbial metabolic processes. Microbes can exude a plethora of organic substances that might drastically alter the chemistry of the porespace, and possibly interact with clay minerals in ways that are difficult to quantify. The proposed edge-inward mechanism of electron transfer (Ribeiro et al. 2009) would theoretically lead to smaller structural impacts than those inflicted by dithionite. Are the effects observed on clay minerals strictly an effect of clay mineral reduction, or are these observable phenomena that occur when clay minerals are placed in the presence of living organisms?

2.3.2 Degrees of irreversibility

Reduction of Fe-bearing clay minerals has been inferred to cause a wide range of structural alterations, including dissolution, octahedral Fe rearrangement, mineral transformation and illitization, dehydroxylation, and more (Dong et al. 2003, Kim et al. 2004, Lee et al. 2006, Ribeiro et al. 2009, Yang et al. 2012, Shi et al. 2021). Some of these effects are thought to be at least partially reversible, and the degree of reversibility depends on the following factors:

Firstly, a major determining variable on the degree of reversibility is the extent of reduction, or the structural Fe(II)/Fe_{Tot} ratio. Multiple papers have suggested that for Fe-rich clay minerals, many effects of reduction are largely reversible when reduction extent is low (Fialips et al. 2002, Ribeiro et al. 2009, Neumann et al. 2011). For instance, Neumann et al. 2011 found that when reduction extent was limited to 50% or below, many of the changes to the structure were found to be largely reversible. At high reduction extents, it is likely that significant crystallographic rearrangements must take place to compensate for the negative charge. Studies have suggested that the dehydroxylation caused by dithionite reduction is only partially restored after reoxidation (Komadel et al. 1995), and might lead to structural instability and leaching of octahedral Fe (Kostka et al. 1999). Other studies have also demonstrated that at

high reduction extents, irreversible changes such as transition from dioctahedral to trioctahedral configuration and dehydroxylation are more likely to occur (e.g. Stucki et al. 2011). Similarly, Ribeiro et al. (2009) found that 100% dithionite-reduced and reoxidised nontronite produced a very different Mössbauer spectrum than nontronite that had been only partially dithionite-reduced and reoxidised.

From these reports, one might conclude that reduction pathways that can achieve the greatest extent of structural Fe reduction (i.e. dithionite) would therefore produce the greatest degree of irreversible alteration. However, clay minerals have also been described to be irreversibly altered by microbial reduction (e.g. Kim et al. 2004, Yang et al. 2012, Shi et al. 2021), where extent of structural Fe(II) is limited. Clearly, the reduction pathway also plays a key role in the extent of irreversible alteration and there is a knowledge gap on how both pathway and reduction extent affect the sustainability of the mineral.

Another key factor affecting the degree of reversibility is the Fe content of the clay mineral. Reduction of clay minerals with low Fe content tends to produce largely reversible effects upon reoxidation, whereas clay minerals with high Fe contents are altered more irreversibly by the effects of redox cycling (Neumann et al. 2011, Gorski et al. 2013). Gorski et al. (2013) observed low Fe-content clay minerals such as Wyoming montmorillonite SWy-2 (2.3 wt % Fe) displaying almost entirely reversible electron transfer, and the colour of the mineral was unchanged. In contrast, clay minerals such as nontronite NAu-1 with comparatively high Fe content (21.2 wt % Fe) displayed a significant colour change alongside an irreversibly altered redox profile upon reoxidation.

Although many of the most dramatic effects of clay mineral redox cycling (e.g. dissolution and transformation) are cited as a result of microbial reduction (e.g. Kostka et al. 1999, Dong et al. 2003, Yang et al. 2012), other research has also indicated that microbial reduction incurred largely reversible impacts on the structure (Gates et al. 1993, Stucki et al. 2011). Lee et al. (2006) demonstrated that Fe-bearing smectite were altered during microbial reduction, but the effects were largely reversible upon reoxidation. This is likely due to the lower achievable reduction extent inherent with microbial reduction. A comparison of partially reduced clay minerals by either

dithionite or microbes showed that at low reduction extents both reduction pathways lead to Mössbauer spectra that were near indistinguishable, and the effects were largely reversible upon reoxidation (Ribeiro et al. 2009). Further work is required to understand whether these effects are truly reversible, and whether the minerals can sustain the effects multiple reduction and oxidation cycles over time.

2.3.3 Introduction to Mössbauer spectroscopy

Previous research on structural changes of Fe-bearing clay minerals utilised Mössbauer spectroscopy and produced compelling evidence on Fe speciation effects caused by reduction, that other techniques could not provide. The Mössbauer effect, discovered by Rudolf Mössbauer in 1958, relies on the recoilless resonant absorption of nuclear gamma rays by ^{57}Fe atoms held within a rigid, solid matrix (Gütlich et al. 2011). Mössbauer spectroscopy allows investigation of properties such as valence state, speciation, and binding environment / coordination of Fe atoms within solid mineral samples. Mössbauer spectroscopy has several advantages over other analytical techniques. For instance, Mössbauer analysis can be applied to a wide range of sample sizes, as the technique allows measurement of atomic scale properties and interactions. Additionally, all atoms and elements other than ^{57}Fe are completely invisible to the measurement making ^{57}Fe -specific Mössbauer free from issues such as matrix effects (Murad and Cashion 2004).

The Mössbauer effect can be simply described as follows: Gamma rays are emitted from a radioactive source. If the gamma radiation is released without the emitting atom recoiling, then the emission can be entirely absorbed without recoil by a receiving Fe atom as no energy is lost. The emitter is moved towards and away from the receiver to apply the doppler effect, this allows for small variations in energy between atoms to be accounted for. The absorption of the gamma radiation can be recorded as a spectrum.

A Mössbauer spectrum can be described using several key parameters. The Mössbauer parameters are effects of hyperfine interactions between Fe atom nuclei and their surrounding electrons, leading to changes to the nuclear and electronic energy levels (Figure 2.6). The parameters can be derived from least square fitting of the data to a theoretical model and subsequently used to interpret the nature of the host material.

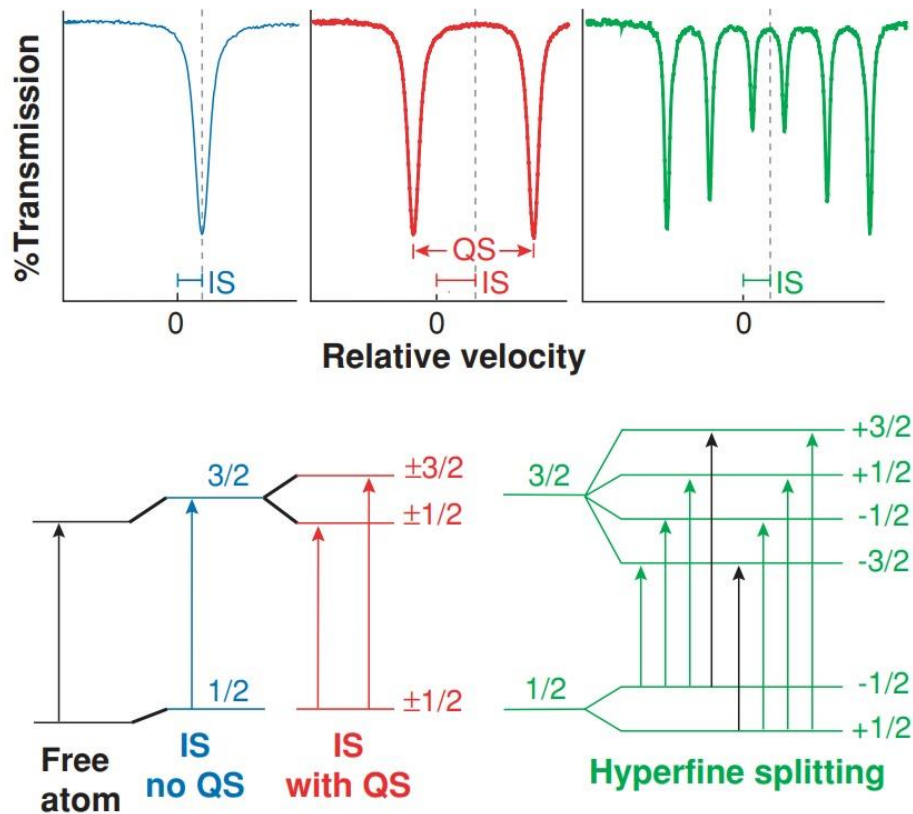


Figure 2.6: Figure demonstrates the effects of hyperfine interactions (Isomer shift, Quadrupole splitting, Hyperfine splitting) on a typical Mössbauer spectrum. Isomer shift (IS) is shown in blue, Quadrupole splitting (QS) is shown in red, Hyperfine splitting (H) is shown in green. Black arrows represent the energy difference between the ground and excited nuclear states. Fractions describe the nuclear spin quantum number of the levels. Illustration is taken from Dyar et al. (2006)

The three main parameters relevant to this study to note are described as follows (Murad and Cashion 2004, Dyar et al. 2006):

- **Isomer shift**, also known as Chemical Shift, or Centre Shift, (will be referred to as CS in later chapters). A shift up or down of nuclear levels, caused by overlap of nuclear and S-electron charge distributions. Presents as a shift of the absorption peak off centre from the zero-point (calibrated against alpha-Fe(0)). This parameter provides information useful for determining the valence state, and ligand bonding state of an Fe atom.
- **Quadrupole splitting**, also known as Electric Quadrupole Interaction (QS hereafter). Orientation of the nuclear quadrupole moment, caused by asymmetric electric field gradient, leading to a splitting of nuclear levels. Presents in a spectrum as the distance between separated peaks. This

parameter is useful for determining properties such as spin state, valence state, bonding properties, and local coordination of an Fe atom. For sextets and octets, QS will become quadrupole shift (for sextets) or the electric quadrupole interaction parameter (in Full-static Hamiltonian fit analysis).

- **Hyperfine splitting**, also known as Magnetic Hyperfine Interaction (H hereafter). This parameter describes orientation of a nuclear magnetic moment in the presence of an externally applied magnetic field, or magnetic ordering occurring across interacting Fe atoms within the sample. Presents in a spectrum as full splitting of nuclear levels. This parameter is used to identify magnetic ordering of Fe within a sample.

Mössbauer spectroscopy will be used throughout this thesis for both quantitative and qualitative analysis of Fe-bearing mineral samples. Manipulation of measurement temperature can provide different use-cases and insights. At higher temperatures (here: 77 K), Fe-rich clay minerals will not present magnetic ordering, and the Mössbauer spectrum can be used as a means of quantifying Fe(II)/Fe(III) stoichiometric ratios from the Fe doublets observed. By decreasing the measurement temperature to liquid helium temperature (4 K), it is possible to induce magnetic ordering in Fe species where it was previously absent. Once magnetic ordering occurred, the Mössbauer spectrum becomes more complex and provides a basis for interpretation of Fe binding environments and speciation within the mineral samples. This approach allow us to probe the impact of reduction on the structure of the clay mineral, the coordination of octahedral Fe, as well as the nature of secondary precipitate minerals formed by the reaction of Fe(II) with clay minerals.

2.4 Effects of redox cycling on clay mineral reactivity towards environmental contaminants

The scope of this project is ultimately to determine the suitability of clay minerals for use in sustainable contaminant remediation. While it has been shown that Fe-bearing clay minerals can be used for transformation of environmentally hazardous substances (e.g. Neumann et al. 2008, Bishop et al. 2011), can clay minerals be used sustainably over multiple cycles of reduction and oxidation? There is evidence to indicate that the clay mineral structure is altered by redox cycling (e.g. Komadel et al. 1995, Gorksi et al.

2013), and irreversible structural changes might impact the long-term efficacy of the minerals as materials for contaminant control.

Research into the effects of microbial reduction-oxidation cycling has produced inconclusive results. One study suggested that redox cycling using *Shewanella* bacteria increased the reactivity of Fe-rich smectites towards contaminant Tc(VII) (Yang et al. 2012). The work found that although the extent of reduction was not changed, the rate of transformation increased after multiple redox cycles. Similarly, another study (Bishop et al. 2019) found that the initial rate of Cr(VI) transformation by Fe-bearing sediments increased with successive redox cycles. However, another study investigating redox cycling Fe-rich smectite with *Shewanella* produced no significant changes towards the reduction of nitrates (Zhao et al. 2015). In each research, the transformation of a different environmental contaminant was measured, and did not include controls for the effects of other minerals (such as Fe-oxide species) that may have been present and influenced the system's reactivity.

Gorski et al. (2012,2013) used mediator compounds to measure how the redox profile of Fe-bearing clay minerals was impacted by chemical reduction (with dithionite) and oxidation. The study observed a dramatic shift in the redox profile of Fe-rich minerals after one cycle of reduction and oxidation. An irreversible shift in redox profile could significantly impact the capacity for the mineral to give and receive electrons, and this might call in to question the long-term sustainability of clay minerals for contaminant control. However, this study measured the effects of 100% structural Fe reduction, but the effects of dithionite-reduction redox cycling to lower reduction extents are still unknown. Additionally, unlike studies using microbial reduction that observed successive increases in rate of reactivity each cycle (e.g. Yang et al. 2012, Bishop et al. 2019), other research (Gorski et al. 2013) has found that subsequent reductions did not alter the profile any further. Importantly, the research conducted by Gorski et al. (2012, 2013) highlighted relationships between redox profile and characteristics of the structure and mineralogy. This would indicate that irreversible structure is linked to reactivity, and irreversible structural alterations could impact the sustainability of clay minerals as reactive materials for contaminant transformation.

The effects of redox cycling with aqueous Fe(II) (i.e. biologically-mediated abiotic reduction) are yet to be confirmed, and studies so far have only investigated the reactivity after a single reduction. It is accepted that the interaction of aqueous Fe(II) and Fe-rich smectites leads to the formation of secondary precipitate minerals (Schaefer et al. 2011). However, the impact of these secondary minerals on reactivity is inconclusive. Some studies have found that the Fe(II) held in secondary minerals dominates contaminant transformation (e.g. Jones et al. 2017, Entwistle et al. 2019), while other studies have found secondary minerals have less effect than clay mineral Fe(II) and reactivity more closely resembles dithionite-reduced samples (Tsarev et al. 2016). More work is required to understand how multiple cycles of reduction with Fe(II) and reoxidation impacts the reactivity of clay minerals, and the role of secondary precipitates in contaminant transformation.

The range of results observed indicate that the effects of multiple redox cycles on the reactivity of Fe-bearing clay minerals are yet to be conclusively understood. The extent of contaminant reduction might vary dependant on the reduction pathway, contaminant chosen, and minerals present.

2.4.1 Introduction to nitroaromatic compounds as contaminants

Reduced clay minerals have been shown effective at transforming a wide variety of environmental contaminants (e.g. Nzungung et al. 2001, Elsner et al. 2004, Ilgen et al. 2017, Neumann et al. 2008, 2009, Bishop et al. 2011, 2019). This project however will focus on the reductive transformation of nitroaromatic compounds as model contaminants and probe compounds.

Nitroaromatic compounds (NACs) are a group of organic compounds featuring a nitro group bound to an aromatic ring. NACs are used ubiquitously as agrochemicals, dyes, explosives, and chemical intermediates and solvents (Klausen et al. 1995, Hofstetter et al. 1999, 2006, Boparai et al. 2008, Ju et al. 2010, Tiwari et al. 2019). The use of NACs has also led to widespread contamination of soil and water resources as remnants of many industrial activities (Hofstetter et al. 1999, Boparai et al. 2008). NACs are persistent under oxic conditions and are of particular concern due to being highly carcinogenic and toxic (Haderlein and Schwarzenbach 1995).

Assessing the sustainability of Fe-bearing clay mineral redox reactions
Introduction and literature review

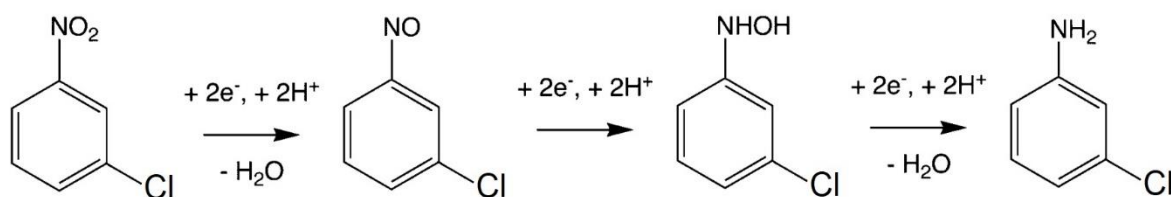


Figure 2.7: Schematic illustrating the 6-electron reduction process transforming kinetic probe compound 3-chloronitrobenzene to product compound 3-chloroaniline. Adapted from Hartenbach et al. (2006)

Nitroaromatics can be readily reduced by Fe-bearing minerals (Ruggè et al. 1998), and reduction of NACs produces corresponding aniline compounds that are often more easily biodegradable than the parent substance (Neumann et al. 2008, Luan et al. 2015b). Hofstetter et al. (2006) investigated the utility of clay mineral Fe towards NAC transformation, and outlined three possible reactive sites on Fe-bearing clay minerals that were capable of reductively transforming NACs. Subsequent papers have demonstrated that structural Fe is primarily responsible for NAC transformation (Neumann et al. 2008).

This project will focus on the transformation of model contaminant 3-chloronitrobenzene as a kinetic probe compound, and model contaminant. NAC compounds make ideal kinetic probes as they are rapidly reduced by mineral Fe(II) and can be transformed into easily detectable products (Klausen et al. 1995). Using 3-chloronitrobenzene as a kinetic probe will allow the quantification of how redox cycling affects the intrinsic reactivity of clay minerals. Nitroaromatics with substituted functional groups such as chloro-, acetyl-, methyl are useful as kinetic probe compounds as substitutions on the aromatic ring allow for analysis of a wide range of reduction potentials and thermodynamic dependencies. The location of the functional group on the aromatic ring will determine the sorptive properties, allowing measurement of various affinities of compounds to mineral surfaces (Neumann et al. 2008, Luan et al. 2015b). In this experiment, 3-chloronitrobenzene was chosen as it has been demonstrated to show negligible adsorption to clay mineral particles (Haderlein and Schwarzenbach 1993, Laird and Fleming 1999, Klausen et al. 1995). 3-Chloronitrobenzene does not strongly sorb to clay mineral surfaces because the negatively charged chlorine substitution is neither electron-withdrawing or electron-delocalizing, meaning there is little interaction between the compound and the negatively-charged clay mineral surface (Haderlein and Schwarzenbach 1993, Laird and

Fleming 1999). Additionally, 3-chloronitrobenzene also makes a suitable probe because the transformation of 3-chloronitrobenzene to its corresponding aniline (3-chloroaniline) can be measured easily with High Pressure Liquid Chromatography (HPLC) (e.g. Neumann et al. 2008).

2.5 Environmental implications of evaluating the effects of multiple reduction-oxidation cycles on the structure and reactivity of Fe-bearing clay minerals

The review has outlined several key points regarding the use of Fe-bearing clay minerals as sustainable materials for control of environmental contaminants. In particular, it has been highlighted that the following are accepted views on redox interactions between clay minerals and contaminants:

1. Fe atoms are commonly incorporated into clay mineral structures, and the variable valence state of structural Fe plays a key role in many subsurface physicochemical processes (Sposito et al. 1999, Kappler et al. 2021). Clay mineral Fe can be reduced via a multiple reduction pathways, and can subsequently reductively transform a wide range of environmental contaminants (e.g. Neumann et al. 2008, Tsarev et al. 2016, Bishop et al. 2019). Clay minerals are thought to be more resistant to dissolution than other Fe minerals, and therefore could provide a renewable source of environmental reduction equivalents (Ernstsen et al. 1998, Fialips et al. 2002). Clay minerals will likely face fluctuating redox condition over time due to changes in porewater chemistry and microbial activity (Dong et al. 2003, Roden et al. 2012, Meng et al. 2021).
2. Electron transfer pathways can include microbial reduction as a means of anaerobic respiration, and chemical / abiotic reduction by compounds such as dithionite (Kostka et al. 1999, Stucki et al. 1984a), or by dissolved Fe(II) atoms (Schaefer et al. 2011, Neumann et al. 2013). Different pathways of reduction lead to different effects on the clay mineral structure, many of which appear to be at least partially irreversible (e.g. Kostka et al. 2002, Dong et al. 2003, Ribeiro et al. 2009, Stucki et al. 2011, Tsarev et al. 2016, Jones et al. 2017, Shi et al. 2021).

3. Irreversible alterations of the clay mineral include significant structural impacts such as dehydroxylation, octahedral rearrangements, and even possibly complete mineral transformation (e.g. Manceau et al. 2000a and b, Dong et al. 2003, Kim et al. 2004, Lee et al. 2006, Neumann et al. in Tratnyek 2011). Changes to structure incurred by reduction are dependant on factors such as structural Fe reduction extent and structural Fe content, and might infer unsustainability of clay minerals as environmental reductants.
4. There is evidence to indicate that redox cycling can impact the reactivity of clay mineral Fe(II) towards contaminants.

Although clay minerals have demonstrated their resilience relative to other Fe minerals as useful materials for contaminant transformation, there is also notable research to indicate that this utility may not be sustainable. Further research is necessary to address the following knowledge gaps in the current understanding:

1. Chemical and microbial reduction have been suggested to affect clay mineral structure and reactivity differently (e.g. Lee et al. 2006, Ribeiro et al. 2009). Research has produced conflicting and contradictory results regarding the effects of each pathway on the clay mineral (e.g. Gates et al. 1993, Stucki et al. 2011, Yang et al. 2012, Zhao et al. 2015). At comparable reduction extents, the effects of redox cycling for each reduction pathway have not been addressed or adequately compared. Furthermore, research has yet concluded whether the observed irreversible alterations scale as the mineral is subjected to multiple reduction-oxidation cycles. Understanding this is crucial to determine whether the minerals can be used as a sustainable form of contaminant transformation.
2. Microbial redox cycling of clay minerals has produced mixed, and sometimes dramatic results (e.g. Kim et al. 2004, Yang et al. 2012, Zhao et al. 2015, Shi et al. 2021). However it has not been established whether the observed effects of microbial interaction with clay minerals are a result of bioreduction of the structural Fe, or other metabolic processes. Is it possible to subject clay minerals to multiple cycles of reduction and oxidation using organic electron shuttling compounds as surrogate for living bacteria? Do the effects of using

shuttle compounds as electron donor differ from the effects of microbial redox cycling?

3. Interactions between aqueous Fe(II) and clay mineral Fe can lead to electron transfer, atom exchange, and precipitation of secondary reactive Fe minerals (Schaefer et al. 2011, Jones et al. 2017, Entwistle et al. 2019). How does abiotic reduction of clay minerals by aqueous Fe(II) impact the structure and reactivity of the clay minerals over multiple redox cycles? What is the nature of the secondary Fe intermediate species, and how do they affect the reactivity of the system towards transformation of contaminants?

The knowledge gaps discussed highlight a need for further research to probe how multiple cycles of reduction and oxidation alter clay minerals. Can clay minerals be used consistently and renewably as a means for transforming harmful environmental contaminants?

2.6 Aims and Objectives

This project aims to assess whether Fe-bearing clay minerals can be used sustainably and renewably as materials for the control and degradation of environmental contaminants. The project will understand how multiple cycles of reduction via various environmentally relevant pathways, and oxidation, impact both the reactivity and the structure of Fe-rich clay minerals. The project will determine whether Fe-bearing clay minerals can be utilized consistently for environmental electron-transfer reactions, and will ultimately outline their potential as materials for long-term control of organic contaminants.

To successfully achieve these aims, the project will:

- Subject Fe-rich clay minerals to multiple cycles of reduction, and subsequent oxidation. Reduction of clay mineral structural Fe will be achieved using three environmentally relevant reduction pathways: Chemical Reduction with dithionite, Microbial proxy reduction using reduced electron shuttling compound (anthraquinone-2,6-disulfonate), and finally via biologically-mediated abiotic reduction with aqueous Fe(II).
- Measure the impact of multiple cycles of reduction and oxidation on the reactivity of clay mineral structural Fe towards model contaminant and probe compound 3-chloronitrobenzene.
- Monitor effects of multiple reduction and oxidation cycles on the structure and morphology of the clay minerals, and determine the degree of reversibility for structural alterations.

Chapter 3: Effects of chemically-induced reduction-oxidation cycling on the structure and reactivity of nontronite

3.1 Introduction

The Fe(II)-Fe(III) redox couple plays a major role in the cycling of nutrients and fate of environmental contaminants in the sub-surface. Fe can be easily incorporated into the structure of clay minerals, and Fe-bearing clay minerals can be found ubiquitously in sediments and soils worldwide (Sposito et al. 1999). Structural Fe can be reduced to Fe(II) by various reduction pathways including microbial activity or by chemical reductants. In natural systems, the redox state of soils and sediments can be dramatically altered by changes in porewater chemistry, often due to seasonality and fluctuations of the water table (e.g. Deng et al. 2014, Calabrese and Porporato 2019). Work has even been conducted to investigate the potential for artificially chemically manipulating the redox state of subsurface sediments for use of contaminant control (Fruchter et al. 2002, Szczody et al. 2004). In their reduced state, Fe-bearing clay minerals have been shown capable of reductively transforming a wide range of hazardous environmental contaminants (e.g. Neumann et al. 2008, 2009, Bishop et al. 2011, 2019). Unlike many other Fe minerals such as naturally occurring Fe-oxides, clay minerals are thought to be more resistant to reductive-dissolution, and could be a potentially renewable source of reduction equivalents in the environment (Fialips et al. 2002). This would mean clay minerals could be a valuable and sustainable tool for engineered pollutant transformation, or a solution for long-term natural attenuation of contaminated land. However, other work has demonstrated that chemical reduction of clay mineral structural Fe can lead to irreversible alterations of the minerals that might call into question their supposed longevity and sustainability.

Dithionite is a common method of chemically reducing clay mineral structural Fe. Dithionite has also been shown to be the most effective reductant, and is capable of accessing almost 100% of structural Fe in Fe-rich clay minerals (1984b). While the use of dithionite as an *in-situ* reductant has been previously discussed (Nzengung et al. 2001), it can also serve as a useful proxy for the effects other chemical reductants that may occur naturally. Previous research has demonstrated that chemical reduction might differ from microbial reduction, and as such produces different effects on the

clay mineral (Lee et al. 2006, Ribeiro et al. 2009). Complete reduction of structural Fe to Fe(II) by dithionite has been shown to leave irreversible alterations to the clay mineral structure, as well as irreversible shifts to the mineral redox potential (Gorski et al. 2013). However, research has also indicated that the degree of irreversibility of clay mineral alterations scale with increasing reduction extent, and at low reduction extent the effects appear indistinguishable from microbial reduction (Ribeiro et al. 2009). Do the irreversible alterations of clay minerals due to chemical reduction impact the sustainability, and can clay minerals persist through successive cycles of chemical reduction and oxidation?

This chapter aims to investigate how multiple cycles of dithionite-reduction and oxidation impact the structure and reactivity of Fe-rich smectite N Au-1. N Au-1 samples are subjected to three cycles of dithionite-reduction, and subsequent reoxidation by hydrogen peroxide (H₂O₂). The effects of redox cycling are measured at both a high reduction extent (75% structural Fe(II)) and a low extent (20% structural Fe(II)). Experiments conducted at a low reduction extent are relevant for comparison with other electron transfer pathways such as bioreduction. High reduction extent experiments provide an insight to the compounding effects of redox cycling when degree of reversibility is lowest, and will be relevant for artificial, *in-situ* reduction techniques. The reactivity of reduced clay minerals for the transformation of kinetic probe compound 3-chloronitrobenzene is measured to assess how reactivity is affected by multiple successive redox cycles. We also measure the effects of redox cycling on clay mineral structure, using variety of spectroscopic analyses including Scanning Electron Microscopy, particle size measurements, and Mössbauer spectroscopy. Overall, we aim to understand whether the alterations caused by chemical reduction will impact the longevity and sustainability of Fe-bearing clay minerals as materials for contaminant control.

3.2 Methods

3.2.1 Mineral Preparation

Nontronite N Au-1 ($M^{+}_{1.05}[Si_{6.98}Al_{1.02}][Al_{0.29}Fe_{3.68}Mg_{0.04}]O_{20}OH_4$, 21.5 wt% Fe) was purchased from the Clay Minerals Society's Source Clays Repository (<https://www.clays.org/source-clays/>). Mineral preparation followed the lab's

standard operating procedure, published previously (e.g. Neumann et al. 2011). In short, the mineral was oven-dried before being crushed to fine powder using a ball mill. The mineral was then suspended in deionised water, size fractionated to a range of 0.2-0.5 μm and finally Na^+ -homo-ionised with 1 M NaCl solution. The mineral sample was then purified to remove any remaining admixed minerals including kaolinite and Fe-oxides. Mineral purity was confirmed using Fourier-Transform Infrared (FT-IR) spectroscopy. The final product was freeze dried, ground with a pestle and mortar and then passed through a 150 μm sieve before being stored prior to use.

3.2.2 Mineral Fe reduction and oxidation

All mineral reduction was undertaken in an anaerobic chamber (GS Glovebox Systemtechnik GmbH, Germany) under a N_2 atmosphere (≤ 1 ppm O_2). Deoxygenation of all solutions and suspensions was carried out by bubbling N_2 for 1 hour. Previous research has demonstrated that this deoxygenation method can remove 100% of dissolved oxygen (Adamou 2020) All dithionite reductions of clay mineral Fe were completed following a modified version (Neumann et al. 2011) of the citrate-bicarbonate-dithionite methods described by Stucki et al. (1984b). Two batches of NAu-1 were subjected to chemical reduction of its structural Fe, one to an intended high (75%) Fe reduction extent and another to an intended low (20%) reduction extent. This was achieved by adding the stoichiometrically equivalent mass of dithionite to reduce 75% and 20% of structural Fe respectively. Samples were left to stir overnight, then homo-ionised with deoxygenated 1 M NaCl solution and subsequently washed with deoxygenated deionised water to remove any remaining dithionite residue. Clay mineral Fe reduction extent was confirmed by both Mössbauer spectroscopy, and with a modified method of hydrofluoric acid (HF) mineral digestion and phenanthroline assay (see Section 3.2.6 for details). Reduced minerals were then suspended in a buffer solution of 10 mM 3-(N-morpholino)propanesulfonic acid (MOPS) and 50 mM NaCl, creating, nominally, a 20 g/L stock suspension. The suspension pH was adjusted to pH 7.5 using aliquots of 1 M NaOH or HCl.

For clay mineral Fe re-oxidation, an aliquot of stock suspension was removed from the glovebox and 1 M hydrogen peroxide (H_2O_2) was added in stoichiometric excess to the concentration of Fe(II), this was left to stir overnight open to the room atmosphere.

The following day, the mineral was washed with 1 M NaCl and deionised water twice in the same manner as with the reduction to remove any possible remaining H₂O₂. Clay mineral was then resuspended, deoxygenated, and moved back into the glovebox ready for the next cycle of reduction.

In total, 3 cycles of reduction-oxidation of N Au-1 were conducted for each reduction extent (75% and 20%). Samples of mineral suspensions were separated from the bulk suspension at each stage of the process before reaction with 3-chloronitro benzene, to be used later in the various solid sample analyses conducted.

Samples and data are categorized by the following naming system, for ease of future reference:

Cycle 1 generally refers to N Au-1 samples that have been reduced once with dithionite.

Cycle 2 generally refers to N Au-1 samples that have been reduced with dithionite, reoxidised with H₂O₂, and subsequently re-reduced with dithionite a second time.

Cycle 3 generally refers to N Au-1 samples that have been reduced for a third time with dithionite, after two preceding reduction-oxidation cycles.

For Mössbauer analysis, each cycle (1-3) also has its respective reoxidised spectrum. For example, "Cycle 1 reoxidised" would refer to measurements of the sample described in Cycle 1 after reoxidation with H₂O₂, and all structural Fe(II) has been oxidised.

3.2.3 Nitroaromatic compound transformation experiments

Transformation experiments involving 3-chloronitrobenzene were only conducted with samples in their reduced stage, i.e. after reduction via dithionite. Control experiments using native (i.e non-reduced) clay minerals were also conducted, but have not been included. There is a significant body of literature previous experiments demonstrating that clay minerals absent of Fe(II) do not react with nitroaromatics under these conditions, and that volatilisation does not occur in the solution (Schulz and Grundl 2000, Hofstetter et al. 2003, Hofstetter et al. 2006, Entwistle 2021).

All transformation experiments were completed and the batch reactors stored inside the anaerobic glovebox, to minimise unintended oxidation. All experiments were conducted in triplicate. For each batch reactor, 1.5 mL of the 20 g/L clay mineral stock suspension and 13.5 mL of buffer solution containing 10 mM MOPS and 50 mM NaCl were added to 20 mL glass vials. The pH of each reactor was adjusted to 7.5 using NaOH or HCl. Reactors were sealed with butylene rubber stoppers, crimp capped to hermetically seal the contents, wrapped in foil or PTFE tape to prevent any risk of unintended photo-oxidation, and then finally placed on an end-over-end rotator.

Probe compound degradation reactions were initiated by injecting 30 μ L of methanolic 3-chloronitrobenzene stock solution to give an initial concentration of \sim 50 μ M, using a Hamilton gas-tight, PTFE luer lock, 0.25 mL glass syringe to achieve a starting concentration of \sim 50 μ M in the reactor. A 500 μ L sample was taken immediately after spiking using a Hamilton gas-tight, PTFE luer lock, 0.5 mL glass pipette and filtered using a luer lock, 0.22 μ m nylon filter (sourced from Thames Restek Ltd) to remove any mineral / solids. The sample was then stored in a clear, 2 mL sealed glass HPLC vial (sourced from VWRTM) with conical glass inserts (from Sigma Aldrich) until analysis. For each reactor, more samples were taken in the same method at pre-determined time steps until the transformation of 3-chloronitrobenzene to 3-chloroaniline had reached completion (i.e. all 3-chloronitrobenzene has been transformed to 3-chloroaniline). All samples were stored in the fridge at 4 °C prior to HPLC analysis.

3.2.4 Organic contaminant quantification

The first sample taken from the reactor immediately after spiking with contaminant was used as measurement for initial concentration.

Samples measured via HPLC were measured against a set of pre-prepared calibration standards containing both methylated contaminant and product, and diluted with DIW, at 5 specific concentrations (1 μ M/L, 12.5 μ M/L, 25 μ M/L, 37.5 μ M/L, and 50 μ M/L) in glass HPLC vials (same as used for reactor samples).

Analysis of samples and concentrations of model contaminant 3-chloronitrobenzene (3CNB) and the degradation product 3-chloroaniline (3CAN) were measured using the Agilent 1260 Infinity II HPLC equipped with DAD detector, using an LC-18 column (XBridge C18 3.5 μ m).

Samples were measured with a custom HPLC method, using deionized water and methanol in varying proportions as eluent. Figure SI 3.1 demonstrates the precision and accuracy of the HPLC method. Figure SI 3.2 shows the custom concentration / time eluent gradient used for each sample.

HPLC method: 10 minute total run time per sample. 1mL / min flow rate, column temperature of 30 °C. 20 mL of sample injected. Measured absorption at wavelengths 214 nm and 252 nm.

3.2.5 Data evaluation and kinetic modelling

The transformation of model probe contaminant 3-chloronitrobenzene to product compound 3-chloroaniline was measured using the measured concentration values of both reactant and product across a time series. The data was modelled applying a second order kinetic rate law to account for two implicit reactive Fe sites (with distinctive reactivities) in the clay mineral, and rate constants were calculated via differential equations as described by Neumann et al. (2008). Equations used to calculate the rate constant values are as follows in Equations 3.1, 3.2, and 3.3.

Equation 3.1; second order kinetic rate law:

$$\frac{\partial[NAC]}{\partial t} = -k_A [Fe(II)_A][NAC] - k_B [Fe(II)_B] [NAC]$$

Where k_A and k_B describe the intrinsic reactivities of highly reactive site “A”, and less reactive site “B”. [NAC] is the measured aqueous concentration of probe contaminant compound 3-chloronitrobenzene, and $[Fe(II)_A]$ and $[Fe(II)_B]$ are the concentration of each reactive site (A and B).

Equation 3.2; boundary condition $[Fe(II)_{Tot}]$, included in mathematical model:

$$[Fe(II)_{Tot}] = [Fe(II)_A] + [Fe(II)_B]$$

For comparison, the measured kinetic data was also fit with a pseudo-first order model describing a single reactive site, shown in Equation 3.3. This was a simplified version of the two-site model described in Equation 3.1.

Equation 3.3; boundary condition $[Fe(II)_{Tot}]$, included in mathematical model:

$$\frac{\partial[NAC]}{\partial t} = -k [Fe(II)_{Total}] [NAC]$$

Equations were solved numerically using Matlab routine ODE15s as described by Neumann et al. (2008). The statistics underlying the best fit model are produced by the following process. The model takes data from 3 replicate reactors and fits all three datasets simultaneously to create a single set of parameters (rate constants k_A and k_B , as well as initial concentration of Fe comprising the highly reactive sites "A"). The mathematical fitting procedure minimized the sum of the squared differences between simulated and measured concentrations based on the Nelder-Mead simplex method, resulting in the estimated values for k_A , k_B and initial $[Fe(II)_A]$ produced in the model output. Standard deviation values were calculated via linear error propagation. This is done by varying parameter values by 10% calculating the resulting error yielded.

The previously mentioned model included an interconversion between each reactive site to account for re-spiking during experiments. However, as the method does not include re-spiking the reactors, this interconversion step was omitted from our calculations and the model was updated to a state similar to a later study (Neumann et al. 2009).

3.2.6 Elemental analysis

Solid phase concentrations of Fe(II) and Fe_{Tot} were measured following HF mineral digestion using a modified 1,10-phenanthroline method (Stucki 1981, Amonette and Templeton 1998) as described in Neumann et al. (2011). Absorbance was measured using UV-VIS spectrophotometer at a wavelength of 510 nm. This method was used to confirm reduction extents of dithionite-reduced minerals, and concentrations of clay mineral Fe(II) were incorporated into kinetic calculations described in Section 3.2.5. Clay mineral loading was back-calculated from the measured total Fe concentration, based on the wt % of Fe in N Au-1, taken to be 22.4% (Neumann et al. 2013).

Clay mineral suspensions were measured for evidence of mineral dissolution due to reduction via dithionite. Samples were taken from supernatant after reduction, filtered with 0.2 µm nylon filter, and measured with a Varian Vista-MPX Inductively-Coupled Plasma Optical Emission Spectrometer (ICP-OES) for dissolved traces of primary smectite elemental components (Si, Al, Mg, Fe). Accuracy is expected to vary within 10% of concentration reading. Measured concentrations were compared to the mineral loading values as a percentage, based on the respective fraction each major element in N Au-1.

Values for wt% of N Au-1 elemental constituents were approximately calculated to be Fe = 22.4% (Neumann et al. 2013), and Al = 8.2%, Mg = 4.2%, Si = 51.5% (Keeling et al. 2000).

3.2.7 Morphological analysis (particle size and SEM / EDX)

Particle morphology was examined using a combination of Scanning Electron Microscopy (SEM) with Energy Dispersive X-ray analysis (EDX), as well as particle size analysis.

Samples for SEM / EDX analysis were prepared under N₂ atmosphere. Samples of mineral suspensions were first diluted to 0.2 g/L mineral loading, and then a drop of the suspension was placed on some carbon tape on an aluminium SEM stub via pipette and allowed to dry overnight. Once all fluid had evaporated, sample stubs were sealed in an airtight container for transport to the SEM. Each sample was gold-coated to improve resolution and minimise risk of oxidation. Samples were analysed using a

Tescan Vega 3LMU scanning electron microscope, fitted with a Bruker XFlash® 6 | 30 for EDX analysis.

EDX analysis was conducted using Imagej software. Elemental mapping images were filtered to show only Fe, Si, and Al, and the relative intensity of each element was measured over representative areas where the mineral was determined to be present. 3 images were taken of each sample, and a minimum of 3 measurements was taken for each image, and mean values were calculated for each sample.

Particle size analysis was conducted as follows: Samples were taken of clay mineral suspensions and diluted to 0.05 g/L using deoxygenated, deionised water. Samples were measured in a sealed screw-cap (to prevent any unintended oxidation), 10 mm x 10 mm (internal width) quartz cuvette sourced from Hellma UK Ltd. Sample particle size was measured using Malvern Panalytical Zetasizer Nano.

3.2.8 Mössbauer analysis

Samples were separated and prepared from the NAu-1 stock suspension before contaminants were added. Solids were separated from supernatant with a 13 mm, 0.2 µM nylon filter under anaerobic atmosphere. The sample solids were sealed in Kapton tape to prevent oxidation during transfer to the Mössbauer spectrometer.

Samples were analysed using and S4 Mössbauer spectrometer (SEE Co., Edina, MN, U.S.A.) in transmission mode and calibrated against 7 µm α-Fe(0) foil. Temperature during spectra acquisition was controlled with a closed cycle cryostat (SHI-850, Janis Research Co., Wilmington, MA, U.S.A.) at either 4 K, 13 K, or 77 K temperature to allow for quantifying Fe oxidation state and the Fe speciation of the clay mineral.

Spectra were analysed using the software Recoil, using Voigt-based fitting routine for spectra measured at 77 K and 13 K temperature, and Full-static Hamiltonian fitting routine for samples measured at 4 K temperature.

3.2.9 Contributions

Dr Jim Entwistle and Dr Katherine Rothwell both assisted with the preparation and measurements of HF digestion experiments. Dr Katherine Rothwell and Dr Rachael Dack provided advice and assistance for developing the HPLC method. Ross Laws

provided operating assistance for SEM imaging. Dr Henriette Christensen conducted measurements with ICP-OES

3.3 Results and discussion

3.3.1 Dithionite-reduced kinetics

To assess how reduction-oxidation cycling using dithionite and H_2O_2 affects the reactivity of clay mineral Fe(II), we reacted model contaminant 3-chloronitrobenzene with nontronite NAu-1 reduced to low (20%) and high extent (75%) of clay mineral Fe reduction ($\text{Fe(II)}:\text{Fe}_{\text{Tot}}$). We monitored the concentrations of both the contaminant and its transformation product 3-chloroaniline. Figure 3.1 shows the changes in 3-chloronitrobenzene concentration over the course of the reaction with 20% dithionite-reduced (left) and 75% dithionite-reduced NAu-1 (right), respectively. Data was converted to values relative to initial measured concentration (c_0) immediately after spiking reactor with contaminant (3CNB) to allow visual comparison.

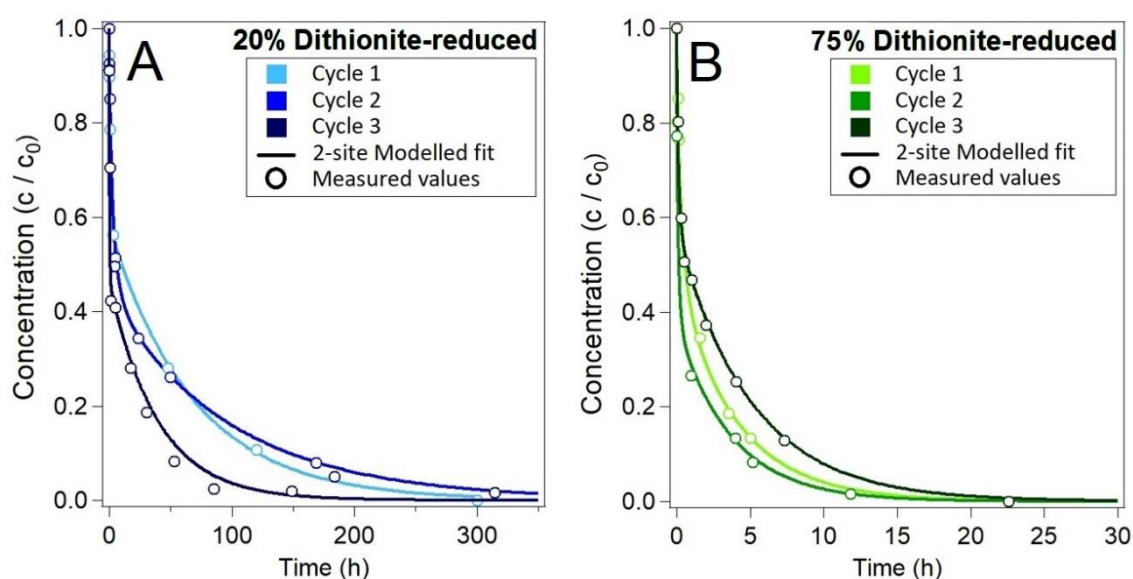


Figure 3.1: Typical time course concentration measurements (circles) of 3-chloronitrobenzene during reaction with NAu-1 that has been reduced with dithionite to (A) 20% Fe(II)/Fe(total) and (B) 75% Fe(II)/Fe(total). Results were obtained in the presence of reduced NAu-1 (Cycle 1), reduced-reoxidised-rereduced NAu-1 (Cycle 2) and reduced-reoxidised-rereduced-rereoxidised-rererduced NAu-1 (Cycle 3), as described in Section 3.2.2. Coloured lines show the fit to the two-site kinetic model (defined in Equation 3.1).

In all experiments: NAC concentration decreased to below detection over the monitoring period; aniline concentrations increased and were equivalent or even higher at the end than initial NAC concentration as shown in Figure SI 3.3. This demonstrates a complete mass balance and indicates that the transformation reaction has reached completion.

Figure 3.1 shows a significant difference between Subfigures A and B: For NAu-1 exhibiting the low Fe reduction extent (20%, blue), the transformation of contaminant reached completion after approximately 300 h, whereas NAu-1 of a high Fe reduction extent (75%) transformed 3-chloronitrobenzene completely to the corresponding aniline after only 24 h. A faster speed of reaction for the high reduction extent (75%) NAu-1 relative to the low reduction extent (20%) NAu-1 is expected, as the former contains a far greater concentration of reactive structural Fe(II). However, the time taken to reach completion for the 75% reduction extent experiments is 10x faster than the 20% reduction extent experiments, whilst Fe(II) content has only increased approximately 2x. This suggests that the relationship between speed of reaction and Fe(II) content is non-linear, and reactivity appears to increase at a rate greater than the increase in Fe(II) content. This might indicate that the increase in reduction extent has impacted the intrinsic reactivity of the clay mineral, rather than just a quantitative increase in reactive material.

Contaminant degradation by NAu-1 of both high and low Fe reduction extents followed a similar overall pattern. There is an initial phase of fast reaction where roughly 50% of the contaminant was transformed within the first few hours. Then, the reaction slowed, and the remaining contaminant was transformed more slowly over the following days (20% reduced NAu-1) or hours (75% reduced NAu-1). This distinct biphasic contaminant degradation has been observed previously for Fe-rich clay minerals reduced to both high (Neumann et al. 2008, 2009) and low Fe reduction extents (Rothwell 2018). It was interpreted to suggest that there are two types of reactive sites in the clay mineral structure capable of reducing and transforming the contaminant: a highly reactive site and a second less reactive site (Neumann et al. 2008, Rothwell 2018). Indeed, fitting the data from all experiments to a model that includes a single reactive Fe site in the clay mineral, produced poor agreement between model fit and the data (Figure SI 3.3). The data was instead fit with a model including two reactive Fe sites in the clay mineral, resulting in excellent agreement between data and model fit (Figure 3.1). The data indicates a presence of two reactive Fe sites, and conforms well with previous research (Hofstetter et al. 2006, Neumann et al. 2008, 2009, Rothwell 2018). This differs from some studies such as Luan et al. (2015b) which despite observing biphasic kinetics, fitted the transformation of bio-

reduced N_{Au}-1 with a single-site, second-order rate law. This finding might be explained by the fact that bioreduction follows a different electron transfer pathway than reduction via dithionite (Rothwell 2018).

For the experiments reduced to a high reduction extent (75%), the kinetic model indicated the rate of contaminant transformation was faster on Cycle 2 than observed for Cycle 1, but Cycle 3 was slower to react than both Cycle 1 and 2. For the experiments reduced to a low reduction extent (20%), the data suggests that Cycle 1 and 2 are largely similar but by Cycle 3 the reaction speed had increased. Overall, the shape of the reaction curve and the time taken to reach completion was similar for each cycle on both experiments. This would indicate that redox cycling does not significantly alter the observed redox reactivity.

The small variation observed between each curve could be due to sample variations between cycles. After conducting the kinetics experiments, a HF mineral digestion and phenanthroline assay was conducted to confirm the reduction extent of the mineral suspension, and measure the mineral loading of each clay mineral suspension (see Table 3.2). The results showed that a significant fraction of the mineral had been lost during the process, and mineral loading concentration was far below the expected value (20 g/L) by Cycle 3. The unexpected loss of mineral meant that the experiments were reduced with a greater stoichiometric concentration of dithionite than would be required to achieve the desired reduction extents (i.e. 75% and 20%). The cause of the decrease in mineral loading was further investigated.

ICP-OES was used to analyse the supernatant of clay mineral suspensions immediately after reduction, to measure for any evidence of reductive dissolution of the mineral. ICP-OES data (Table SI 3.1) shows negligible concentrations of N_{Au}-1 elemental components immediately after reduction with dithionite, confirming that the loss of mineral loading was not due to reductive dissolution. It was concluded in retrospect that quantities of clay mineral were being lost unintentionally from suspension during the comprehensive washing procedure (details in Section 3.2.2) to remove remnant dithionite and hydrogen peroxide from the samples between phases of reduction and oxidation.

Variations in mineral loading and reduction extent will have impacted the observed contaminant transformation. This demonstrates that comparing degradation kinetics qualitatively (i.e. using shape of curve and time to completion) maybe insufficient, particularly as variables such as Fe(II) content and clay mineral loading might vary between sets of reactor. Hence, analysis using a mathematical model will allow a more accurate comparison as the model accounts for variation of variables. The kinetic model takes into account the measured concentration of Fe(II) present in the system provided by the phenanthroline assay, in order to produce rate constant values to describe the intrinsic reactivity.

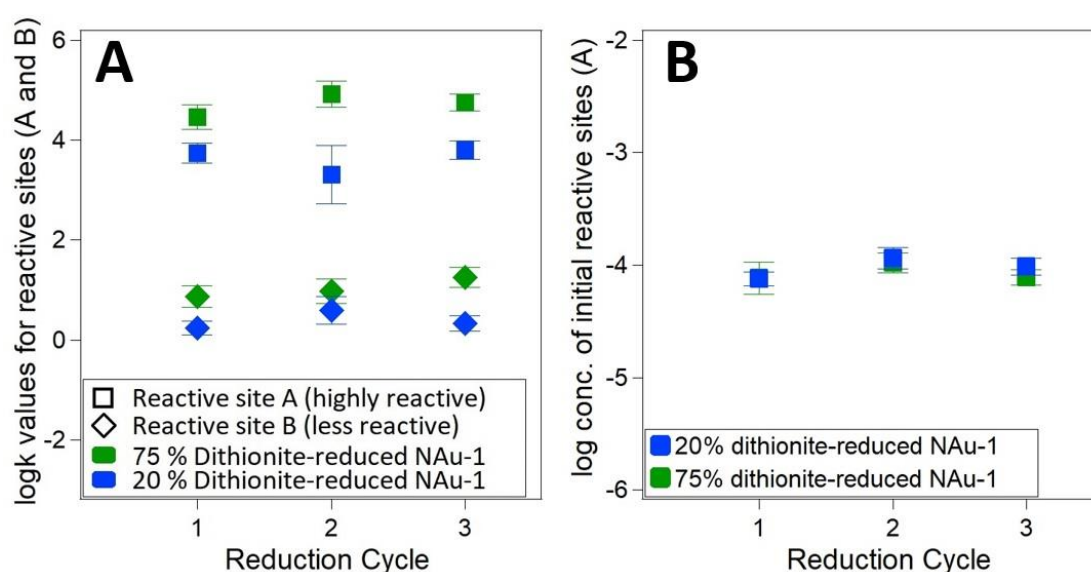


Figure 3.1: Kinetic parameters for 3-chloronitrobenzene transformation obtained from all data to the second order rate model (Equation 3.1): second order rate constant k (Subfigure A), and initial concentration of highly reactive Fe(II) (Subfigure B). Parameter values are plotted as logarithms, showing values for degradation in the presence of both 20% reduction extent (blue) and 75% reduction extent (green), dithionite-reduced NAu-1. Error bars are defined by 1 standard deviation. All parameter values can be found in Table SI 3.2.

Figure 3.2A shows the second-order rate constant (k) log values for the transformation of 3-chloronitrobenzene in the presence of NAu-1 reduced with dithionite to a high reduction extent (75%, green) and a low reduction extent (20%, blue). Includes log k values for both highly reactive and less reactive Fe(II) sites. The data indicates that NAu-1 reduced with dithionite to a high reduction extent has increased rate constant values compared to NAu-1 reduced with dithionite to low reduction extents. The measured increase is consistent across three cycles of reduction and oxidation. The kinetic model calculates intrinsic reactivity of the clay mineral, and takes account of the concentration of Fe(II) in the system (as measured by HF digestion). The greater k

values measured for 75% reduced NAu-1 suggest that the clay mineral is intrinsically more reactive at high reduction extents compared to low reduction extents. Previous work (Rothwell 2018) highlighted the relation between clay mineral Fe reduction extent and observed redox reactivity towards contaminants, and found that reactivity increases significantly with increasing reduction extent. The study also found that rate constants plateaued once the mineral had reached a specific reduction extent of around approximately 30-40% Fe(II)/Fe_{Tot}. The 20% Fe(II) NAu-1 data is typically below this threshold, whereas the 75% Fe(II) NAu-1 is above the threshold, so these results are consistent with previous work. In addition, the rate constant values for both reactive sites are highly comparable to those measured previously for the reaction of high reduction extent, Fe-rich clay minerals with 3-chloronitrobenzene (Neumann et al. 2008).

Both experiments (75% and 20% reduction extent) do not indicate any significant change (i.e. values within ranges of error) in rate constant values across 3 redox cycles, for either reactive site. This finding reflects the modelled fit data presented previously in Figure 3.1, and suggests that redox cycling with dithionite does not significantly impact the reactivity of the mineral.

There has been little previous research into the effects of dithionite reduction-oxidation cycling on the reactivity of nontronites. Gorski et al. (2012, 2013) investigated the effects of cycling on Ferruginous smectite SWa-1 (12.1 wt% Fe) and observed a significant, irreversible shift in redox profile leading to a more positive E_H after one reduction. A more positive E_H could have a detrimental impact on the reductive capacity of the mineral towards a contaminant. However, the effect was observed after the first reduction but did not accumulate with further cycling. If similar shift in redox profile has occurred in this case with NAu-1, any effects on reactivity would be in place before reaction with 3-chloronitrobenzene. In this respect the results from Gorski et al. may confer well as we do not see any changes past the first reduction.

The kinetic model can also be used to calculate the initial concentration of highly reactive sites. The calculated concentrations suggest that highly reactive sites comprise 0.85-1.5%, and 0.2-0.5% of the total structural Fe(II) in 20% and 75% reduced NAu-1

samples respectively. It has been previously demonstrated that although the highly reactive sites comprise of only a minute fraction of the total Fe(II), they are responsible for a significant volume of contaminant transformation (Neumann et al. 2008). The data presents no significant change over three reduction-oxidation cycles to the concentration of initial highly reactive sites for either high or low reduction extent. This further confirms that reactivity of the clay mineral is not significantly affected by reduction-oxidation cycling with dithionite. Most interestingly, the data suggests that there is no difference in the initial concentration of the highly reactive Fe sites between the high Fe reduction extent and low Fe reduction extent samples. This would imply that despite more than twice the relative percentage of Fe(II) in the structure, increased reduction extent did not lead to the formation of significantly more highly reactive sites. Previous research (Rothwell 2018) observed the relation between Fe(II) content and concentration of highly reactive sites (CA0), and found that CA0 increased with increasing reduction extent up to a maximum at around 48% Fe(II)/Fe_{Tot} before decreasing as reduction extent increased further. Rothwells data suggest that NAu-1 reduced to ~20% and ~75% reduction extent should have largely equivalent concentration of highly reactive sites, which would subsequently mean that the results align well with previous studies.

3.3.2 Effects of redox cycling on clay mineral morphology and size

Repeated reduction and oxidation of clay mineral structural Fe is thought to incur a wide range of effects on the morphology and structure of clay minerals (Stucki et al. 2011). Research so far has largely focused on the effects of microbial reduction-oxidation cycling. Studies have discussed how redox cycling with microbes can cause dissolution of fine particles, aggregation, dissolution pits, mineral transformation, and various other effects that significantly alter the shape or size of the clay mineral particles (Dong et al. 2003, Kim et al. 2004, Dong et al. 2005, Jaisi et al. 2007b, Yang et al. 2012, Shi et al. 2016). There has however been less work examining the morphological impacts of chemical cycling. To understand the extent to which reduction-oxidation cycling with dithionite impacts the morphology of the clay minerals, a series of structural analyses were conducted using particle size measurements, and scanning electron microscopy (SEM) combined with energy-dispersive X-ray spectroscopy.

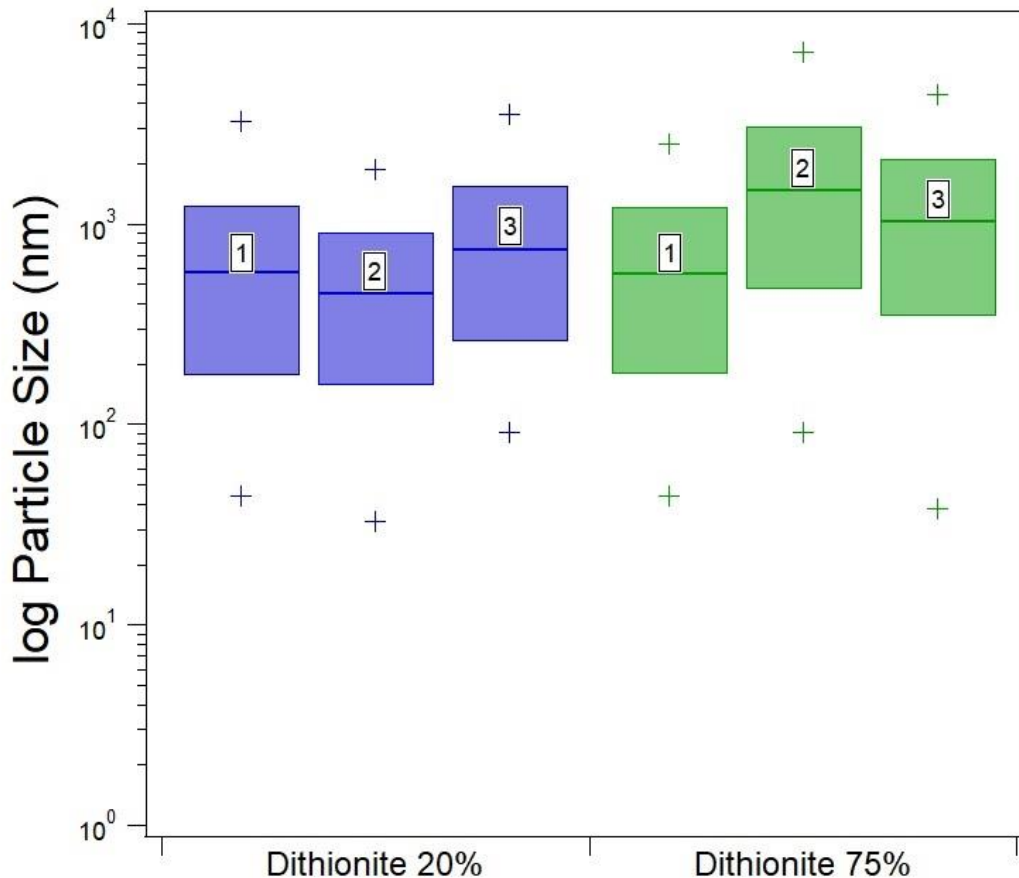


Figure 3.2: Particle size analysis of NAu-1 dithionite-reduced to a high (75 %, green) and low (20 %, blue) reduction extent, measured in a reduced state over 3 reduction-re-oxidation cycles. Limits of the range are marked by “+” and the bars define the mean value and 1 standard deviation above and below.

Figure 3.3 shows collated particle size measurements for dithionite-reduced NAu-1 at both high and low reduction extent, showing change in reduced clay mineral particle size over 3 cycles of reduction and oxidation. The mean particle size of NAu-1 with structural Fe reduced to 20% (blue) ranged from 0.424 μm – 0.705 μm , which is well within the size fraction isolated during the mineral preparation (Section 3.2.1). Samples retrieved after each reduction-oxidation cycle and exhibiting 75% Fe reduction extents varied more in mean particle size (0.458 μm – 1.177 μm), yet all particle size distributions had significant overlap in standard deviations. A preliminary inspection of the data shows that there is some variation between each cycle, with the greatest differences apparent in the high reduction extent samples. There does not appear to be any prevailing trend of direction over the three cycles. Interestingly, the high reduction extent and the low reduction extent samples do not follow the same pattern of size change.

A statistical single-factor ANOVA was conducted on both the 20%, and 75% dithionite-reduced N_{Au}-1 particle size distribution sets to determine whether variation between reduction cycles are statistically significant. The analysis for the values for N_{Au}-1 reduced to 20% reduction extent produced a *p*-value of 0.386, and the 75% dithionite-reduced samples returned a *p*-value of 0.183. The *P*-values for both experiments were greater than a significance level of 0.05. Similarly, 20% dithionite reduced distribution sets returned an *F*-value of 0.955, while 75% dithionite-reduced sets returned an *F*-value of 1.714. Both *F*-values were below the *F*-critical value of 3.039. The results from the ANOVA analysis confirm that for both experiments, variation in particle size across reduction cycles is not statistically significant.

This finding contradicts previous studies (e.g., Yang et al. 2012) which state that reduction-oxidation cycling causes the dissolution of smaller less-crystalline mineral particles, and the preservation and recrystallisation of larger more crystalline particles. However, the Yang et al (2012) study used bioreduction with living microbes present in the system which may have caused the observed dissolution. If dissolution was occurring in our experiments, one would expect a significant increase in particle size, which was absent. Similarly, clay mineral dissolution would be accompanied by the release of structural cations (Al, Mg, Fe, Si) into solution. As discussed, (Section 3.3.1, and Table SI 3.1) the concentrations of relevant atoms were measured in the supernatant during the reduction via ICP-OES, and the analysis did not measure any significant concentrations that would indicate any notable dissolution. Our combined results suggest that dithionite reduction of clay mineral Fe, irrespective of Fe reduction extent and repeated cycles of reduction and reoxidation, caused minimal mineral dissolution and align well with previous studies (Stucki et al 1984, Rothwell 2018, Entwistle 2021).

However, particle size analysis alone is insufficient to determine whether morphology of the clay mineral is impacted in other ways. Some papers have cited morphological effects due to redox cycling such as dissolution pits that are visible with SEM (Yang et al. 2012, Zhao et al. 2015), and the preferential dissolution of Fe from the structure (Russel et al. 1979). To examine the samples for any visible traces of dissolution, SEM analysis was conducted, and to measure whether Fe is preferentially dissolved by

reduction EDX was employed to measure the relative intensity of relevant structural atoms (Fe, Si, Al).

A collection of SEM images was taken of N Au-1 samples reduced to both high (75%) and low (20%) reduction extent with dithionite (Figure SI 3.4). Due to the sub-micron scale of the clay minerals, the SEM microscope was incapable of capturing images of individual clay mineral particles at sufficient resolution. In addition, it was difficult to determine exactly which visible features were representative of clay mineral. EDX scans were utilised in tandem with SEM images to highlight clay mineral structures based on their elemental emission (Figure SI 3.6). The pink features in Figure SI 3.6B and E demonstrate how some structures visible in the SEM image could be categorized as NaCl crystals formed during sample drying based on their colour in the EDX scan. When EDX scans were filtered (Figure SI 3.6 C and F) to show only Fe, Si, and Al (primary elemental constituents of N Au-1), it became apparent that clay minerals formed a largely homogenous film across the carbon tape of the SEM stub. The images taken show little distinguishable features that could be indicate distinct variation between samples due to cycling or Fe(II) content. The SEM analysis did not provide sufficient evidence to indicate that the clay mineral is affected morphologically by reduction-oxidation cycling. The issue of insufficient resolution to appropriately image clay mineral particles is inherent to SEM imagery. For this reason, previous claims (e.g. Yang et al. 2012) of visible evidence of dissolution pitting may be inaccurate. Microscopy techniques with greater resolution such as atomic force microscopy should be considered in future studies for adequate morphological imaging.

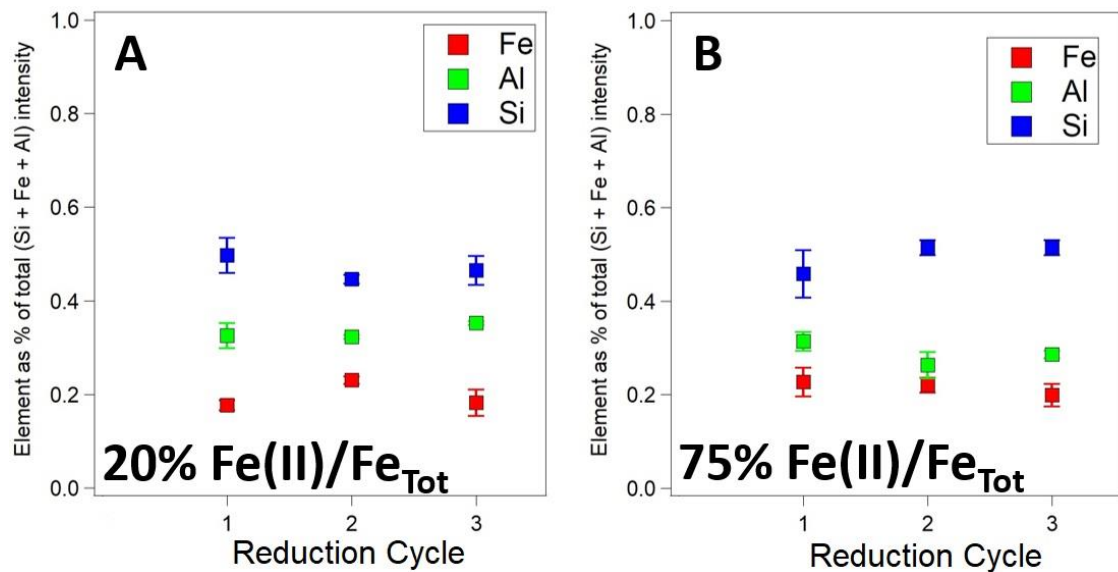


Figure 3.3: EDX elemental intensity data of key smectite structural elements (Fe, Si, Al) for dithionite-reduced NAu-1 samples, taken as average over multiple scans. Figure A shows the % elemental intensity for 20% dithionite-reduced NAu-1 over three reduction cycles, and Figure B shows the % elemental intensity of 75% dithionite-reduced NAu-1 over 3 reduction cycles. Red = Fe, Blue = Si, Green = Al. Error bars determined by 1 standard deviation.

Figure 3.4 presents the average elemental % intensity measured with EDX of Si, Fe, and Al for NAu-1 samples reduced with dithionite to a high (75%) and low (20%) reduction extent. The ratio of Fe : Si intensity remains at a ratio of approximately 1 : 2.5, a ratio that matches natural NAu-1 elemental composition perfectly. The intensity of Al is greater than would be expected (when considering the compositional percentage it encompasses in NAu-1) (Keeling et al. 2000), this may be an unintended effect produced by the aluminium SEM stubs used for the analysis. The values indicate that there is the same relative proportion of each of the three structural elements at both reduction extents (75% and 20%), and across all three reduction cycles. The ratio between the elements does not significantly change (within error). This data is further evidence that composition is not significantly affected by redox cycling with dithionite. Furthermore, the values would indicate that if any dissolution occurred, it was congruent. The results of this study however show no evidence for congruent dissolution either with ICP-OES (Table SI 3.1). The EDX data also further demonstrates that there was no preferential dissolution, or loss, of Fe from the mineral. These findings do not align with previous studies (e.g. Russell et al., 1979, Kostka et al. 1999, Jaisi et al. 2008b) which indicated incongruent Fe dissolution from clay minerals upon reduction. Russell et al. (1979) found that the degree of Fe loss increased with

increasing extent of tetrahedral Fe in the nontronite sample, and it was this tetrahedral species of structural Fe that was preferentially dissolved. Considering for this study that NAu-1 nontronite was chosen, tetrahedral Fe content should be minimal to none. This might offer an explanation as to why the samples show little evidence of preferential Fe dissolution.

The analysis with SEM and EDX does not suggest any significant alterations to the clay mineral, but these analyses are limited to structural effects at a microscopic scale. It is possible that Fe redox cycling is causing structural rearrangements within the clay mineral at an atomic scale. Previous research has discussed how reduction of structural Fe can cause octahedral rearrangement, resulting in the transition of Fe configuration from dioctahedral to trioctahedral (e.g. Manceau et al. 2000a and 2000b, Ribeiro et al. 2009). To further probe the structural impacts of dithionite reduction, a comprehensive Mössbauer analysis was conducted.

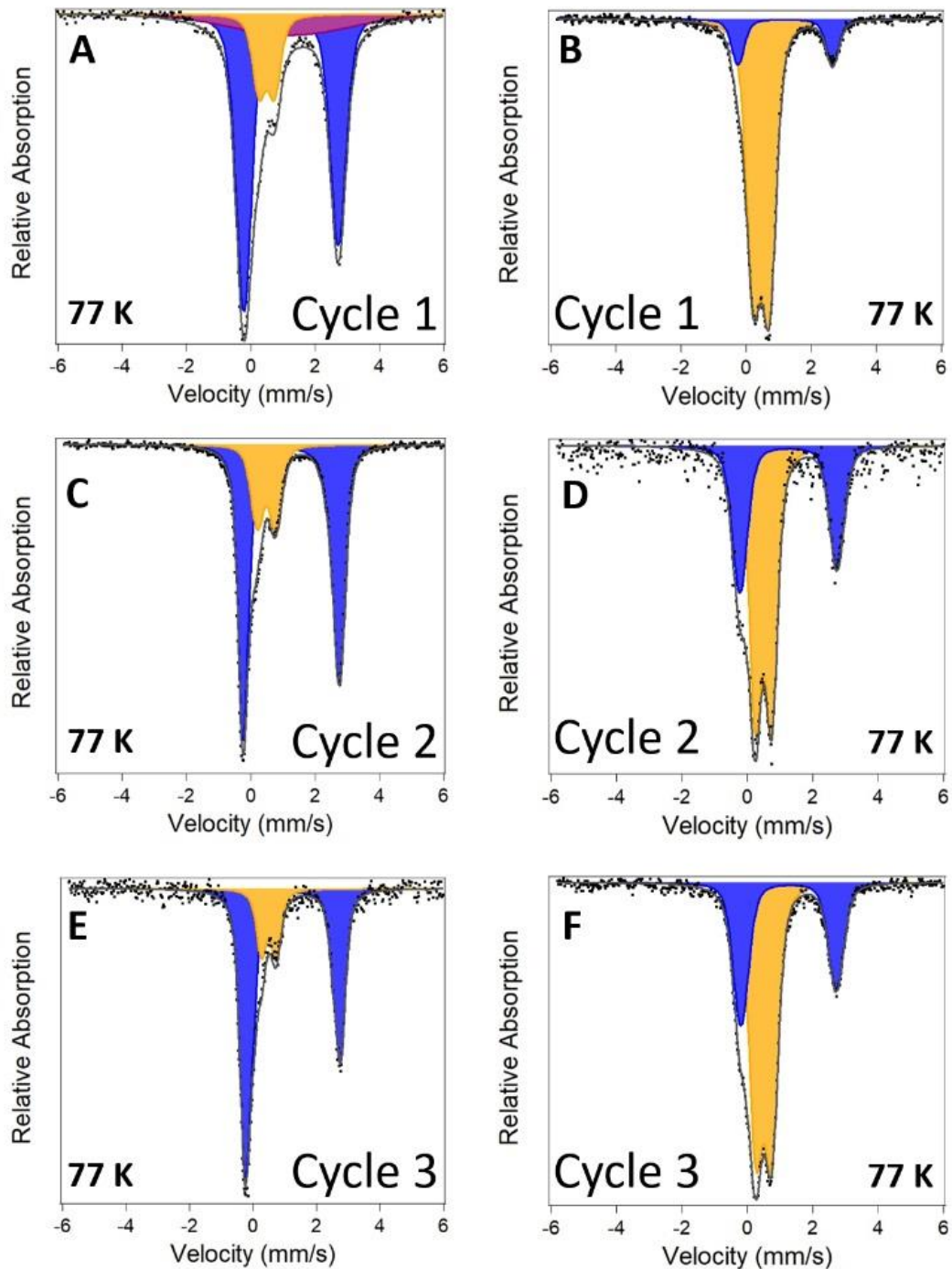
3.3.3 Effects of redox cycling on clay mineral structure and Fe speciation

For a more accurate understanding of the effects of redox cycling on the clay mineral Fe binding environment, a comprehensive Mössbauer analysis was conducted on dithionite-reduced NAu-1 samples. Figure 3.5 shows the Mössbauer spectra of samples measured at a temperature of 77 K. Within Figure 3.5, Subfigures A, C, and E, show the spectra of samples reduced to a high extent (75% Fe(II)/Fe(total)) for reduction cycles 1, 2, and 3 respectively. Subfigures B, D, F, show the spectra of samples reduced to a low extent (20% Fe(II)/Fe(total)), for cycles 1, 2, and 3 respectively. The spectra confirm successful electron transfer from the reducing agent (dithionite) to the clay mineral structural Fe as indicated by the presence of an Fe(II) doublet species (blue), which is absent in native NAu-1 (Figure 3.7A). Consistent with the presence of only Fe(III) in native NAu-1, the central doublet (orange) represents clay mineral Fe(III) in all spectra. Table 3.1 shows the measured hyperfine parameters and relative areas of each Fe species. The different spectra are largely similar across all three cycles.

One observation is the presence of the poorly resolved species (shown in purple) creating a wide base in Figure 3.5A. This feature is only present in this spectrum and has a high centre shift (CS) value of 1.204 mm/s. This value is within the range

expected for Fe(II) species (Murad and Cashion 2004), and aligns well with that of the Fe(II) doublet species (1.202 – 1.206 mm/s). This feature could thus be an indication for the presence of an additional Fe(II) or Fe(II)-containing species. Previous research also observed a poorly resolved feature at the base of the Mössbauer spectra of NAu-1 dithionite-reduced to > 30 % Fe(II)/Fe_{Tot} (Rothwell et al. 2018) which were interpreted as Fe(II) material in the onset of magnetic ordering. However, the feature was observed at a lower temperature (13 K), and many Fe speciations will begin to magnetically order at lower temperatures (Murad and Cashion 2004). The presence of this purple species in the first reduction cycle combined with its absence after subsequent reoxidation-reduction cycles could be the result of structural rearrangements in the clay mineral. When roughly one third of structural Fe was reduced, the nontronite octahedral sheet has been seen to begin transitioning from dioctahedral to trioctahedral (Manceau et al. 2000). More recent studies have further shown that Fe-bearing clay minerals reduced to a high extent underwent significant structural alterations during the first reduction process and remained largely unchanged in subsequent re-oxidation and reduction (Gorski et al. 2013).

High reduction extent Low reduction extent



Legend:

- Fe(III) doublet
- Fe(II) doublet
- Poorly-resolved feature
- Observed values
- Calculated fit

Figure 3.3.4: Mössbauer spectra measured at 77 K of dithionite-reduced NAu-1 over 3 cycles of reduction-oxidation. Left side shows NAu-1 reduced to a high reduction extent (75 %) and right side shows NAu-1 reduced to a lower reduction extent (20 %). Spectra were fitted with Voigt-based fitting technique

Based on our evidence, the poorly resolved feature is an Fe(II) species, and hence the reduction extents indicated by the Mössbauer spectra for the “75%” dithionite-reduced N_{Au}-1 samples are 83%, 79% and 81% Fe(II) for Cycle 1, 2, and 3 respectively. The reduction extents measured for the “20%” dithionite-reduced N_{Au}-1 samples were equal to 15%, 36%, and 35% Fe(II) for cycles 1, 2, and 3 respectively. These Fe(II)/Fe(total) values measured by Mössbauer align well with those measured after mineral digestion (see Table 3.2).

For the high reduction extent samples dithionite achieved largely consistent reduction extent after each cycle around the intended extent (75%). The low reduction extent samples were less consistent with each cycle, and displayed a marked increase in reduction extent after the first cycle. This is due to the unintended loss of mineral during the washing process between each reduction cycle. This was confirmed by the mineral loading data presented in Table 3.2, and the lack of evidence for reductive dissolution as shown by ICP-OES data in Table SI 3.1. As previously discussed in Section 3.3.1 (in tandem with the HF mineral digestion data presented in Table 3.2), the unintended loss of mineral caused a stoichiometric imbalance where more dithionite was added than necessary to achieve the desired reduction extent, leading to an over-reduction of the mineral. For the low reduction extent (20%) experiment, this led to a doubling of reduction extent on Cycle 2, coinciding with a loss of half the mineral loading concentration (Table 3.2). The high reduction extent experiment was conducted after, and while stoichiometry was controlled for during the reduction process, mineral loss during washes still occurred (most evidently in Cycle 3).

Although the reduction extent achieved differs from the intended concentrations (i.e. 20% and 75%), the reduction extents achieved in both experiments do not suggest that the reduceability or achievable reduction extent is impacted by cycling. Similarly, the hyperfine parameters (i.e. centre shift and quadrupole splitting) values remain unchanged for both the Fe(II) doublet and Fe(III) doublet species (Table 3.1) across both high and low reduction extent samples, and across 3 cycles of reduction and oxidation. This does not indicate any compounding structural effects caused by successive reductions. Previous papers have suggested chemical redox cycling can lead to irreversible changes, including a shift in redox profile of clay minerals (Gorski et al.

2012) which might impact the thermodynamics of electron transfer into and out of the structural Fe. The Gorski study found that the shift of redox profile occurred in the first redox cycle, and subsequent cycles were largely identical. This is similar to the trend observed in the Mössbauer data (Figure 3.5) where cycles 2 and 3 are almost indistinguishable but differ from Cycle 1. The Gorski study however focused on ferruginous smectite SWa-1 with 12.6 wt% Fe, which makes direct comparisons difficult due to differences in mineralogy. A later study (Gorski et al. 2013) found that there was less notable a shift of redox profile when NAu-1 was reduced. The presence of the poorly resolved base feature in the high reduction extent Cycle 1 spectrum (Figure 3.5A) might be evidence of irreversible structural changes occurring at high reduction extents, however this is yet to be confirmed.

In comparison, other research has observed a decrease in reduction extent of clay minerals after multiple redox cycles (e.g. Zhao et al., Yang et al 2012). Unlike this experiment, the papers employed live microbes as reductants and biological reduction has been well documented to enact different effects on the clay mineral structure than those observed with chemical reduction (e.g. Ribeiro et al. 2009).

Table 3.1: Hypofine parameters derived from spectra fitting of Mössbauer spectra of dithionite-reduced NAu-1 exhibiting high and low Fe reduction extents. Spectra were measured at 77 K. Centre shift (CS) relative to α -Fe(0). Voigt-based fitting was used to establish the Mössbauer parameters. (*) \pm % error based on uncertainty

			CS (mm/s)	QS (mm/s)	σ (mm/s)	A ⁻ /A ⁺	% Area (*)
High reduction extent (75 %) NAu-1	Cycle 1	Fe(II)	1.26	2.93	0.38	1.27	64.60 (0.846)
		Fe(III)	0.50	0.47	0.31	1	15.75 (0.781)
		Poorly resolved	1.20	0.01	3.92	1	19.64 (1.599)
			CS (mm/s)	QS (mm/s)	σ (mm/s)	A ⁻ /A ⁺	% Area (*)
	Cycle 2	Fe(II)	1.25	2.96	0.27	1.28	78.90 (0.344)
		Fe(III)	0.49	0.52	0.24	1	21.09 (0.284)
			CS (mm/s)	QS (mm/s)	σ (mm/s)	A ⁻ /A ⁺	% Area (*)
	Cycle 3	Fe(II)	1.25	2.93	0.28	1.68	82.99 (1.366)
		Fe(III)	0.51	0.46	0.18	1	17.00 (0.994)
Low reduction extent (20 %) NAu-1			CS (mm/s)	QS (mm/s)	σ (mm/s)	A ⁻ /A ⁺	% Area (*)
	Cycle 1	Fe(II)	1.20	2.90	0.28	1	15.05 (0.574)
		Fe(III)	0.46	0.49	0.32	1	84.94 (0.479)
			CS (mm/s)	QS (mm/s)	σ (mm/s)	A ⁻ /A ⁺	% Area (*)
	Cycle 2	Fe(II)	1.25	2.96	0.35	1.19	36.51 (1.106)
		Fe(III)	0.49	0.49	0.26	1	63.48 (0.970)
			CS (mm/s)	QS (mm/s)	σ (mm/s)	A ⁻ /A ⁺	% Area (*)
	Cycle 3	Fe(II)	1.25	2.91	0.36	1.33	35.63 (0.573)
		Fe(III)	0.48	0.48	0.30	1	64.36 (0.822)

Assessing the sustainability of Fe-bearing clay mineral redox reactions

Chapter 3: Chemically-induced redox cycling with dithionite

Table 3.2: Data taken from HF mineral digestion and phenanthroline assay (Section 3.2.6) showing measured reduction extent as Fe(II)/Fe_{Tot} and calculated mineral-loading of initial stock suspension. () ± standard deviation

	High reduction extent NAu-1		Low reduction extent NAu-1	
	Fe(II)/Fe _{Tot} (%)	Stock suspension mineral loading (g/L)	Fe(II)/Fe _{Tot} (%)	Stock suspension mineral loading (g/L)
Cycle 1	82.61 (3.549)	18.88 (0.770)	15.42 (0.400)	16.06 (0.799)
Cycle 2	79.22 (2.163)	16.23 (0.249)	37.95 (1.651)	9.34 (0.195)
Cycle 3	86.65 (0.393)	7.61 (0.050)	35.11 (1.651)	6.22 (0.197)

The hyperfine parameters of the Fe components are similar across the three reduction-re-oxidation cycles, with the exception of one parameter. The results show a visible, gradual increase in asymmetry of the Fe(II) doublet peaks across the three reduction-oxidation cycles from $A = 1.278$ to $A = 1.681$ for NAu-1 samples reduced to a high extent, and from $A = 1.000$ to $A = 1.337$ for NAu-1 samples reduced to a low reduction extent (20%). Without implementing an asymmetry ($A-/A+ \neq 1$) for the Fe(II) doublet, the spectra could not be reasonably fit (Figure SI 3.5A). There are several possible effects that can cause a doublet to display variations in line symmetry such as the Goldanskii-Karyagin effect, and effects caused by sampled orientation and texturing. The Goldanskii-Karyagin effect is caused by lattice vibrational anisotropy, where the vibrational amplitude of atoms is different in different directions (Murad and Cashion 2004). The effect is very rarely observed in ^{57}Fe spectra. However, while often mistaken for the rare Goldanskii-Karyagin effect (Murad and Cashion 2003), asymmetry in the Fe(II) doublet is most commonly due to the texturing effect often seen with fine needle or thin plate-shaped minerals. The thin plate shape of the clay minerals have might lead to a preferred orientation once settled out of suspension. This might be partially evidenced by the SEM results which indicated the minerals tend to settle out of suspension to form a film over the sample stub. Similarly, multiple washes of the suspension with 1 M NaCl solution will lead to continued delamination of the clay mineral particles, this combined with centrifugation could lead to a preferred orientation of minerals once solids are separated from solution (as described for sample preparation processes in Sections 3.2.1, and 3.2.2). Over time, the sample orientation might become increasingly less random. This causes an anisotropic effect on gamma absorption leading to asymmetry in line intensities. Pfannes and Gonser

(1972) demonstrated that small deviations from mineral particle orientation randomness can lead to exaggerated asymmetry in line intensities, whereas the occurrence of the Goldanskii-Karyagin effect would require largely unrealistic levels of lattice vibrational anisotropy. The extent of asymmetry in the dithionite reduced samples further suggests the effect is more likely due to texturing rather than the aforementioned Goldanskii-Karyagin effect. Texturing effects are best accounted for in sample preparation by assuring irregular and heterogeneous orientation of sample before analysis (Murad and Cashion 2004), sometimes with additives such as activated charcoal to prevent settling or by adjusting the angle of the gamma beam. However, the addition of supplementary additives to the suspension to improve the orientation poses a large risk of introducing species that might lead to unintentional oxidation or solutes that may coat the mineral and leave them unsatisfactory for analysis (Stucki et al. 1984). In this instance it was opted that no external additions to the system was preferable to any risk of sample oxidation.

The Mössbauer spectral data acquired at 77 K temperature provide important insight into the redox state of the clay mineral Fe, however a more comprehensive analysis of the structure requires Mössbauer spectra measurement at a lower temperature. Reducing the temperature to 4 K causes many Fe species to magnetically order (Murad and Cashion 2004) and allows us to examine the binding environment and speciation of Fe within the clay mineral structure. A further analysis was conducted at 4 K temperature to probe how Fe speciation is altered by multiple cycles of dithionite-reduction and oxidation with H_2O_2 . The analysis focused on N Au-1 samples dithionite-reduced to high reduction extents (i.e. 75%). This is because many previous papers have highlighted how the degree of irreversibility increases with reduction extent (Kostka et al. 1999, Fialips et al. 2002, Neumann et al. 2011, Gorski et al. 2012,2013), and reduction to high extents is therefore most likely to cause significant alterations that might impact the longevity and sustainability of Fe-rich clay minerals.

High reduction extent – 4 K spectra

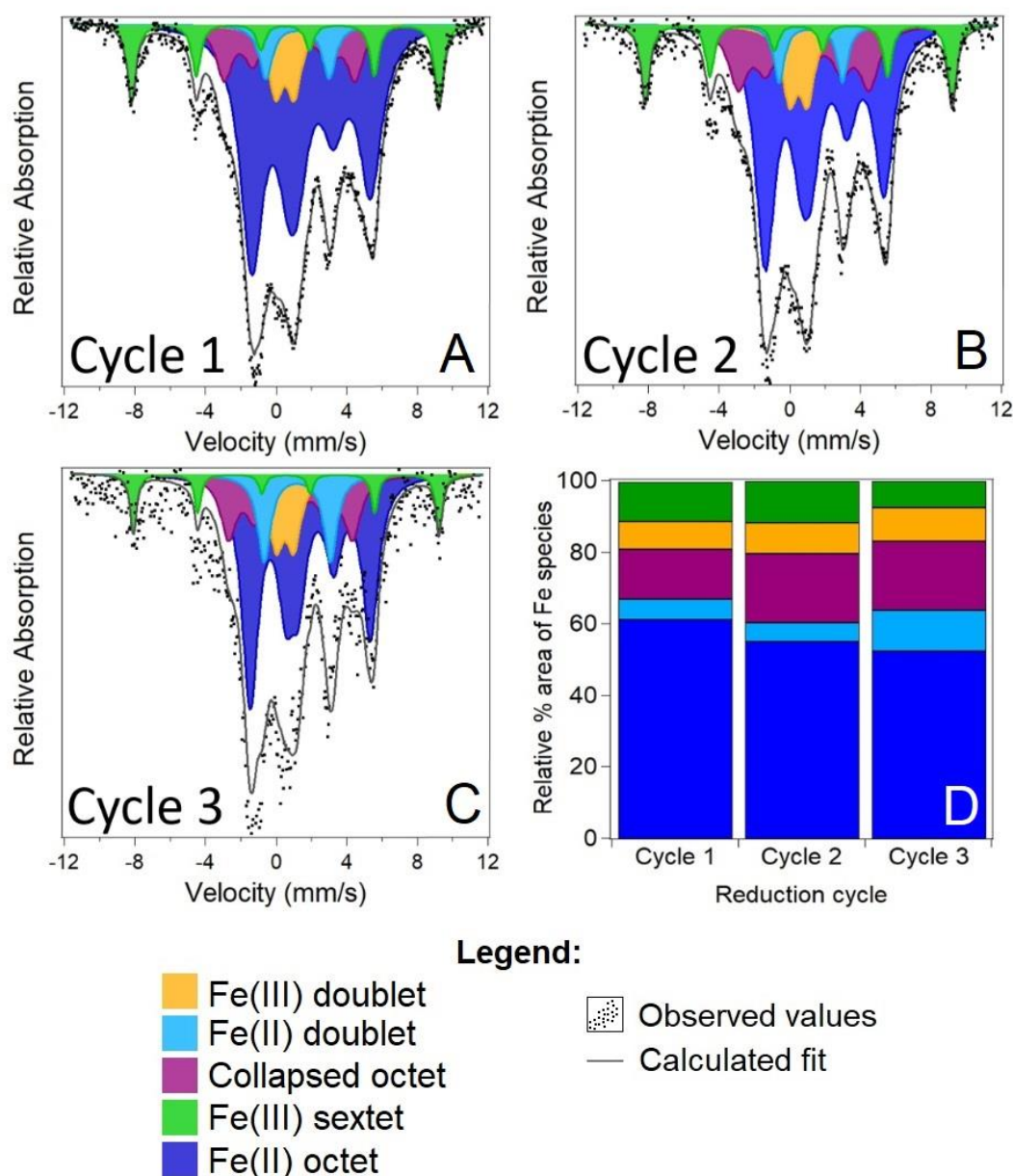


Figure 3.5: Mössbauer spectra of NAu-1 dithionite-reduced to a high extent (75%), and measured at 4 K temperature. Subfigures A, B and C show the spectra for reduction cycles 1, 2, and 3 respectively. Spectra were fit using a variable line width fitting technique (Full-static Hamiltonian). Figure D shows the change in relative area of each Fe speciation over the 3 reduction-oxidation cycles.

Figure 3.6A, B, and C shows the Mössbauer spectra of the NAu-1 dithionite-reduced to a high reduction extent over three cycles of reduction. Figure 3.6D shows the change in relative area of Fe species over the 3 cycles. Strikingly, all three spectra look very similar and thus all spectra can be fit with the same five Fe species: a large ordered octet (dark blue), a sextet species (green), a broad collapsed feature (purple), and 2 doublets (orange and light blue). The parameters defining each species are listed in

Table 3.3. The light blue doublet component has a high CS value (1.21-1.22 mm/s) and a wide quadrupole split (QS) value of 3.58-3.75 mm/s. This species characterised as Fe(II) as these parameters are higher than would be considered possible for Fe(III) (Murad and Cashion, 2003). The lack of magnetic ordering suggests the doublet represents Fe(II) atoms with limited interaction with neighbouring Fe, and therefore likely represents Fe such as sorbed / surface bound Fe(II) or Fe(II) bound to other octahedral cations such as Al and Mg. The dark blue octet species with a CS value of $\sim 1.418 - 1.466$ mm/s and QS values ranging from 2.990-3.151 mm/s and suggests the presence of magnetically ordered Fe(II). This component holds the largest fraction of reduced structural Fe and this species has been observed before in previous research (Rothwell 2018, Entwistle 2021) with equivalent parameters. The ability for this species to magnetically order suggests it is material with high Fe-Fe interactions, this is possible with clay minerals with very high Fe content such as nontronites due to multiple neighbouring octahedral Fe atoms. The orange doublet has a CS of 0.5 mm/s and a QS of 1 mm/s, values which indicate this is non-ordered Fe(III) (Murad and Cashion 2004). The green species also has a CS of 0.5, and formation of a sextet also indicates this is Fe(III) but with increased Fe-Fe interactions. The purple phase is a collapsed octet with a relatively high CS (~ 0.8 mm/s), but lower than that of the other Fe(II) components. This species is potentially a mixed valence, magnetically incompletely ordered Fe component. Examining the relative area of each species in comparison with the HF digestion data (Table 3.2) suggests that the combined total area of both the blue doublet and blue octet (total area is $\sim 67\%$) is less than the measured reduction extent ($\sim 82\%$). The difference between these two values indicates that this species should be largely Fe(II). When combining both the confirmed Fe(II) species and the collapsed purple species, the total area is equivalent to the expected reduction extent ($\sim 82\%$). Therefore, this species is potentially a mixed valence (due to the relatively low CS value), magnetically incompletely ordered Fe component.

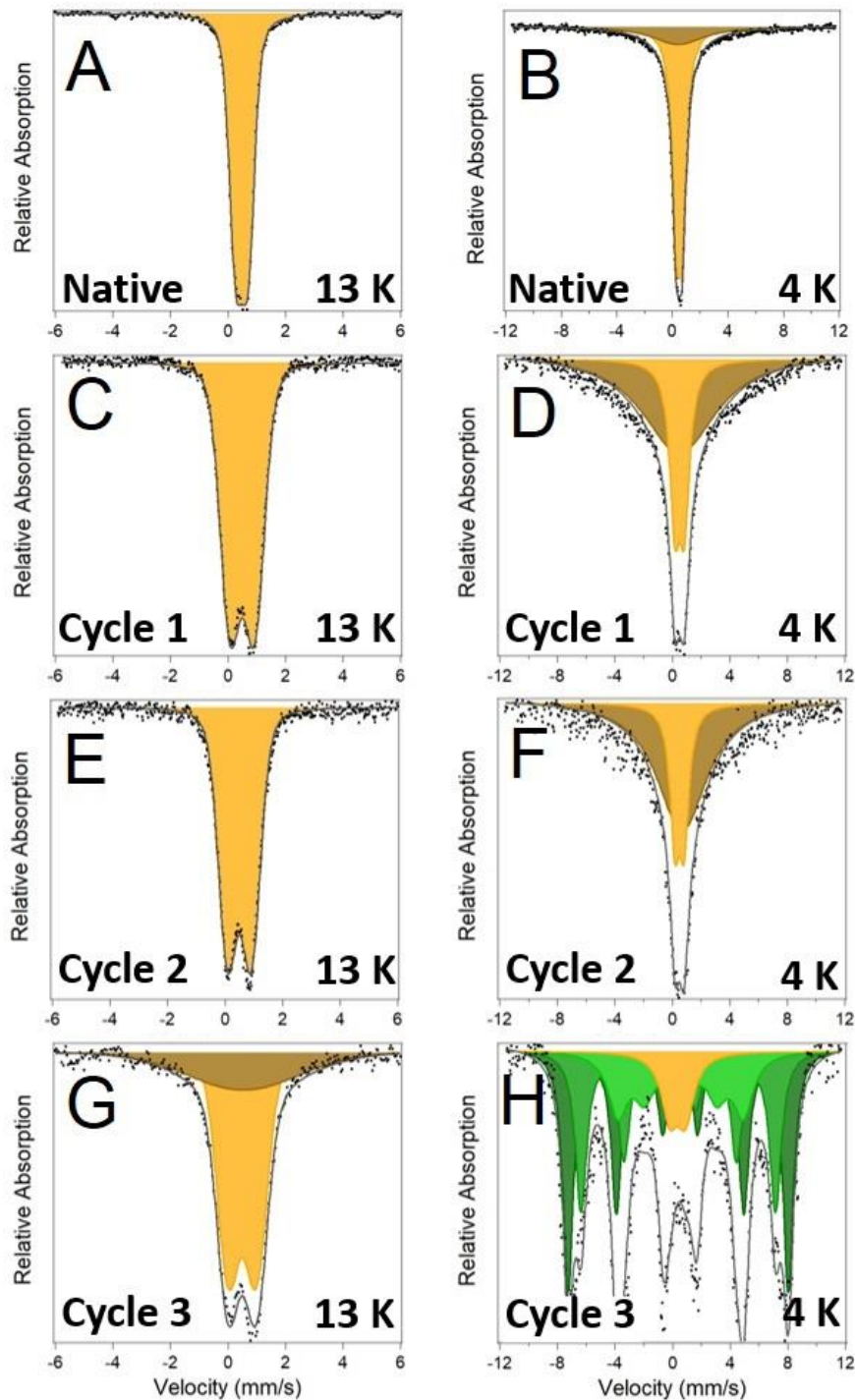
Table 3.3: Mössbauer hyperfine parameters for NAu-1 reduced to high reduction extent by dithionite, measured at 4 K temperature using a variable line width fitting method (Full Static Hamiltonian). Fe species are colour-coded to match the species present in the spectra of Figure 3.6

		CS (mm/s)	H (T)	$e^2qQ/2$ (mm/s)	η (-)	w (mm/s)	θ (-)	Area (%)
Cycle 1	Fe(II) octet	1.466	17.034	-2.955	0	0.768	90	61.278
	Fe(III) sextet	0.519	54.016	0	0	0.299	0	11.130
	Fe(II) doublet	1.212	0	3.579	0	0.455	0	5.797
	Fe(III) doublet	0.520	0	1.052	0	0.511	0	7.655
	Collapsed feature	0.802	22.992	-0.061	0	0.561	0	13.898
Cycle 2	Fe(II) octet	1.464	16.943	-2.990	0	0.650	90	55.210
	Fe(III) sextet	0.514	53.881	0	0	0.297	0	11.581
	Fe(II) doublet	1.220	0	3.584	0	0.368	0	5.214
	Fe(III) doublet	0.509	0	1.044	0	0.554	0	8.691
	Collapsed feature	0.811	23.011	0	0	0.663	0	19.304
Cycle 3	Fe(II) octet	1.418	16.720	-3.151	0	0.541	90	52.545
	Fe(III) sextet	0.570	53.570	0	0	0.222	0	7.377
	Fe(II) doublet	1.216	0	3.755	0	0.454	0	11.302
	Fe(III) doublet	0.510	0	1.033	0	0.527	0	9.522
	Collapsed feature	0.820	21.783	0	0	0.565	0	19.254

The Hyperfine parameters (Table 3.3) show little change with clay mineral Fe redox cycling. The Mössbauer fittings for NAu-1 dithionite-reduced to a high extent all show species with similar parameters, and in somewhat consistently similar proportions. The most notable impact of successive reduction cycles appears to be a visible decrease (shown in Figure 3.6D) in the relative area the magnetically ordered Fe species (dark blue octet, and green sextet), coinciding with an increase in the more poorly ordered Fe(II) species (purple and light blue species). This could suggest redox cycling is causing structural alteration that leads towards more Fe binding environments with less and/or weaker Fe-Fe interactions. Previous studies have shown how different Fe(II) speciations in relation to clay minerals can have vastly differing intrinsic reactivities (Hofstetter et al. 2003). Hofstetter found that some poorly-ordered species such as surface-bound or sorbed Fe(II) had significantly greater reactivity than some structural Fe species. Whilst this study did not observe a significant effect on clay mineral reaction kinetics over three reduction-oxidation cycles (Section 3.3.1), if the observed structural effects are leaving irreversible alterations this could affect the sustainability of redox cycling clay minerals over greater time scales.

To examine whether the successive reduction and oxidation of NAu-1 leads to significant alterations to the clay mineral Fe structure, a comparison was conducted of the spectrum of unaltered, native NAu-1 with those of reoxidised samples after each cycle or reduction and re-oxidation (Figure 3.7). It has been shown that the extent of irreversibility of alterations caused by structural Fe reduction increases with reduction

extent, and that at low reduction extents effects on the structure are largely reversible (Russel et al. 1979, Neumann et al. 2011, Gorski et al. 2012 and 2013, Zhao et al. 2015). For this reason, this experiment focused on the high reduction extent (>75%) samples as these could offer improved insight into the sustainability of redox cycling clay minerals at greater scales.



Legend:

- Fe(III) doublet
- Poorly-resolved feature
- Fe(III) sextets
- Observed values
- Calculated fit

Figure 3.6: Figure shows spectrum for native sample (Subfigures A and B), and Mössbauer spectra of NAu-1 dithionite-reduced to high reduction extent (>75%) and subsequently reoxidised with H₂O₂ after 3 cycles of reduction and oxidation. Subfigures C, E, and G show the spectra of the reoxidised samples for cycles 1, 2, and 3 (respectively) when measured at 13 K, fitted using Voigt-based fitting technique. Subfigures D, F, and H show the spectra of reoxidised samples for cycles 1, 2, and 3 (respectively) when measured at 4 K temperature, fitted using variable line width fitting technique (Full-static Hamiltonian).

Figure 3.7 shows the Mössbauer spectra measured at 4 K and 13 K temperature for both the unaltered native sample, as well as the spectra for NAu-1 dithionite-reduced to a high reduction extent and subsequently reoxidised with H₂O₂ over 3 redox cycles. All hyperfine fitting parameters can be found in Table SI 3.3. The Mössbauer spectra of the native mineral at both temperatures (Subfigures A and B) is dominated by an Fe(III) doublet. The central doublet (orange) of the native sample spectra at 13 K has a CS of 0.48 mm/s and a QS of 0.44 mm/s, the doublet at 4 K has a CS of 0.50 mm/s and a QS of 0.45 mm/s. These are values typically expected for native nontronites (Murad and Cashion 2004). A visual comparison of the native spectra with the reoxidised sample spectra after the following reduction cycling would suggest that cycling caused changes to the binding environment of Fe in NAu-1. For the 13 K data (Figure 3.7 left column), after the first reduction and oxidation (Figure 3.7 C) the spectrum presents a larger QS value of 0.85 mm/s. Increased quadrupole split values upon reoxidation have been observed previously (e.g. Ribeiro et al. 2009, Zhao et al. 2015). Ribeiro et al. (2009) described this as a distortion of the electric field environment caused by the reduction, perhaps due to the structural rearrangement from *cis*- to *trans*-octahedral Fe sites. The distortion of the electric environment suggests that the structural Fe is in a more distorted environment after reoxidation (Stucki 2011), this is strong evidence to suggest that the first reduction causes an irreversible alteration to the structure. Irreversible changes upon the initial reduction cycle are not unexpected at such high reduction extents. Gorski et al. (2012, 2013) similarly observed increased quadrupole splitting after reoxidation when compared with the native sample, this structural rearrangement occurred in tandem with a shift in the minerals redox profile.

The Gorski et al. (2012,2013) study found no significant changes on the second cycle which was interpreted to indicate that the irreversible changes occurred after only the initial cycle. Similarly, our results indicate little difference between the reoxidised spectra of the 1st and 2nd redox cycle (Figure 3.7 C and E). The Gorski et al. (2012, 2013) studies however did not investigate beyond 2 cycles of reduction-oxidation. In the 3rd cycle of this experiment, there is a clear visible difference in the spectrum measured at 13 K compared to the spectra of cycles 1 and 2. Unlike the spectra for

cycles 1 and 2 at 13 K, Cycle 3 shows the appearance of a broad, but poorly resolved feature at the base. This could indicate that there has been a change in speciation after 3 cycles. While a poorly resolved species can be difficult to interpret, measuring the sample at a lower temperature can provide a greater insight into the speciation of structural Fe.

The right column of Figure 3.7 shows the spectra of both native and reoxidised NAu-1 samples over 3 cycles of reduction and oxidation when measured at 4 K temperature. Analysis of the sample spectra measured at 4 K provides more detailed insights into the structural transitions taking place, and the speciations of structural Fe. The spectra of reoxidised NAu-1 after both 1 and 2 redox cycles (Figure 3.7 D and F) look similar at 4 K to the spectrum of the native, but with some key differences. As with the native, the reoxidised samples present a prominent Fe(III) doublet (orange) with a centre shift of ~ 0.5 mm/s, but once again show an increased QS value at 0.7 mm/s. However, the reoxidised sample spectra for cycles 1 and 2 (Figure 3.7 D and F) spectra display an exaggerated base, which requires the inclusion of a poorly resolved species. The spectral area of this base feature remains similar from Cycle 1 to Cycle 2 (Table SI 3.3). The sample after a third cycle of reduction-oxidation however produced an entirely different spectrum, with almost all Fe(III) showing magnetic ordering. The spectrum for NAu-1 after 3 cycles includes 3 magnetically ordered sextet species, the largest with a CS of 0.48 mm/s, a hyperfine field width of 47.44 T. The smallest sextet has a CS of 0.57 mm/s and a hyperfine field width of 27.0 mm/s. The spectra of reoxidised NAu-1 after 3 redox cycles indicates that reduction-oxidation cycling indeed caused significant irreversible alterations, as repeated cycling led to a Mössbauer spectrum significantly dissimilar to the original native.

For comparison, Figure SI 3.5B shows a Mössbauer spectrum measured at 4 K of NAu-1 after 3 reduction-oxidation cycles when the sample is dithionite-reduced to a low reduction extent (20%). The spectrum appears essentially unchanged from the native spectrum, with a single Fe(III) doublet. This finding aligns well with previous data that found the reversibility of structural Fe reduction impacts is decreased with increasing reduction extent (e.g. Fialips et al. 2002, Neumann et al. 2011), however this also demonstrates that the effect is consistent across multiple redox cycles.

The Mössbauer data shows without doubt that repeated clay mineral Fe reduction to a high extent, followed immediately by complete and rapid reoxidation caused rearrangement of the structural Fe. In the reduced samples a gradual shift from magnetically ordered material towards more poorly ordered Fe can be observed. This may represent a shift of Fe atoms within the octahedral sheet from a well-ordered lattice to more labile configuration. The spectra of NAu-1 samples after reoxidation showed a trend towards increased magnetic ordering. This observation implies that during the reduction structural Fe is re-ordered within the octahedral sheet, and upon reoxidation the Fe then transitions towards binding environments with high Fe-Fe interactions that allow for magnetic ordering. Studies have discussed structural rearrangement caused by clay mineral Fe reduction, and effects such as dehydroxylation and the transition from dioctahedral to trioctahedral configuration have been well documented (Manceau et al. 2000, Stucki et al. 2011, Neumann et al. 2011). Structural alterations of the clay mineral occur to compensate for the excess negative charge caused by the change in Fe oxidation state (Tratnyek et al. 2011). It is possible that further structural movement could be possible. Ribeiro et al. (2009) investigated dithionite reduction and reoxidation of Garfield nontronite. After complete (i.e. 100%) reduction with dithionite and reoxidation, the spectrum of the reoxidised samples showed significant magnetic ordering in the form of large sextet species (which were not present at lower reduction extents). The sextet species had a mean hyperfine field of 44 T, similar to the results seen here in cycles 3 (Figure 3.7H). The Ribeiro study later confirmed that the magnetically ordered Fe material was internal to the clay mineral, and was not a secondary Fe-oxide mineral, indicating a major irreversible structural rearrangement. It is possible that while the reduction was leaving measurable impacts on the Fe speciation (such as increased QS, and the broad base feature), the quantity of structural Fe impacted by reduction did not breach a negative charge threshold that was structurally unstable. The spectrum of Cycle 3 (Figure 3.7H) could be evidence that a sufficient quantity of octahedral Fe was affected by reduction to require a major structural shift beyond reversibility to maintain structural integrity. It is possible that the rearrangement of Fe speciation seen in Cycle 3 may be connected to the shift in redox profile after complete (100%) structural Fe reduction described by Gorski et al. (2012,2013). This is because this research finds no

evidence that the intrinsic reactivity of the structural Fe is affected by multiple cycles before the change occurs that could indicate a change in redox properties.

Simultaneously, all previous cycles (i.e. Cycle 1 and 2) reoxidation reverts the Mössbauer spectrum to a state reminiscent of the native without magnetic ordering, and a prominent central doublet.

3.3.4 Connecting structural changes and observable clay mineral Fe redox reactivity towards contaminants (Environmental Impact/Conclusions)

The data collected from both the kinetic experiments and structural mineral analysis indicate that redox cycling of NAu-1 with dithionite can be conducted sustainably. Multiple cycles of dithionite-reduction and oxidation with H₂O₂ were shown to have little impact on the reactivity of the clay minerals, even when reduced to a very high reduction extent. At a low reduction extent, results show no discernible impact on intrinsic reactivity, particle size, morphology, or Fe speciation that was not reversible upon reoxidation. At a high reduction extent however, some irreversible changes occur to the speciation of structural Fe, but the changes did not relate to a change in reaction kinetics during the experiment. The most notable impact (i.e. the transition of the Mössbauer spectrum after Cycle 3 reoxidation – Figure 3.7H) only occurred after 3 complete cycles of reduction and oxidation, and therefore its impact on mineral reactivity was not measured. Future work should investigate whether this major speciation transition does indeed impact the reaction kinetics.

The results of this study have important implications for natural systems as they demonstrate that chemically altering the oxidation state of clay minerals could provide a renewable and sustainable source of reduction equivalents towards environmental contaminants. Although there were some irreversible mineral alterations, these were only present at exceptionally high reduction extents. While there are multiple pathways that can reduce clay mineral structural Fe (e.g. Rozenson and Heller-Kallai 1976a and 1976b, Stucki et al. 1984a, Stucki and Kostka 2006, Schaeffer et al. 2011), to the best of the author's knowledge there are no naturally occurring reductants that can successfully achieve nontronite reduction extents equivalent to those of dithionite. This would imply that the reduction extents required to cause irreversible or unsustainable alterations are difficult to reproduce in natural systems. The data from the experiments involving clay minerals reduced to low reduction extent could be

considered more environmentally relevant, and the results in that experiment demonstrate that chemical reduction cycling is sustainable. Although dithionite would not be expected to occur naturally in high concentrations, previous studies have proposed that it could be injected *in-situ* to promote abiotic mineral reduction and improve land remediation (Amonette et al. 1998, Istok et al. 1999 Fruchter et al. 2000). Even in these circumstances where dithionite is employed to artificially achieve *unnaturally* high reduction extents of minerals, this research has also shown that the minerals would be renewable for consistent contaminant transformation over at least three reduction-oxidation cycles.

3.4 Supporting information

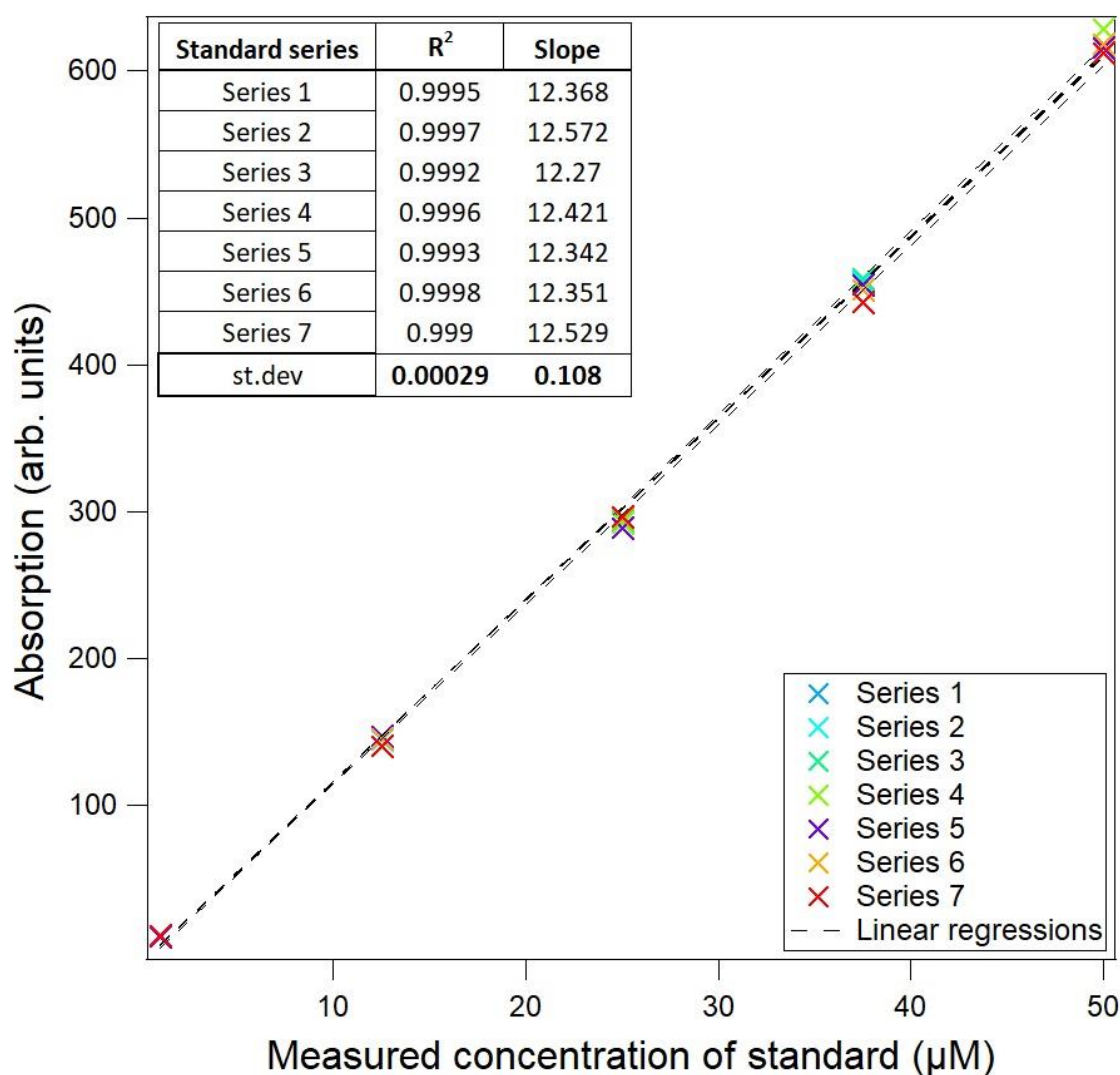


Figure SI 3.1: Graph plotting the absorption values of 7 sets of reference standards at 5 concentrations (1, 12.5, 25, 37.5, 50 µM) as measured using the described HPLC method (see Section 3.2.4). Dotted lines show the linear regressions of each standard series. Table shows the R² value for each series of standards, the slope of each regression, and the standard deviations of both. Figure demonstrates a high level of precision and accuracy for the HPLC method.

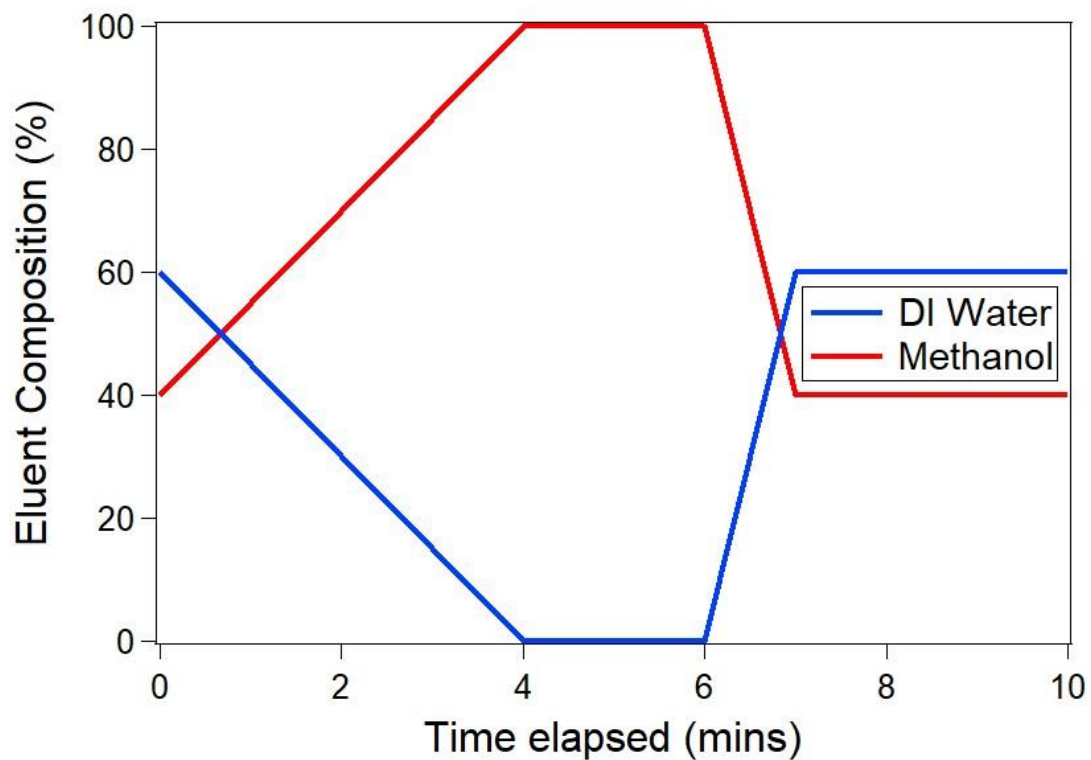


Figure SI 3.2: Diagram shows the composition of the eluent used in the HPLC method for each sample as described in Section 3.2.4. Total run time 10 minutes per sample. Red line represents % Methanol, and Blue line represents % deionised water.

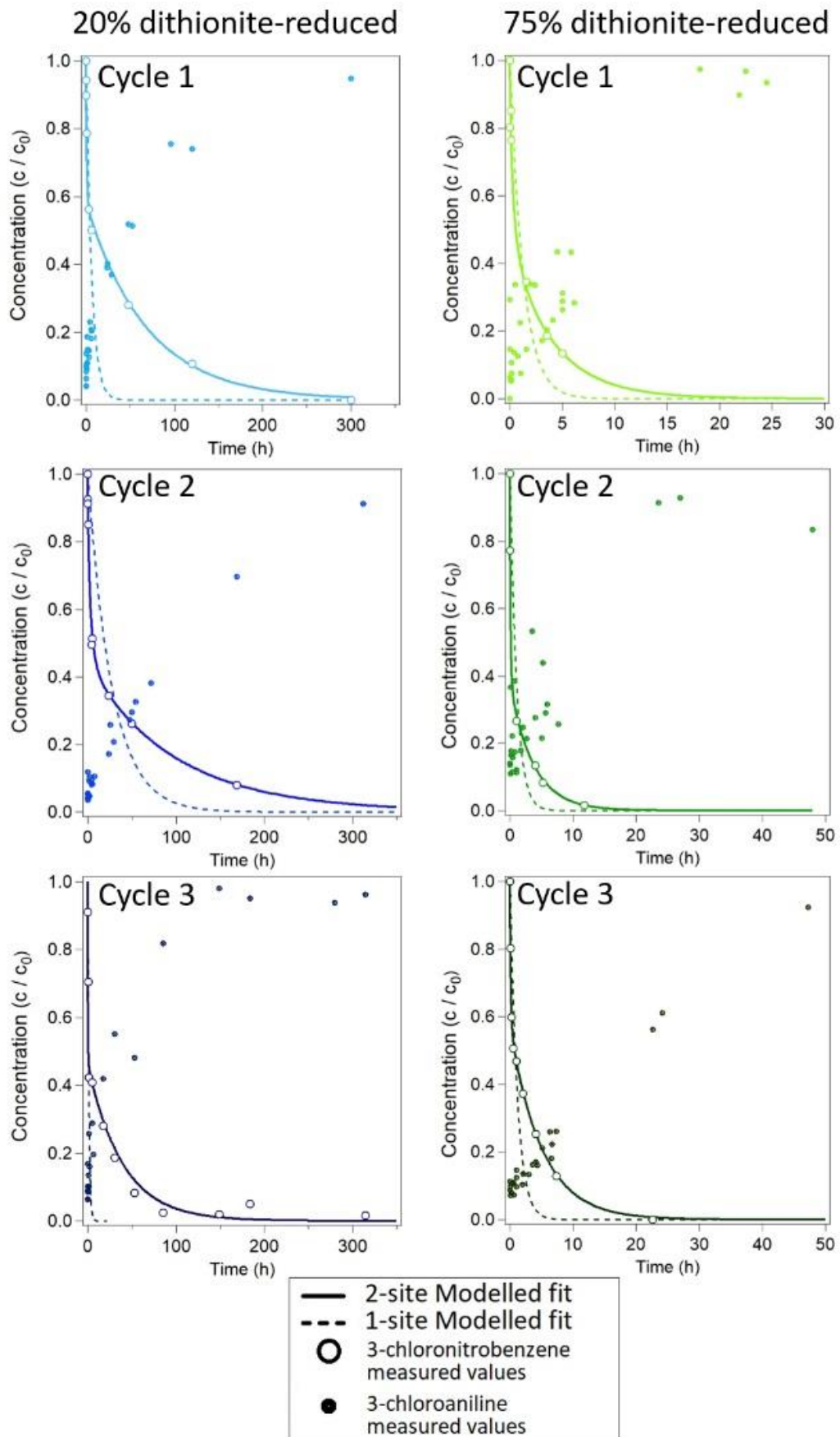


Figure SI 3.3: Complete kinetic data across 3 reduction cycles for both NAu-1 dithionite reduced to 20% and 75% Fe(II). Figures include measured concentration values for 3-chloronitrobenzene and corresponding aniline product, and both 1-site and 2-site modelled fittings.

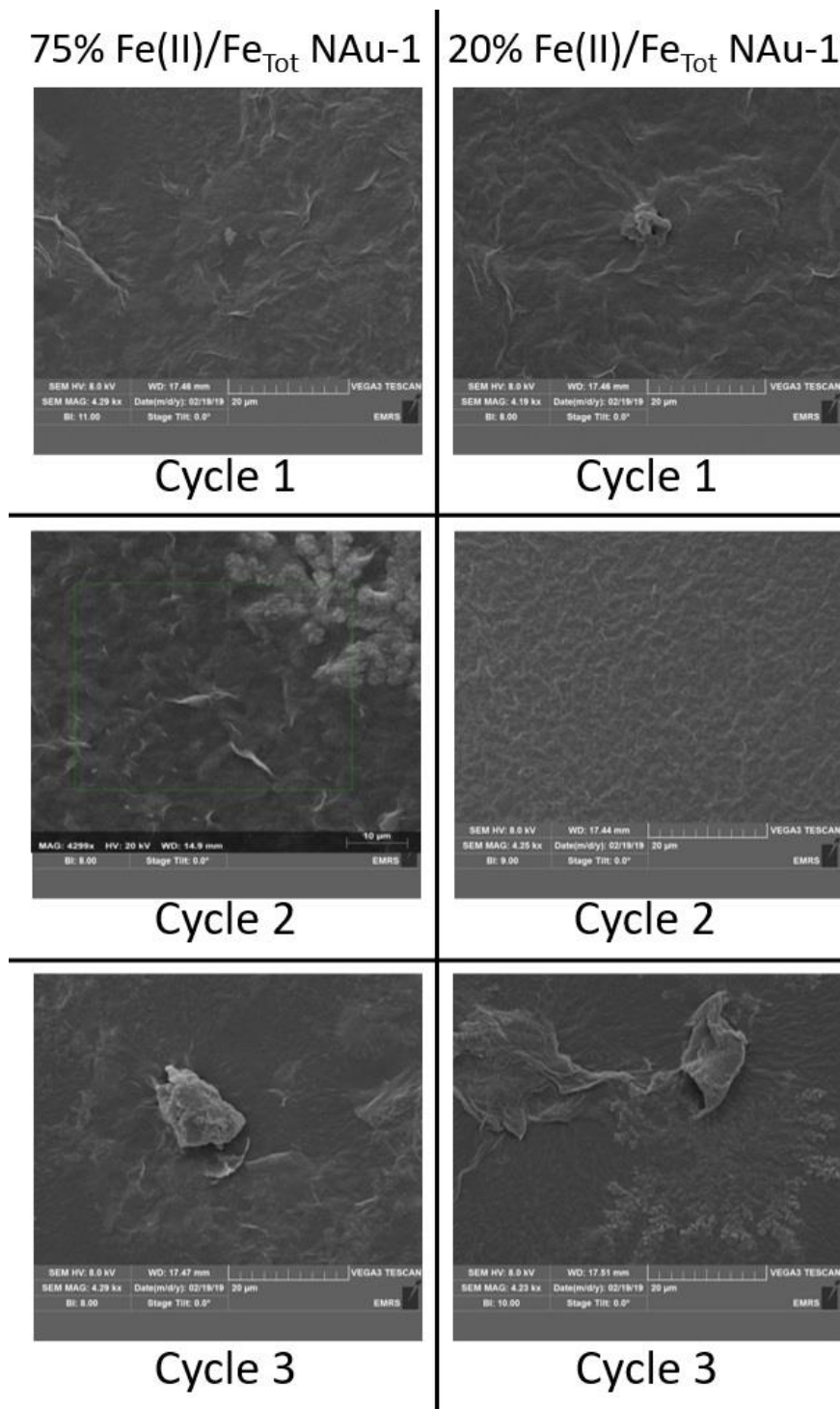


Figure SI 3.4: Collection of SEM images captured of dithionite-reduced NAu-1 samples across 3 cycles of reduction-oxidation. Left column shows 75% dithionite-reduced NAu-1 images, and right column shows 20% dithionite-reduced NAu-1 images.

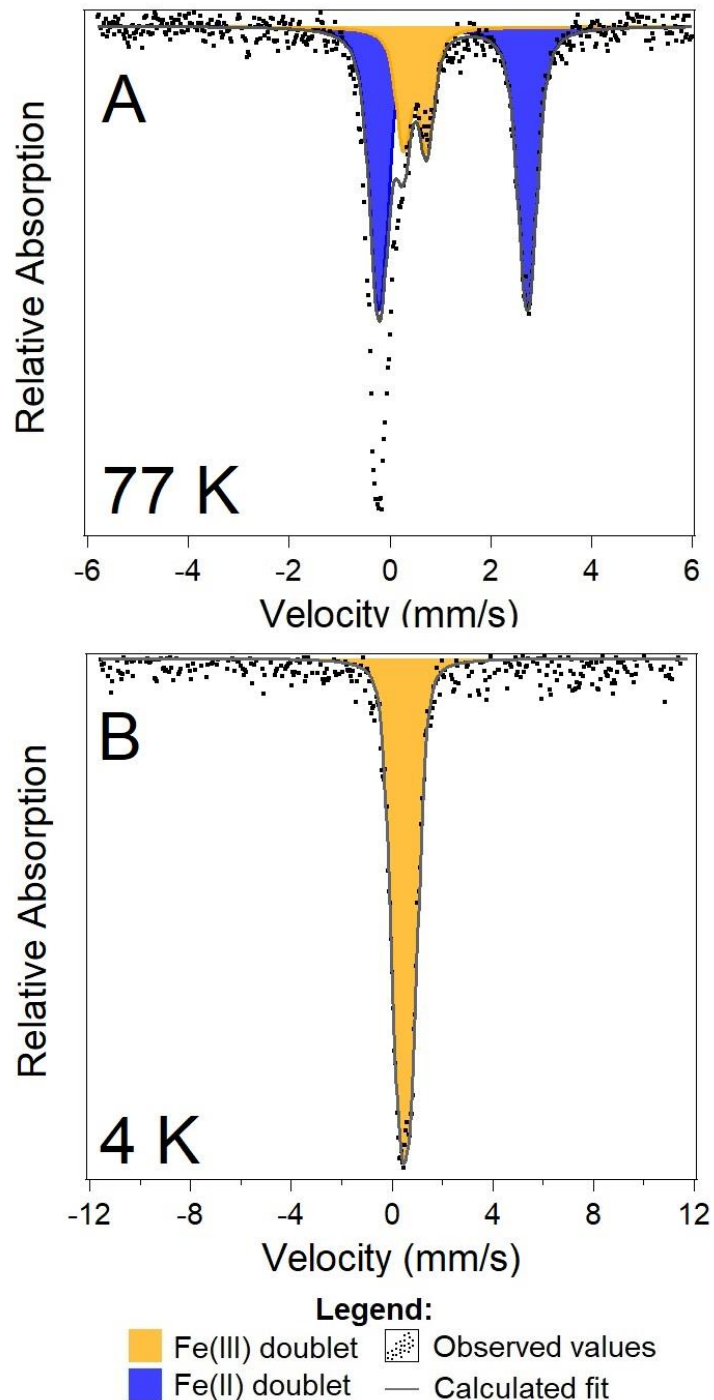


Figure SI 3.5: Figure A shows Mössbauer spectrum measured at 77 K temperature of dithionite-reduced N Au-1 in the third reduction cycle (i.e. re-re-reduced) to a high reduction extent (>75%). Spectrum was fitted without any change to the asymmetry parameter ($A+/A- = 1$). Demonstrates how the spectrum cannot be appropriately fit without altering the asymmetry of the Fe(II) doublet. Figure B shows the spectrum of N Au-1 reduced with dithionite to a low reduction extent (20%) for 3 successive redox cycles and oxidised with H_2O_2 , measured at 4 K temperature. Both spectra A and B were fitted with Voigt-based fitting technique.

Assessing the sustainability of Fe-bearing clay mineral redox reactions
Chapter 3: Chemically-induced redox cycling with dithionite

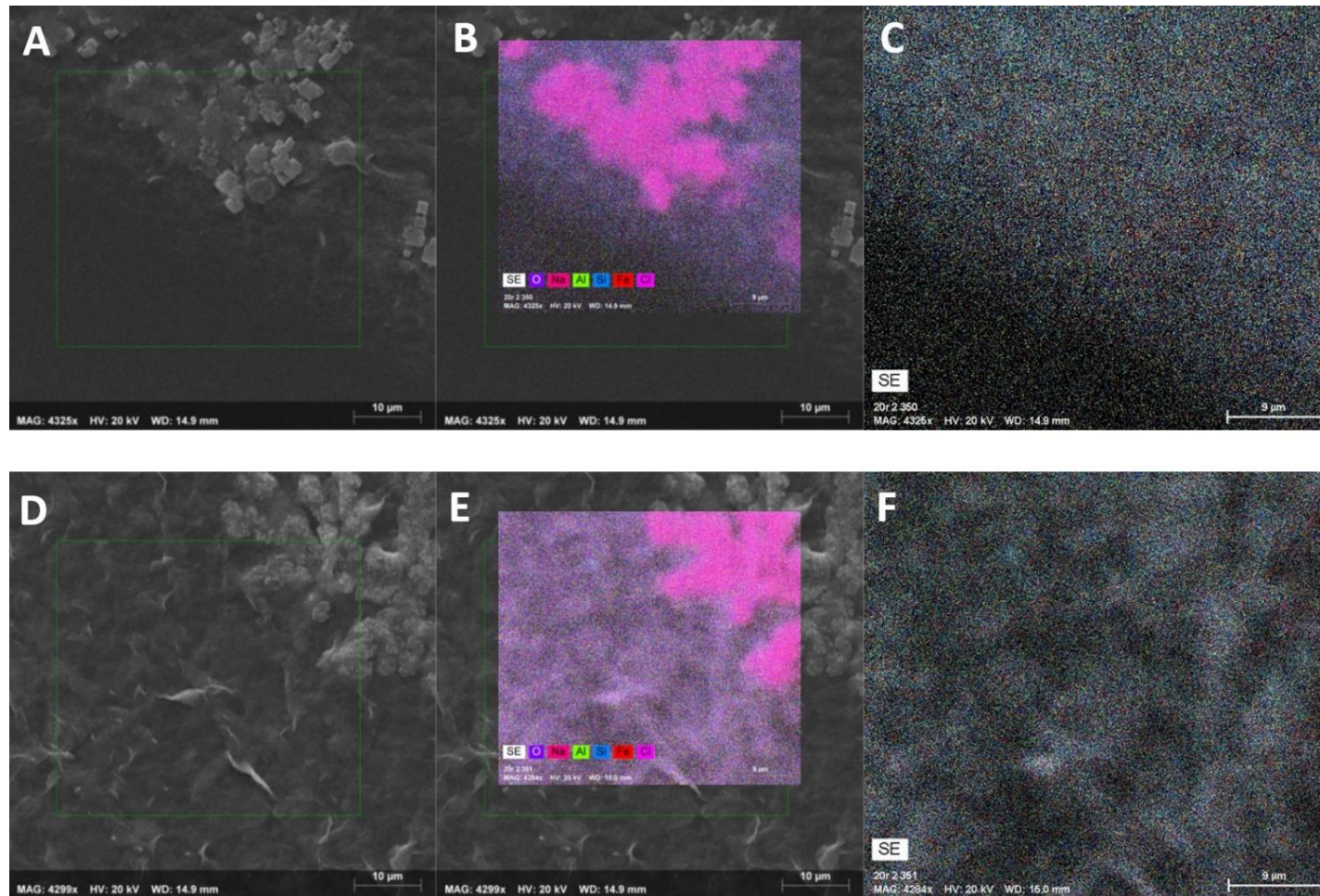


Figure SI 3.6: Comparison of SEM images with EDX scan images. Image A shows an SEM image of 75% dithionite-reduced NAu-1, Image B shows the same image partially overlain by EDX scan with full suit of relevant elements (O, Al, Si, Fe, Cl), Image C shows the EDX scan when filtered to show only nontronite structural elements (Fe = red, Al = green, Si = blue). Image D shows an SEM image of 20% dithionite-reduced NAu-1, Image E shows the same image partially overlain by EDX scan with full suit of relevant elements (O, Al, Si, Fe, Cl), Image F shows the EDX scan when filtered to show only nontronite structural elements (Fe = red, Al = green, Si = blue). Note that for images B and E, pink colours represent Na and Cl.

Assessing the sustainability of Fe-bearing clay mineral redox reactions

Chapter 3: Chemically-induced redox cycling with dithionite

Table SI 3.1: ICP-OES measurements for Fe, Al, Si, and Mg, for supernatant samples taken from NAu-1 suspensions after reaction with dithionite to achieve 20% and 75% Fe(II)/Fe_{Tot} over 3 cycles of reduction-oxidation. Data shows measured concentration of each respective element, and how much as a percentage that concentration relates to the content of NAu-1 present in the suspension.

		Fe		Al		Mg		Si	
		Conc. (g/L)	% of clay mineral						
High reduction extent (75%) NAu-1	Cycle 1	0.00327	0.0773	0.00116	0.0753	0.000576	0.0728	0.00898	0.0921
	Cycle 2	0.00432	0.119	0.00222	0.167	0.00162	0.238	0.00516	0.0617
	Cycle 3	0.00170	0.0993	0.000808	0.130	0.000304	0.0952	0.00355	0.0903
Low reduction extent (20%) NAu-1	Cycle 1	0.00114	0.0333	0.00100	0.0805	0.00025801	0.0403	0.00135	0.0172
	Cycle 2	0.00324	0.155	0.00108	0.142	0.000318781	0.0815	0.00276	0.0573
	Cycle 3	0.000693	0.0497	0.000316	0.0624	0.000264553	0.102	0.000988	0.0308

Table SI 3.2: All kinetic parameters for 20% and 75% dithionite-reduced N Au-1 over 3 cycles of reduction and oxidation, parameters are displayed in Figure 3.2. Data includes the log k rate constant values for both highly reactive sites (log k A) and less reactive sites (log k B), as well as initial log concentration of highly reactive sites (CA0). Standard deviation for each parameter (δ) is included.

		log k A	δ	log k B	δ	log CA0	δ
20% dithionite-reduced NAu-1	Cycle 1	3.748	0.193	0.244	0.137	-4.121	0.0621
	Cycle 2	3.318	0.137	0.587	0.274	-3.937	0.0956
	Cycle 3	3.798	0.185	0.338	0.160	-4.017	0.0722
75% dithionite-reduced NAu-1	Cycle 1	4.458	0.249	0.863	0.222	-4.115	0.146
	Cycle 2	4.925	0.258	0.985	0.241	-3.977	0.0888
	Cycle 3	4.756	0.170	1.255	0.072	-4.108	0.0702

Table SI 3.3: Mössbauer hyperfine parameters for both native, unaltered NAu-1, as well as NAu-1 reduced to high reduction extent by dithionite and subsequently reoxidised by H₂O₂ over 3 reduction-oxidation cycles. Top table shows fitting parameters for NAu-1 samples measured at 13 K temperature, fitted using Voigt-based fitting technique. Bottom table shows fitting parameters for NAu-1 samples measured at 4 K temperature using a variable line width fitting method (Full Static Hamiltonian). Fe species are colour-coded to match the species present in the spectra of Figure 3.7

	T (K)	Species	CS (mm/s)	QS (mm/s)	σ (mm/s)	Area (%)
Native	13	Fe(III)	0.48	0.44	0.34	100
(cycle 1)	13	Fe(III)	0.499	0.851	0.609	100
(cycle 2)	13	Fe(III)	0.498	0.824	0.559	100
(cycle 3)	13	Fe(III)	0.497	0.971	0.667	73.031
		Fe(III)	0.499	0.181	3.771	26.969

	T (K)	Species	CS (mm/s)	H (T)	$e^2qQ/2$ (mm/s)	w (mm/s)	θ (-)	Area (%)
Native	4	Fe(III)	0.502	0	0.425	0.352	0	74.777
		Fe(III)	0.448	0	0	2.282	0	25.223
	T (K)	Species	CS (mm/s)	H (T)	$e^2qQ/2$ (mm/s)	w (mm/s)	θ (-)	Area (%)
Cycle 1	4	Fe(III)	0.510	0	0.661	0.431	0	28.279
		Fe(III)	0.497	0	0	3.152	0	71.721
	T (K)	Species	CS (mm/s)	H (T)	$e^2qQ/2$ (mm/s)	w (mm/s)	θ (-)	Area (%)
Cycle 2	4	Fe(III)	0.508	0	0.639	0.418	0	26.186
		Fe(III)	0.681	0	0	2.144	0	73.8608
	T (K)	Species	CS (mm/s)	H (T)	$e^2qQ/2$ (mm/s)	w (mm/s)	θ (-)	Area (%)
Cycle 3	4	Fe(III)	0.509	0	1.103	0.701	0	8.567
		Fe(III)	0.571	27.083	0	0.830	0	19.770
		Fe(III)	0.483	41.912	-0.140	0.489	0	30.429
		Fe(III)	0.478	47.446	-0.140	0.437	0	41.234

Chapter 4: Effects of Fe redox cycling by electron shuttles on the reactivity and structure of clay minerals

4.1 Introduction

In the previous chapter (Chapter 3), the impact of chemical reduction-oxidation cycling on the structure and reactivity of Fe-rich smectites was assessed. The results demonstrated that redox cycling was sustainable over at least three reduction cycles. We compared results at a high reduction extent, as well as the effects at a low reduction extent. The low reduction extent data was conducted to be comparatively relevant to the effects of other reduction pathways, such as microbial reduction.

In natural sediments, the primary natural influence on fluctuating redox states is the activity of microbes (Stucki et al. 1987). Microbes have been shown capable of reducing structural Fe in clay minerals (e.g., Kostka et al. 1996, Dong et al. 2003). Unlike dithionite reduction, microbial reduction cannot achieve 100% extent Fe(II) in Fe-rich clay minerals (Lee et al. 2006). Although microbes reduce a much smaller extent of structural Fe reduction than dithionite, studies have observed a wide range of irreversible impacts supposedly caused by microbial reduction. The structural effects of microbial reduction can range from dissolution (e.g., Dong et al. 2003, Yang et al. 2012, Shi et al. 2021), to complete mineral transformation / illitization of smectitic minerals (e.g. Kim et al. 2004, Zhang et al. 2007). Research into the impact of microbial redox cycling on the reactivity of clay minerals has also produced mixed results. Some studies have suggested that microbial redox cycling can increase initial rates of reaction (e.g., Yang et al. 2012), while other papers have cited no significant change to reactivity (e.g. Zhao et al. 2015).

The use of microbes as reductants for Fe-bearing clay minerals introduces additional levels of complexity to experiments. Firstly, living microbes require additives and solutes such as trace metals and nutrients to encourage metabolism (e.g. Kostka et al. 1996) which may complicate system chemistry. Additionally, microbial metabolism results in the production of a multitude of poorly-categorised organic byproducts such as extracellular polymeric substances and electron shuttling compounds (Gao et al. 2019). The impact of these substances on the clay mineral is unclear. In natural

systems, extracellular organic compounds such as humic acids and microbial exudates are used by bacteria as a means of increasing accessibility of Fe for respiration (Lovely et al. 1996, Melton et al. 2014). Electron transfer via shuttling compounds accounts for a high percentage of microbial reduction, and electron shuttles such as anthraquinone-2,6-disulfonate (AQDS) are often added in laboratory conditions to improve mineral reduction (e.g. Dong et al. 2003, Jaisi et al. 2005). Using reduced electron shuttles as reductant, it might be possible to simulate microbial reduction without the presence of living microbes. This will allow the measurement of redox cycling effects, without the ambiguity inherent with microbial metabolic processes.

In this experiment we subject Fe-rich clay mineral NAu-1 to multiple cycles of reduction and oxidation, using a reduced electron-shuttle as the reductant. Electron-shuttling compound anthraquinone-2,6-disulfonate (AQDS) is electrochemically reduced, and then reacted with NAu-1 smectite for three successive cycles of reduction, and oxidation by hydrogen peroxide. We measure the effects of redox cycling on the reactivity of the minerals towards transformation of 3-chloronitrobenzene, as well as monitor structural alterations using particle size analysis and Mössbauer spectroscopy. The chapter will investigate whether redox cycling with reduced electron shuttles produces effects more similar to pure microbial reduction, or more similar to chemical reduction by dithionite. Ultimately, the aim is to determine whether electron shuttles alone can act as appropriate abiotic surrogates for microbial reduction, in the absence of Fe-reducing bacteria.

4.2 Methods

4.2.1 Mineral preparation

Nontronite NAu-1 ($M^{+}_{1.05}[\text{Si}_{6.98}\text{Al}_{1.02}][\text{Al}_{0.29}\text{Fe}_{3.68}\text{Mg}_{0.04}]\text{O}_{20}\text{OH}_4$, 21.5 wt% Fe) was purchased from the Clay Mineral Repository. The samples were suspended in deionised water, size fractionated via centrifuge to a range of 0.2 μm – 0.5 μm and then Na^+ -homo-ionised with 1 M NaCl solution. The mineral sample was then purified to remove any additional unwanted minerals including kaolinite and Fe-oxides. Mineral purity was confirmed using Fourier-Transform Infrared spectroscopy (FT-IR). The final product was freeze dried, ground with a pestle and mortar and then passed through a 150 μm sieve before being stored prior to use.

4.2.2 Electrochemical reduction of anthraquinone-2,6-disulfonate

Anthraquinone-2,6-disulfonate (AQDS) was used as a representative electron shuttling compound (Curtis and Reinhard 1994, Lovley et al. 1996) and electrochemically reduced to Anthrahydroquinone-2,6-disulfonate (AH₂DS) to act as reducing agent. AQDS was sourced from Santa Cruz Biotech as a dry powder. The reduction of AQDS to AH₂DS was achieved within the anaerobic glovebox (GS Glovebox Systemtechnik GS040113)) using an electrochemical cell with the following set-up described in Figure 4.1. A photograph of the experimental setup is also available in the SI (Figure SI 4.1).

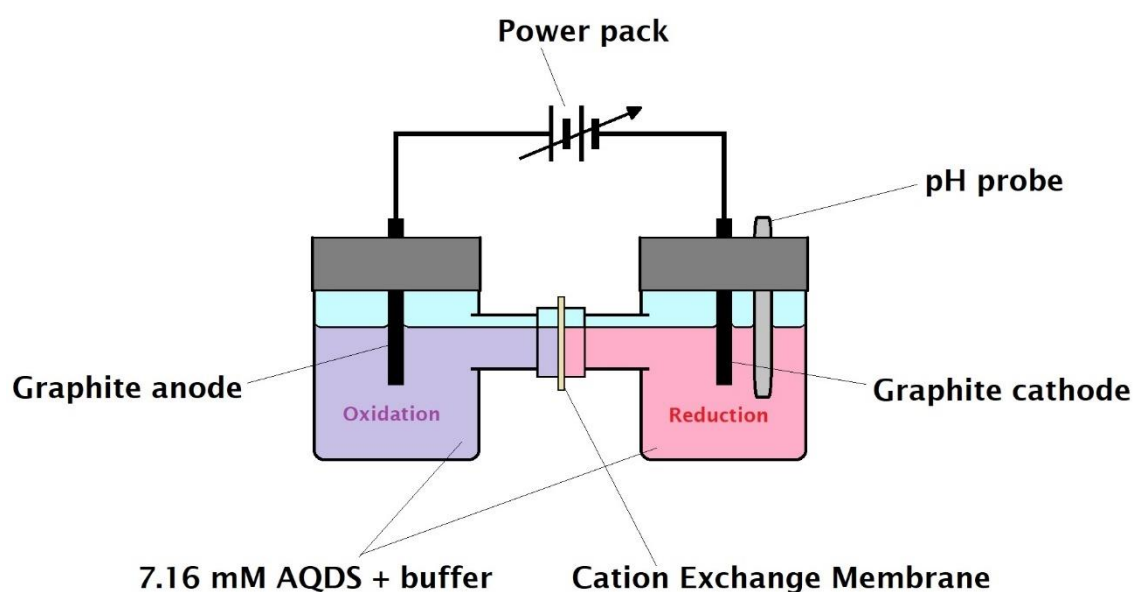


Figure 4.1: Diagram describing the experimental setup of electrochemical cell used to reduce AQDS to AH₂DS

An electrochemical cell was created using a burex H-cell consisting of two identical half-cells clamped together, connected by a central tube. Each side was filled with 200 mL of 7.16 mM AQDS (calculated to be stoichiometrically capable of reducing 200% of NAu-1 structural Fe), dissolved in buffer solution (10 mM MOPS, 50 mM NaCl in deoxygenated deionized water). The two half-cells were separated along the connected tube by a fabric-reinforced, Nafion cation exchange membrane, this was to prevent unintended oxidation of AH₂DS by the anode during electrolysis. Each side of the cell was connected to a partially submerged graphite electrode, both of which were connected to a powerpack supplying 15 V to the system to drive the electrochemical reduction. pH was monitored using a pH meter with glass electrode from Thermofisher Ltd submerged in the half cell containing the cathode. Aliquots of 1 M HCl and NaOH were added to the cathode half-cell when necessary to maintain a

constant pH of 7.0 ± 0.05 . 14 μL samples were taken at regular intervals, diluted with DIW, and analysed with ultraviolet-visible spectrophotometry (UV-VIS) to monitor the transformation from AQDS to AH_2DS and establish the time required to reach complete reduction. UV-VIS samples were analysed in a sealed screw-cap (to prevent any unintended oxidation), 10 mm x 10 mm (internal width) quartz cuvette sourced from Hellma UK Ltd.

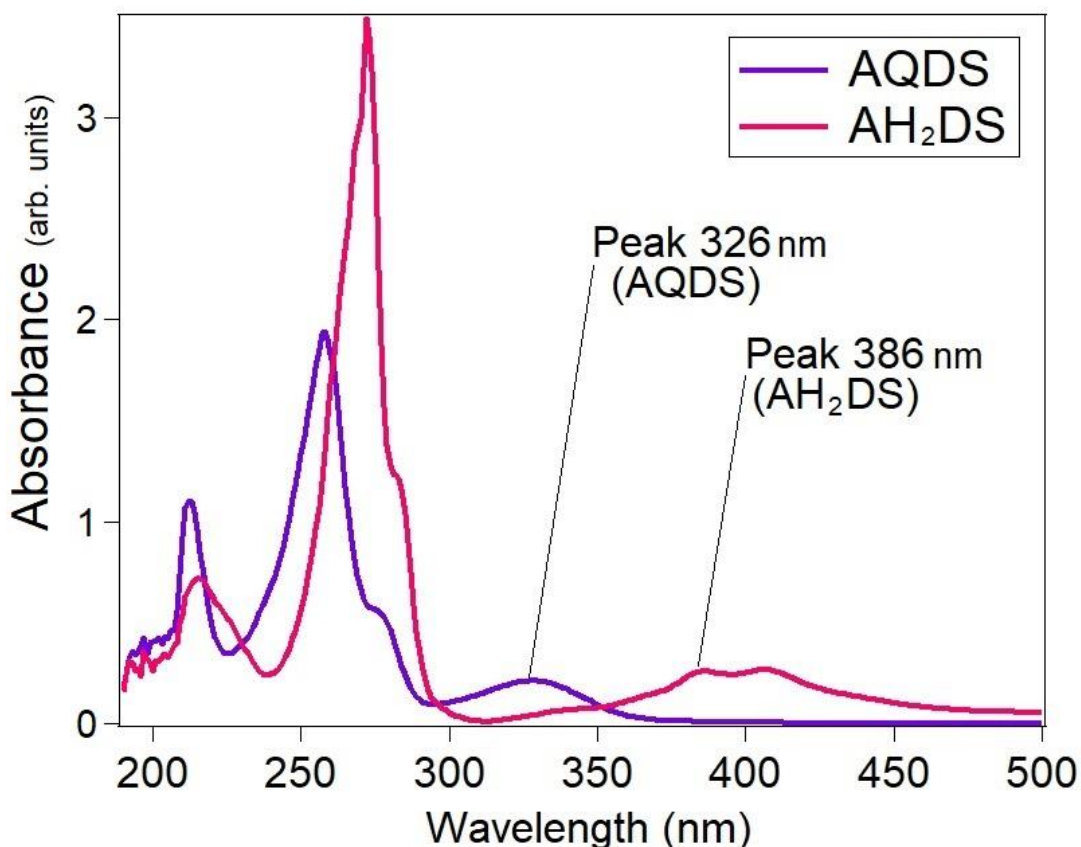


Figure 4.2: The absorption spectra for AQDS and AH_2DS measured with UV-VIS spectrophotometer. Purple represents AQDS and pink represents the reduced form AH_2DS

The changes in concentration of AQDS and AH_2DS were calculated by measuring absorbance at wavelengths of 326 and 386 nm, using the following equations (Equation 4.1, and 4.2) derived version of Beer's law as described in Jaisi et al. (2007a).

Equation 4.1; Concentration of AQDS (M):

$$= \frac{(MA_{326}^{AH_2DS} \times A_{386} \times t) - (MA_{386}^{AH_2DS} \times A_{326} \times t)}{t^2 \times [(MA_{326}^{AH_2DS} \times MA_{386}^{AQDS}) - (MA_{386}^{AH_2DS} \times MA_{326}^{AQDS})]}$$

Equation 4.2; Concentration of AH₂DS (M):

$$= \frac{A_{326} - (MA_{326}^{AQDS} \times AQDS \times t)}{MA_{326}^{AH_2DS} \times t}$$

Where MA is the molar absorptivity (molar extinction coefficient), A_x is the measured absorbance at the corresponding wavelength and t is the path length used in the spectrometer. The value for MA of AH₂DS is 650 and 6700 at wavelengths 326 and 386 respectively. The value for MA of AQDS is 5200 and 270 at 326 and 386 nm, respectively (Jaisi et al. 2007a). The transformation was gradual and reached completion (100% reduction of AQDS) after 10 hours (see Figure SI 4.2 showing the transformation of the spectrum). Figure 4.3 (and Figure SI 4.2) demonstrates that AQDS was successfully reduced from AQDS to AH₂DS, as it aligns well with UV spectra observed in previous studies (Shi et al. 2012).

4.2.3 Reduction-oxidation cycling of NAu-1

Once the reduction of AQDS was complete, and the UV-VIS spectra showed a complete transformation from AQDS to AH₂DS (see Figure SI 4.2) the reduced solution was added to powdered NAu-1 and left overnight to stir. The following morning the solution was centrifuged to separate solids from solution, and a sample of the supernatant was taken to measure the change in concentration of both AH₂DS and AQDS. By measuring the concentration of AQDS/AH₂DS using the method described in Section 4.2.2, it is possible to calculate the concentration of electrons transferred from reductant to the clay mineral. The supernatant was added once again to the electrochemical cell, and the solution was recycled and re-reduced. The reduced NAu-1 was washed with deoxygenated 1 M NaCl solution, and then DIW to assure that all AQDS solution was removed from the mineral. Finally, reduced NAu-1 was resuspended in 10 mM MOPS, 50 mM NaCl buffer solution at a concentration of 20 g/L, and pH was adjusted to 7.5 ± 0.02 using 1 M NaOH. Reactors were made using 1.5

mL of N_{Au}-1 stock suspension diluted to 15 mL with buffer solution to create a concentration of 2 g/L.

The remaining stock suspension was re-oxidised with 1 M hydrogen peroxide in stoichiometric excess, and left stirring overnight to aerate in the room atmosphere, as described in Section 4.2.2.

For re-reduction, clay mineral suspensions were again centrifuged to separate solids from supernatant. Solid material was then brought into the anaerobic N₂ chamber and washed with deoxygenated 1 M NaCl solution and DIW before restarting the reduction process. The process was repeated for 3 cycles of reduction with AH₂DS and oxidation with H₂O₂.

4.2.4 Kinetic batch experiments

All kinetic experiments were completed and stored overnight inside an N₂ atmosphere (<1 ppm O₂) anaerobic glovebox, to minimise all unintended oxidation. All experiments were conducted in triplicate. For each batch reactor, 1.5 mL of the 20 g/L clay mineral stock suspension and 13.5 mL of 10 mM MOPS 50 mM NaCl buffer solution were added to 20 mL glass vials. The pH of each reactor was adjusted to 7.5 using small increments of NaOH or HCl. Reactors were sealed with butylene rubber stopper, crimp capped to hermetically seal the contents, and then placed on a rotator.

Kinetic reactions were initiated by injecting 30 µL of methanolic 3-chloronitrobenzene stock solution using a gas-tight glass syringe to achieve a concentration of ~50 µM in the reactor. A 500 µL sample was taken immediately after spiking and filtered via a 0.22 µm nylon filter to remove any excess mineral. The sample was then stored in a sealed glass HPLC vial ready for analysis. This initial sample was taken as measurement for initial concentration. For each reactor, more samples were taken in the same method at incremental time steps until the reaction had reached completion. All samples were stored in the fridge at 4 °C prior to HPLC analysis.

Analysis of samples and concentrations of model contaminant 3-chloronitrobenzene (3CNB) and the degradation product 3-chloroaniline (3CAN) were measured using the Agilent 1260 Infinity II HPLC equipped with DAD detector, using an LC-18 column

(XBridge C18 3.5 μm). Analysis used same technique as described in Section 3.2.2. Figure SI 3.2 shows the eluent compositional gradient / method.

Contaminant transformation experiments were conducted, measured, and modelled following the same methodology as described previously in Sections 3.2.3, 3.2.4, and 3.2.5.

4.2.5 Particle size analysis

Samples were taken of clay mineral suspensions and diluted to 0.05 g/L using deoxygenated, deionised water. Samples were measured in a sealed screw-cap (to prevent any unintended oxidation), 10 mm x 10 mm (internal width) quartz cuvette sourced from Hellma UK Ltd. Sample particle size was measured using Malvern Panalytical Zetasizer Nano.

4.2.6 Mössbauer Spectrometry

Samples were separated and prepared from the NAu-1 stock suspension before contaminants were added. Solids were separated from supernatant with a 13 μm nylon filter under anaerobic atmosphere. The sample solids were sealed in Kapton tape to prevent oxidation during transfer to the Mössbauer spectrometer.

Samples were analysed using and S4 Mössbauer spectrometer (SEE Co., Edina, MN, U.S.A.) in transmission mode and calibrated against 7 μm $\alpha\text{-Fe(0)}$ foil. Temperature during spectra acquisition was controlled with a closed cycle cryostat (SHI-850, Janis Research Co., Wilmington, MA, U.S.A.) at either 4 K or 77 K to allow for quantifying the Fe speciation of the clay mineral.

Spectra were analysed using the software Recoil, using Voigt-based fitting routine for spectra measured at 77 K, and Full-static Hamiltonian fitting routine for samples measured at 4 K.

4.2.7 Fe analysis

Aqueous Fe(II) and Fe(total) concentrations were measured using the 1,10-phenanthroline method (Schilt 1969). Solid phase Fe concentrations were measured following HF digestion using a modified 1,10-phenanthroline method (Stucki 1981, Amonette and Templeton 1998), as described previously (Neumann et al. 2011).

4.2.8 Contributions

MSc student Shaikha Almesbah helped with the development of the AQDS reduction process. Maggie White assisted with the preparation and measurements of HF digestion experiments

4.3 Results and Discussion

4.3.1 Clay mineral Fe reduction with AH₂DS

Examining the UV-VIS spectra of the AQDS solution before and after reaction with NAu-1 shows a change from reduced state (AH₂DS) to oxidised state (AQDS) as shown in Figure 4.3. The figure demonstrates that the peak at 386 nm representative of AH₂DS has decreased and the peak at 326 nm representative of AQDS has increased (Jaisi et al. 2007a, Shi et al. 2012). This indicates that AH₂DS was oxidised after reaction with the clay mineral and suggests electron transfer has occurred into the clay mineral. It was also noted a change in colour of the NAu-1 from light green / orange to a dark green / blue. The change of colour from light green to dark green / blue in NAu-1 (see Figure SI 4.3.) has been widely described as evidence of reduction of octahedral Fe(III) to Fe(II) (e.g. Komadel et al. 1990). Using the equations 4.1 and 4.2, it was calculated that the oxidation of AH₂DS was the electron molar equivalent of 9.7 %, 10.8 %, and 10.6% reduction (see Table SI 4.1) of the clay mineral structural Fe present for cycles 1, 2, and 3 respectively. A separate phenanthroline assay measured the reduction extent of NAu-1 to be 7.2 %, 8.5 %, and 9.8 % for cycles 1, 2, and 3 respectively (also see Table SI 4.1 for comparison). The calculated values for both reduction extent and electrons transferred align very well. Other research investigating reduction of NAu-1 with AH₂DS achieved a similar result in the first 24 hours (Jaisi et al. 2005, Shi et al. 2021), but achieved a greater reduction extent when left to react for much longer time periods (Jaisi et al. 2007a). It is possible that over longer time periods a higher reduction extent would be achievable, however it is unclear whether the study (Jaisi et al. 2007a) replenished the reductant over that time with newly produced AH₂DS which could have impacted the reductive capacity of the solution.

To investigate whether the reaction had reached equilibrium at the point of measurement, it is possible to calculate the overall, non-standard reduction potential (E_H). The E_H for the reduction of NAu-1 with AH₂DS was calculated using Equation 4.3, consisting of two reaction half-cell equations. The reduction potential of NAu-1

structural Fe was calculated using a modified version of the Nernst equation (Equation 4.4) taken from Gorski et al. (2013). This is used to account for the broadening of E^0_H values unique for each smectite, which lead to wider range than expected for a typical Fe(II)/Fe(III) redox couple (Luan et al. 2014). The oxidation potential of AH₂DS to AQDS was calculated using the Nernst equation (Equation 4.5).

Equation 4.3; calculating the overall, non-standard E_H :

$$E_H = E_{H\ NAu1} - E_{H\ AH2DS}$$

Equation 4.4; Modified Nernst Equation to calculate NAu-1 reduction half equation:

$$E_{H\ NAu1} = E^0_{H\ NAu1} - \left(\frac{1}{\beta}\right) \times \frac{RT}{zF} \ln \frac{[Fe(II)]}{[Fe(III)]}$$

Equation 4.5; Nernst Equation used to calculate reduction potential of AH₂DS half-cell reaction:

$$E_{H\ AH2DS} = E^0_{H\ AH2DS} - \frac{RT}{zF} \ln \frac{1}{\left(\frac{[AQDS][H^+]^2}{[AH_2DS]}\right)}$$

Where E^0_H is the standard reduction potential and values for both the NAu-1 Fe(II)/Fe(III), and the AH₂DS/AQDS redox couples were taken from published literature. The E^0_H for the oxidation reaction of AH₂DS to AQDS was taken to be -0.18 V (Luan et al. 2014). The E^0_H value for NAu-1 Fe reduction was taken to be -0.45 V (Gorski et al. 2013). β is the dimensionless factor used to describe the broadening effect of smectite E^0_H values, and for NAu-1 is 0.56 (Gorski et al. 2013). R is the universal gas constant (8.314 J·K⁻¹·mol⁻¹), T is the temperature in Kelvin (298 K, z is the ion charge / moles of electrons transferred per unit (2 electrons per mole of AH₂DS oxidised, 1 electron per mole of Fe(III) reduced), F is the Faraday constant (96,485.3365 C mol⁻¹). The equations use the Molar concentrations of both redox couples after reaction, and [H⁺] is included for the AQDS/AH₂DS redox pair.

The overall, non-standard E_H values for the reaction of AH₂DS with NAu-1 are 0.011 V, 0.016 V, and 0.019 V for cycles 1, 2 and 3 respectively. These values are sufficiently close to 0 suggesting that the reaction did indeed reach equilibrium.

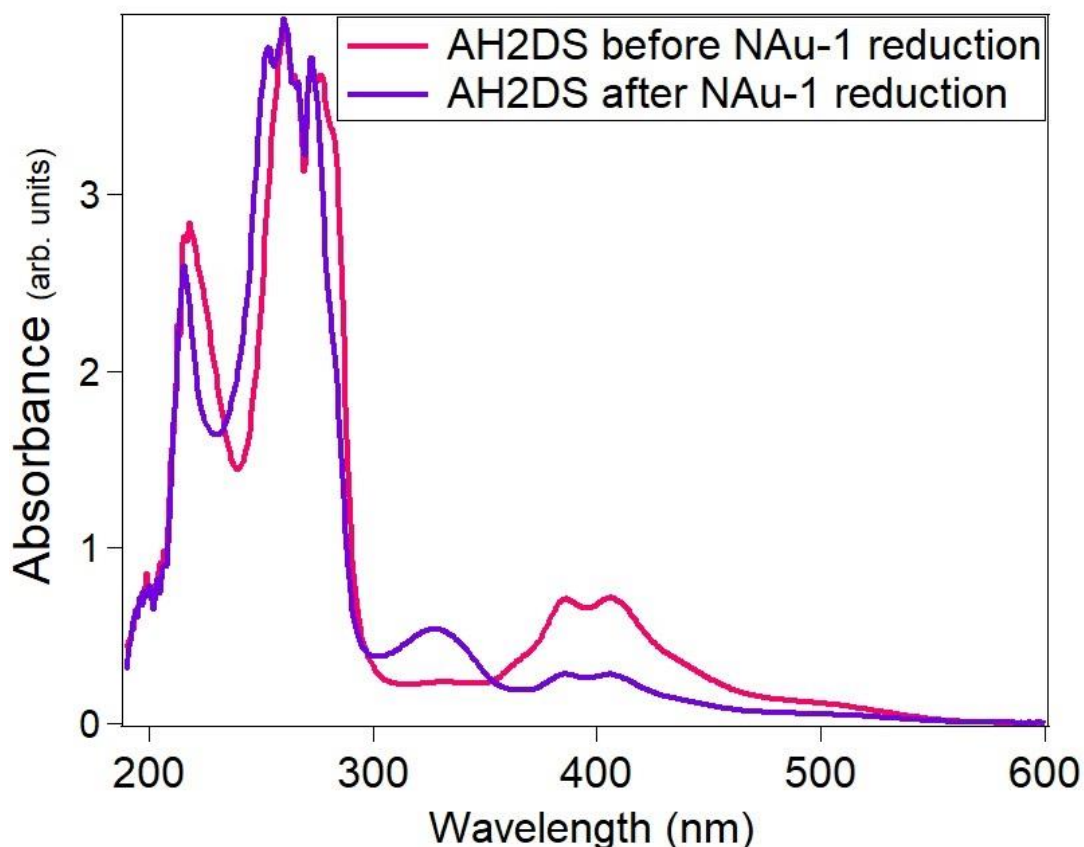


Figure 4.3: UV-VIS spectrum of the reduced AQDS solution (AH₂DS) before (pink) and after reaction with NAu-1 (purple) for Cycle 1.

The results from the spectrophotometrically determined AQDS / AH₂DS concentrations show that the reduction extent achieved remained constant across the three cycles of reduction and re-oxidation. In each reaction, the reductant was not fully oxidised and there was adequate AH₂DS remaining in solution for further reduction. This would suggest that unlike dithionite, AH₂DS is incapable of completely reducing the structural Fe of the clay mineral.

Luan et al. (2014) used AH₂DS to reduce Nontronite NAu-2, and also found that the achievable reduction extent was consistently capped regardless of initial concentration of AH₂DS. The study determined that AH₂DS alone was insufficient to completely reduce the available structural Fe due to thermodynamic limitations.

4.3.2 Contaminant transformation kinetics of AQDS-reduced NAu-1

AH₂DS-reduced NAu-1 was reacted with 3-chloronitrobenzene and its transformation to the corresponding aniline was measured using HPLC. The 3-chloronitrobenzene concentration data for all three cycles (Figure 4.4) shows that contaminant transformation occurred in two distinct phases. First, an initial rapid decrease in

concentration occurred, resulting in approximately 50% of the 3-chloronitrobenzene being transformed in less than 3 hours. After, the remaining contaminant was more slowly transformed, with the reaction reaching completion at approximately 900 hours after the initial spiking. Figure SI4.4 shows the complete kinetic data set including the corresponding aniline product concentration. The same biphasic contaminant transformation behaviour was observed previously for dithionite-reduced N Au-1 (section 3.3.1), however the time required to reach complete contaminant transformation is much longer for the AH₂DS-reduced N Au-1. This is likely due to the lower reduction extent, meaning there is half as much reactive Fe(II) accessible for contaminant transformation. There is little difference between the 3 cycles, however the reaction was quickened slightly after Cycle 1, but Cycle 2 and Cycle 3 show very similar results. First examination of the reaction kinetics suggests that reduction-oxidation cycling using AH₂DS as reductant did not cause any significant changes to the clay mineral Fe(II) reactivity, similar to what was previously observed when dithionite was used as the reductant (see Figure 3.1).

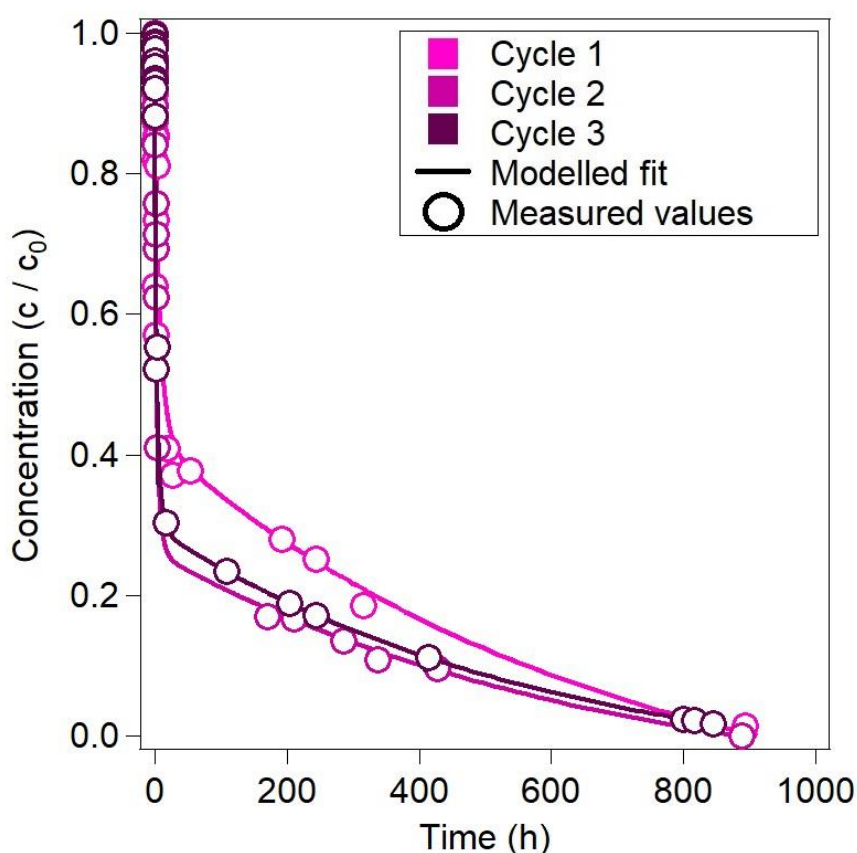


Figure 4.4: Typical concentration data of 3-chloronitrobenzene in the presence of N Au-1 that was subjected to one (pink circles), two (purple circles), or three (dark purple circles) cycles of reduction with AH₂DS and re-oxidation with H₂O₂. Lines show the fit obtained using the two-site kinetic model (eq.).

To better understand the effects of multiple cycles of reduction and oxidation on reactivity, the transformation kinetics were fit with both a single-site and a two-site model as described in Chapter 3.2.5. As previously observed with the dithionite-reduced N_{Au}-1, the one-site model was not able to correctly fit the data (Figure SI 4.4) whereas the two-site model more accurately described the measured values (Figure 4.4). The conformity with the two-site model would indicate the presence of two distinct reactive sites, as has been described for Fe-rich minerals in various papers (e.g. Hofstetter et al. 2006, Neumann et al. 2008, Rothwell 2018). Biphasic kinetics have also been observed in bio-reduced nontronite samples (Yang et al. 2012), who suggested the rapid transformation phase was due to highly reactive clay mineral Fe edge-sites. This however, differs from one study that modelled kinetics using a single reactive site, second order rate law for nitroaromatic reduction by bio-reduced N_{Au}-2 (Luan et al. 2015b). The differing results proposed in Luan et al. (2015b) could indicate that AH₂DS- reduction and bio-reduction follow different reduction pathways (Rothwell 2018). From the kinetic model fits, rate constant values and the initial concentration of highly reactive sites were obtained (Figure 4.5).

Figure 4.5(A) shows that the rate of reaction does not change significantly over 3 cycles of reduction and oxidation. The log k values for Cycle 1 are 2.9 and -0.4 for the highly reactive sites and the less reactive sites respectively. There is a small, but statistically significant increase in Cycle 2 for the log k value of the highly reactive sites to 3.3. This might be due to the slight increase in reduction extent measured in multiple analyses (possibly as great an increase as ~7-10% depending on which analysis of Fe(II)/Fe_{Tot} is referenced (see Section 4.3.1). It has been demonstrated that even small increases in Fe(II) content can reflect significant increases in reactivity in N_{Au}-1 when the reduction extent is below 30 % Fe(II):Fe_{Tot} (Rothwell 2018), which might have caused this increase in rate constant values.

There is no statistically significant difference between the measured log k values of Cycle 2 and 3. The calculated rate constant values of AH₂DS-reduced N_{Au}-1 align well with the observations made on the kinetic model (Figure 4.4); there is a small increase in the speed of reaction on Cycle 2, followed by largely equivalent reaction for Cycle 3.

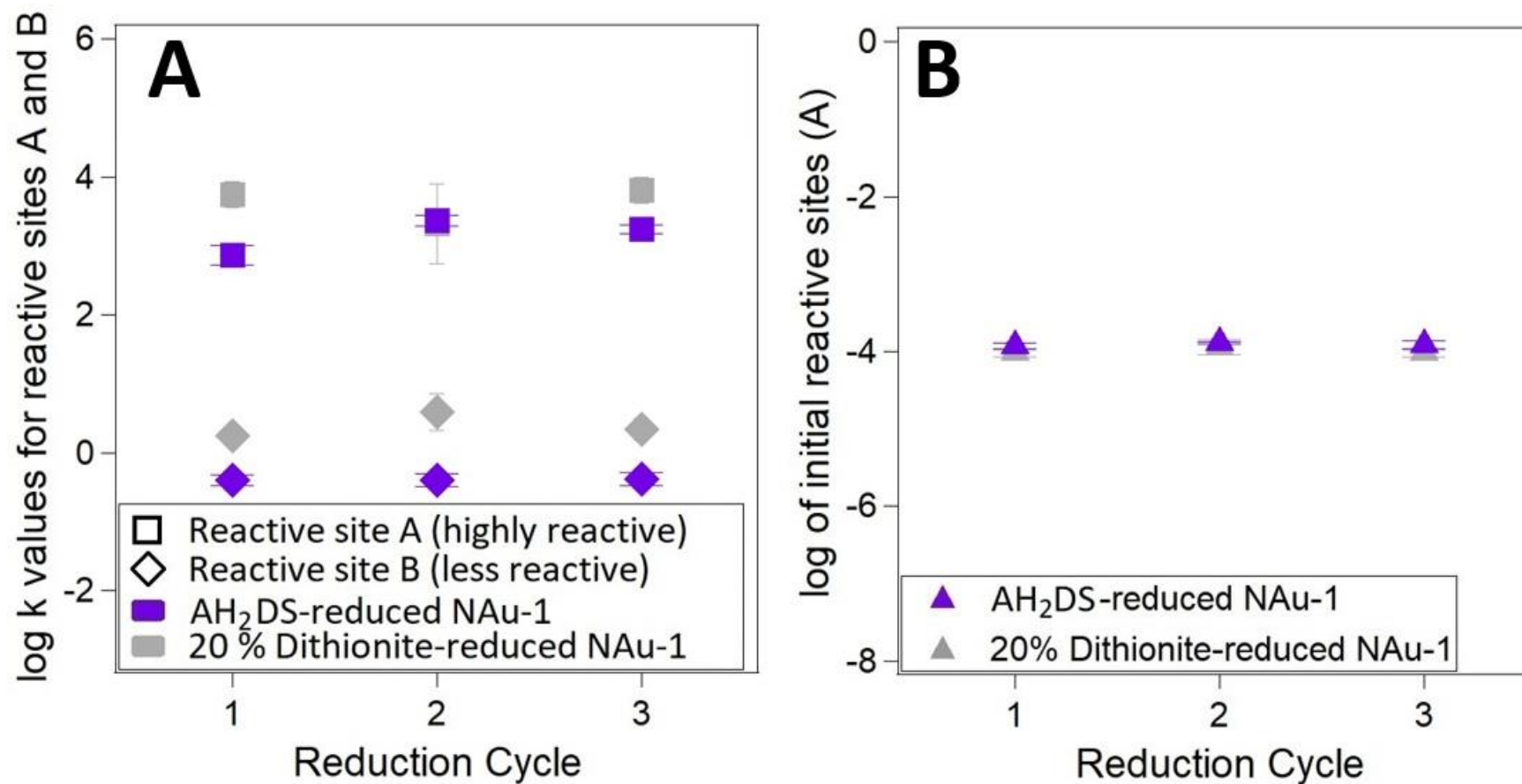


Figure 4.5: Log of rate constants of 3-chloronitrobenzene transformation by AH₂DS-reduced NAu-1 shown in purple versus 20% dithionite-reduced NAu-1 shown in grey. Figure shows for both highly reactive sites (square), and less reactive sites (marked with diamonds) of the clay mineral (left). Right figure (B) shows log of initial concentration of highly reactive sites, and compares both AQDS-reduced (purple) and dithionite-reduced (grey) – values as calculated by the two-site kinetic model. Error bars show 1 standard deviation.

Figure 4.5 also shows the values achieved using dithionite as reductant to achieve a low reduction extent (taken from previous chapter, Section 3.3.1) for comparison. The AH₂DS-reduced log k values are similar to those of the dithionite-reduced N_{Au}-1, but marginally (but statistically significant) smaller. This difference most likely due to the lower Fe reduction extent obtained with AH₂DS (~9%) compared to dithionite (~15-36%, refer to Section 3.3 for exact dithionite-reduction extent values).

Previous work by Rothwell (2018) measured the effects of dithionite reduction on N_{Au}-1 on rate constants over a range of reduction extents. The study demonstrated that rate constants for N_{Au}-1 increased with increasing reduction extent, until reaching approximately 30% Fe(II)/Fe_{tot} where rate constants began to plateau. The results by Rothwell show that dithionite-reduced minerals produce log k values that are highly comparable to the AH₂DS-reduced mineral log k values produced in this study, when reduced to equivalent reduction extents. However, the AH₂DS-reduced mineral log k values for less reactive sites are lower than those for dithionite-reduced minerals. It is possible that AH₂DS-reduced N_{Au}-1 is less reactive than dithionite-reduced N_{Au}-1. AH₂DS is intended to act as a suitable abiotic proxy for microbial reduction, and it has been suggested that microbially-reduced clay minerals react less quickly than dithionite-reduced clay minerals (Luan et al. 2015b). Another factor to take into account is that the Rothwell study used a different probe compound (2-acetylnitrobenzene), which makes direct comparison of rate constant values non-viable. The study (Rothwell 2018) did not investigate the effects of multiple redox cycles. There has currently been no previous research investigating the effects of multiple reduction cycles using electron shuttling compounds as the sole reducing agent.

The model also yields, as one of its fit parameters, the initial concentration of highly reactive sites within the clay mineral structure. The data in Figure 4.5(B) highlights that the initial concentration of highly reactive sites did not demonstrate any significant change over 3 cycles of reduction oxidation (i.e. values within range of error). The Figure also presents data from the dithionite-reduced samples, and the values are generally equivalent with no statistically significant difference (based on calculated error) in initial concentration of highly reactive sites.

Overall, it appears that reduction-oxidation cycling with AH₂DS does not cause significant changes to the reactivity. It is unknown whether reduction-oxidation cycling of NAu-1 using AH₂DS as reductant should more closely emulate the effects biological or chemical reduction. AH₂DS is intended in this experiment to act as an abiotic proxy for microbial / biological reduction. Biological reduction cycling of NAu-2 has shown mixed results, from dissolution and significantly increased kinetics (i.e. Yang et al. 2012), to largely sustainable and reversible effects with negligible impact on reaction kinetics (Zhao et al. 2015). Our kinetics results so far more closely align with the latter study, but the study has not yet measured how the structure and morphology is affected. Zhao et al. (2015) however also suggested that the presence of AQDS during bioreduction (used as an electron mediator) allows the reduction of interior structural Fe, which was inaccessible to bioreduction when AQDS is absent. This would indicate that using AH₂DS as the sole electron donor could follow a pseudo-random pattern of electron transfer into the clay mineral octahedral sheet, more typically associated with chemical (dithionite) reduction (Ribeiro et al. 2009). Indeed, the measured kinetics results of this experiment indicate little discernible difference between the results achieved using dithionite versus AH₂DS.

Overall, it appears that reduction-oxidation cycling with AQDS and H₂O₂ does not cause significant changes to the reactivity. The results do not however highlight whether reduction with AH₂DS impacts the structure / morphology of the clay mineral, or whether AH₂DS is an appropriate substitute for microbial reduction. A comprehensive assessment of the physicochemical effects on the clay mineral was conducted to further understand how the electron transfer from electron shuttling compounds interact with structural Fe.

4.3.3 Impacts of reduction-oxidation cycling with AH₂DS and H₂O₂ on clay mineral structure

To better understand whether reduction-oxidation cycling with reduced AQDS leads to structural changes or alterations of the clay mineral particles, a number of analyses were conducted. An assessment of electron transfer and Fe speciation using Mössbauer spectroscopy, and particle size analysis was used to measure morphological changes.

Figure 4.6 presents particle-size measurements for AH₂DS-reduced NAu-1 suspensions over 3 cycles of reduction. The distribution of particles is spread over a wider range than initially size-fractionated for via centrifugation (i.e. 0.2 μm – 0.5 μm). However the mean particle size is well within the expected range. There appears to be almost no change in particle size between each cycle for AH₂DS-reduced NAu-1. A statistical ANOVA was conducted on the AH₂DS-reduced NAu-1 particle size distribution sets. The analysis produced a *p*-value of 0.778 above a significance level of 0.05, and an *F*-value of 0.251 below the *F-critical* value of 3.039. These statistical parameters confirm that the variation between the three reduction cycles is not statistically significant. This indicates that redox cycling with AH₂DS does not significantly impact particle size.

A consistent particle size distribution across 3 cycles of reduction and oxidation is also strong evidence that smaller particles are not dissolved preferentially in favour of larger more crystalline particles during the process. This finding is contrary to what has been suggested by some research to occur during biological reduction-oxidation cycling (Yang et al. 2012). However, Yang et al. (2012) achieved bio-reduction of structural Fe with live microbes present in the system, which may have had a more intrusive impact on the minerals than the electron transfer process alone. The study also used nontronite NAu-2 rather than NAu-1, and a previous paper (Jaisi et al. 2005) found that biological reduction led to a change in particle thickness for NAu-2 but not for NAu-1.

Figure 4.6 also shows the measured particle size distribution of NAu-1 chemically reduced with dithionite to a low reduction extent. The particle size distribution of dithionite-reduced NAu-1 is very similar to the AH₂DS-reduced values, and the difference is also not considered statistically significant. This would indicate that both reduction pathways produce similar (i.e. negligible) effect on particle size.

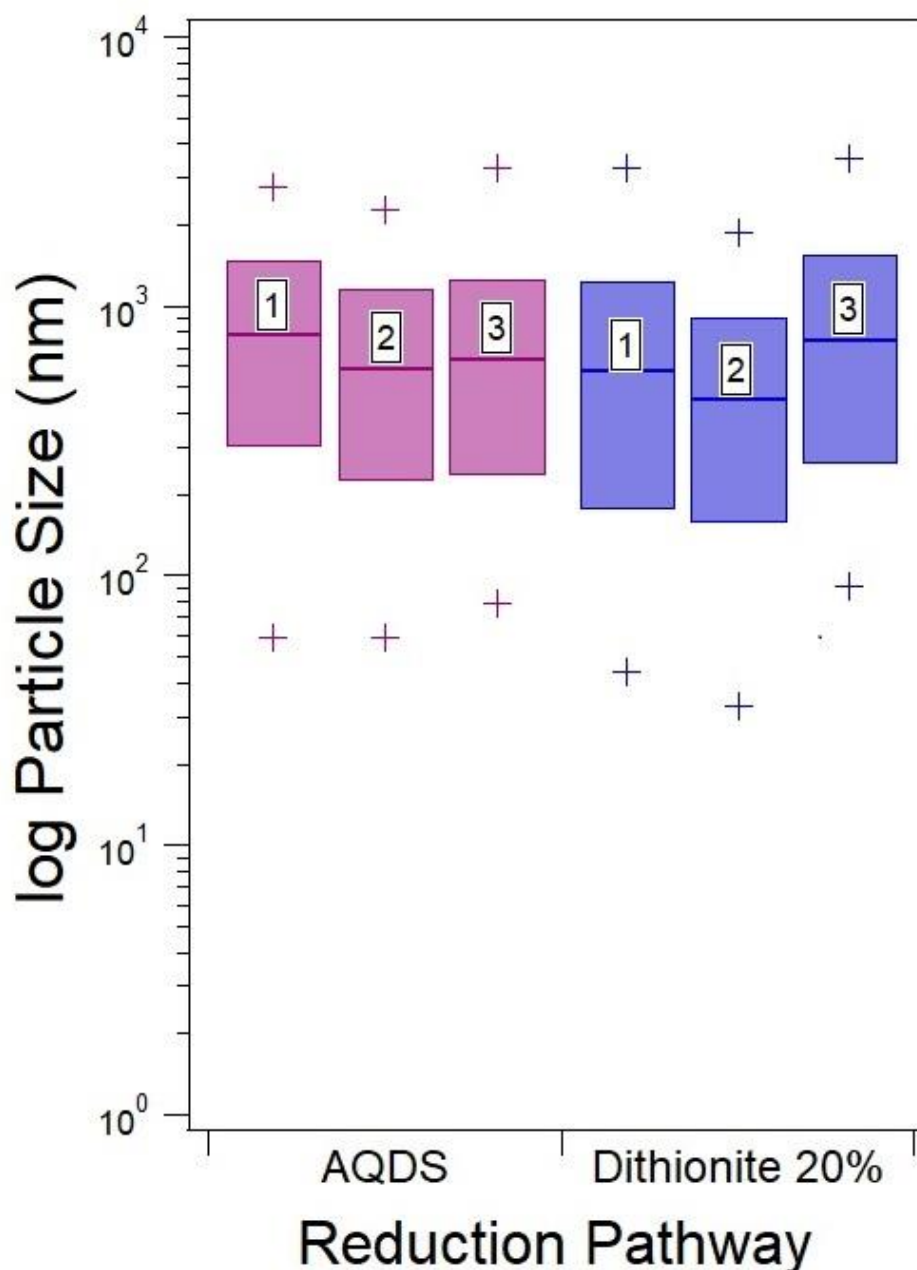


Figure 4.6: Graph shows the changes in particle sizes measured for AH₂DS-reduced NAu-1 over 3 cycles (shown in purple), data are also compared with dithionite-reduced NAu-1 to low reduction extent (blue). Figure shows the range of sizes, marked with +, the mean, and 1 standard deviation above and below (marked by the coloured column).

However, although results suggest that reduction-oxidation cycling is not significantly impacting the morphology / size of the clay mineral suspension, this does not provide insight into alterations to the mineral structure. A comprehensive analysis was conducted using Mössbauer spectroscopy to probe the binding environments of structural Fe at atomic resolution. Figure 4.7 shows the Mössbauer spectra of AH₂DS-reduced NAu-1 over 3 redox cycles. Samples were measured at both 77 K to examine the reduction extent, and at 4 K to understand how cycling impacts Fe speciation.

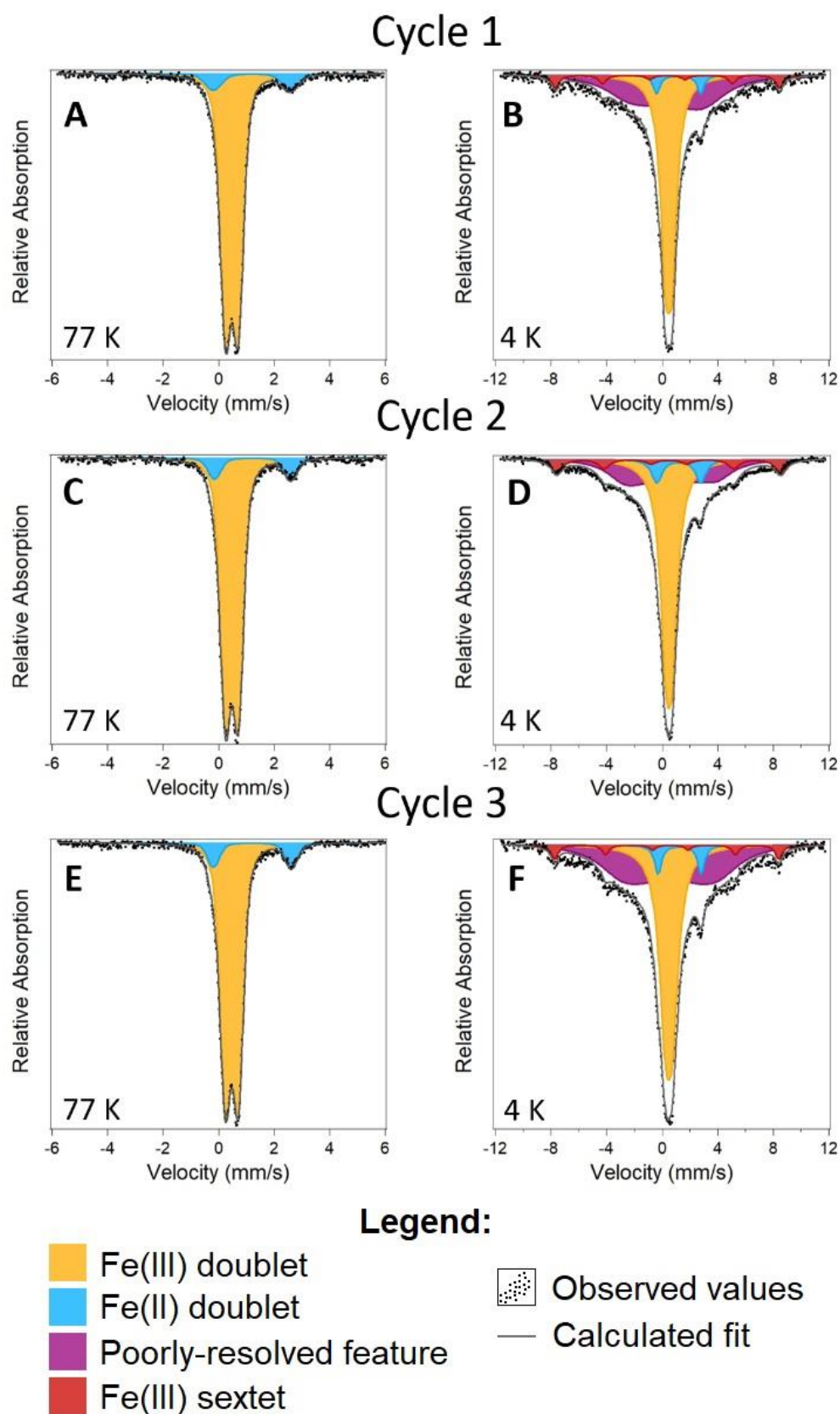


Figure 4.7: Mössbauer spectra for NAu-1 reduced with AH₂DS, measured at both 77 K temperature (Figures A, C, E) and 4 K temperature (Figures B, D, F) for cycles 1, 2, and 3 (respectively). Spectra measured at 77 K were fitted with Voigt-based fitting technique. Spectra measured at 4 K were fitted using variable line-width (Full Static Hamiltonian) fitting technique.

The left side of Figure 4.7 (Sub-figures A, C, E) shows the spectra for AH₂DS-reduced N_{Au}-1 over 3 reduction cycles, measured at 77 K temperature (all fitting parameters are shown in Table 4.1). The spectra measured at 77 K of the AH₂DS-reduced N_{Au}-1 for all 3 cycles look very similar, and all three spectra display 2 doublets. The first doublet present in each spectrum has a CS of 0.48 mm/s and a QS of 0.47, values typical for Fe(II) and rep. The blue doublets have CS values between 1.20-1.23 mm/s and QS values of 2.75-2.81 mm/s, which are within ranges typical for Fe(II) (Murad and Cashion 2004). For comparison the spectrum of the native, unaltered N_{Au}-1 can be viewed in Figure 4.8, and does not contain this blue doublet species. The blue Fe(II) doublets comprise 9.1%, 9.3%, and 10.1% of total absorption for cycles 1, 2, and 3 respectively (see Table SI 4.1). These values align very closely with the reduction extent values measured in both the HF digestion (7.2%-9.8%, Table SI 4.1), and those calculated by the oxidised AH₂DS concentrations (9.7%-10.8% Table SI 4.1). The Mössbauer spectra for AH₂DS-reduced N_{Au}-1 measured at 77 K temperature are further evidence that electron transfer has occurred from the AH₂DS, and that reduction extent remained stable over 3 cycles of reduction and oxidation.

The parameters measured for the Fe(II) doublet are very similar to those measured previously for the dithionite-reduced N_{Au}-1 (CS = 1.20 - 1.26 mm/s, QS = 2.90 – 2.95 mm/s, see Table 3.1) albeit with a marginally smaller QS value, and are within the range for dithionite-reduced N_{Au}-1 as measured in previous work (Rothwell 2018). The values also align well with the values measured for clay mineral Fe after microbial reduction in the presence of live organisms. Previous studies investigating biological reduction of nontronite by *Shewanella* measured highly comparable parameters for the achieved Fe(II) doublet. Ribeiro et al. (2009) measured a doublet species with CS and QS values of CS = 1.26 mm/s, QS = 2.69 mm/s whereas Yang et al. (2012) observed an Fe(II) doublet with parameters CS = 1.22 mm/s, QS = 2.69 mm/s using VBF fitting. These results are distinctly similar to the parameters achieved in this experiment, however both studies used N_{Au}-2 rather than N_{Au}-1 which could complicate comparison.

The spectra measured at 77 K temperature indicate that the Fe(II) content is similar to both dithionite and biologically reduced samples of previous studies. Mössbauer

measurements at 77 K alone are insufficient to appropriately determine whether reduction via AH₂DS more closely resembles biological or chemical reduction. Spectra collected at 4 K can offer a more accurate insight into how reduction via this pathway impacts the binding environment of Fe within the mineral structure. Previous studies have shown that Mössbauer spectra collected at 4 K present different patterns, depending on whether biological reduction or reduction with dithionite was applied (Ribeiro et al. 2009).

Figure 4.7 (right side) also shows the spectra collected for AH₂DS-reduced NAu-1 provides insight into the speciation of Fe within the system. Again, all three cycles produced spectra that are virtually indistinguishable from each other. The spectra comprise 4 species, including the central doublet (yellow) typical of Fe(III) within NAu-1, a small Fe(II) doublet (blue), a large collapsed feature at the base (purple), and a small sextet species (red).

The sextet phase is unexpected as a sextet of this width has not been observed in comparable samples of dithionite-reduced or biologically-reduced NAu-1 at similar reduction extents (e.g. Ribeiro et al. 2009). After re-analysing the batch of native NAu-1 used for this experiment, the Mössbauer spectrum of the unaltered NAu-1 sample used in this batch of experiments (Figure 4.8), it was found that the native sample also contains this sextet species with equivalent parameters (Table 4.1). The relative spectral area of the sextet is 4% in the spectrum of native NAu-1 and all three spectra of reduced NAu-1. It is most likely that this sextet species represents an Fe-oxide impurity that were not removed during the size-fractionation and extensive clean-up procedure (see Section 4.2.1) filtered out during the precipitation stage. As the sextet area and Mössbauer parameters are unaffected by the reaction with AH₂DS, this component is most likely not redox active and will be disregarded for the remainder of the analysis.

Assessing the sustainability of Fe-bearing clay mineral redox reactions

Chapter 4: Redox cycling with reduced electron-shuttling compounds

Table 4.1: Mössbauer spectra parameters for AH₂DS-reduced NAu-1, over 3 cycles of reduction and oxidation. Top table shows fit parameters for spectra measured at 4 K temperature using full-static hamiltonian technique. Bottom table shows fit parameters for spectra measured at 77 K temperature using from Voigt-based fitting technique. Fe species are colour coded as displayed in Figure 4.7. CS = Centre shift, H = magnetic hyperfine field, QS = quadrupole splitting

	T (K)	Species	CS (mm/s)	H (T)	QS (mm/s)	η (-)	w (mm/s)	θ (-)	Area (%)
Native NAu-1	4	sextet	0.49	49.93	-0.14	0	0.4	0	3.89
		Fe(III) doublet	0.49	0	0.46	0	0.45	0	96.11
AH ₂ DS-reduced (cycle 1)	4	sextet	0.42	49.44	0.01	0	0.33	0	4.62
		Fe(III) doublet	0.48	0	0.49	0	0.43	0	46.25
		Fe(II) doublet	1.19	0	3.18	0	0.30	0	3.74
		Collapsed	0.57	17.82	-0.44	0	2.00	0	45.40
AH ₂ DS-reduced, reoxidised, reduced (cycle 2)	4	sextet	0.47	49.61	-0.15	0	0.23	0	3.27
		Fe(III) doublet	0.48	0	0.47	0	0.44	0	47.01
		Fe(II) doublet	1.25	0	3.11	0	0.35	0	4.81
		Collapsed	0.53	18.47	-0.05	0	2.00	0	44.91
AH ₂ DS-reduced, reoxidised, reduced, reoxidised, reduced (cycle 3)	4	sextet	0.46	49.40	-0.19	0	0.32	0	5.03
		Fe(III) doublet	0.48	0	0.51	0	0.54	0	43.31
		Fe(II) doublet	1.26	0	3.10	0	0.30	0	4.86
		Collapsed	0.51	22.48	0	0	1.86	0	46.79

	T (K)	Species	CS (mm/s)	QS (mm/s)	σ (mm/s)	Area (%)
Native NAu-1	77	Fe(III)	0.48	0.44	0.34	100
(cycle 1)	77	Fe(II)	1.20	2.76	0.50	9.06
		Fe(III)	0.48	0.46	0.30	90.94
(cycle 2)	77	Fe(II)	1.23	2.75	0.36	9.32
		Fe(III)	0.48	0.47	0.30	90.68
(cycle 3)	77	Fe(II)	1.22	2.81	0.33	10.11
		Fe(III)	0.48	0.47	0.28	89.89

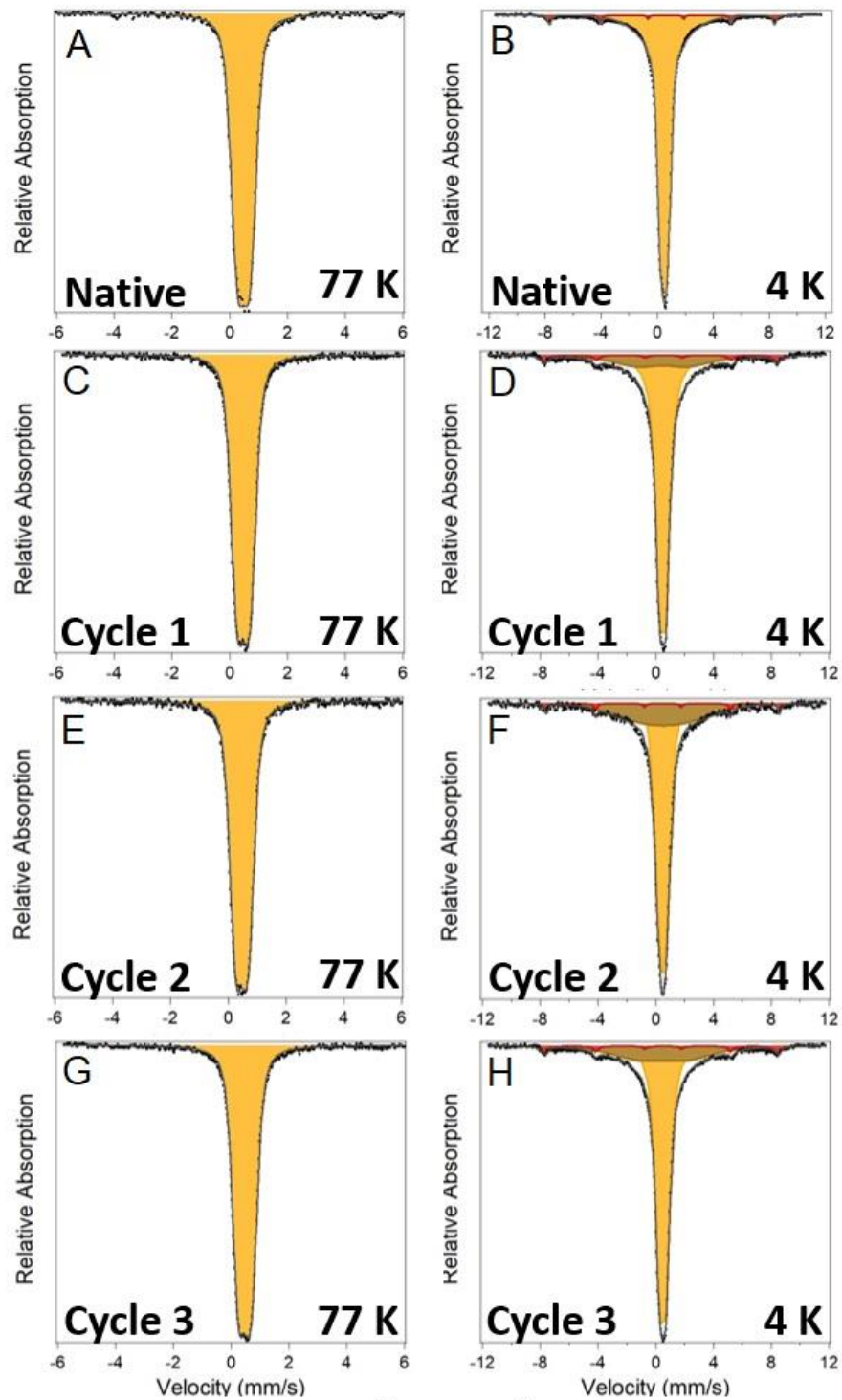
For a more accurate comparison, a sample of the native NAu-1 was reduced with dithionite to 9 % reduction extent using the methods described in section 3.1.2. Once again, the Mössbauer spectrum measured at 4 K (see Figure SI 4.5) shows a sextet with a hyperfine field of 50 T is present in the spectrum and exhibits a similar spectral area as in native NAu-1 and NAu-1 after reduction with AH₂DS. It appears that this species is not dissolved by dithionite reduction as might be expected for most Fe-oxide species, however this may be due to the relatively low concentration of dithionite used to achieve this low reduction extent (9%). While we cannot characterise or determine the nature of this sextet species, it does not appear to be influenced by reduction or play a significant role in the cycling process.

Aside from the sextet, the remaining species observed in the AH₂DS-reduced NAu-1 at 4 K temperature align very closely with the NAu-1 spectrum reduced to an equivalent reduction extent with dithionite at 4 K (Figure SI 4.5). Both dithionite-reduced and AQDS-reduced NAu-1 produce almost identical spectra and all show the same species with equivalent parameters. Ultimately this indicates that the effects of reduction by these two pathways lead to similar effects on Fe speciation within the clay mineral.

To determine whether the effects of AH₂DS-reduction on NAu-1 are reversible requires examination of the sample after reoxidation. After reoxidation with H₂O₂, samples were again measured with Mössbauer at 4 K temperature to examine whether the effects of reduction alter the mineral to a state different from the native.

Figure 4.8 demonstrates the differences between the native, unaltered sample of NAu-1 and a sample of NAu-1 that had been reduced with AH₂DS and then reoxidised with hydrogen peroxide. The left column of spectra in the figure compares the native, unaltered NAu-1 (Figure 4.8 A and B) with the AH₂DS-reduced-reoxidised NAu-1 samples over 3 reduction-oxidation cycles (Figure 4.8 C,E,G) at 77 K temperature.

AH₂DS-reduced, reoxidised NAu-1 spectra



Legend:

- Fe(III) doublet
- Poorly-resolved feature
- Fe(III) sextet
- Observed values
- Calculated fit

Figure 4.8: Figure shows the Mössbauer spectra of native NAu-1 (unaltered) vs AH₂DS-reduced, reoxidised NAu-1. The top row (figures A and B) shows the native sample, and below are the re-oxidised samples over 3 cycles. Left column shows samples measured at 77 K temperature, and right shows samples measured at 4 K temperature

Both spectra (native and reoxidised) have equal parameters, and were fit with a CS of 0.48 mm/s and a QS of 0.44 mm/s. The right side of Figure 4.8 compares the native (Figure 4.8 B) and the reoxidised samples over 3 reduction-oxidation cycles (Figure 4.8 D,F,H) measured at 4 K temperature. Again, there is little difference between the native and the subsequent reoxidised cycles, with each spectrum showing a central doublet with a CS of 0.49 mm/s and a QS of 0.43 mm/s. The reoxidised spectra do however have a wider base, which has been fitted with an additional poorly resolved feature (brown). Ribeiro et al. (2009) also noted a wider, flared base of the central Fe(III) doublet after both biological and abiotic reduction of Fe in a structurally similar nontronite (Garfield). The spectrum for the reoxidised N Au-1 sample highly resembles the spectrum produced previously by N Au-1 reduced with dithionite to a low reduction extent (Figure 4.9).

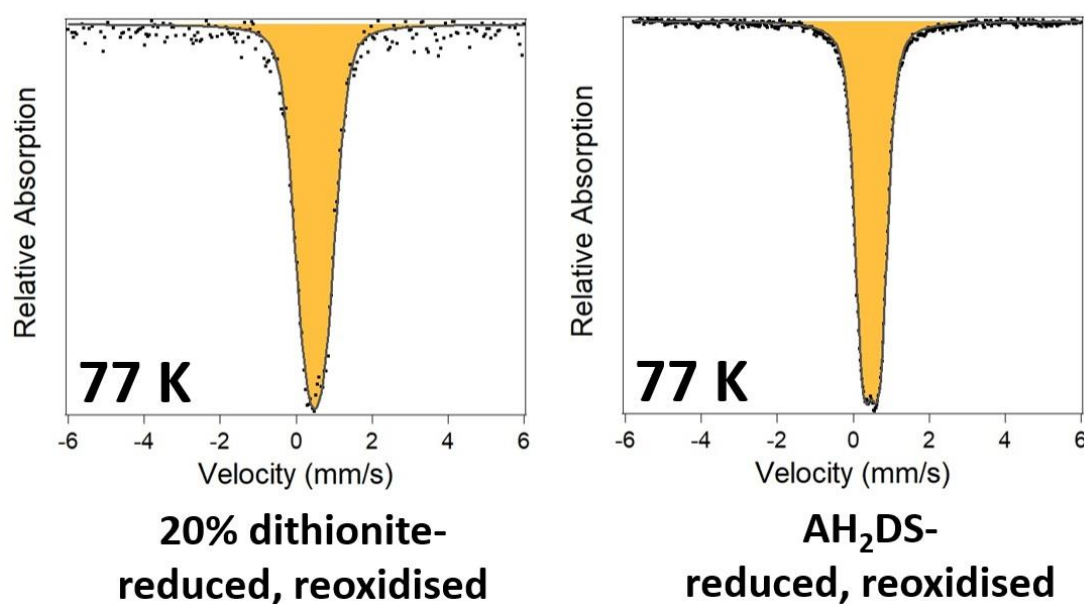


Figure 4.9: Mössbauer spectra taken at 77 K temperature - comparison of 20% dithionite-reduced, reoxidised N Au-1 (left) versus N Au-1 AH₂DS-reduced, reoxidised N Au-1 (right)

When overlaid, the two spectra of Figure 4.9 are virtually identical. Both have a CS value of 0.49 mm/s, however the dithionite reduced spectrum has a slightly higher QS value of 0.52 mm/s. It is likely that the greater QS is caused by the greater extent of reduction achieved. Results from Chapter 3 (see Section 3.3.3) also indicated more significant structural impacts at higher reduction extents. This also aligns well with previous research which has demonstrated how the extent of irreversible alterations

to the structure increases with increasing reduction extent (e.g. Neumann et al. 2011, Gorski et al. 2012, 2013).

The Mössbauer spectra for the second and third cycles of AH₂DS-reduced, reoxidised NAu-1 were almost identical to first cycle, and did not show any changes at either temperature measured (77 k or 4 k). This means that the impacts to the structure were caused by the first reduction, and did not increase with multiple cycles. This result is not unexpected, as the reduction extent was low and remained constant across all three cycles. As stated, the impacts to structure caused by reduction grow with increasing reduction extent, and at low reduction extents the effects are largely reversible (Fialips et al. 2002, Neumann et al. 2011). Previous research has also described how large structural transitions from a dioctahedral to trioctahedral configuration occur once reduction extent reaches a threshold of roughly 1/3 of the clay mineral octahedral Fe(III) being reduced to Fe(II) (Manceau et al. 2000). The reduction extent achieved with AH₂DS in this experiment was too low to reach this threshold, meaning the reduction is not extensive enough to cause significant structural rearrangements.

4.3.4 Is AH₂DS a feasible and appropriate surrogate for biological reduction of clay mineral Fe?

How similar are the results produced using AH₂DS as reductant to those observed when live microbes are present? The achievable reduction extent appears limited to roughly 10% Fe(II)/Fe_{Tot}, which is similar to the limits observed when using biological reduction with NAu-1 (Jaisi et al. 2005, Shi et al. 2016). The inability to achieve a reduction extent above 10% despite stoichiometric excess could be evidence for the limited fraction (10%) of bio-accessible structural Fe as suggested by Shi et al. (2016). If this were confirmed it might indicate that electron transfer from AH₂DS occurs from the edge inwards as is the case with biological reduction (Ribeiro et al. 2009).

Other studies (Zhao et al. 2015) have suggested that AH₂DS can transfer electrons across the clay mineral basal plane in a pseudo-random manner to reduce interior structural Fe. This would potentially produce an effect on the clay mineral more closely resembling dithionite reduction, which has been well-documented to be capable of reducing >99% structural Fe (e.g. Manceau 2000b, Lee et al. 2006, Ribeiro et al. 2009). The study has demonstrated in our E_H calculations (see section 4.3.1) that the reaction

of AH₂DS and N_{Au}-1 did reach an equilibrium state confirming that the reaction reached completion. This would indicate that reduction by AH₂DS is thermodynamically incapable of reaching 100% reduction of the N_{Au}-1, rather than being limited by a limited accessible pool of structural Fe(II). However, this finding alone does not confirm the electron transfer mechanism of AH₂DS.

Previous research has suggested that multiple reduction-oxidation cycles with live microbes leads to a progressively smaller achievable clay mineral reduction (Yang et al. 2012, Shi et al. 2021). In contrast, this study found that achievable reduction extent was unaffected by multiple cycles of AH₂DS-reduction and oxidation. Previous studies also suggest that redox cycling can lead to the preferential reductive dissolution of smaller, less crystalline clay mineral particles; an effect which may contribute to the changes in achievable reduction extent (Dong et al. 2003, Yang et al. 2012, Zhao et al. 2015, Shi et al. 2021). We observed no evidence of preferential dissolution, as particle size was demonstrated to show no significant change (Figure 4.6). In this instance, there are few similarities between the effects of redox cycling with AH₂DS, and the effects described for microbial redox cycling.

When examining the structural effects of reduction-oxidation cycling with AH₂DS, Mössbauer analysis indicated there was little observable difference between the spectra produced by AH₂DS-reduced N_{Au}-1 and dithionite-reduced N_{Au}-1 at either 77 K or 4 K temperature. Results showed that Cycle 1 lead to a widening of the base of the Fe(III) doublet upon reoxidation, an effect which has been documented for both biological and chemical reduction (e.g. Ribeiro et al. 2009). Similarly, other research (Lee et al. 2006) has demonstrated that biological reduction produces effects on smectite structure that are largely indistinguishable from dithionite-reduced smectites at comparable extents of Fe(II). We also observed that successive cycles of reduction and oxidation did not cause any further changes to speciation after Cycle 1. This aligns well with previous research (e.g. Gorski et al. 2012) which found that structural effects of chemical reduction-oxidation cycling on smectites were most pronounced on the first cycle and negligible on subsequent cycles. The Mössbauer data suggests that redox cycling with AH₂DS is has minimal impact on structure, and is largely reversible after the 1st cycles. A review by Stucki (2011) concluded that reduction-oxidation

cycling with bacteria led to the greatest degree of reversibility which reflects the results presented here. The review also found that reduction with dithionite to the high reduction extents led to the greatest degree of irreversible changes. We postulate that the reversibility of biological-reduction as quoted by Stucki (2011), might be an effect of the limited achievable reduction extent, and not the reduction pathway. Although, our Mössbauer spectra of AH₂DS-reduced N_{Au}-1 resemble those of dithionite-reduced-N_{Au}-1, this does not imply that they are dissimilar to biologically-reduced N_{Au}-1 reduced.

The biphasic kinetics observed align well with previous studies using microbes for bioreduction of nontronite (e.g. Yang et al. 2012, Luan et al. 2015b). However, our data also aligns well with a model depicting two reactive Fe sites as has been demonstrated in multiple studies using dithionite as reductant (e.g. Hofstetter et al. 2006, Neumann et al. 2008, 2009, Rothwell 2018). In contrast, Luan et al. (2015b) fitted the kinetics of nitroaromatic transformation by bio-reduced clay minerals using a single-site, second-order rate law, in contrast to our two-site model. The inference of a single reactive site has been suggested to possibly reflect the difference in electron transfer pathway (Rothwell 2018) between bioreduction and dithionite-reduction. Bioreduction has been suggested to follow an edge-inwards migration of electron transfer (Ribeiro et al. 2009), but other papers have suggested that AH₂DS-reduction is capable of pseudo-random transfer across the clay mineral basal plane (Zhao et al. 2015). This might mean that more reactive Fe sites are accessible using electron shuttling compounds. However, the term “bioreduction” encompasses a number of electron transfer pathways including transfer via direct contact, nano-wires, biofilms, chelating agents and electron-shuttling compounds (Melton et al. 2014, Reguera et al. 2020). In the absence of living organisms, differences between the effects of a single pathway of electron transfer (in this case electron shuttling) versus the multiple electron transfer mechanisms available to microbes do not necessarily indicate that AH₂DS is an inappropriate surrogate. This is especially true when considering the significant degree of increased reduction extent achieved when using AQDS in combination with bacteria (e.g. Jaisi et al. 2005, Bishop et al. 2011, Yang et al. 2012), and the prevalence / abundance of shuttling compounds that are used and produced by microbes (Lovley et al. 1996, Melton et al. 2014).

In summary, our results demonstrate that reduction-oxidation cycling with AH₂DS is sustainable and does not cause significant irreversible alterations to the structure or kinetic reactivity of N_{Au}-1. The results of this experiment differ from studies which have employed live microbes present in the system, as results show no dissolution, mineral transformation, or change in reduction extent (Dong et al. 2003, Kim et al. 2004, Zhang et al. 2007, Yang et al. 2012, Shi et al. 2021), but simultaneously there is little to categorically distinguish the effects of AH₂DS-reduction from either biological or chemical reduction. Previous studies have demonstrated that biological reduction of Fe-rich clay minerals is limited to low reduction extents (Kostka et al. 1999, Dong et al. 2003, Yang et al. 2012), that effects of a low reduction extent on the mineral are largely reversible (Fialips et al. 2002, Neumann et al. 2011), and that at low reduction extents both biological and chemical reduction lead to similar effects on the mineral (Lee et al. 2006, Ribeiro et al. 2009). It is proposed that many of the more notable results (e.g. mineral transformation, dissolution) described in previous studies, are a product of the complex range of reactions and organic waste products associated with microbial metabolism, but are not effects of electron transfer to the mineral. Mineral dissolution and transformation may occur in tandem with anaerobic respiration (i.e. mineral reduction), but the former is not a product of the latter. By this reasoning, AH₂DS-reduction is an appropriate surrogate for bacterial reduction, but not an appropriate substitute for the presence of bacteria. AH₂DS is limited in that it cannot emulate the effects of all biochemical processes associated with living organisms.

4.4 Supporting information

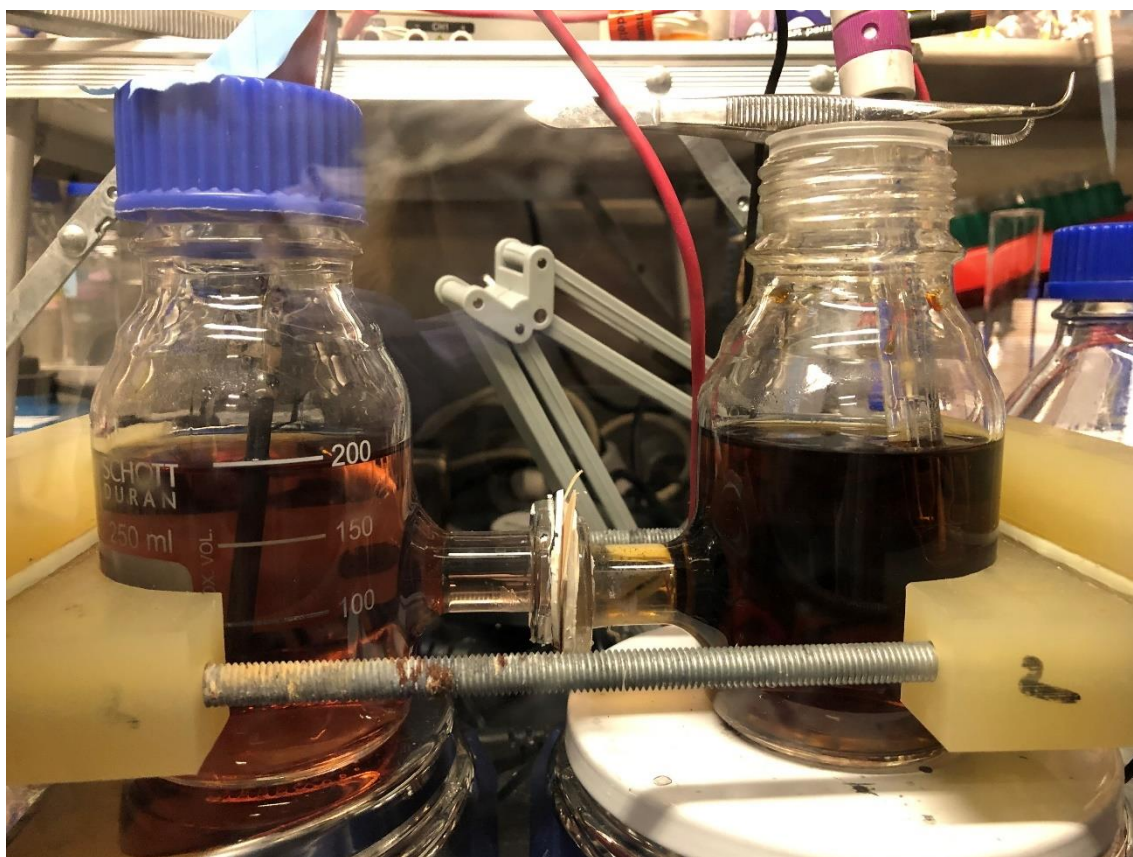


Figure SI 4.1: Image taken showing the electrochemical cell set-up, used in the reduction of AQDS to AH₂DS.

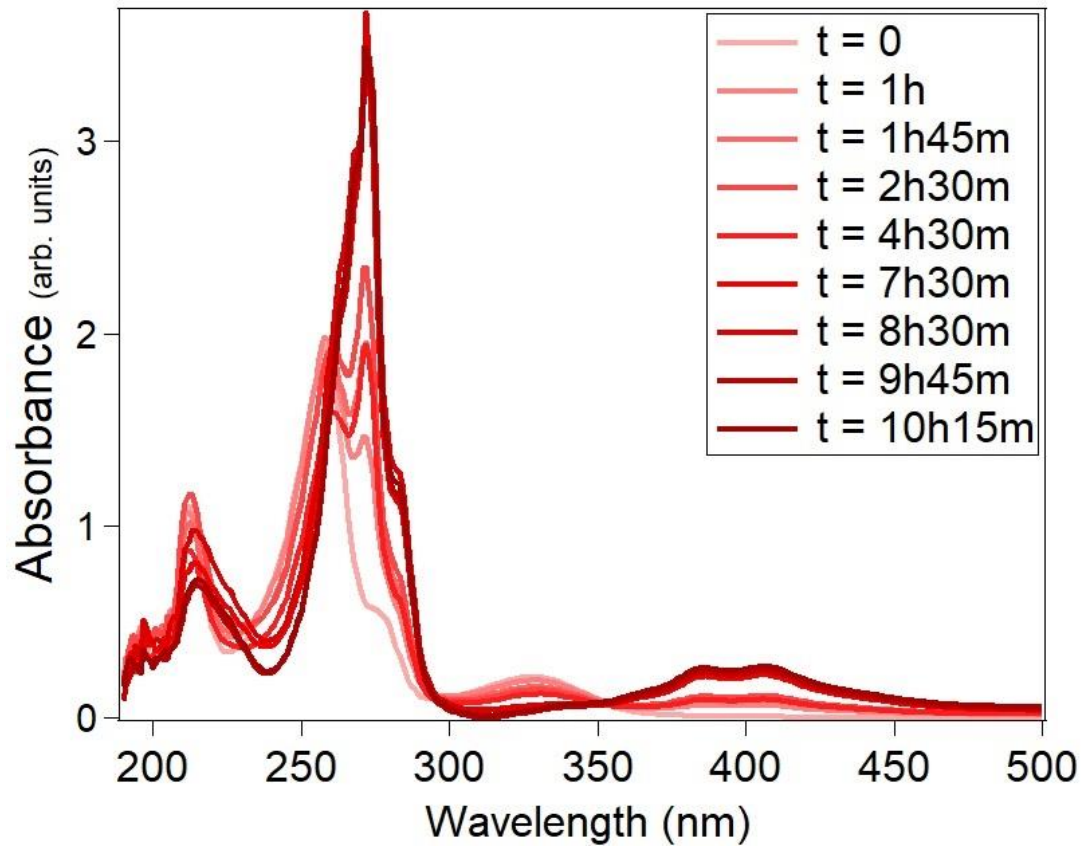


Figure SI 4.2: The transformation of AQDS to AH₂DS over time. Samples were taken at various stages during the reduction process, and measured with UV-VIS spectrometry. Colours change from light pink to dark red as time progresses, showing the measured UV-VIS spectrum of AQDS solution as it is reduced to AH₂DS.



Native (unaltered) NAu-1



AH₂DS-reduced NAu-1

Figure SI 4.3: Images demonstrating the change in colour of NAu-1 in suspension after reaction with AH₂DS. Left image shows unaltered, native sample of NAu-1 in suspension of DIW, right image shows AH₂DS-reduced NAu-1 suspended in DIW.

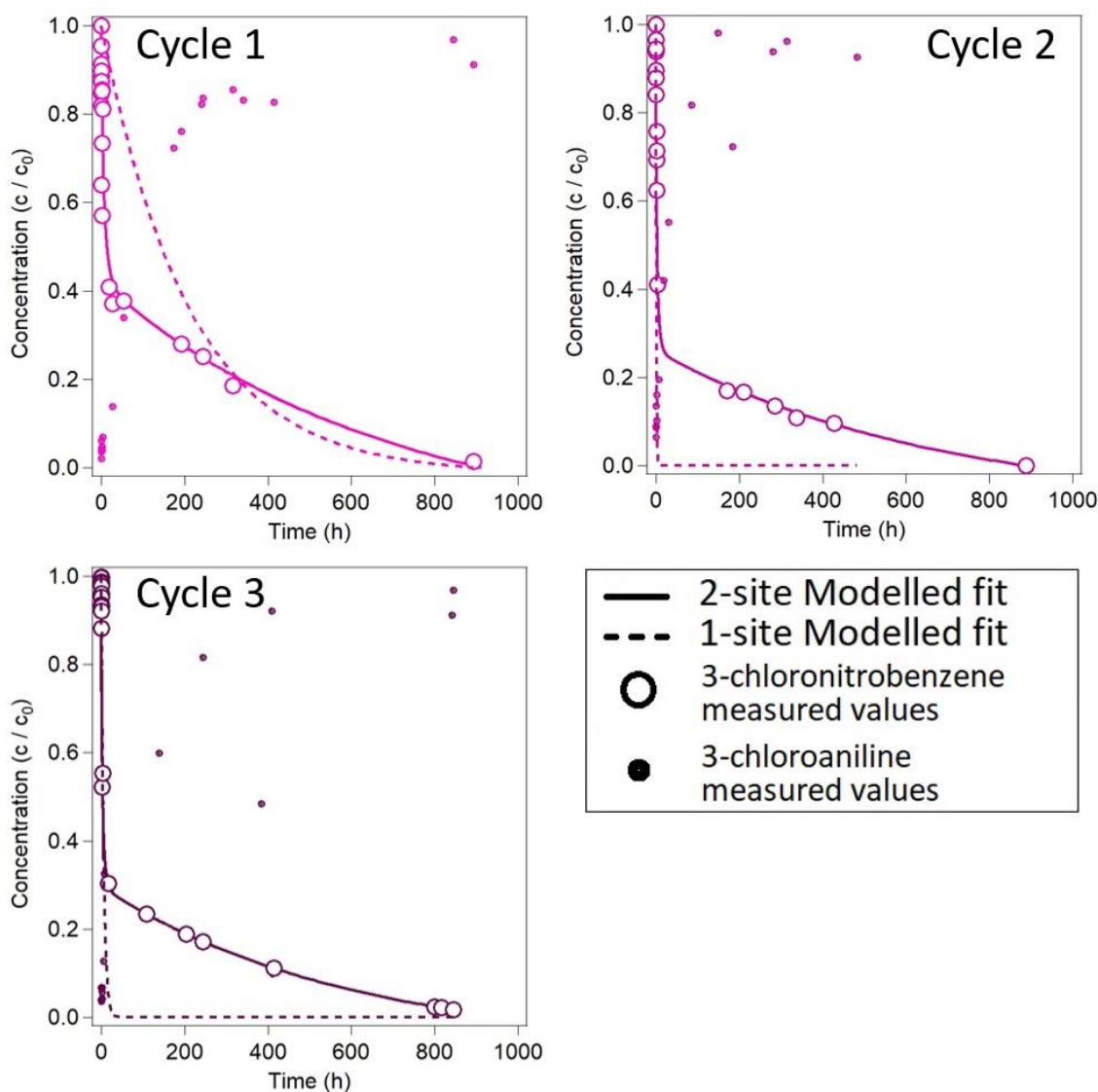


Figure SI 4.4: All kinetic data collected for reaction of AH_2DS -reduced $NAu-1$ with 3-chloronitrobenzene over 3 cycles of reduction. Measured data is large rings, 2-site modeled fit is unbroken line, 1-site modeled fit is dashed line, measured values for 3-chloroaniline product are small coloured dots.

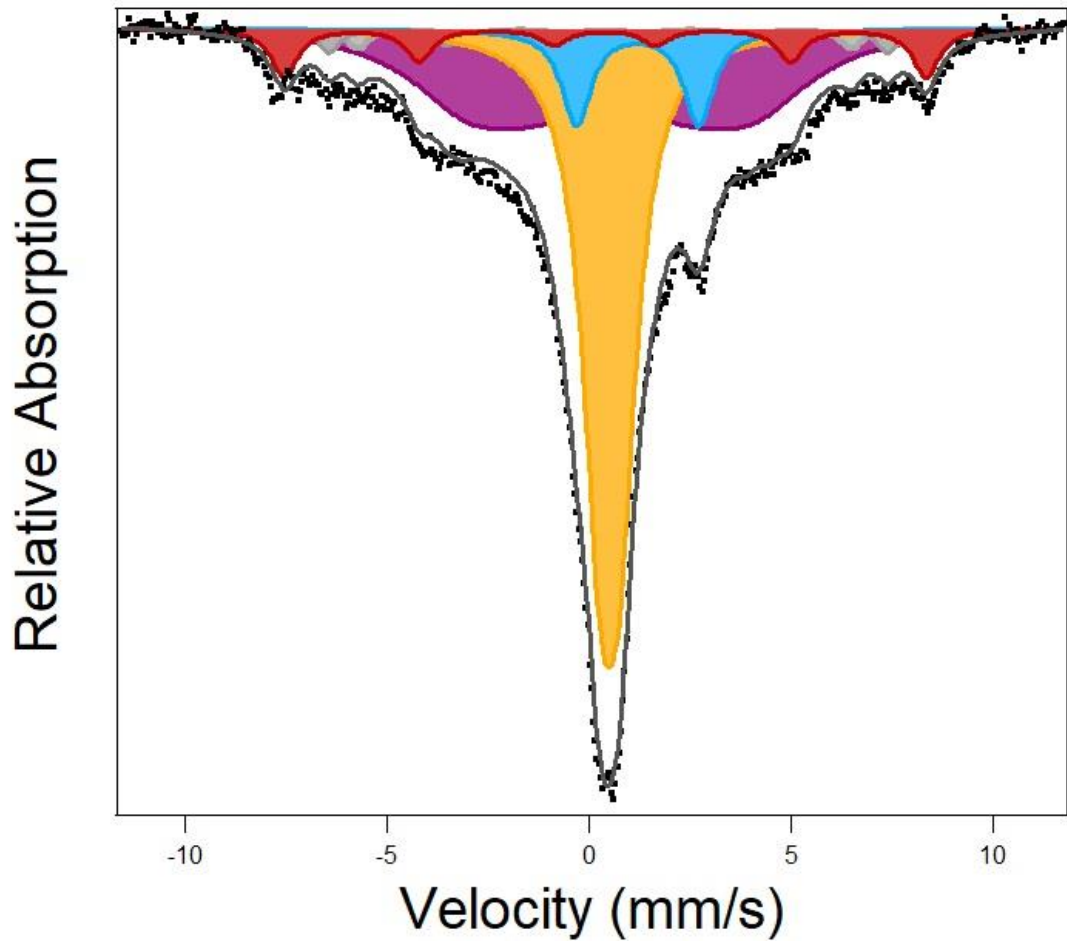


Figure SI 4.5: Mössbauer spectrum of Nau-1 dithionite-reduced to 9% Fe(II)/Fe_{Tot}, measured at 4k temperature, fitted with full-static Hamiltonian technique. Orange is Fe(III) doublet, Blue is Fe(II) doublet, purple is poorly-resolved feature, red is Fe(III) sextet species

Assessing the sustainability of Fe-bearing clay mineral redox reactions

Chapter 4: Redox cycling with reduced electron shuttling compounds

Table SI 4.1: Electron balance to calculate electron transfer during oxidation of AH₂DS and reduction of NAu-1. Includes calculated reduction extent expected based off electron balance, and includes measured NAu-1 reduction extent values from HF mineral digestion and Mössbauer spectroscopy.

	Cycle 1	Cycle 2	Cycle 3
AQDS calculated before reaction with NAu-1 (M)	0.000167	0.0000284	0.0000606
AQDS calculated after reaction with NAu-1 (M)	0.000516	0.000349	0.000307
AH ₂ DS calculated before reaction with NAu-1 (M)	0.000549	0.000562	0.000397
AH ₂ DS calculated after reaction with NAu-1 (M)	0.000200	0.000241	0.000151
AH ₂ DS oxidised to AQDS by reaction with NAu-1 (M)	0.000349	0.000321	0.000246
Electrons transferred to NAu-1 (M)	0.000698	0.000642	0.000492
Total structural Fe present in suspension (M)	0.00716	0.00590	0.00464
Equivalent structural Fe reduced to Fe(II) (%)	9.7	10.8	10.6
Reduction extent measured via HF digestion and phenanthroline assay (%)	7.2	8.5	9.8
Reduction extent measured with Mossbauer Spectrometry (%)	9.1	9.3	10.1

Chapter 5: Effects of redox cycling via biologically-mediated, abiotic reduction – impact on clay mineral structure and secondary precipitates

5.1 Introduction

In the preceding chapter (Chapter 4) experiments demonstrated that redox cycling clay minerals using electron shuttle AQDS (electrochemically reduced to AH₂DS) as reductant was sustainable. The results indicated that reduction by the electron shuttle had little effect on either structure or reactivity, and any changes were reversible upon reoxidation. The reversibility of electron-shuttle reduction could suggest that it is not microbial *reduction* that causes irreversible transformations of clay minerals, but perhaps instead the various other biogenic processes and products resulting from microbial metabolism. Microbes have a substantial impact on the chemistry of natural systems, and there are a plethora of ways in which microbial activity can impact clay minerals.

The value of clay minerals with regards to redox reactions is that clay minerals are believed to be more resistant to reductive dissolution than other Fe minerals. Naturally occurring Fe-oxide and -oxyhydroxide minerals such as goethite, lepidocrocite, and hematite are readily dissolved by microbial reduction (Arnold et al. 1988, Bonneville et al. 2004). The dissolution of Fe minerals by microbial reduction leads to increased concentrations of aqueous Fe(II) within sediments and porewaters (Zachara et al. 2002). Aqueous Fe(II) atoms can interact with clay mineral surfaces. Studies have demonstrated interfacial electron transfer from Fe(II) atoms sorbed to clay mineral surfaces (Schaefer et al. 2011, Neumann et al. 2013). In the environment, the reduction by aqueous Fe(II) is an indirect result of microbial activity (i.e. mineral dissolution) within the system, and as such is described as biologically-mediated, abiotic reduction. A study by Latta et al. (2017) demonstrated that electron transfer from Fe(II) can occur by either edge-sites or via the basal plane. Additionally, further work has demonstrated that electron transfer from sorbed Fe(II) can cause significant atom exchange between the aqueous and mineral phase (Neumann et al. 2015). Research has not yet understood how this reduction pathway might impact the sustainability of clay minerals over multiple reduction-oxidation cycles.

Furthermore, the oxidation of aqueous Fe(II) by electron transfer to structural Fe(III) also results in the formation of secondary precipitate minerals including Fe-oxyhydroxides, and mixed valent minerals similar to green rusts (Schaefer et al. 2011, Tsarev et al. 2016, Jones et al. 2017). Previous work has indicated that the formation of these secondary minerals can influence the reactivity of system towards contaminants (Rothwell 2018, Entwistle et al. 2019).

This chapter investigates how subjecting Fe-rich clay minerals to multiple cycles of reduction by Fe(II) and reoxidation with hydrogen peroxide impacts both the structure and reactivity of the clay mineral. Fe(II)-reduced clay minerals are reacted with probe contaminant 3-chloronitrobenzene to measure the effects of redox cycling on transformation kinetics. Solid sample analyses are conducted using X-ray Diffraction (XRD) and Mössbauer spectroscopy to study changes in structure and Fe speciation caused by Fe(II) redox cycling. Additionally, we attempt to characterise the secondary Fe minerals formed during the process. Isotope specific Mössbauer allows the precision measurement of both clay mineral structural Fe, and the secondary minerals separately. This chapter aims to answer the following questions:

Do multiple cycles of reduction by Fe(II) impact the sustainability of the clay mineral?

What secondary Fe minerals form, and how do they impact the system reactivity?

How are the secondary minerals altered during the redox cycling process?

5.2 Methods

5.2.1 Reduction-oxidation cycling of N_{Au}-1 with aqueous Fe(II)

All reduction-oxidation, and contaminant transformation experiments were conducted in an anaerobic chamber (GS Glovebox Systemtechnik GmbH, Germany) under a N₂ atmosphere (≤ 1 ppm O₂) unless stated otherwise. Deoxygenation of all solutions and suspensions was carried out by bubbling N₂ for 1 hour.

5.2.1.1 Mineral preparation

Native N_{Au}-1 clay mineral samples were prepared for experiments following the procedures described in Chapter 3 (Section 3.2.1.)

5.2.1.2 Stock solution preparation

A 100 mM stock solution of $\text{Fe(II)}_{\text{aq}}$ was prepared to be used as reductant for the NAu-1 in contaminant transformation experiments. Metal Fe(0) powder at natural isotopic abundance was dissolved in 1 M HCl by mixing with magnetic stirrer for 3 hours at 60 °C. The solution was then diluted with deoxygenated, deionized water (DIW) to a final concentration of 100 mM, and finally, filtered using a luer lock, 0.22 μm nylon filter (sourced from Thames Restek Ltd) to remove any remaining solids.

Additional Fe(II) stock solutions were also prepared via the same method, but instead using Fe(0) metallic powder that has been isotopically enriched in the ^{56}Fe (sourced from Trace Sciences International Inc., Purity = 99.92 % ^{56}Fe) or the ^{57}Fe isotope (Isoflex, San Francisco. Purity = 95.02 % ^{57}Fe). These isotopically enriched stock solutions were used in later experiments for Mössbauer analysis.

A pH and ionic strength buffer solution was prepared in excess consisting of 10 mM 3-(N-morpholino)propanesulfonic acid (MOPS) and 50 mM NaCl, dissolved in deoxygenated DIW.

5.2.2 Transformation of contaminant 3-chloronitrobenzene and reaction kinetics experiments

This experiment investigated how redox cycling nontronite NAu-1 using $\text{Fe(II)}_{\text{aq}}$ as the reductant impacted the reaction kinetics towards the reductive transformation of model nitroaromatic contaminant, and kinetic probe compound 3-chloronitrobenzene.

NAu-1 clay mineral samples were subjected to three successive cycles of reduction, using $\text{Fe(II)}_{\text{aq}}$ as reducing agent, and oxidation via H_2O_2 .

Samples and data are categorized by the following naming system, for ease of future reference:

Cycle 1 generally refers to NAu-1 samples that have been reduced once with $\text{Fe(II)}_{\text{aq}}$.

Cycle 2 generally refers to NAu-1 samples that have been reduced with $\text{Fe(II)}_{\text{aq}}$, reoxidised with H_2O_2 , and subsequently re-reduced with $\text{Fe(II)}_{\text{aq}}$ a second time.

Cycle 3 generally refers to NAu-1 samples that have been reduced for a third time with $\text{Fe(II)}_{\text{aq}}$, after two preceding reduction-oxidation cycles.

For some experiments such as solid sample analyses, “Cycle 1 reoxidised” would refer to measurements of the sample described in Cycle 1 after reoxidation with H_2O_2 , and all structural Fe(II) has been oxidised to Fe(III).

5.2.2.1 Reduction-oxidation cycling of N_{Au}-1, using Fe(II)_{aq} as reductant and H₂O₂ as oxidant

Initial reduction (Cycle 1) of N_{Au}-1 with Fe(II)_{aq} was conducted by the following procedure:

Fe stock solution with natural isotopic abundance (Section 5.2.1.2) was added to the deoxygenated buffer solution to achieve a desired concentration of 3.5 mM Fe. 10 μ L samples of buffer + stock solution were taken aside to measure initial concentrations of Fe(II)_{aq} and Fe_{Tot} via colourimetric 1,10-phenanthroline assay (following method described in Schilt (1969)). Powdered N_{Au}-1 nontronite was added to the buffer + Fe-stock solution to achieve a desired mineral loading concentration of 2 g/L. The pH was then adjusted to 7.5 with aliquots of 1 M HCl or NaCl, and the mixture was left overnight to stir via a magnetic stirrer. The following morning, batch reactors were produced from the stock suspension by removing 3 x 15 mL samples and adding to 3 separate 20 mL glass vials. Each batch reactor (15 mL of 2 g/L clay mineral suspension in 20 mL glass vial) was pH-adjusted to 7.5 with 10 μ L aliquots of 1 M NaOH or HCl (as necessary). Reactors were sealed with a butylene rubber stopper, crimp-capped to hermetically seal the contents, then wrapped in aluminium foil to prevent any risk of photo-oxidation. Batch reactors were set aside for contaminant transformation (described later in Section 5.2.2.2), and stored in the anaerobic chamber on an end-over-end rotator. The remaining clay mineral stock suspension was then centrifuged to separate solid material from supernatant and remaining Fe(II)_{aq}. Centrifugation was carried out in centrifuge tubes, sealed and wrapped with PTFE tape to prevent any risk of oxidation. Once solids were separated from supernatant, 10 μ L samples were taken of the supernatant for 1,10-phenanthroline analysis (Schilt 1969) to measure the change in concentration of Fe(II)_{aq} and Fe_{Tot} of solution after reaction with N_{Au}-1. The separated solids were then washed to remove remnant Fe(II)_{aq} and re-suspended in buffer solution at 2 g/L mineral concentration using a magnetic stirrer and left until adequately mixed. Once solid material was adequately resuspended and mixed, the

suspension was removed from the anaerobic chamber. H_2O_2 was added in molar excess in order to assure all Fe(II) present in the suspension was able to be oxidised to Fe(III). The suspension was left exposed to the natural atmosphere overnight, mixing with magnetic stirrer to allow for complete oxidation.

The following day, the oxidised material was washed carefully multiple times with DIW to remove any remnant H_2O_2 , and solids were resuspended in DIW at an equivalent mineral loading concentration (2 g/L). A 20 mL sample was taken from the suspension and set aside for later solid sample analyses.

The bulk, oxidised clay mineral suspension was deoxygenated for 1 hour by bubbling with N_2 , and the solution was brought back into the anoxic, N_2 atmosphere anaerobic chamber. The solution was then centrifuged to separate solid material from supernatant, and the reduction process would be restarted (with some adjustments to concentrations) to initiate Cycle 2.

Using the data collected by 1,10-phenanthroline assay in Cycle 1 for samples of supernatant taken before and after NAu-1 reduction, the difference between the values can be used to calculate the concentration of $\text{Fe(II)}_{\text{aq}}$ that was removed from the solution after reaction with NAu-1 to become solid-associated. The concentration of solid-associated Fe(II) was combined with the total clay mineral present in suspension, to give a molar concentration of total solid Fe present after the Cycle 1 reoxidation.

For the second reduction (Cycle 2), Fe stock solution was added to the deoxygenated buffer solution to achieve a desired concentration of 3.5 mM Fe. 10 μL samples of buffer + stock solution were taken aside to measure initial concentrations of $\text{Fe(II)}_{\text{aq}}$ and Fe_{Tot} via colourimetric 1,10-phenanthroline assay. Solid material from Cycle 1 was added to the buffer + Fe-stock solution and mixed to achieve a suspension with a desired mineral loading concentration of 2 g/L. The pH was then adjusted to 7.5 with aliquots of 1 M HCl or NaCl and the mixture was left overnight to stir via a magnetic stirrer. The following morning, the suspension was then diluted with buffer solution to achieve a total Fe molar concentration (combined solid, structural, and aqueous) equivalent to that of the reactors of Cycle 1. Three 15 mL batch reactors were produced (as described above) from the stock suspension and set aside for

Assessing the sustainability of Fe-bearing clay mineral redox reactions

Chapter 5: Redox cycling with aqueous Fe(II). Biologically-mediated, abiotic reduction

contaminant transformation experiments. The remaining suspension was centrifuged to separate solids from supernatant, and supernatant was analysed via 1,10-phenanthroline assay to measure the change in Fe(II) and Fe_{Tot}. Solids were resuspended at 2 g/L in buffer solution and removed from anaerobic chamber for oxidation via H₂O₂ (as described for Cycle 1). After 24 hours of oxidation, solids were washed to remove remnant H₂O₂, resuspended in DIW, and a 20 mL sample was taken for later solid sample analyses.

The clay mineral suspension was deoxygenated for 1 hour by bubbling with N₂, and the solution was brought back into the anaerobic chamber. The solution was then centrifuged to separate solid material from supernatant, and the reduction process would be prepared for Cycle 3. Again, the concentration of total solid Fe present was calculated using the values measured before and after reaction of Fe(II) with N_{Au}-1 by 1,10-phenanthroline assay.

Cycle 3 followed the same reduction procedure as described for Cycle 2, and again the suspension was diluted after reaction with the aqueous phase to achieve an equivalent total Fe molar concentration as present in Cycle 1 reactors. Three 15 mL batch reactors were prepared as described above and set aside for contaminant transformation. Remaining solid material was separated from supernatant and reoxidised as described in Cycle 2. A 20 mL sample of the reoxidised suspension was set aside for solid sample analyses.

5.2.2.2 Nitroaromatic compound transformation experiments

Probe compound degradation reactions were initiated by injecting 30 µL of methanolic 3-chloronitrobenzene stock solution to give an initial concentration of ~50 µM, using a Hamilton gas-tight, PTFE luer lock, 0.25 mL glass syringe to achieve a starting concentration of ~50 µM in the reactor. A 500 µL sample was taken immediately after spiking using a Hamilton gas-tight, PTFE luer lock, 0.5 mL glass pipette and filtered using a luer lock, 0.22 µm nylon filter (sourced from Thames Restek Ltd) to remove any mineral / solids. The sample was then stored in a clear, 2 mL sealed glass HPLC vial (sourced from VWR™) with conical glass inserts (from Sigma Aldrich) until analysis. For each reactor, more samples were taken in the same method at pre-determined time steps until the transformation of 3-chloronitrobenzene to 3-chloroaniline had reached

completion (i.e. all 3-chloronitrobenzene has been transformed to 3-chloroaniline). All samples were stored in the fridge at 4 °C prior to HPLC analysis.

5.2.2.3 Organic contaminant quantification

The first sample taken from the reactor immediately after spiking with contaminant was used as measurement for initial concentration. Samples measured via HPLC were measured against a set of pre-prepared calibration standards containing both methylated contaminant and product, and diluted with DIW, at 5 specific concentrations (1 µM/L, 12.5 µM/L, 25 µM/L, 37.5 µM/L, and 50 µM/L) in glass HPLC vials (same as used for reactor samples).

Analysis of samples and concentrations of model contaminant 3-chloronitrobenzene (3CNB) and the degradation product 3-chloroaniline (3CAN) were measured using the Agilent 1260 Infinity II HPLC equipped with DAD detector, using an LC-18 column (XBridge C18 3.5 µm).

Samples were measured with a custom HPLC method, using deionized water and methanol in varying proportions as eluent. Figure SI 3.2 shows the custom concentration / time eluent gradient used for each sample.

The HPLC method was conducted as follows: 10 minute total run time per sample. Flow rate was 1 mL / min, and column temperature was kept at 30 °C. 20 mL of sample was injected per analysis. Absorption was measured at wavelengths 214 nm and 252 nm.

5.2.2.4 Data evaluation and kinetic modelling

All measured contaminant transformation were fitted with kinetic models to calculate the intrinsic reactivity of the system. Kinetic modelling followed the methods and equations described previously in Chapter 3 (Section 3.2.5)

5.2.2.5 Solid sample analyses with X-ray diffraction (XRD)

Mineral samples were analysed for characterisation via XRD. Reoxidised XRD samples were produced by centrifuging reoxidised mineral suspensions to separate solid material from the supernatant. The solids were then freeze-dried overnight to remove excess moisture, leaving a solid powder. The dry mineral powders were placed on a zero-background sample holder, and smoothed over with a silicon slide.

The dry mineral samples were measured with a PANalytical X'Pert with X'Celerator detector using the following setup:

Optics: Soller slit = 0.04 rad, Divergence slit = 0.5 °, Beam mask = 20 mm, Anti-scatter slit = 1 °

2theta range: 5–100 °, step size = 0.0334 °, 1 s step⁻¹

5.2.3 Mössbauer analysis with Fe isotopes

As well as understanding the effects of Fe(II)_{aq} redox cycling on the reactivity of the system, a secondary experiment was conducted in tandem. This experiment applied isotope-specific Mössbauer analysis to measure how Fe(II)_{aq} redox cycling impacts the structural Fe coordination within the clay minerals, and to quantify the reduction extent (i.e. % Fe(II) content) of clay mineral structural Fe, as well as the Fe(II):Fe_{tot} ratio of the whole reactor system. The experiment also investigated whether secondary Fe minerals are formed during the process, how these are altered by successive cycles, and what role these might play in the transformation of nitroaromatics.

Using isotopically enriched Fe(II)_{aq} solutions allows isolated measurement and characterisation of different pools of Fe present in the system. Using Mössbauer-visible (⁵⁷Fe), or Mössbauer-invisible ⁵⁶Fe allows the measurement of either clay mineral structural Fe, or of the added Fe(II) reductant separately. A more in-depth explanation, and labelling regime is available later in Section 5.3.3.1.

For the Mössbauer analysis, only 2 reduction oxidation cycles were examined. Samples and data are categorized by the following naming system, for ease of future reference:

Cycle 1 generally refers to NAu-1 samples that have been reduced once with Fe(II)_{aq}.

Cycle 2 generally refers to NAu-1 samples that have been reduced with Fe(II)_{aq}, reoxidised with H₂O₂, and subsequently re-reduced with Fe(II)_{aq} a second time.

For note: each cycle also has its respective reoxidised spectrum. For example, "Cycle 1 reoxidised" would refer to measurements of the sample described in Cycle 1 after reoxidation with H₂O₂, and all structural Fe(II) has been oxidised.

5.2.3.1 Redox cycling process used to create samples for Mössbauer analysis

The following section describes the redox cycling process for N_{Au}-1 samples to be used for Mössbauer analysis. Unlike the kinetic experiments (Section 5.2.2), samples measured by Mössbauer were not sub-samples separated from a bulk suspension. Instead, new samples were processed each time, and redox cycling was ceased at the desired stage of examination. For instance, for a Mössbauer spectrum of "Cycle 2 reoxidised N_{Au}-1", a new sample would be prepared and cycled, with the process stopped after the second reoxidation. The sample would then be analysed by Mössbauer.

The redox cycling process is as follows: 30 mg of powdered, native N_{Au}-1 was added to a 20 ml glass vial (wrapped in foil to prevent any later unintentional photo-oxidation) and brought into the N₂ atmosphere anaerobic chamber. 100 mM Fe(II)_{aq} stock solution enriched with required isotope (⁵⁶Fe or ⁵⁷Fe) was added to deoxygenated buffer stock solution (Section 5.2.1.2) in a separate 50 mL glass beaker to achieve a concentration of 3.5 mM Fe(II)_{aq}. The stock solution mixture was adjusted to pH 7.5 by adding minute increments of 1 M NaOH or HCl as required, and a 10 µL sample was taken and stored for a later 1,10-phenanthroline assay (Schilt 1969) to measure the initial concentration of Fe(II) and Fe_{Tot}. The stock solution buffer mixture was then added into the aluminium foil-wrapped glass vial containing the 30 mg of powdered N_{Au}-1, to a mineral loading concentration of 2 g/L. The vial was then sealed with a butylene rubber stopper, crimp-capped to hermetically seal the contents, mixed using a vortex mixer for 10 seconds to allow particle dispersal, and left to stir overnight on an end-over-end rotator. The following day, the reactor vial was decrimped and the contents were added to centrifuge tubes, sealed with PTFE tape and centrifuged at 11000 rpm for 15 minutes to separate solid minerals from supernatant. The centrifuged tubes were then returned to the anaerobic chamber and the supernatant poured into a separate vessel; a sample of supernatant was taken for a later 1,10-phenanthroline assay.

Samples to undergo further second and third reductions were resuspended in DIW and removed from the anaerobic chamber for subsequent oxidation via H₂O₂ oxidation. Oxidation followed the same procedure as described in Section 5.2.2.1, but no sub-

samples were separated for solid analysis. After washing with DIW and deoxygenation solid samples were transferred back to the anaerobic chamber, and Cycle 2 would repeat the process to the oxidised solid mineral material.

Mössbauer spectra were fitted using the commercial software Recoil (Ottawa, Canada) using Full Static Hamiltonian site analysis for samples displaying magnetic ordering and Voigt based fittings for samples where magnetic ordering was not visible. Reduction extent was the principal analysis objective.

5.2.3.2 Mössbauer analysis

Solids were separated from supernatant via either prolonged centrifugation or with a 0.2 µm nylon filter under anaerobic atmosphere. The sample solids were sealed in Kapton tape to prevent oxidation during transfer to the Mössbauer spectrometer.

Samples were analysed using an S4 Mössbauer spectrometer (SEE Co., Edina, MN, U.S.A.) in transmission mode and calibrated against 7 µm α-Fe(0) foil. Temperature during spectra acquisition was controlled with a closed cycle cryostat (SHI-850, Janis Research Co., Wilmington, MA, U.S.A.) at either 77 K or 4 K temperature to allow for quantifying Fe oxidation state and the Fe speciation of the clay mineral.

Spectra were analysed using the software Recoil, using Voigt-based fitting routine for spectra measured at 77 K temperature, and Full-static Hamiltonian fitting routine for samples measured at 4 K temperature.

5.2.4 Contributions

Dr Jamie Gould provided technical guidance and operational assistance for XRD measurements.

5.3 Results and Discussion

5.3.1 Contaminant transformation with Fe(II)-reduced NAu-1

To understand how multiple cycles of reduction via Fe(II)_{aq} and reoxidation (with hydrogen peroxide) impacts the reactivity of the minerals, reduced NAu-1 was used to reductively degrade a probe compound. Fe(II)-reduced NAu-1 was reacted with 3-chloronitrobenzene and the concentration of both the model contaminant and product (3-chloroaniline) were measured in time course experiments. The concentrations of these reactants and products were measured with HPLC, and

transformation curves were fitted using the kinetic model defined by the equations described in Chapter 3 (Section 3.2.5).

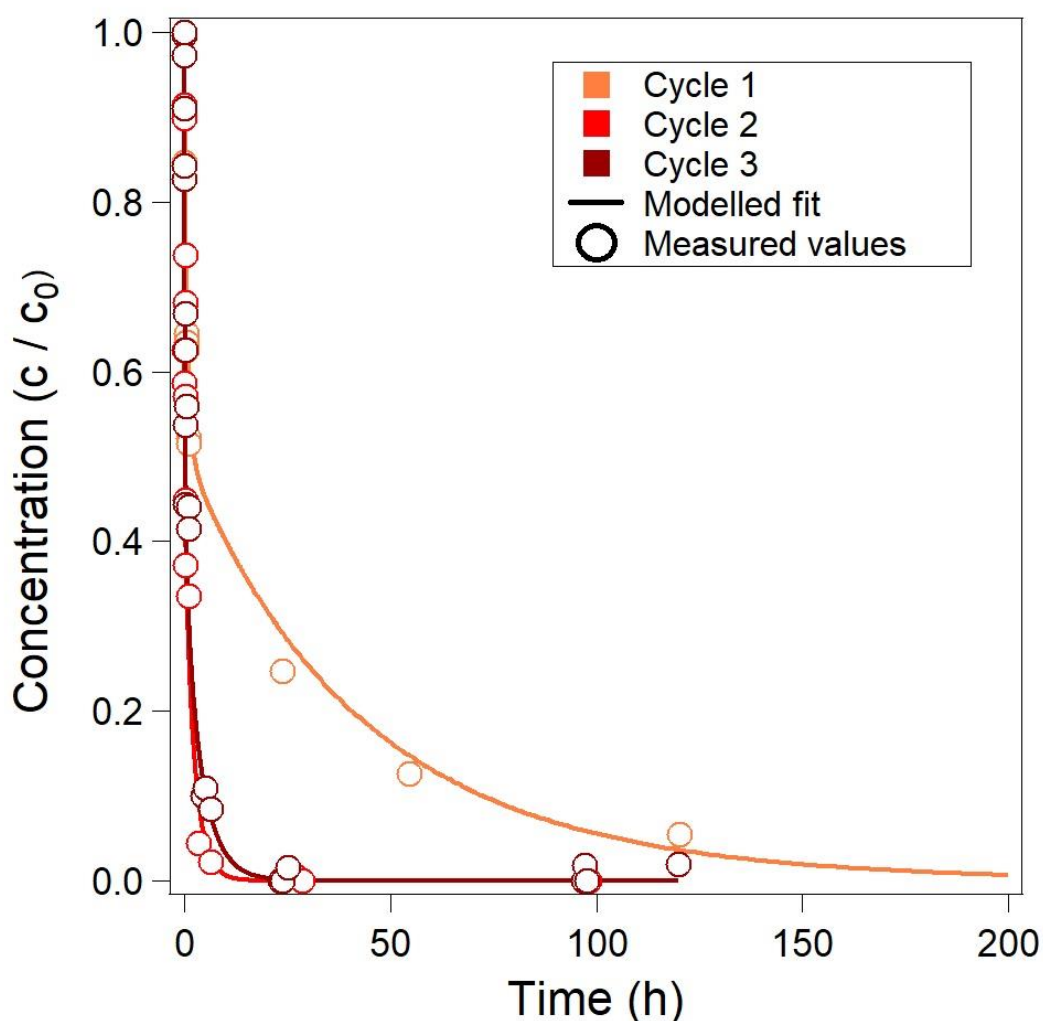


Figure 5.1: Typical time course concentration measurements (circles) of 3-chloronitrobenzene during reaction with NAu-1 that has been reduced with Fe(II)_{aq}. Results were obtained in the presence of reduced NAu-1 (Cycle 1), reduced-reoxidised-rereduced NAu-1 (Cycle 2) and reduced-reoxidised-rereduced-rereoxidised-rererduced NAu-1 (Cycle 3), as described in Section 5.2.2. Coloured lines show the fit to the two-site kinetic model (defined in Equation 3.1).

Figure 5.1 shows the measured concentrations of 3-chloronitrobenzene (3CNB) during reaction with NAu-1 reduced by 3.5 mM aqueous Fe(II) over 3 successive reduction cycles, and the corresponding modelled fits of kinetic degradation. In Cycle 1 the concentration of 3CNB decreases gradually over time, and the reaction reaches completion after roughly 200 hours. The degradation profile is confirmed to reach completion in the measured accumulation of the product compound 3-chloroaniline (as shown in Figure SI 5.1), where there is an increase until the concentration of the product equals that of the initial spike of 3CNB.

The measured concentration data was initially fitted with a one-site reactive model to conform to a first order rate law (see Figure SI 5.1). However, it is evident that the measured values and the one-site model do not agree, and that the first order rate model was insufficient to appropriately describe the data.

When examining the first reduction cycle, the 3CNB transformation appears to follow two distinct phases. First, an initial stage of rapid transformation where around 50% of the contaminant was transformed in the first 12 hours of reaction. Then, the reaction changed to a more gradual change with the concentration declining over the following few days. The measured data was then fitted with a kinetic model comprising two reactive sites for contaminant degradation, which was developed previously for highly reduced Fe-rich clay minerals (Neumann et al. 2008). This model is the same as used previously in both of the previous Chapters 3 and 4, and was described in detail previously (see Section 3.2.5). It is evident from visual inspection of the modelled curves that this two-site model produces a far more accurate description of the measured data. The good agreement between experimental data and model fit implies the existence of two distinct reactive Fe(II) sites present in the system that determine the transformation rate and curve shape. A first highly reactive site that dominates transformation during the initial stages, and a second less reactive site which gradually becomes the prevailing influence over time. The adherence to a two-site reactive model is typical for reduced, Fe-rich clay minerals (e.g. Neumann et al. 2008, Neumann et al. 2009).

When compared with other experiments, the contaminant transformation of Cycle 1 observed in isolation produces results comparable to those of other reduction pathways. For instance, the first cycle degradation fitting looks similar to the fittings produced in the dithionite-reduced and AQDS-reduced NAu-1 of Chapters 3 and 4 (see Section 3.3.1, Section 4.3.2). This fitting pattern has also been demonstrated in previous research. Rothwell (2018) investigated the transformation of 2-acetylnitrobenzene in the presence of Fe(II)-reduced NAu-1, and observed a similar rate and profile of degradation. This study also demonstrated that the two-site model is applicable to Fe(II)-reduced, Fe-rich clay minerals, and that rates are comparable with those of dithionite-reduced minerals. The study however did not investigate

beyond the initial reduction for any potential effects of multiple cycles. Previous experiments demonstrated that three successive reduction-oxidation cycles using either dithionite or AQDS as reductants did not lead to any significant changes to the rate of reaction (Figures 3.1, 3.2, and Figures 4.4, 4.5). In contrast, Figure 5.1 shows that for Fe(II)-reduced NAu-1 the rate of reaction rapidly increased after the first cycle, and in Cycle 2 the reaction reached completion in under 24 hours. This rapid degradation is also reflected in the corresponding aniline concentrations (see Figure SI 5.1). Both Cycle 2 and 3 were also tested with a one-site model, and as with the first cycle in both cases the one-site model was insufficient to appropriately describe the measured data values (see Figure SI 5.1). Cycles 2 and 3 both also show the same biphasic pattern of the initial rapid decrease in concentration followed by a more gradual decline afterwards, although the reaction takes place on a much shorter time scale. Cycle 3 appears similar to Cycle 2, and there is no increase to the speed of transformation to the extent seen in the previous cycle. The transformation curves displayed in Figure 5.1 appear to indicate that reactivity is dramatically improved after Cycle 1, but then remains consistent after Cycle 2.

Assessing the impact of redox cycling to the rate of contaminant transformation qualitatively is limiting. However, the kinetic model can also provide quantitative analysis of the observed changes to reactivity seen after Cycle 1.

5.3.2 Analysis of contaminant degradation kinetics

The kinetic model takes into account the concentration of Fe(II) present in the system, and this can be used to quantitatively assess the intrinsic reactivity of the system. The kinetic fit can yield the rate constant values for the contaminant transformation, as well as calculate the concentrations of both highly reactive and less reactive sites on the clay surface, implicit in the adherence to the two-site model. The two reactive sites will be referred to hereafter as site A (highly reactive), and site B (less reactive).

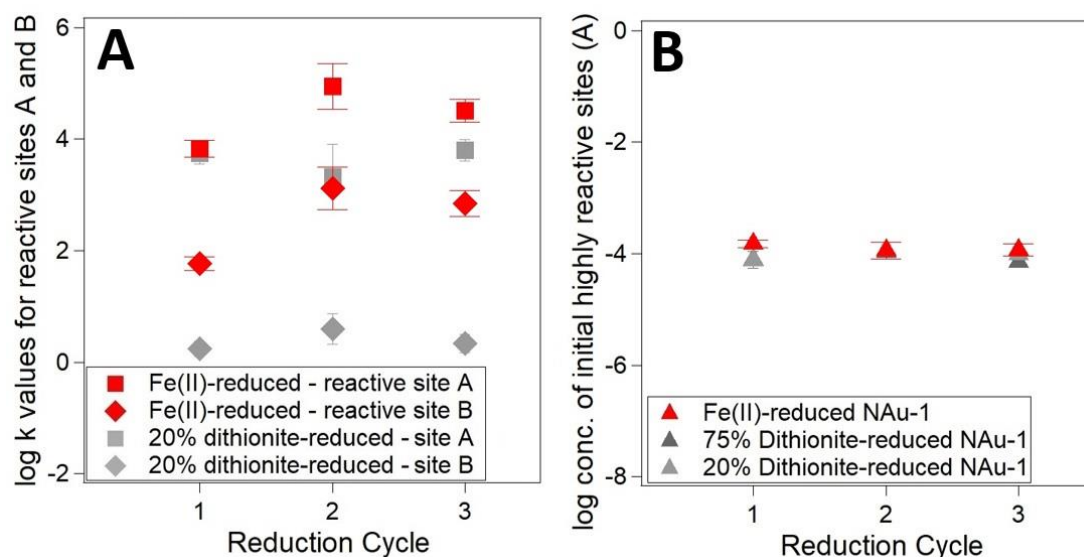


Figure 5.2: Figure A shows the logarithm of rate constants (k) for 3CNB degradation with 3.5 mM Fe(II)-reduced NAu-1 (red markers) and low (20 %) extent dithionite-reduced NAu-1 (grey markers, data from chapter 3) resulting from each of the 3 reduction-oxidation cycles. Squares mark highly reactive site log k values, and diamonds represent less reactive site log k values. Figure B shows the logarithms of the initial concentrations of highly reactive sites (A) in 3.5 mM Fe(II)-reduced NAu-1 (red) and dithionite-reduced NAu-1 to high (75 % - dark grey) and low (20 % light grey) extent. Error bars are defined by 1 standard deviation.

Figure 5.2 shows the calculated kinetic parameters for Fe(II)-reduced NAu-1 over 3 reduction-oxidation cycles. In Figure 5.2 (A) the changes in the log of the kinetic rate constant (k) are visible. The kinetic rate constant in this instance is described as the intrinsic reactivity of a defined electron donor species. For Cycle 1 it is evident that the rate constant values for site A (highly reactive) are two orders of magnitude greater than those of site B (less reactive). Rate constant values for both reactive sites significantly increase over an order of magnitude on Cycle 2, with the log k value for site A rising from 3.8 to 4.9, and the log k value for site B rising from 1.8 to 3.1. This increase in reactivity reflects the modelled fittings where there was a clear increase in the rate of reaction between Cycle 1 and 2. The rate constant values of Cycle 3 decrease slightly in comparison to Cycle 2, however the change is not significantly different after accounting for error (based on 1 standard deviation). This result also aligns with the modelled fitting where Cycle 2 and 3 are largely similar. The difference between the rate constant values for site A versus site B remains similar across all three cycles (a difference of roughly 2 orders of magnitude), which suggests cycling does not impact one reactive site to a greater extent than the other.

Figure 5.2 also features kinetic parameters calculated for 20 % dithionite-reduced NAu-1 (taken from Figure 3.2) for comparison. The site A rate constant for both Fe(II)-

reduced and dithionite-reduced NAu-1 are almost identical, with a log k of 3.8 and 3.4 respectively. However, the rate constant value of site B for the Fe(II)-reduced sample is 1.5 orders of magnitude greater than the value for the dithionite-reduced sample. This result aligns well with previous research. Rothwell (2018) investigated the effect of one reduction with Fe(II) on the reactivity of NAu-1 towards the transformation of 2-acetylnitrobenzene. The study compared the results with NAu-1 reduced with dithionite to equivalent reduction extents and observed that the rate constant values for the highly reactive sites did not differ significantly, whereas the less reactive sites were significantly increased. The different choice of probe compounds (2-acetylnitrobenzene vs 3-chloronitrobenzene) in each study means the log k values determined are not directly comparable, because different nitroaromatic contaminants have different one-electron reduction potentials ($E_h^{1'}$) values and therefore will react with the minerals at different rates (Klausen et al. 1995). However, it is reasonable to expect similar trends of transformation. The log k values measured by Rothwell were lower than those achieved in this study despite equal conditions (pH, mineral loading, and concentrations of contaminant and Fe). This result might be due to 3-chloronitrobenzene having a more positive $E_h^{1'}$. This could mean that it possesses a greater tendency to be reduced than 2-acetylnitrobenzene. Indeed, Klausen et al. (1995) also measured increased rate constant values for 3-chloronitrobenzene reduction by Fe-minerals, compared to 2-acetylnitrobenzene.

While the specific rate constant values may differ between the two studies, the findings and conclusions proposed by Rothwell are consistent with the data of this experiment. The increased log k values in the less reactive site B were determined by Rothwell as evidence for the formation of new reactive Fe(II) sites in the system. The differing reaction kinetics between dithionite-reduced and Fe(II)-reduced nontronite (at equal *structural* Fe(II):Fe_{tot}) is likely to be due to the differing *total* Fe(II) content within the system. While it has been shown that aqueous Fe(II) alone cannot reduce nitroaromatics (e.g. Klausen et al. 1995), the Rothwell study proposed a number of possible explanations to the effects of Fe(II) reduction on the kinetics. Firstly, the increased Fe(II) may have allowed a recharging effect of the NAu-1 structural Fe, providing improved reactivity for site B. Secondly, the study noted a significant fraction of aqueous Fe(II) was removed from solution and became solid-associated. This effect

Assessing the sustainability of Fe-bearing clay mineral redox reactions

Chapter 5: Redox cycling with aqueous Fe(II). Biologically-mediated, abiotic reduction

was also observed in this study (see table 5.1), where in Cycle 1 85% of aqueous Fe(II) was removed from solution after contact with NAu-1. It is possible that the solid-associated Fe formed additional reactive Fe sites in secondary solid phases.

Table 5.1: Concentration values for the added Fe stock solution before and after reaction with NAu-1, describing the volume of Fe removed from solution to become solid associated, and as a percentage of the initial aqueous Fe(II) added. Table also displays the as the Fe(II)/Fe_{Tot} ratio of the reactor at the moment before kinetic experiments commence.

Reduction cycle	Aqueous Fe(II) conc. before Nau-1 reduction (mM/L)	Aqueous Fe(II) conc. post Nau-1 reduction (mM/L)	Aqueous Fe(II) conc. post Nau-1 reduction (% of initial stock solution)	Solid-associated Fe(II) conc. post NAu-1 reduction (mM/L)	Solid-associated Fe(II) post reduction (% of initial stock solution)	Fe(II)/Fe _{Tot} ratio
1	3.5	0.54	15.40	2.96	84.60	0.33
2	3.5	0.20	5.80	3.29	94.20	0.30
3	3.5	0.16	4.60	3.33	95.40	0.25

The study by Rothwell however only measured the first cycle, and did not measure the effects of subsequent re-oxidation and re-reduction of the mineral with Fe(II). Our modelled fitting data shows that the second cycle of reduction has a severe impact on the rate of reaction, an effect previously unseen by prior research. As with the modelled fit (Figure 5.1), reduction Cycle 2 shows notably increased reactivity with significant rise in K values when compared with Cycle 1 and with dithionite-reduced values. Both reactive sites increased by over an order of magnitude, with the log k values for the highly reactive sites changing from 3.83 to 4.94, while the less reactive sites increased from 1.76 to 3.12. The cause of this increase on the second cycle must be investigated.

In the second reduction, samples were reduced with the same concentration of Fe(II) (3.5 mM) and Table 5.1 shows that a greater percentage (94%) of aqueous Fe(II) concentration was removed from solution into the solid phase than Cycle 1 (85%). However, in Cycle 2 the concentration of reduction equivalents in the system (i.e. concentration of Fe(II)) cannot explain the observed effects on kinetics for the following reasons. After the clay mineral reduction with aqueous Fe, Cycle 2 and Cycle 3 reactors were diluted to ensure an equal concentration of total Fe to the Cycle 1 reaction, before contaminant transformation occurred. Table 5.1 shows the Fe(II)/Fe_{Tot} ratio within the reactor for each cycle, and shows that the ratio remains relatively unchanged albeit with a minor decreasing trend due to the increased Fe(III) from the reoxidation. This means that Cycle 2 achieved over an order of magnitude greater

reactivity towards the probe compound than Cycle 1 despite an equal concentration of total Fe, and an equal or smaller Fe(II):Fe(III) ratio in the system.

For Cycle 3, rate constant values are similar to those of Cycle 2 but both reactive sites show a minor decrease. The decrease in rate constants is within error and therefore is not considered significant. This result is comparable to the modelled fittings of Figure 5.1, where there were very similar results between cycles 2 and 3, with a slight decrease in speed of reaction on the latter. This result indicates that the most significant effect on the reactivity of the system occurs after the first cycle has been oxidized. Additionally, after Cycle 2 has been re-oxidized, any further redox cycling causes negligible impact on the system reactivity.

The kinetic model can also be used to calculate the initial concentration of highly reactive sites (CA0 hereafter) present in the clay mineral. Interestingly, the results (Figure 5.2B) suggest that reduction-oxidation cycling causes no measured changes to the initial concentration of initial highly reactive sites over 3 cycles. In addition, the concentration values calculated for Fe(II)-reduced nontronite are equivalent to the values resulting from the analysis of the kinetics of 3CNB degradation by dithionite-reduced N Au-1. The Rothwell study (2018) also found Fe(II)-reduced N Au-1 produced highly comparable CA0 values to dithionite-reduced experiments.

Rothwell (2018) also investigated the nature of the intrinsic reactive sites described by the fitting in N Au-1 reduced with aqueous Fe(II). The study concluded that when reduction extent of the mineral is below 30%, the highly reactive sites (i.e. site A) are most likely to be a dioctahedral Fe(II) atom bound to an Fe(III). At greater reduction extents, increased Fe(II)-Fe(II) interaction led to a trioctahedral configuration, however the study did not achieve such reduction extents when using Fe(II) as the reducing agent. The study also found that the highly reactive sites showed similarities, and were highly comparable in nature for both dithionite and Fe(II)-reduced N Au-1. The less reactive sites (i.e. site B) did not show the same similarities between the two reduction pathways and were very different in nature. The study suggested that the less reactive Fe sites were comprised of different species for both dithionite and Fe(II)-reduced N Au-1, and that in the latter case the sites were new Fe(II) species associated with phases formed by the electron transfer reaction between aqueous and structural Fe.

The observed rise in rate constant values for Cycle 2, but negligible difference in initial concentration of highly reactive sites suggests that reactivity is increased despite no change in relative abundance of highly reactive sites. One explanation for this effect is that cycling with Fe(II) causes impacts to the clay mineral structure that make octahedral Fe substantially more reactive than when reduced with dithionite. However, there are many arguments as to why this is unlikely. Firstly, if this were the case it would be expected that these alterations would be observed in Cycle 1, or that one might see an additive effect with each subsequent cycle. We would expect to see the changes begin on the first reduction cycle, with similar or cumulative effects on the second. When exactly repeating the same reduction process there is no logical reason why this would cause significant changes on the second cycle but not the first. Similarly, if the changes to reactivity measured are intrinsic to the clay mineral it does not follow that Cycle 1 and Cycle 2 would each cause different effects. Rothwell (2018) has shown that reduction with either Fe(II) or dithionite produces the same species of highly reactive sites on the first reduction cycle. As the electron transfer mechanism produces the same reactive sites for Cycle 1, it does not follow that a different mechanism would occur on the second cycle under the same conditions.

Secondly, previous research has shown that reducing Fe-bearing clay minerals to a low % of structural Fe(II)/ Fe_{Tot} (reduction extent) tends to produce results that are largely indistinguishable, regardless of reduction pathway (Ribeiro et al. 2009). In addition, previous studies have shown that electron transfer from Fe(II)_{aq} to Fe-rich clay minerals only tends to achieve low reduction extents (e.g. Schaefer et al. 2011, Neumann et al. 2013, Rothwell 2018, Entwistle 2021). The experiments of the previous chapters similarly demonstrated that at low reduction extents there was little difference between the kinetic effects of reduction via dithionite versus electron shuttles such as AQDS (i.e. Section 4.3.4). There is therefore little evidence to suggest that changing the source of the electron donated should impact the kinetics to the extent observed with Fe(II).

Another explanation for the rise in reactivity after Cycle 2 is that rather than an increase in the intrinsic activity of the reactive sites, the results instead reflect the formation of new reactive species. The kinetic model was designed to describe the

kinetics of the reactive Fe within the system, and initially it was assumed that this reactive Fe was within the clay mineral. The model takes into account the total concentration of Fe(II) and allocates this reactive Fe into two pools, one with high rate constant values and one with a low rate constant value. While it was designed for discriminating the presence of variability in clay mineral structural Fe, the model itself cannot determine exactly what Fe species the two pools represent. It is clear that the model works well to describe this system, which has been demonstrated to possess increased solid-associated Fe(II). It is therefore possible that the model is describing new reactive sites external to the clay mineral.

There are multiple points of evidence that could suggest the formation of new reactive Fe species. Firstly, previous research (Rothwell 2018) concluded that the increased reactivity of the less reactive sites observed in Fe(II)-reduced N_{Au}-1 was caused by formation of additional reactive sites. It was determined that these additional reactive sites were formed by the electron transfer reaction between the aqueous Fe ion and the structural Fe on the initial reduction, but the exact nature of the sites was largely undefined.

Secondly, it has been well documented that the oxidation of aqueous Fe by solid minerals can lead to the formation of secondary minerals such as magnetite, surface-sorbed / complexed Fe(II), or green rust species (e.g. Misawa et al. 1974, Genin et al. 2005, Tsarev et al. 2016, Jones et al. 2017). It is possible that the secondary minerals are also reactive towards nitroaromatics (e.g. Klausen et al. 1995, Hostetter et al. 2006) which might explain the newly formed reactive sites described by Rothwell (2018). Concomitant to this, the complete reoxidation of the system after Cycle 1 means that Cycle 2 reactors contained a new previously absent pool of solid Fe formed by the oxidation of the added Fe from Cycle 1. Previous studies have shown that the reaction of aqueous Fe(II) with Fe-oxides and -oxyhydroxides can promote transformation to reactive mixed valent species (e.g. Tamaura et al. 1984, Pedersen et al. 2005, Colón et al. 2006, Gorski et al. 2009). The interaction between the residual oxidized Fe from Cycle 1, and the new aqueous Fe of Cycle 2 may lead to the further transformation and formation of new highly reactive Fe sites absent in Cycle 1.

Considering the changes in reactivity are possibly due to the formation of secondary Fe species, a further spectroscopic analysis was conducted to characterize the solid-associated Fe present within the system.

5.3.3 Characterisation of Fe species, and impacts of Fe(II) redox cycling on mineralogy

To understand the cause of the observed increase in reactivity towards nitroaromatic contaminants, the study analysed the effects of reduction oxidation cycling on the Fe speciation of the system. The experiment involved a combination of wet-chemical analyses, isotope-specific ^{57}Fe -Mössbauer spectroscopy and XRD analysis to identify and monitor different solid-associated pools of Fe in our system, specifically: (1) Fe bound in the structure of clay minerals and; (2) solid-associated Fe that resulted from the removal from solution / precipitation of aqueous Fe(II) in the presence of added solids (Cycle 1: NAu-1/ cycles 2+3: NAu-1 plus Fe oxidation product).

5.3.3.1 Characterisation of clay-associated Fe species and mineralogy with Mössbauer spectroscopy

Mössbauer spectroscopy allows ultra-high-resolution analysis of the binding environment of Fe atoms, allowing a deeper insight into how solid-bound Fe is organised within the system.

A combination of Mössbauer-visible and Mössbauer-invisible Fe isotopes were used to allow targeted measurement of each specific pool of Fe (i.e. clay mineral structural Fe, and added Fe(II)). Solutions enriched with ^{56}Fe are Mössbauer-invisible, meaning using this isotope as the reductant allows us to study the impacts of Fe(II) reduction on the clay mineral structural Fe alone. Alternatively, ^{57}Fe isotope is highly Mössbauer-visible. Clay minerals naturally have a very low abundance of ^{57}Fe , which means using solutions enriched with ^{57}Fe as the reducing agent can produce a Mössbauer reading for the aqueous phase orders of magnitude greater than the clay mineral structural Fe content. This produces a spectrum where the reading of the enriched $^{57}\text{Fe(II)}$ reductant masks the absorption of the structural Fe, making the reading of the structural Fe essentially invisible. Isotope-specific Mössbauer allows the precision observation of specific pools of Fe within the system, allowing us to examine how both the clay mineral and the added Fe(II) are altered by the reaction.

Assessing the sustainability of Fe-bearing clay mineral redox reactions

Chapter 5: Redox cycling with aqueous Fe(II). Biologically-mediated, abiotic reduction

To simplify the description of the analysis conducted, a visual symbol system was produced to help label each spectrum. Figure 5.3 describes the labelling process that has been applied to our Mössbauer analysis.

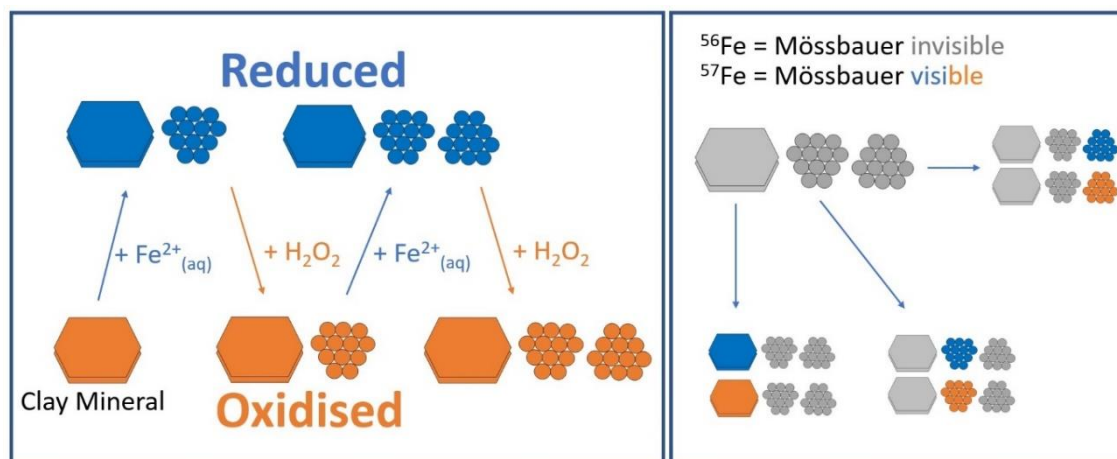


Figure 5.3: diagram describing the process of redox cycling with Fe(II) (left), where the hexagon represents the clay mineral structural Fe, and the cluster shapes represent the added Fe(II) reductant. Blue symbolises that the Fe pool is in a reduced state (i.e. contains Fe²⁺) and Mössbauer visible, orange indicates an oxidised state and Mössbauer visible, grey indicates the Fe pool is Mössbauer invisible. (right) demonstrates which Fe pools are visible / invisible per experiment.

To begin, ⁵⁶Fe (i.e. Mössbauer-invisible) was used as reductant in order to examine the effects of redox cycling on the clay mineral structural Fe. This experiment was conducted to provide an insight into whether interaction of NAu-1 with Fe(II)_{aq} causes any alterations to the clay mineral structure that might be responsible for the observed kinetics. Preliminary Mössbauer measurements were conducted at 77 K temperature, allowing a quantitative assessment of sample oxidation state. As the most significant kinetic alterations occurred between Cycle 1 and Cycle 2, the Mössbauer analysis focused primarily on only 2 cycles of reduction and oxidation.

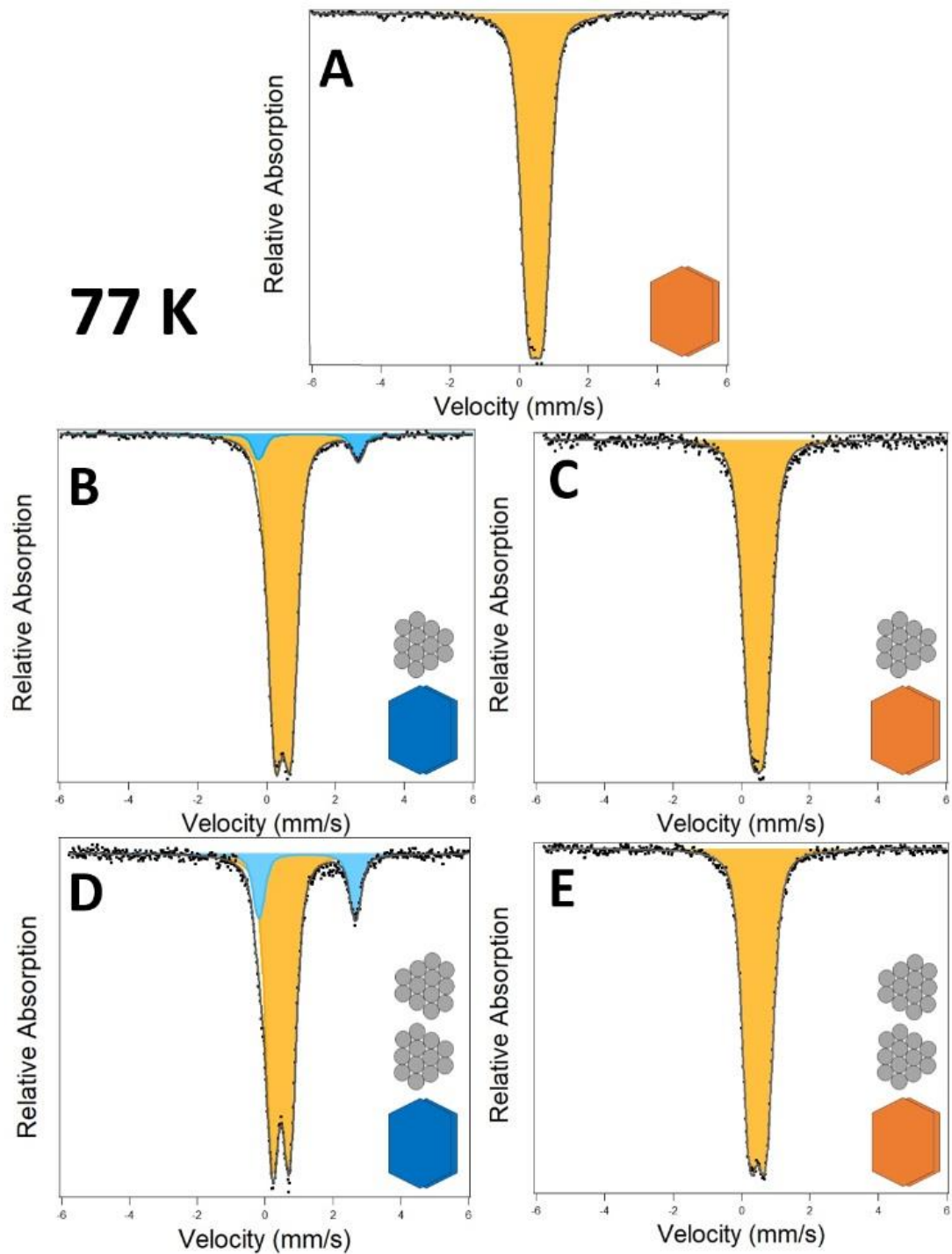


Figure 5.4: Mössbauer data measured at 77 K temperature showing effect of Fe(II) reduction on clay mineral *'structural Fe'* over 2 cycles of reduction-oxidation. A) Native Spectra, B) ^{56}Fe -reduced NAu-1, C) ^{56}Fe -reduced-reoxidised NAu-1 at 77 K, D) ^{56}Fe -reduced-reoxidised-reduced NAu-1, E) ^{56}Fe -reduced-reoxidised-reduced-reoxidised NAu-1. Fit using Voigt-based fitting technique.

Figure 5.4 shows the Mössbauer spectra of NAu-1 reduced by aqueous $^{56}\text{Fe}(\text{II})$ 77 K. A complete set of Mössbauer parameters can be found in Table 5.2. Figure 5.4 A shows the spectrum for native, untreated NAu-1 produces a single doublet (shown in yellow) with a center shift (CS) parameter of 0.48 mm/s, and quadrupole splitting (QS) value of

Assessing the sustainability of Fe-bearing clay mineral redox reactions

Chapter 5: Redox cycling with aqueous Fe(II). Biologically-mediated, abiotic reduction

0.44 mm/s. These are expected parameters for untreated NAu-1 typical for many nontronite samples, as have been previously documented (e.g. Neumann et al. 2013, Murad and Cashion 2003). A single peak with a low CS and QS suggests that the native mineral contains no Fe(II). A single species also suggests that there are no admixtures or mineral contaminants such as Fe-oxides present. In comparison, Figures B and D represent the spectra for the samples after the addition of $^{56}\text{Fe(II)}_{\text{aq}}$. Both show the presence of a doublet (shown in light blue) with high CS and a high QS values (~ 1.23 mm/s and 2.85 mm/s respectively) indicative of structural Fe(II). The presence of the doublet in these figures confirms that Fe(II) is now present, and since the added $\text{Fe(II)}_{\text{aq}}$ is ^{56}Fe and Mössbauer-invisible, the source of this doublet must be clay mineral Fe that has become reduced within the clay structure due to electron transfer from the aqueous Fe(II). The parameters of the Fe(II) doublet agree with those measured in previous studies investigating electron transfer between $\text{Fe(II)}_{\text{aq}}$ and clay mineral Fe (i.e. Neumann et al. 2013).

Table 5.2: Table describing the fitting parameters used for the $^{56}\text{Fe(II)}$ -reduced NAu-1 77 K, over 2 cycles of reduction and oxidation. Table also includes the parameters used to fit the native, unaltered NAu-1 sample.

		CS (mm/s)	QS (mm/s)	σ (mm/s)	% Area
Native NAu-1	Fe(III) doublet	0.48	0.44	0.34	100
^{56}Fe -reduced	Fe(III) doublet	0.48	0.48	0.31	92.95
	Fe(II) doublet	1.22	2.88	0.23	7.05
^{56}Fe -reduced, reoxidised	Fe(III) doublet	0.48	0.47	0.37	100
^{56}Fe -reduced, reoxidised, ^{56}Fe -reduced	Fe(III) doublet	0.47	0.51	0.29	83.14
	Fe(II) doublet	1.24	2.83	0.23	16.86
^{56}Fe -reduced, reoxidised, ^{56}Fe -reduced, reoxidised	Fe(III) doublet	0.47	0.47	0.34	100

In the first cycle, the doublet occupied a relative spectral area of 7 %, indicating a clay mineral Fe reduction extent ($\text{Fe(II)}/\text{Fe}_{\text{Tot}}$) of 7 %. The achieved reduction extent agrees well with previous research where reduction of NAu-1 with aqueous Fe at pH 7.5 typically achieved a $\text{Fe(II)}/\text{Fe}_{\text{Tot}}$ between 5-10% (Neumann et al. 2013). Previous work by Rothwell achieved a marginally higher reduction extent of 8 % $\text{Fe(II)}/\text{Fe}_{\text{Tot}}$ at the same concentration of aqueous Fe(II). The difference between these two values is

Assessing the sustainability of Fe-bearing clay mineral redox reactions

Chapter 5: Redox cycling with aqueous Fe(II). Biologically-mediated, abiotic reduction

negligible and within error, which is 3-5% of spectral area in Mössbauer spectroscopy. Interestingly, the Fe(II) doublet area in spectrum D indicates a Fe reduction extent of 16%, suggesting that twice as much structural Fe in the clay mineral was susceptible to reduction after reoxidation (i.e. in Cycle 2). Although the increase in electron transfer in the second cycle results in higher clay mineral Fe(II) concentration, we suggest that this cannot explain the measured differences in reactivity, as observed as reduction kinetics of the probe compound (Figure 5.2). Comparison with the dithionite-reduced data (see Figure 5.2) shows that the second cycle Fe(II)-reduced kinetics achieved 1.5 orders of magnitude greater than dithionite-reduced samples even with a lower reduction extent. For this reason, the kinetic changes observed in Cycle 2 cannot simply be explained by increased structural Fe(II) content, and instead must imply there has been a qualitative change to the intrinsic reactivity of the system.

Both spectra of reoxidised NAu-1 (Figure 5.4 C and E) revert to a form similar to the native, showing a large central Fe(II) doublet with largely equivalent parameters. The Fe(II) doublets of spectra B and D are no longer present in the spectra after reoxidation which suggests that all the structural Fe(II) has been re-oxidised by hydrogen peroxide. Previous research into reduction-oxidation cycling via dithionite and microbes to low reduction extents has found similar effects, with re-oxidation of the mineral reverting the Mössbauer spectrum to resemble the native (Ribeiro et al. 2009, Stucki 2011). Various studies have shown that the effects of reduction on nontronite are largely reversible, and the degree of reversibility decreases with increasing reduction extent (Lee et al. 2006). In both Cycle 1 and Cycle 2, the extent of reduction is relatively low meaning that any effects on structure due to are reduction would be largely reversible after re-oxidation. Research has not yet investigated the structural impacts of reoxidation after reduction with Fe(II).

The 77 K Mössbauer data indicates that there is electron transfer from the aqueous Fe to the Fe originating in the clay mineral. It appears that the fraction of reducible Fe originating in the clay mineral is increased on the second cycle. Although there is a greater degree of electron transfer in the second cycle, the increase in Fe(II) is relatively small and cannot alone explain the measured effects on reactivity. The questions that need to be addressed are: how is reactive Fe(II) allocated within the

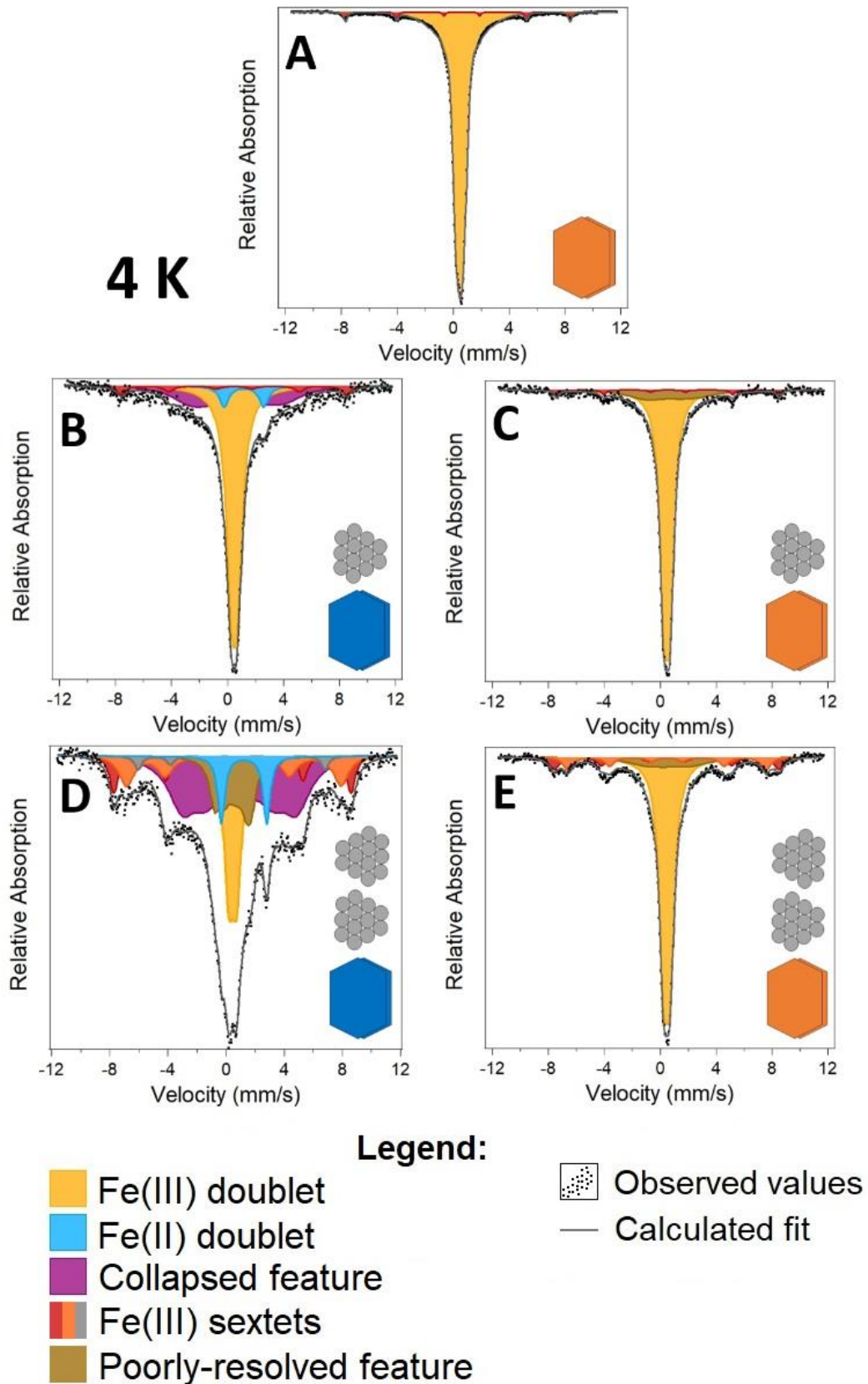


Figure 5.5: Mössbauer spectra collected at 4 K of clay mineral structural Fe over 2 cycles of reduction using Mössbauer-invisible aqueous $^{56}\text{Fe(II)}$ (3.5 mM) and oxidation with hydrogen peroxide. Figure includes: a Native sample spectra (A), a Reduced sample (B), a Reduced, re-oxidized sample (C), a Reduced, re-oxidized, re-reduced sample (D), and a Reduced, re-oxidised, re-reduced, reoxidized sample (E). Spectra fitted using variable line-width (full static Hamiltonian) fitting technique

system and; how does redox cycling impact the speciation of reactive species? A further analysis was conducted on the samples at 4 K temperature to further probe the nature of the clay mineral Fe.

To better understand the binding environments of the clay mineral Fe, Mössbauer analysis of the system at 4 K temperature was conducted, and the spectra are shown in Figure 5.5. Lowering the temperature of measurement from 77 K to 4 K produces a different spectrum, and magnetic interactions between structural Fe atoms begin to occur. The magnetic interactions provide insight into the speciation of Fe within the clay mineral, allowing a more detailed observation of the atomic conditions of structural Fe, and the nature of Fe binding environments.

To allow effective comparison, a spectrum of the unaltered sample was taken (Figure 5.5 A) at 4 K temperature. Like the spectrum taken at 77 K temperature (Figure 5.4 A) it primarily shows only one large doublet. The doublet was fitted with a CS value of 0.50 mm/s and a QS of 0.43 mm/s. NAu-1 absorption spectra typically only shows the presence of Fe(III) doublets (e.g. Murad and Cashion 2004) with low quadrupole splitting values (0.4-0.5 mm/s). The spectrum also features a sextet species with a CS value of 0.48 mm/s, and a hyperfine field of 50 T comprising 5.4 %. This sextet was also seen in the previous chapter (e.g. see Section 4.3.3) and is likely an Fe-oxide contaminant that was not removed during purification.

There are a number of visible differences between the native NAu-1 spectrum (Fig. 5.5 A), and the spectrum of $^{56}\text{Fe(II)}_{\text{aq}}$ reacted with NAu-1 (Fig. 5.5 B), suggesting that reaction with aqueous Fe(II) has affected the structural Fe binding environment. As with the data measured at 77 K temperature (Figure 5.4), the spectrum of NAu-1 reacted with $\text{Fe(II)}_{\text{aq}}$ features an additional doublet (blue) with a high CS and QS parameters (1.2 mm/s and 3 mm/s respectively), indicative of Fe(II). The presence of Fe(II) in spectrum B is further confirmation that electron transfer has occurred from the aqueous phase. The blue doublet has an area of 5.7 %, similar but slightly less than the Fe (II) doublet area from the spectrum collected at 77 K. This would suggest that the majority of the clay mineral Fe(II) in the system is present as this Fe(II) doublet species.

In spectrum B, the base of the spectrum is even broader and has been fitted with a large collapsed feature (shown in purple) with a relative spectral area around 30 %. This collapsed feature has a centre shift (CS) of 0.56 mm/s, which would be typically considered too low to be Fe(II) (Murad and Cashion 2004). This feature has slightly higher CS value than other Fe(III) species measured, however the value still fits within the expected range for Fe(III). It is possible that this is the culmination of multiple species that when overlain are not highlighted individually by the fitting. The increased presence of this species in the reduced state (relative to the native and oxidised state) implies that this may be related to or contain some fraction of Fe(II). By these observations it is reasonable to suggest that this species represents structural Fe(III) that has been influenced by the presence of nearby Fe(II).

There remains a small sextet displayed (shown in red), comprising 6% of the spectral area. The sextet parameters obtained were CS of 0.48 mm/s (indicating ferric iron), and a hyperfine field value of 50 T. This implies that the reduction has had little effect on the Fe-oxide contaminant species.

Upon re-oxidation, the Mössbauer absorption spectrum (Figure 5.5 C) largely resembles that of the native mineral. The central Fe(III) doublet remains and has essentially equivalent parameters to the native spectrum (CS = 0.49 mm/s, QS = 0.44 mm/s). The base of the doublet is however notably wider than in the native spectrum, and has been fitted with an additional poorly resolved feature (brown). The sextet has the same CS and hyperfine field values as those seen in the reduced spectrum and occupies the same relative percentage area. The re-oxidised spectrum suggests that some changes have occurred due to the first Fe(II)-reduction (notably the poorly resolved feature), however the changes appear to be negligible and the spectrum looks largely very similar to the native state. The low reduction extent achieved after the reaction with Fe(II)_{aq} means that this result is largely expected as studies have shown that low reduction extent tends to produce largely reversible impacts on the clay mineral structure (e.g. Gorski et al. 2012). The Fe(II)-reduced, reoxidised spectrum looks similar to the reoxidised spectra produced after reduction by both AQDS and dithionite (see Section 3.3.3, and Section 4.3.3).

In the second reduction cycle with $\text{Fe(II)}_{\text{aq}}$ (Figure 5.5 D), the structural impacts of reduction appear far more pronounced. Results show a growth in relative area of all Fe species (relative to the central Fe(III) doublet) during the re-reduced phase. The spectrum shows the re-appearance of the blue doublet, purple collapsed feature and sextet species except each represents a larger relative % area. The spectrum has also been fitted with an additional poorly resolved feature (brown) with an H value of around 8 T. The low CS value (0.48 mm/s) suggests this species is largely Fe(III). This species could represent Fe material in the onset of magnetic ordering. The Fe(II) doublet maintains a relative area of 6 %, which is equivalent to the first cycle but lower than what was observed in the 77 K spectrum which showed 16 % Fe(II). This indicates that the doublet is only a fraction of the total Fe(II) in the 2nd cycle. The peak of the sextet area (shown in red) has equivalent parameters to the sextet of the re-oxidized Cycle 1 (e.g. CS = 0.5 mm/s, QS = 0.1 mm/s and hyperfine field = 50 T). The spectrum has also been fitted with other sextet species, including one with a H value of 45.5 mm/s. The total % area of Fe that is organized as a sextet has increased from ~6 to ~21 %. The increasing area of sextets with each reduction suggests that structural Fe is being rearranged to form new species with high Fe-Fe interactions allowing the material to magnetically order.

The second cycle spectrum of the Fe(II)-reacted NAu-1 again presents a wide collapsed feature (purple) with a relative area of 40 % of the total Fe. Interestingly, the collapsed species now has a higher CS value (0.87 mm/s) than that of the 1st cycle. The high CS value indicates this species is more associated with Fe(II) than previously in Cycle 1. As the Fe(II) doublet (blue) consists of less % area than the doublet of the 77 K spectrum, some Fe(II) is unaccounted for and the collapsed feature is the most likely Fe species to contain these additional electrons based on the high CS value. The collapsed feature has very similar parameters to the purple collapsed feature observed previously in dithionite-reduced NAu-1 (see Section 3.3.3). In the previous experiments the collapsed feature was described as a mixed-valent species, and it was also seen to increase with multiple cycles as appears to be the case in this experiment. The collapsed feature occupies 40 % of the spectrum, and mathematically must contain the remaining 10 % of the Fe(II) (implicit in the 77 K spectrum). This means that although containing Fe(II) the species will be largely Fe(III), and therefore like the collapsed

feature from Cycle 1, likely highlights that structural Fe(II) is impacting neighbouring Fe(III). Another possible explanation is that the collapsed feature is the culmination of multiple Fe species, formed from material that has been dissolved from the clay mineral and mixed external secondary minerals. If clay mineral Fe has been dissolved and redistributed into secondary minerals, this might lead to a mixed-valent Mössbauer reading with poor resolution. This dissolution and redistribution might also explain why the reducible Fe is increased on the second cycle, as structural Fe has been redistributed to secondary minerals which are more accessible to reduction. Previous research has investigated the extent of atom exchange between aqueous Fe(II) and NAu-1 at pH 7.5 (Neumann et al. 2015) and noted that less than 5 % was exchanged within the first 24 hours. If the sextet species alone are evidence for preferential Fe dissolution and re-precipitation, the potential extent of atom exchange could be much greater than 5 %. However, this previous study only examined the initial reaction of NAu-1 with Fe(II)_{aq} (i.e. Cycle 1), and did not account for a system where other Fe-minerals were present as may well be the case in this sample. Overall, the second reduction of NAu-1 with Fe(II)_{aq} appears to produce more exaggerated effects on the structure of the clay mineral than the first reduction, and it is possible this might relate to the increased kinetics.

The Cycle 2 reoxidized spectrum (Figure 5.5 E) looks highly similar to the Cycle 1 spectrum (Figure 5.5 C), and all Fe(II) species such as the blue doublet have disappeared which indicates that all Fe(II) has been successfully oxidized. The central Fe(III) doublet is fit with similar parameters to those of both the native and the Cycle 1 re-oxidized spectra, but there is a significant increase in relative area for the magnetically ordered sextet species. The sextet component present after reaction of NAu-1 with aqueous ⁵⁶Fe(II) was preserved into oxidation (21% total spectral area), and the additional distinct sextet is confirmed in the spectrum (orange). The red sextet (50 T) has an area of 10% (almost double the area of the sextet in Cycle 1), and the additional sextet (orange) composes an area of 11 %. The orange sextet has been fitted with hyperfine parameters typically indicative of lepidocrocite (specifically, H of 46 T). This is significant as any species visible to Mössbauer must be produced with Fe originally within the clay mineral. This result is strong evidence to suggest that

structural Fe has been dissolved out of the clay mineral, and has been incorporated into the external secondary Fe-oxide minerals.

Both the wide collapsed feature, and the narrow poorly resolved species have disappeared, which suggests that these alterations were largely reversible. The disappearance of the large collapsed feature of the reduced state (purple) upon reoxidation strengthens the hypothesis that this feature is an effect of reduction the clay mineral octahedra, rather than the formation of a separate mineral phase.

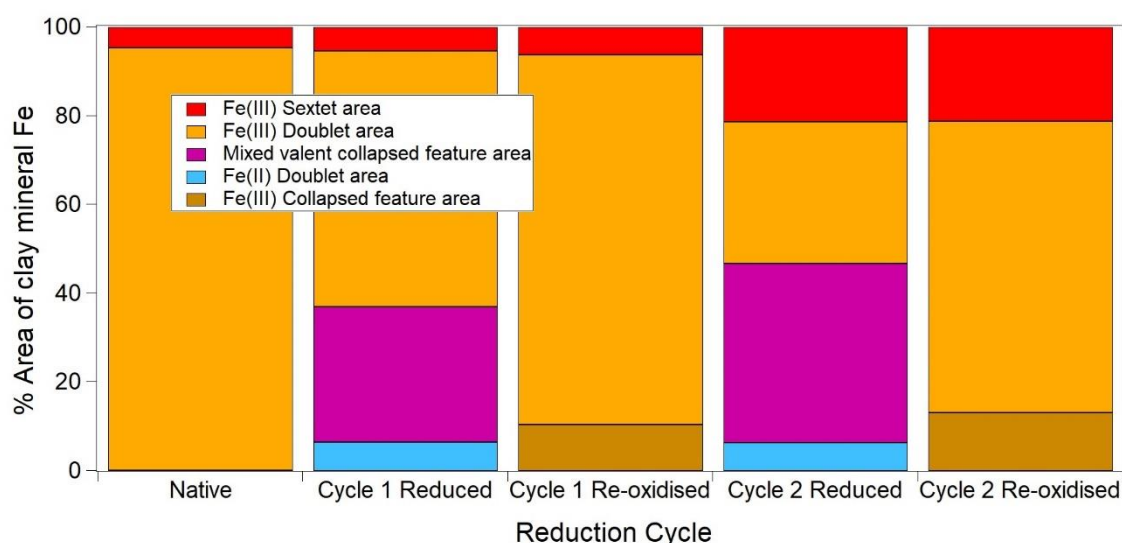


Figure 5.6: Relative areas of Fe components resulting from Full-static Hamiltonian fits of Mössbauer spectra of samples across cycles 1 and 2, . Mössbauer spectra were collected at 4 K.

Figure 5.6 shows how the relative proportions of each Fe binding environment change over the two cycles of reduction with $\text{Fe(II)}_{\text{aq}}$ and reoxidation. The figure demonstrates the gradual transformation of the native spectrum from a single (orange) doublet to a mixture of speciations, over the 2 cycles.

The combined evidence from Mössbauer analysis of the clay mineral Fe indicates that reduction-oxidation cycling with aqueous Fe(II) does cause some irreversible alterations to the clay mineral structure. Firstly, the increasing extent of reduced Fe suggests that changes to the structure create more Fe that is accessible to receive electrons from the added $\text{Fe(II)}_{\text{aq}}$. In addition, the increased area of the Fe(III) sextets indicates that a portion of the structural Fe is re-organized into structures with greater magnetic ordering, and similar binding environments to the external Fe-oxides produced by oxidation. This is strong evidence to indicate that octahedral Fe is dissolved out and reincorporated into the secondary intermediate minerals. The

greater relative % of the purple collapsed feature between Cycle 1 and Cycle 2 suggests that reduction is causing rearrangements of the structural Fe within the octahedral sheet that accumulate with each cycle. Ultimately, the area of the original Fe(III) doublet decreases on each cycle to be replaced by other distinct components (such as the sextets) implying that Fe(II)-reduction cycling causes irreversible structural alterations, despite only achieving a low reduction extent.

While the evidence implies that the clay mineral structure is impacted by reaction with the $\text{Fe(II)}_{\text{aq}}$, the observed changes alone do not provide a clear explanation for the effects on kinetics. New Fe speciations that arise in the Fe(II)-reacted N Au-1 spectra (Figure 5.5 B and D) are either Fe(III) (e.g. the sextets) and therefore unreactive, or are species that have been previously observed in the dithionite-reduced N Au-1 experiments such as the purple collapsed feature. The reduction extent does increase from Cycle 1 to Cycle 2, but the extent is still far smaller than that achieved with dithionite. Furthermore, many of the structural effects appeared reversible upon oxidation, whereas the kinetics suggest that a major and permanent change occurred on the second reduction (evidenced by the negligible difference in reactivity between Cycle 2 and 3). These observations further the hypothesis that clay mineral structural Fe alone cannot be primarily responsible for over an order of magnitude increase in reactivity measured on reduction Cycle 2 (Figure 5.2 A). If the clay mineral Fe does not provide a clear explanation, then the remaining added Fe(II) must play a significant role in the observed kinetics.

5.3.3.2 X-ray Diffraction Spectroscopy Results

It is possible that reduction-oxidation cycling with Fe(II) and H_2O_2 leads to the formation of secondary minerals within the system. Visual examination of the oxidised samples showed that the colour changed to a light orange colour (shown in Figure SI 5.2), this colour is typical for Fe-oxyhydroxides such as lepidocrocite, which strongly suggests that secondary Fe-oxide minerals have formed. X-ray diffraction (XRD) can provide an accurate assessment of the various crystalline minerals present in a sample. Samples were taken from the bulk suspension for XRD analysis during the previous kinetics experiments (Sections 5.3.1, 5.3.2), providing solid mineral samples for 3 successive reduction-oxidation cycles.

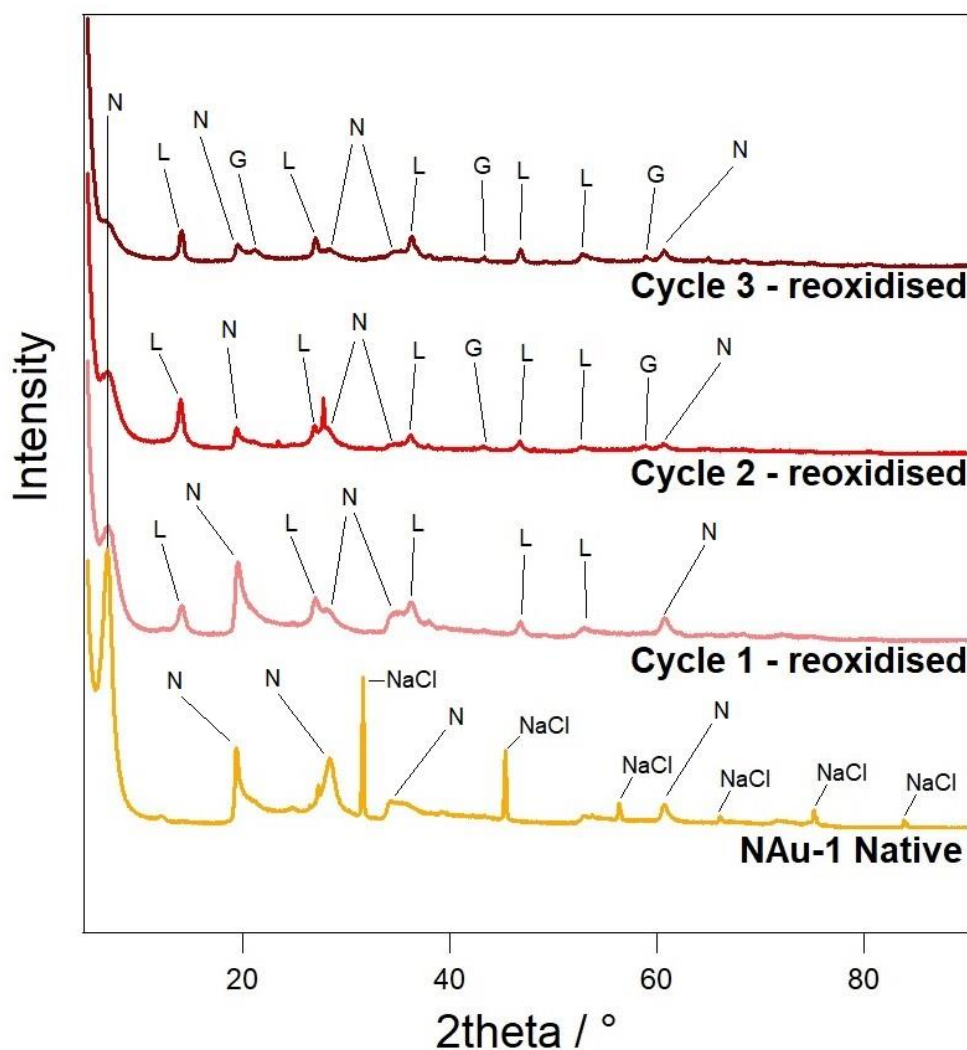


Figure 5.7: X-ray diffraction spectra of the Fe(II)-reduced, re-oxidized NAu-1 over 3 cycles: Cycle 1 = pink, Cycle 2 = red, Cycle 3 = brown. Also shown is the spectrum of the native NAu-1 sample for comparison (orange). Relevant peaks have been highlighted with "N" as the native NAu-1 peaks, "L" highlighting lepidocrocite, "G" highlighting goethite, and "NaCl" highlighting unintended NaCl crystal contaminations.

A series of XRD scans were conducted on samples taken during the experiment to understand the bulk mineralogical changes of crystalline phases within the system, and to investigate whether redox cycling causes the formation of any secondary minerals. Initial scans focused on the re-oxidised samples from each stage of the cycle, as these could be examined outside the anaerobic chamber without any risk of accidental oxidation. Reduced samples required the use of an anaerobic dome holder to prevent oxidation, yet the geometry of this holder produced a large background between 12 and 35° 2θ that impaired phase identification (see Figure SI 5.4). Figure 5.7 shows the XRD spectrum for the native, untreated NAu-1 as well as the re-oxidized samples from cycles 1, 2 and 3. The native spectrum (orange) presents several large peaks, which remain visible across the 3 cycles of reduction and oxidation, but diminish in intensity.

The loss of intensity in the peaks is uniform across all the N Au-1 peaks, which could suggest that there the N Au-1 crystals are becoming less crystalline with each reduction-oxidation cycle (McCusker et al. 1999). While the peaks decrease in relative intensity, the 2-theta value of each peak stays consistent suggesting that despite a trend towards becoming less crystalline, there are no significant changes in composition occurring. The native spectrum also contains an unintended contamination of NaCl crystals highlighted in the figure, which are absent in the other spectra due to removal by dissolution. When comparing the re-oxidized spectra with the native, it is clear several secondary peaks appear which were previously absent in the native spectrum. A diffraction pattern closely aligned with lepidocrocite was present in all 3 cycles, and small traces of what appeared to be goethite was also present (most noticeably in Cycle 3). This information is strong evidence to indicate that lepidocrocite is the primary oxidation product after addition of H₂O₂. The results also confirm that solid Fe-oxide minerals were present in the system during the reduction phase of Cycles 2 and 3. However, lepidocrocite is a typically expected product for the rapid oxidation of solid mixed-valent Fe minerals (such as green rusts), as well as aqueous Fe(II) (Misawa et al. 1974). Subsequently, the XRD data alone cannot provide an insight into the nature of the solid-associated Fe in the reduced phase, or any oxidation product of aqueous Fe(II) after reaction with the clay mineral. Mössbauer spectroscopy can provide more insight to the state of the Fe precipitates before oxidation.

5.3.3.3 Formation of secondary minerals – effects of cycling on precipitates

It is evident that the clay mineral structural Fe alone cannot be responsible for the significant increase in reaction kinetics observed for N Au-1 reduction-oxidation cycled with Fe(II)_{aq}. The experiment has demonstrated that the system also contains another pool of solid-associated Fe(II) that could potentially be the source of the increased reactivity.

The results from the preliminary XRD scans highlight the mineralogy present after oxidation with H_2O_2 , but do not provide insight into the nature of solid-associated Fe in the reduced phase. Understanding the oxidised mineral content alone also cannot explain the changes in reaction kinetics measured, particularly the significant increase in reactivity measured in reduction Cycle 2.

Previous research (Entwistle 2021) noted that the reaction of $\text{Fe(II)}_{\text{aq}}$ with N Au-1 can lead to the formation of secondary reactive intermediate minerals which can play a crucial role in the transformation of organic contaminants. Although the study monitored the transformation of a different contaminant and at a higher pH, the research concluded that the reactors containing secondary Fe materials were more effective at contaminant transformation than reactors containing reduced N Au-1 alone. The study conducted a further ^{57}Fe isotope-specific Mössbauer analysis to interpret how the nature and speciation of the solid-associated Fe(II) added as a reductant is altered over multiple cycles of reduction and oxidation.

To monitor the fate of the added aqueous Fe(II) and changes in its binding environment over the first two reduction-re-oxidation cycles, we collected Mössbauer spectra at 77 K of samples that were reacted with Mössbauer-visible $^{57}\text{Fe(II)}$ as the reducing agent. Using aqueous Fe(II) enriched in the ^{57}Fe isotope allows observation of the impact to the $\text{Fe(II)}_{\text{aq}}$ upon reaction with the clay mineral. The ^{57}Fe isotope is Mössbauer-visible but comprises only 2.2 % of natural abundance. By enriching the reducing $\text{Fe(II)}_{\text{aq}}$ solution with ^{57}Fe , it is possible to diminish the relative reading of the clay mineral Fe to less than 3 % of the total spectral absorption. This allows us to focus on the spectra produced by the reducing agent, and therefore understand how this pool of Fe is impacted during the reduction-oxidation cycling. It is also possible to understand how the added $\text{Fe(II)}_{\text{aq}}$ of one cycle is affected in another cycle. By repeating the experiment and precisely choosing either ^{57}Fe or ^{56}Fe as the reducing agent, it is possible to visualise the changes in speciation of the added $\text{Fe(II)}_{\text{aq}}$ for both the 1st or 2nd reduction and across multiple cycles.

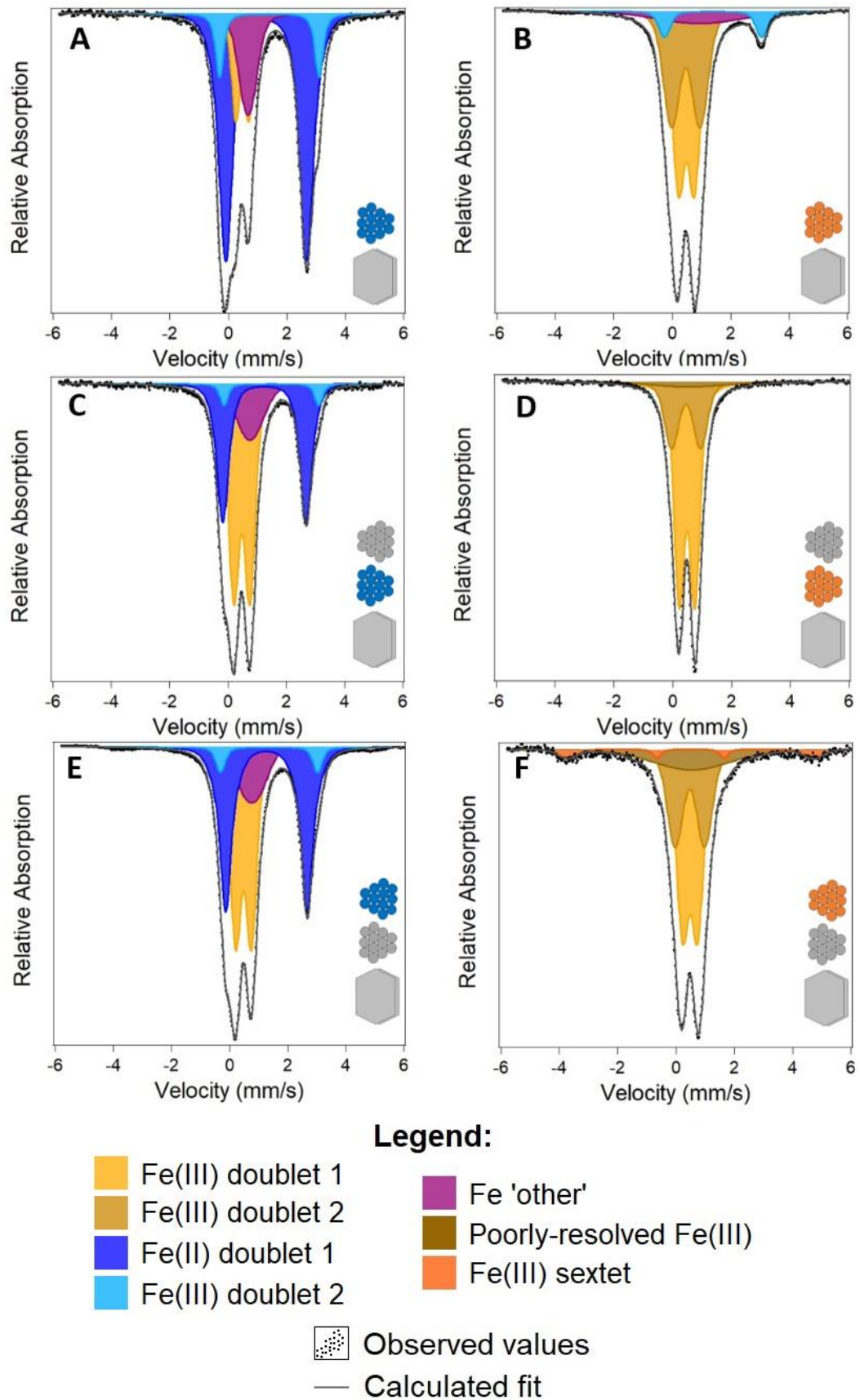


Figure 5.8: Mössbauer fitting spectra of the ^{57}Fe -reduced NAu-1 at 77 K temperature. Figure includes the first reduction cycle ^{57}Fe -reduced (A) and re-oxidized (B), ^{57}Fe -reduced-reoxidized- ^{56}Fe -reduced (C) and subsequent re-oxidised (D), and also ^{56}Fe -reduced-reoxidised- ^{57}Fe -reduced (E), and subsequent reoxidised spectrum (F). All spectra fitted with voight-based fitting technique

Figure 5.8 shows the Mössbauer spectra for the added Fe(II)_{aq} reductant after reaction with NAU-1 over 2 cycles of reduction and oxidation with H₂O₂. The fitting parameters are outlined in Table SI 5.2. Initial observation shows that the spectra differ significantly from the clay mineral spectra (see figure 5.5). As the samples were filtered and washed sufficiently to remove all traces of the supernatant before measurement, the presence of spectra dissimilar to NAU-1 confirms that a large fraction of the added Fe(II)_{aq} has been removed from solution to become solid-associated. This is consistent with previous research that has shown that the reaction of Fe(II)_{aq} with NAU-1 at pH 7.5 leads to nearly complete removal of Fe(II) from solution (Neumann et al. 2013, Rothwell 2018). From the results collected in Section 5.3.3.2 results have determined that electron transfer occurs from the added Fe(II)_{aq} to the clay mineral structural Fe. Electron transfer from the aqueous phase causes partial oxidation of the added Fe(II)_{aq}, and so far results have confirmed the presence of the oxidised product. Figure 5.8 A shows the spectrum of ⁵⁷Fe(II)_{aq} with NAU-1, and shows 4 distinct doublet species. The orange doublet has a relative area of 14 % of the spectrum and was fitted with a CS value of 0.47 mm/s and a QS of 0.44 mm/s, which are consistent parameters typically expected for Fe(III) (Murad and Cashion 2003). The presence of the orange doublet is further evidence that oxidation of the added Fe(II)_{aq} has occurred, and in its place is the product Fe(III).

Figure 5.8 A also shows two doublets (light and dark blue) with high CS and QS values, typical for Fe(II) (Murad and Cashion 2003). It is expected that the remainder of spectral area would be Fe(II), as almost all Fe(II) was removed from solution but only a small fraction was oxidised by the clay mineral. The larger doublet (dark blue) comprises 61% of the spectral area and was fitted with two components and has a CS of 1.29 mm/s, and the average QS of the two components is 2.81 mm/s. The smaller doublet (light blue) has a CS of 1.40 mm/s and a QS of 3.40 mm/s. A study by Neumann et al. (2013) investigated the adsorption of Fe(II)_{aq} to smectitic clay minerals over a range of pH values. The study highlighted the differing Mössbauer parameters of sorbed Fe(II) to different clay mineral sites. The parameters of the large dark blue doublet of Fig. 5.8 align very closely with the parameters of either edge-bound Fe(II) at pH 7.5, or is also similar to the Fe(II) doublet parameters of octahedral Fe(II) as observed in the dithionite-reduce NAU-1 (see section 3.3.3). The parameters of the

smaller light blue doublet align well the parameters of Fe(II) sorbed to the basal plane.

The ratio of small doublet : large doublet is 1:6.

The spectrum has also been fitted with a rounded single peak (purple) comprising 14.5 % of the area, with a CS of 0.68 mm/s, and a QS of 0.3 mm/s. Parameters for this species are lower than the range typically expected for Fe(II), but similarly the CS value is higher than most other Fe(III) species observed thus far which might indicate it is an Fe(III) species affected by the neighbouring presence of Fe(II). This species was also observed in the results of Entwistle (2019) where it was also characterised as Fe(III).

In total, the relative percentages of oxidation state indicates that approximately 29 % of the solid-associated Fe(II) was oxidised after reaction with the clay mineral which equates to 0.26 mM of Fe. In contrast, the clay mineral spectrum (see Figure 5.5 B) had a reduction extent of approximately 7 %, which would equate to 0.12 mM of Fe. This discrepancy in the results suggests there is a disconformity, and 0.1 mM of Fe (approximately 10-13 % of the reductant) has been oxidised, for which the electrons are unaccounted for. This discrepancy might be due to heterogeneities between samples, and accounting for the margin of error inherent with Mössbauer fittings. Nevertheless, the presence of Fe(III) in the sample is evidence that the aqueous phase has been oxidised by the clay mineral. Fe(III) is much less soluble than Fe(II) so most at pH 7.5 would be expected to have precipitated out of solution. Previous studies have reported that the interaction between aqueous Fe(II) and clay minerals can lead to the formation of secondary solid Fe species including ferrihydrite, and mixed valent Fe-oxyhydroxides such as “green rusts” (e.g. Schaefer et al. 2011, Tsarev et al 2016, Jones et al. 2017). From this information it is reasonable to suggest that secondary Fe precipitate minerals are formed after the reaction of Fe(II)_{aq} with N Au-1.

Upon reoxidation (Figure 5.8 B), the spectrum changes to show 2 ferric doublets, with similar CS but differing QS values. Most notably, spectrum B still contains a ferrous Fe(II) doublet suggesting that a fraction of Fe(II) is not reoxidised, despite addition of hydrogen peroxide and prolonged exposure to the oxic atmosphere. The doublet fits the same parameters as the smaller light blue doublet of Fig 5.8 A, which suggests it might represent Fe(II) sorbed to the basal plane (Neumann et al. 2013). The source of this Fe(II) doublet is uncertain. One explanation might be that subjecting the solid-

associated Fe(II) fraction to rapid oxidation via H_2O_2 produced a layer of Fe(III)-oxide minerals that isolated pockets of Fe(II), armouring or occluding fractions from oxidation. However, if this was the case one would expect to see a fraction of unoxidized Fe(II) in the second cycle too. Another explanation is that after reaction with the clay mineral, the oxidation of $\text{Fe(II)}_{\text{aq}}$ causes precipitation of Fe and the formation of secondary minerals where a fraction of Fe(II) is inaccessible to oxidation at the surface. The 77 K spectrum does not offer sufficient information to conclusively determine the nature of this doublet.

While 77 K Mössbauer alone cannot accurately characterise mineral content, it is possible to compare these results with parameters that might be expected based on the contents of the reoxidised sample. XRD data suggested that the primary mineral component of in the reoxidised sample was lepidocrocite. Lepidocrocite is a typically expected Fe-oxide mineral that forms when Fe(II) is rapidly oxidised (Misawa et al. 1974), as is the case here. The Mössbauer spectrum parameters of lepidocrocite at ≥ 77 K can produce a broad distribution of values defining potential doublets, dependant on multiple factors such as crystallinity, water content and surface effects (Murad and Schwertmann 1984, De Grave et al. 1986). The Fe(III) doublets in Figure 5.8 (B) are fitted with parameters within the expected range for lepidocrocite.

Figure 5.8 C and E represent the spectra from the reduced phase of Cycle 2. Figure 5.8 C shows the spectrum of the $^{57}\text{Fe(II)}_{\text{aq}}$ added in Cycle 1, after being re-reduced with new (Mössbauer invisible) $^{56}\text{Fe(II)}$ in Cycle 2. This allows us to view what happens to the oxidized precipitate (i.e. mostly lepidocrocite) once more Fe(II) has been added to the system, and further electron transfer into the clay mineral occurs. In contrast, Figure 5.8 E represents the reductant Fe(II) of Cycle 2, made visible with $^{57}\text{Fe(II)}$ while the Fe(II) added in Cycle 1 is now invisible (^{56}Fe). This allows us to view how in the second cycle the added Fe(II) is altered after interacting with the clay mineral and oxidized precipitates.

Examination of Figure 5.8 C shows the presence of Fe(II) doublet species (blue), comprising approximately 40 % of the spectrum. When compared with the oxidised sample spectra for Cycle 1 (Fig 5.8 B), it is apparent that the Fe(II) doublets are significantly larger. This means that in Cycle 2 there has been significant electron

transfer from the added Fe(II)_{aq} into the oxidized precipitate minerals leading to a 40 % reduction extent. The smaller, light blue doublet is has decreased in relative area compared to both the first NAu-1 reduction (i.e. Figure 5.8 A) as well as the previous spectra of the reoxidised sample (Fig 5.8 B). This would suggest that addition of new Fe(II)_{aq} has affected this portion of Fe(II) even though oxidation via H₂O₂ could not. The ratio of small doublet to large doublet has decreased to 1 : 9. This is evidence to indicate a shift in the binding environment of Fe(II) between Cycle 1 and 2, as one Fe(II) species partially transitions to another after reaction with Fe(II)_{aq}.

The reduction of Fe-oxyhydroxides such as lepidocrocite can lead to the formation of mixed valent minerals. Ona-Nguema et al. (2002) used microbes to bioreduce lepidocrocite and documented the formation of green rust minerals with doublet species fitted with a CS of 1.27 mm/s and QS values of 2.89 mm/s and 2.51 mm/s. Green rust species are mixed valent layered double hydroxide species, and have can also be produced by the oxidation of ferrous solutions (Misawa et al. 1974). Multiple quadrupole-split doublets are also typical to the Mössbauer effect produced by green rusts (Trolard et al. 1996, Genin et al. 2005).

The remaining species are Fe(III) and encompass 60% of the spectrum. They include the typical doublet (orange) with a CS of 0.48 mm/s (present in both Fig 5.8 A and B), and the secondary doublet (purple). The second Fe(III) species (purple) comprises an almost exactly equivalent relative area to that of Cycle 1 (Fig 5.8 A) at 14.6%, and also shows an increased centre shift value to 0.75 mm/s. As it has been hypothesised that this species represents Fe(III) affected by neighbouring Fe(II), an increase in CS towards values more associated with Fe(II) is of interest. With a decreasing relative fraction of Fe(II) (40 % Fe(II) compared to 70 % in Cycle 1), it could be expected that one would also observe a decreasing effect of the Fe(II) on the remaining Fe(III). One explanation for this observation might be connected to the change in ratio between the two different Fe(II) species. The relative decrease of the smaller Fe(II) doublet, (and subsequent relative increase in the large Fe(II) doublet) could highlight that Fe(II) is preferentially reorganised to one type of binding environment. This could perhaps suggest that the system is trending towards a pool of Fe(II) that is more distinctly separate from the remaining Fe(III), rather than a more homogenous and disorderly

mixture of Fe atoms. This might mean that the effects of this distinct Fe(II) fraction are increased on the neighbouring Fe(III), despite there being fewer interactions between atoms of each oxidation state.

Figure 5.8 E highlights the effects on the 2nd Fe(II)_{aq} added to the system after reacting with both the clay mineral and the oxidized Fe precipitate minerals. Both Cycle 2 spectra measured before total oxidation (Figure 5.8 C and E) appear almost identical to each other, and parameters show almost no variation between each sample. In addition, the reduction extent of both the pre-existing Fe-oxide precipitates from Cycle 1, and the solid-associated Fe(II) of Cycle 2 are approximately equal. The precipitate from Cycle 1 (Fig. 5.8 C) has roughly 40 % reduction extent, and the newly added Fe(II) (Fig. 5.8 E) has approximately 47 % reduction extent. It was calculated that a total of 0.35 mM of electrons are present in the solid phase (sum of both clay mineral and oxidised precipitates) based on the reduction extent (see Figures 5.4 D, and 5.8 C). The second reductant Fe(II) is 53% oxidized, which is calculated to be 0.4 mM of electrons transferred to the oxidant. These values align well and show a complete electron balance within the reasonable range of error associated with Mössbauer fittings. This finding is significant as it appears that the electron concentration is shared equally between both pools of Fe, and shows that the oxidation of the aqueous phase leads to a product with a similar binding environment to the (now) reduced solid phase. Electron transfer between sorbed Fe(II) and Fe-oxyhydroxides has been previously observed (Williams and Scherer 2004). The study investigated Fe(II) sorption to goethite, hematite, and ferrihydrite and also noted the reaction resulted in the formation of a distinct solid-bound Fe(II) species that was structurally similar to the bulk Fe-oxide material.

The remaining two spectra of Figure 5.8 (D and F) show the state of the system after the second reoxidation with peroxide. Both spectra are similar to the Cycle 1 spectrum and are primarily composed of ferric doublets, similar in parameters to those of Cycle 1. One clear difference between the re-oxidised spectrum of Cycle 1 is that there is remnant fraction of Fe(II) (seen in Figure 5.8B) persisting beyond oxidation by H₂O₂. Fe(II) that was previously occluded to oxidation in Cycle 1, is now no longer protected. This could suggest that the structure of the external Fe precipitate minerals undergo

rearrangements during the cycling that makes the previously resistant Fe(II) in the precipitate now accessible to re-oxidation. This may be because the first cycle was oxidised by the clay mineral only, and therefore was limited by the extent to which the Fe(II)_{aq} could interact with oxidising species. In contrast, for Cycle 2 the Fe(II)_{aq} is able to interact with the pre-existing Fe-oxide precipitates from the previous oxidation. This would offer a greater scope for oxidation (due to more accessible Fe), and in doing so might also incur significant atom exchange as has been demonstrated in previous research (i.e. Pedersen et al. 2005). The greater interactions between the aqueous and solid phase in Cycle 2 could have led to formation of structurally different precipitate minerals to Cycle 1, where Fe(II) is more accessible to oxidation. Although we cannot precisely determine any feature which might have prevented complete oxidation in Cycle 1, it is clear that all Fe(II) is now accessible to oxidation by H₂O₂.

Another key difference is that in Figure 5.8 F there is now the presence of what appears to be a small sextet (shown in orange). The sextet has a hyperfine field of 46 T, and therefore resembles the sextet of lepidocrocite. One possible explanation is that this is the formation of small quantities of an Fe-oxyhydroxide species that is magnetically ordered at temperatures above 77 K such as goethite. Our XRD data showed that there could be trace quantities of goethite present in the latter cycles, and this was most evident in Cycle 3. However, a pure goethite would typically present a sextet with a wider hyperfine field parameter (Fysh and Clark 1982). Another possible explanation for the appearance of this sextet is that the Neel temperature for lepidocrocite lies on or around 77 K. The onset of ordering is not immediate, and both the doublet and the sextet can coexist over a range of around 10 K (Johnson 1969). Any fluctuations between samples or over this temperature boundary could lead to magnetic ordering of the lepidocrocite present. This has been demonstrated in previous papers such as Guyodo et al. (2016), which demonstrated magnetic ordering of a lepidocrocite sextet with comparable hyperfine field parameters at 77 K. We conclude that the latter explanation is the most likely scenario, due to the pronounced presence of lepidocrocite confirmed in previous spectral analyses (i.e. Figure 5.7).

Previous research has shown that the reaction of aqueous Fe(II) with clay minerals can lead to the formation of mixed-valent secondary minerals (e.g. Schaefer et al. 2011,

Entwistle 2021). Results have already shown that Fe(II) that is reacted with clay minerals becomes solid-associated, and this Mössbauer data demonstrates the Fe is speciated. In all reduced states of this experiment, it was noted that the colour of the solids visibly changed to a dark blue / green. The change of colour to blue/green indicates the presence of Fe(II)-O-Fe(III) bonds (Komadel et al. 1990). However, it is unclear whether this change would be due to the formation of new mixed valent minerals such as green rusts, or due to the reduction of the clay mineral octahedral sheet. It is possible that both the oxidation of Fe(II)_{aq}, and the reduction of solid ferric precipitates in this experiment led to the formation of mixed valent species similar to green rusts. Jones et al. (2017) suggested that the reduction of clay minerals with aqueous Fe(II) does indeed lead to the formation of green rusts. However, previous research conducted by Entwistle (2021) under directly comparable conditions contested the conclusions of the Jones et al. study, and determined that both the Mössbauer parameters and XRD spectra of these secondary minerals were dissimilar to green rusts, but the exact nature of the solid precipitates was undetermined. Conducting Mössbauer analysis at 4 K temperature on the precipitates can offer further insight into the Fe speciation of the solid-bound Fe(II) precipitate species.

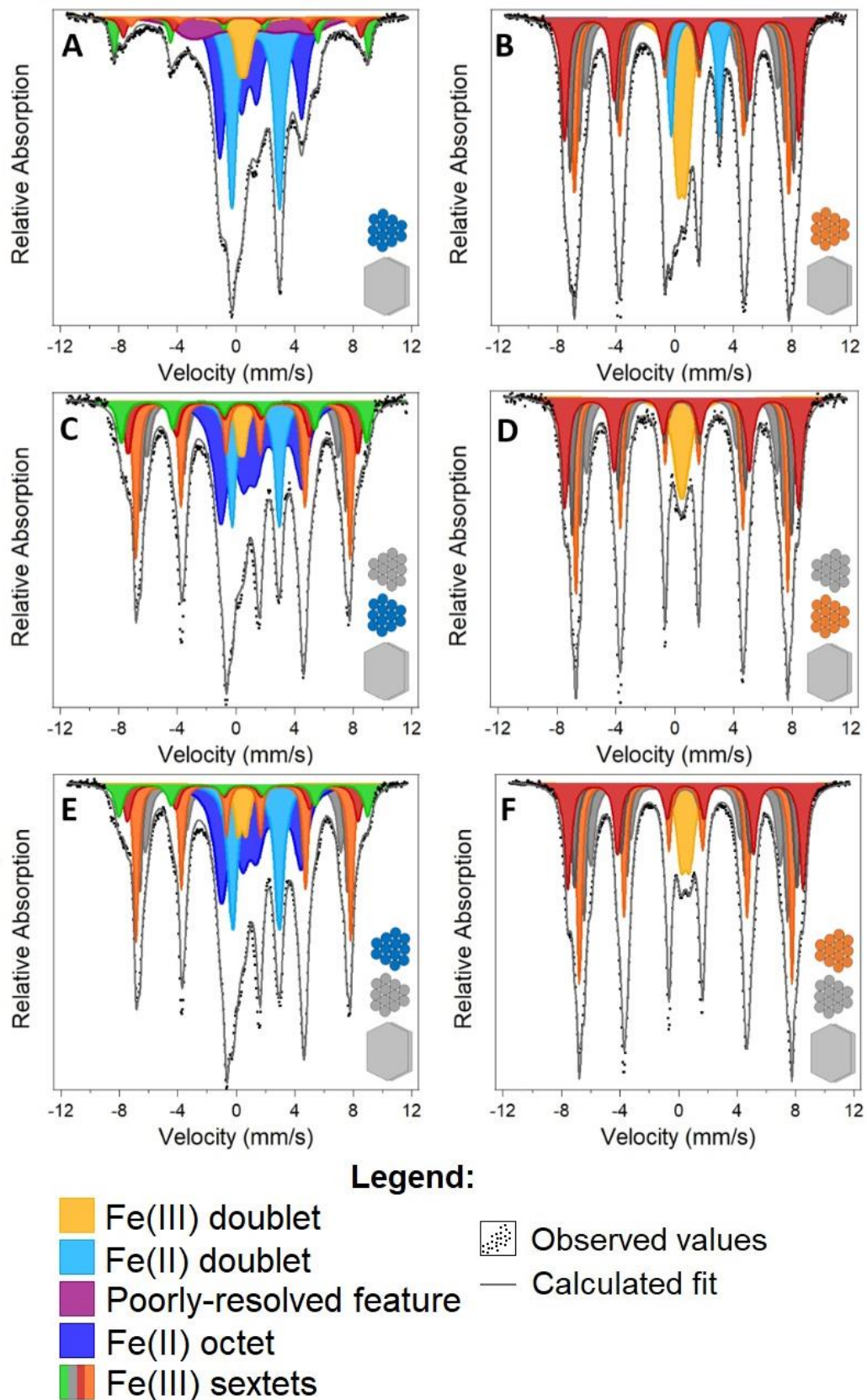


Figure 5.9: Mössbauer spectra at 4 K temperature when using $^{57}\text{Fe(II)}_{\text{aq}}$ as the reducing agent, showing speciation of secondary precipitate minerals formed over two cycles of reduction and oxidation. Figure includes First cycle precipitate (A), First cycle re-oxidised precipitate (B), First precipitate after re-reduction (C), First precipitate after second re-oxidation (D), Second precipitate formed (E), Second precipitate after re-oxidation (F). Each spectrum was fit using variable line width fitting technique (Full static Hamiltonian).

Figure 5.9 shows the Mössbauer spectra at 4 K of the added aqueous Fe(II) in reaction with clay minerals over 2 reduction and oxidation cycles. A full list of Mössbauer parameters are available in Table SI 5.3. Spectrum A represents the speciation of the added Fe(II) on the first cycle after contact with the NAu-1 for <18 h. In the centre of the spectrum, a large fraction of the total Fe is held as a large octet species occupying 38 % of area (shown in dark blue), and a doublet with a large quadrupole splitting occupying 30 % of the area (light blue). The octet has a CS value of 1.3 mm/s and a QS of 2.97 mm/s, similarly the doublet species has a CS of 1.34 mm/s and a QS of 3.25 mm/s. The high centre shift and quadrupole splitting values for these species indicates that these are both Fe(II), and therefore demonstrates that the majority of Fe in this sample is Fe(II). This would be expected as the data has demonstrated that only a small percentage of the added Fe(II) should be oxidised, based on the measured electron transfer into the clay mineral (Figure 5.4). The significance of the ordered Fe(II) species is that it indicates that the Fe(II) has formed a structure that allows enough Fe-Fe interactions to magnetically order. This would not be the case if the Fe(II) was only adsorbed or loosely complexed to the clay mineral surface, and is further confirmation that the added Fe(II) formed a precipitate species. The ordered Octet species has been observed in previous work (Rothwell 2018, and Entwistle 2021) and the parameters are well aligned with both studies showing an octet with a hyperfine field of 12-13 mm/s, and a similar relative area. A comparison by Entwistle of the octet parameters found the species to most closely resemble those of Fe(II)/Fe(III) minerals such as greenalite and biotite.

Interestingly, for the initial reduction (Figure 5.9 A) it appears that a large fraction of the added Fe(II) remains as a doublet, which suggests it is not in a binding environment rich in Fe, or with sufficient Fe-Fe interactions to magnetically order. This could suggest that in Cycle 1 a large fraction of the Fe(II) remains sorbed, rather than forming a distinct secondary mineral species.

The total sum of the relative areas for both the blue octet and the blue doublet is 65% of the spectrum, which aligns well (within error) with the expected value for Fe(II)/Fe_{Tot} according to the spectrum measured at 77 K temperature (Figure 5.8A).

However, the ratio between the Fe(II) octet and Fe(II) doublet at 4 K is very different to the ratio between the two Fe(II) species observed at higher temperatures. This means it is difficult to draw comparisons between the two spectra with regards to the Fe(II) content.

The remaining species visible in spectrum A include a small doublet (yellow) and multiple sextets (green, red, and orange). The (yellow) doublet has a CS of 0.48 mm/s, and a QS of 0.49 mm/s. These values are typically too low to be Fe(II), therefore this likely represents Fe(III) that is poorly ordered. The largest sextet (green) displays a larger hyperfine field (54 T) than previously observed in the Fe-reduced clay mineral spectra (i.e. Figure 4.6), but has been observed in previous work (Rothwell 2018, and Entwistle 2021). The sextet also disappears after oxidation, a characteristic also observed in previous research by Entwistle, which suggests the species is connected in some way to the presence of Fe(II). The sextet has a hyperfine field width similar to that of hematite, an Fe-oxide mineral consisting of closely-packed Fe(III)-octahedra with minimal vacancies. However, hematite would be visible at 77 K as it magnetically orders at high temperatures (Murad and Cashion 2003). Also, hematite is relatively thermodynamic stable and is typically an end-member Fe-oxide species that does not form easily without sufficient time or significant applied heat (Schwertmann and Murad 1983, Liu et al. 2007). For this reason the species is unlikely to be hematite. The wide sextet also has equivalent parameters to the sextet observed in the dithionite spectra (see Chapter 3, Figure 3.6). When examining dithionite-reduced NAu-1 spectra, the sextet with these parameters is only visible once the extent of reduction is above a certain threshold of ~30 % (Rothwell 2018). It has been proposed that when a Fe-rich clay mineral is reduced beyond a specific % reduction extent that octahedral rearrangements occur and trioctahedral domains begin to form within the clay mineral octahedral sheet (Manceau et al. 2000). It is possible this species represents octahedrally bound Fe external to the clay mineral that has an altered local environment in close proximity to surrounding Fe(II).

The spectrum also features a purple collapsed species with a CS of 0.67 mm/s, and comprising 14.50 % of the spectral area. It is possible this represents the same species, but has begun to magnetically order due to the lower temperature. A similar species

was observed by Entwistle (2021), but this was only at much higher concentrations of added Fe(II) (20 mM). The CS value and relative area are equivalent to the poorly defined Fe(III) species seen previously in the spectra taken at 77 K (see Figure 5.8 A).

Upon re-oxidation (spectrum B) the dark blue Fe(II) octet species disappeared, and the light blue doublet decreased significantly, although it still comprises 10 % of the spectral area, similar to what was observed in the spectra collected at 77 K (see Figure 5.8). This shows that the majority of Fe(II) has been oxidised to Fe(III) and aligns well with expectations. The resulting spectrum is composed primarily of sextets with hyperfine field widths between 40-50 T. The spectrum could be fitted with multiple possible sextet species likely representing a mixture of Fe-oxides, but our fitting has used 5 individual sextets and labelled with colour only the largest (46 T - orange) and widest (50 T – dark red) areas as these can be fitted without ambiguity around the fitting parameters. The dominance of sextet species within the reoxidised spectrum indicates the Fe in the sample has taken forms that are naturally magnetically ordered. This transformation is expected as oxidation of aqueous Fe(II) will lead to the precipitation of Fe(III) oxyhydroxides (Misawa et al. 1974), many of which produce sextets within this observed range of hyperfine field widths at 4 K (Murad and Cashion 2004). The visible colour of the sample changed from green to a light orange, also indicative of ferric oxyhydroxide minerals (see Figure SI 5.2). The sextet with the largest relative area within the spectrum has a hyperfine field of 46 T, which fits the parameters of lepidocrocite (Murad and Cashion 2004). Lepidocrocite is also a light orange colour (Schwertmann et al. 2000), and is formed by the rapid oxidation of ferrous iron or of “green Fe(II)-Fe(III) intermediates” (Misawa et al. 1974) which based on our observations is a justifiable description for the ordered species observed in Fig. 5.9, graph A. Lepidocrocite has also been observed to be present in the oxidised sample in the previous XRD analysis (see section 5.3.3.1). These points provide further evidence that lepidocrocite is the dominant mineral produced upon reoxidation.

D and F show the spectra for the second cycle reoxidised samples. Both spectra look very similar to each other and to the reoxidised spectrum of Cycle 1 (B) but with the absence of the Fe(II) doublet. Once again the primary species is the sextet with a

hyperfine field of 46 T, which has been determined to be lepidocrocite. This indicates that any subsequent reduction will interact with the same Fe-oxide materials.

After the second addition of aqueous Fe(II), the Mössbauer spectra of the initially added Fe and the second added look almost identical (Figure 5.9 graphs C and E) with each showing the similar Mössbauer components that occupy similar relative areas in the spectra.

When compared with the spectrum for Cycle 1 (Figure 5.9 A), it is apparent that the spectrum is much more heavily dominated by sextets suggesting an increased relative content of Fe(III). Increased Fe(III) is expected based on the reduction extent data acquired in Figure 5.8. Like the Cycle 1 spectrum (Fig 5.9 A), the outer sextet has a H of 54 T, however in Cycle 2 the sextet with largest relative area is now one with a H of 46 T, as with the reoxidized sample spectrum. This finding is likely the result of the lepidocrocite present in the system after the preceding reoxidation.

Additionally, the relative contribution of Fe in each spectra occupied by the Fe(II) doublet has decreased significantly from 45 % of the Fe(II) content in Cycle 1, to only 30 % of the total Fe(II) content in Cycle 2. Simultaneously the fraction of Fe(II) that is magnetically ordered (i.e. dark blue octet) has increased from 55 % to 70 % of the total Fe(II) in the sample. In Cycle 1, the ratio of ordered Fe(II) : poorly ordered Fe(II) is approximately 1:1, whereas in Cycle 2 the ratio is 2:1. This indicates that Fe(II) is restructured in Cycle 2 preferentially into forms that have more Fe-Fe interactions. Poorly-ordered Fe species could include sorbed or surface complexed Fe atoms, a decrease in the relative area of the doublet could indicate an incorporation of sorbed atoms into more rigid structures where atoms are capable of interacting magnetically.

One possible explanation for this change is that in Cycle 1, only 30 % of the aqueous Fe(II) is oxidised (by the clay mineral) and then precipitates. The partial oxidation of Fe(II)_{aq} has been shown to be capable of forming mixed valent materials such as green rusts (Misawa et al. 1974). However mixed valent Fe minerals are typically stoichiometrically limited by the ratio of Fe(II):Fe(III) (e.g. Genin et al. 2005, Gorski et al. 2009). This could mean that secondary mineral formation is limited by the concentration of available Fe(III). The remaining fraction of the Fe(II)_{aq} concentration can be removed from solution in one of two ways. One possible way is known as the

“conveyor belt model” where an $\text{Fe(II)}_{\text{aq}}$ atom donates an electron to a Fe(III) atom within a precipitate species. The donated electron is conducted through the bulk precipitate to potentially cause reductive dissolution of an atom elsewhere on the precipitate surface. The donating atom then immediately precipitates onto the surface of the bulk Fe-oxide due to oxidation (Neumann et al. 2015), leaving no net difference in the $\text{Fe(II)}:\text{Fe(III)}$ ratio. The other possible interaction is sorption of $\text{Fe(II)}_{\text{aq}}$ to the oxide or clay mineral surface (e.g. Neumann et al. 2013, Tsarev et al. 2016). Overall, this would imply that the system in Cycle 1 is stoichiometrically insufficient to allow widespread mineralisation of the added $\text{Fe(II)}_{\text{aq}}$, and a large fraction will therefore remain sorbed. In contrast, aside from the increased reduction extent of the clay mineral, Cycle 2 will have sufficient capacity for oxidation due to the presence of the Fe-oxides from the reoxidation (as demonstrated in section 5.3.3.1), thus allowing unlimited formation of secondary precipitate minerals as stoichiometric limitations are removed.

Another key difference between the first and second cycle spectra is the absence of the collapsed feature visible in Figure 5.9A. This reflects the significant decrease in relative area in Cycle 2 for the poorly resolved feature visible in the 77 K spectra (see Figure 5.8 C and E). As with the high temperature analyses, this highlights a shift away from poorly-ordered Fe species, and might also indicate Fe material is organising towards two distinct solid phases of each oxidation state, rather than a more homogenous and disorderly mix of Fe atoms.

The distinct similarity of the Mössbauer spectra obtained for the initially added Fe and the second added Fe as present after the second Fe(II) addition indicates an interaction between both pools of Fe that causes a transformation of both leading to the same speciation. This finding could be explained by different hypotheses. Firstly, electron transfer from the secondary added aqueous Fe(II) caused transformation of the initial, fully oxidised Fe precipitate minerals (Figure 5.9 B) into a mixed-valent mineral similar to that observed in reduction Cycle 1 (Figure 5.9 A). Studies have shown that Fe-oxide minerals can be reduced by $\text{Fe(II)}_{\text{aq}}$ to form mixed-valent minerals such as magnetite and green rusts (Misawa et al. 1974, Tamaura et al. 1984, Pedersen et al. 2005). The $\text{Fe(II)}_{\text{aq}}$ oxidised by the electron transfer would precipitate out of

solution as Fe(III), and some Fe(II) would be removed through sorption to the newly formed precipitates. This would lead to the formation of solid, mixed-valent Fe material. Simultaneous precipitation and sorption has been observed in previous research (e.g. Neumann et al. 2013, and Williams and Scherer 2004), and this is a possibility based on the multiple Fe(II) species observed in both the 77 K and 4 K Mössbauer. Electron transfer would cease once both the initially present and newly formed Fe phase(s) reach equal reduction extents.

Another possible pathway involves the dissolution of $^{57}\text{Fe(II)}$ formed during the initial electron transfer from aqueous $^{56}\text{Fe(II)}$, atom mixing with aqueous phase ^{56}Fe , and re-precipitation into secondary minerals (Latta et al. 2017, Pedersen et al. 2005). The striking similarity between the two solid-associated Fe pools is consistent with previous research suggesting atom exchange between aqueous Fe(II) and lepidocrocite. Atom exchange between aqueous Fe(II) and Fe-oxyhydroxides has been observed in previous research, and studies have observed rates of over 50% of Fe exchanged in less than 24 hours under pH and concentrations (Handler et al. 2008, Pedersen et al. 2005). However, our experimental setup does not allow for monitoring atom mixing between aqueous and solid Fe pools, which requires the quantification of Fe isotope ratios in both pools over time (e.g. Handler et al. 2014). We can hence neither unambiguously confirm nor rule out that Fe atom exchange occurred in our experiments.

In summary, Mössbauer analysis provides a number of significant insights into how reduction-oxidation cycling with aqueous Fe(II) affects the mineralogy of the system. In Cycle 1 it is possible to determine that aqueous Fe is partially oxidised by the clay mineral leading to various mixed-valent solid phases. The percentage of Fe(II) that is magnetically ordered suggests that the Fe(II) is precipitated as a secondary solid-bound mineral, rather than purely adsorbed or complexed to clay mineral surfaces. The re-oxidation of the added Fe(II)_{aq} by hydrogen peroxide leads to the formation of ferric oxides, with the primary mineral being lepidocrocite. Finally, results indicate that the second cycle of reduction causes significant interaction between the first oxidized precipitates and second added Fe(II)_{aq}, which leads to essentially identical binding environments for both pools of Fe. There also appears to be a shift towards the system

becoming generally more ordered from Cycle 1 to Cycle 2. How do these observations relate to the kinetic data and, could these mineralogical transformations lead to the observed changes in reactivity towards nitroaromatics?

5.3.4 Relating structure to reaction kinetics

Several parallels can be drawn between the measured kinetics and the changes in mineralogy and Fe speciation as seen through Mössbauer spectroscopy. In Section 5.3.2, results suggested that the reactive Fe sites were affected by redox cycling. In Cycle 1 the highly reactive Fe site achieved an equivalent level of reactivity to that of dithionite-reduced NAu-1, whilst the less reactive sites were dramatically increased compared with dithionite-reduced NAu-1. In Cycle 2, data indicates a distinct increase in rate constant values by over an order of magnitude for both reactive sites. Cycle 3 produced rate constant values largely similar to those of Cycle 2, and throughout all 3 cycles the initial concentration of highly reactive sites calculated by the model remains largely unchanged. It was clear that the greatest effects on reactivity occurred after the 1st reoxidation in Cycle 1.

The ⁵⁶Fe Mössbauer results (see Figures 5.5 and 5.6) also indicate that significant structural changes occur between Cycle 1 and 2 for the clay mineral. Firstly, in Cycle 1 the ⁵⁶Fe-reduced NAu-1 achieved an extent of 7 % Fe(II)/Fe_{Tot} in Cycle 1, whereas a reduction extent of 16 % was achieved in Cycle 2. There is no question that an increased concentration of reactive Fe(II) could lead to increased reactivity, and it is likely that this change may have contributed to the observed difference in rate constants between Cycle 1 and 2. However, it was concluded that the achieved reduction extent and the structural alterations to the clay mineral alone were insufficient to account for the drastic impacts of cycling on the reactivity, and the increased kinetics must be somehow related to the Fe(II) content external to the clay mineral.

Previous research has provided strong evidence that Fe(II)-reduction of clay minerals leads to the formation of secondary reactive Fe minerals. Rothwell (2018) demonstrated the simultaneous formation of solid-associated Fe material, and increased k values for the less reactive sites after reaction of Fe(II)_{aq} with NAu-1. This result was replicated in our initial reduction. The Rothwell study stated that the

increased rate constant values for Fe(II)-reduced NAu-1 was due to the formation of new reactive Fe sites. It was considered possible that the new reactive sites are found within secondary Fe precipitates. Tsarev et al. (2016) similarly observed increased reduction kinetics of Fe-reduced nontronites towards Uranium, and stated that the increased reactivity was likely due to the formation of reactive secondary Fe(II)/Fe(III) oxyhydroxide precipitates. Previous work (Entwistle 2021) also observed the formation of secondary precipitate minerals, which appeared to positively impact mineral reaction kinetics. The results thus far present adequate evidence to suggest the presence of a mixed-valent secondary precipitate minerals in the reduced phase, and that these secondary minerals appear connected to the improved transformation kinetics. However, there has currently been no research conducted to measure the effects of multiple cycles of Fe(II)-reduction and oxidation, and therefore no direct corollary for the major kinetic impacts measured after the first cycle.

A further analysis with ^{57}Fe -enriched solutions outlined further changes occurring in the solid-associated, added Fe(II) pool. For Cycle 1, the Mössbauer spectrum taken at 4 K showed 36% of the solid-associated Fe(II) was speciated as a magnetically-ordered octet species (see Figure 5.9). This is further evidence to indicate that secondary reactive precipitates have formed. It was also clear that after the reoxidation of Cycle 1, Fe-oxyhydroxides (namely lepidocrocite) were consistently present in the system. The data also provided insight towards the changes to reactivity over multiple cycles, and highlighted several important differences between the spectra of Cycle 1 and 2. Firstly, our results demonstrate that there are significant interactions between the oxidized precipitates of Cycle 1 and the added Fe(II) of Cycle 2, leading to an even spread of Fe(II) between both pools. This paper has observed that the reaction transformed the speciation of both pools of Fe to produce two almost identical spectra. This meant in Cycle 2, both the added Fe(II), and the oxidized precipitates from Cycle 1 were altered to resemble one another.

How do the changes to the precipitated material between Cycle 1 and 2 relate to the observed kinetics? Fe(II) is the reactive fraction of the mineralogy, and is the source of reduction equivalents for contaminant transformation. The Fe(II) content of Fe minerals has been shown in multiple experiments to be the driving force for

contaminant reduction, and studies have highlighted the importance of the Fe(II):Fe(III) towards influencing the reactivity and redox potential of Fe minerals (i.e. Lee and Batchelor 2003, Gorski et al. 2009, Usman et al. 2018). There are a number of distinct differences visible in the Fe(II) content of the secondary (i.e. external to the clay mineral) Fe precipitates between Cycle 1 and Cycle 2. In the spectra measured at 77 K (see Figure 5.5), the Fe(II) content is split unequally between 2 sets of doublets. The smaller of the two doublets can be fitted with parameters previously used to describe Fe(II) adsorbed to the clay mineral basal plane (Neumann et al. 2013), and is relatively diminished in the second cycle for both the 1st and 2nd Fe precipitates. This could indicate that there is less basally-sorbed Fe(II) in the second cycle. While Fe(II)_{aq} can transfer electrons to structural Fe across the basal plane, at pH 7.5 the extent of sorption and electron transfer would be significantly less than that at edge sites (Neumann et al. 2013). For this reason, the effects of basally-sorbed Fe(II) on the reduction extent and reactivity of the clay mineral is likely negligible. However, electrostatically-bound Fe(II) on the basal surface can in fact impede reactivity, as it can limit the access of nitroaromatic molecules to reactive surface sites where electron transfer can occur from octahedral Fe(II) (Hofstetter et al 2006). The decrease in basally-sorbed Fe(II) might reflect both an increase in accessible reactive structural Fe, as well as demonstrating a preference for Fe(II) speciations with greater reactivity.

Another key difference between the precipitate material of Cycle 1 versus Cycle 2, is that in Cycle 1 a fraction of the Fe(II) is resistant to oxidation even by H₂O₂. In Cycle 1, the reoxidation of the sample with H₂O₂ leaves 7% of the added Fe remaining as a Fe(II) doublet. If a fraction of the Fe(II) in the precipitate material is inaccessible to oxidation via a strong oxidant such as H₂O₂, then it also may have been inaccessible to oxidation by the NAC contaminant. In Cycle 2 it is clear that all Fe(II) was completely oxidised by H₂O₂, therefore this could indicate a greater portion of the reactive Fe(II) was capable of reducing the NAC which may have contributed to the greater reactivity of Cycle 2.

The Mössbauer spectra collected at 77 K temperature for the precipitate material also shows a significant decrease from Cycle 1 to Cycle 2 in the relative area of the poorly resolved Fe(III) doublet with a CS value of ~0.7 mm/s. This species was hypothesised to

represent Fe(III) with an altered local environment due to being in close proximity to neighbouring Fe(II) atoms. The measured decrease of this species between Cycle 1 and 2 could indicate that the two oxidation states of Fe become more distinct and separate rather than a homogenous mix.

Differences between Cycle 1 and 2 are also reflected when examining the Mössbauer spectra measured at 4 K (Figure 5.9). The precipitate material spectra at 4 K show that Fe(II) is speciated as either primarily a large octet species (dark blue) or a doublet with a large quadrupole splitting (light blue). Like the data collected at 77 K temperature, in Cycle 2 there is similarly a relative diminishing of the smaller Fe(II) fraction (in this case the doublet) and in its place Fe(II) is preferentially speciated as a magnetically ordered doublet. The data reflects a shift in the ratio of poorly ordered : ordered from 1:1 for Cycle 1, to 1:2 for Cycle 2. It is unexpected that this result would lead to greater reactivity, as it has previously been shown that species such as sorbed or surface-complexed Fe are highly reactive towards nitroaromatic compounds (Klausen et al. 1995, Hofstetter et al. 1999).

An explanation for this finding may be as follows: Firstly, increased ordering / Fe(II)-Fe(II) interactions could allow for greater ease of electron transfer across the bulk mineral. This would mean interior Fe atoms would be more accessible to oxidation by the contaminant at the surface. This might not be the case in poorly-ordered material with low Fe interactions as electron conduction may not be favourable due to for instance greater distance required for electron transfer between atoms. Greater magnetic ordering implies greater interactions between Fe atoms, and therefore reduced void space and holes which hinder electron transfer. This has been demonstrated previously in materials such as hematite, where there are orders of magnitude differences in conductivity and resistance across different planes of the crystal lattice due to the heterogeneity of holes (Iordanova et al. 2005).

Next, the increased fraction of magnetically-ordered Fe(II) in Cycle 2 signifies that Fe is re-organised to allow increased Fe(II)-Fe(II) interactions. Increased Fe(II)-Fe(II) interactions (and decreased Fe(II)-Fe(III) interactions) is further evidence to suggest that the two oxidation states are becoming increasingly more spatially distinct. This might make electron transfer to the contaminant easier for 2 reasons. Firstly, if there is

a region with a high concentration of interacting Fe(II) atoms this might mean a larger percentage of the reactive material is accessible to the surface and therefore is available for contaminant transformation. This is feasibly the case as the study has demonstrated that some Fe(II) was inaccessible to oxidation in Cycle 1, whereas all Fe(II) could be oxidised in Cycle 2. Secondly, in a region of highly interacting Fe(II) atoms, any Fe atom oxidised at the surface by the contaminant might be rapidly replenished and re-reduced due to electron transfer and conduction from multiple neighbouring Fe(II) atoms. This efficient electron transfer might not be the case for Fe(II) atoms homogenously dispersed in a matrix of Fe(III) material, as the potential gradient is not localised like an isolated oxidised surface site, and any conduction would be more isotropic. Bulk conduction of electrons through Fe-oxide minerals across has been demonstrated (Yanina and Rosso 2008, Handler et al. 2009), and a distinct region with high concentration of interacting Fe(II) atoms would create an increased charge concentration and therefore a sufficient potential gradient to drive electron transfer to surface sites oxidised by contaminant transformation. Overall, this effect would mean contaminant-oxidised Fe(II) atoms are quickly replenished by electron transfer from their interacting neighbours.

This trend towards distinct phases of each oxidation state could be caused by different pathways for Fe precipitation between Cycle 1 and 2. The data has demonstrated that only a small fraction of clay mineral structural Fe is reduceable, and at pH 7.5 most electron transfer occurs via the edge sites (Neumann et al. 2013). This means that only a small portion of the Fe(II)_{aq} in Cycle 1 can be immediately oxidised and precipitated as a new mineral, the remaining fraction of Fe(II)_{aq} is removed from solution largely by sorption leading to a spectrum dominated by poorly-ordered Fe material. Cycle 2 on the other hand would have much greater extent of oxidation and subsequently precipitation due to the greater concentration of possible electron receivers in the form of the pre-existing Fe-oxides. Oxidation of Fe(II)_{aq} by an Fe-oxide surface could lead to the immediate epitaxial growth of the oxide at the point of electron transfer due to immediate precipitation of Fe(III). The transferred electrons would theoretically be transferred through the bulk material elsewhere by conduction (Yanina and Rosso 2008). The greater proclivity for immediate precipitation by oxidation would create an overall binding environment for the added Fe that is well-ordered, with high Fe-Fe

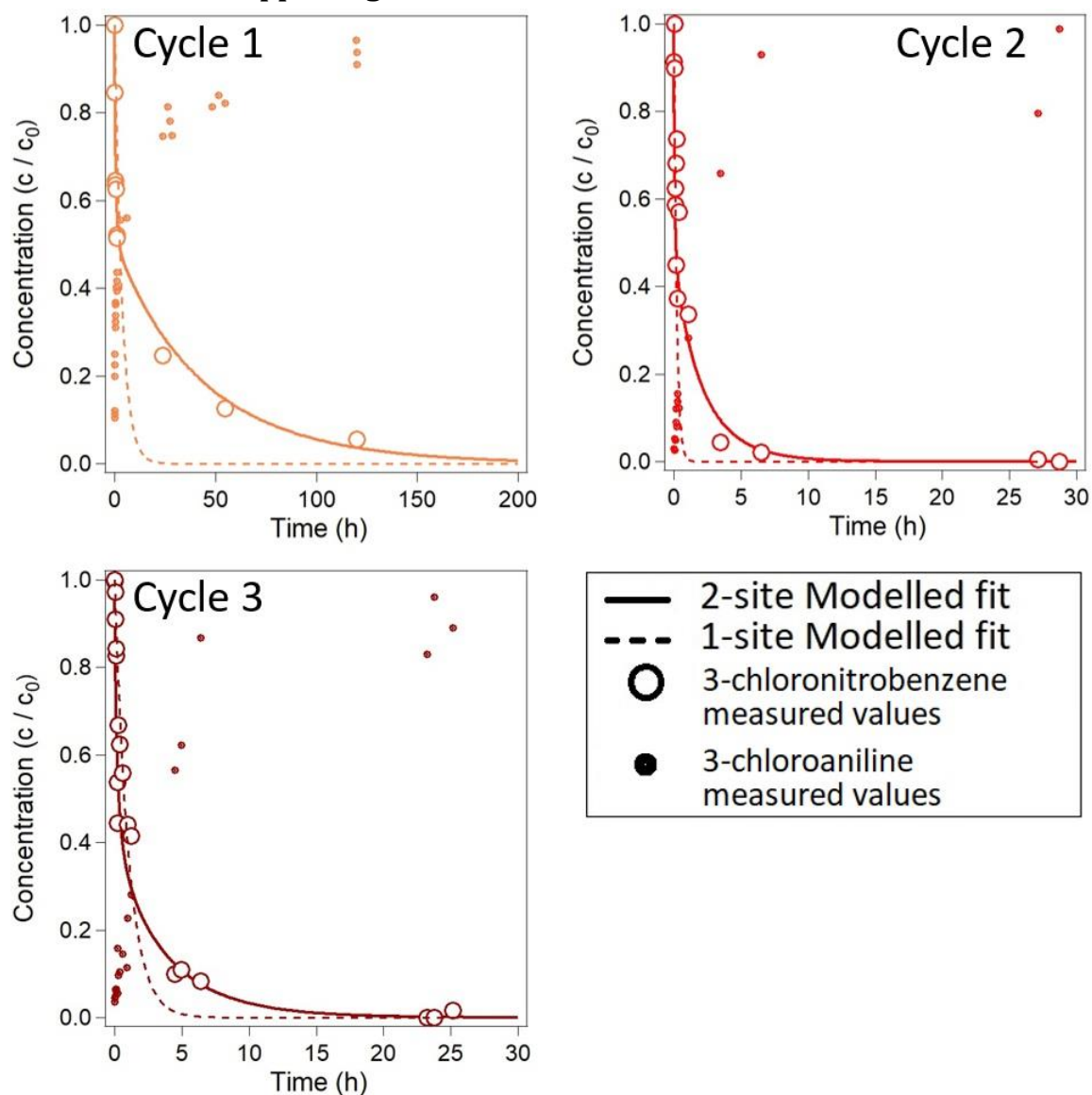
interactions. This could lead to 2 distinct phases of well-ordered Fe with different oxidation states, as electrons move from one region of the precipitate to another across a potential gradient.

In summary, reaction of $\text{Fe(II)}_{\text{aq}}$ with Fe-bearing clay minerals results in electron transfer into structural Fe, and the subsequent formation of secondary precipitates. The secondary precipitate minerals significantly improve contaminant transformation. Results describe a shift in ordering of Fe in the precipitate mineral from poorly ordered to well-ordered material between Cycle 1 and 2. This also correlates with a significant increase in the reaction kinetics between Cycle 1 and Cycle 2. We hypothesise that the presence of Fe-oxides in Cycle 2 allows for the formation of Fe material with increased Fe(II)-Fe(II) interactions, possibly reflective of distinct, concentrated phases of each oxidation state. The precipitate material formed in Cycle 2 is also more reactive towards the nitroaromatic reduction due to increased capacity and accessibility for electron transfer. Increased capacity for electron transfer could explain why intrinsic reactivity is seen to increase, whilst the concentration of initial highly reactive sites remains unchanged.

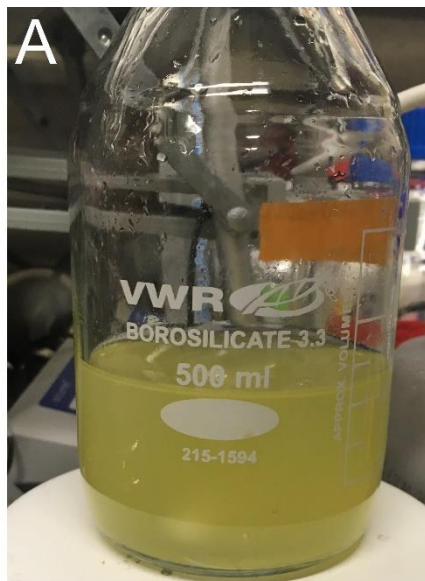
5.3.5 Conclusions / summary

The results demonstrate that reduction-oxidation cycles of N Au-1 with aqueous Fe(II) impacts both the structure of the clay mineral and the overall system's reactivity towards nitroaromatic contaminants. Kinetic experiments show that contaminant transformation is significantly increased after 2 cycles of reduction with Fe(II) and oxidation with hydrogen peroxide. Isotope-specific Mössbauer spectroscopy highlights that the reaction of aqueous Fe(II) with clay mineral octahedral Fe leads to irreversible structural changes to the clay mineral, possibly due to Fe atom exchange. The oxidation of the $\text{Fe(II)}_{\text{aq}}$ leads to the formation of a reactive Fe(II)-rich precipitate species. The presence of these secondary Fe precipitates has a significant effect on the reactivity of the system towards the reductive transformation of 3-chloronitrobenzene. Reaction kinetics show the greatest increase after Cycle 1, and it is proposed that this is due to the presence of remnant Fe-oxides in Cycle 2 which encourage the formation of reactive material with greater capacity for electron transfer to the contaminant.

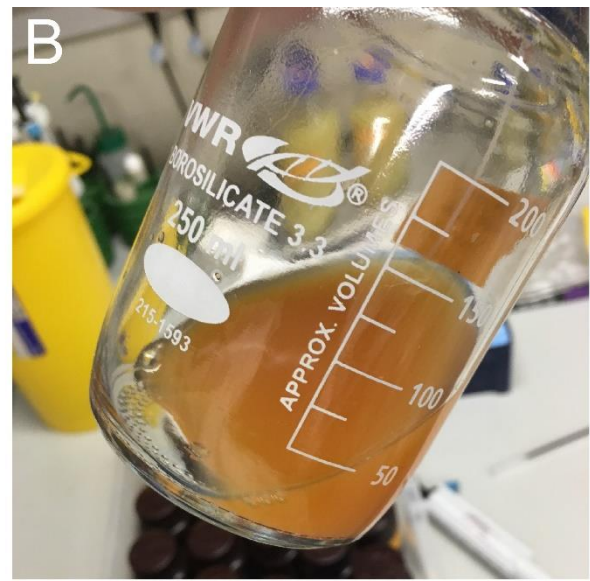
5.3.6 Supporting information



SI Figure 5.1: All collected kinetic data for Fe(II)-reduced NAu-1 for all reduction cycles. Contains the measured concentration values for both 3-chloronitrobenzene, and product compound 3-chloroaniline. Figure also contains modeled fittings when measured with both 1-site model and 2-site model.



Native NAu-1



Fe(II)-reduced,
reoxidised NAu-1

Figure SI 5.2 : Image A shows native, unaltered NAu-1 in suspension with DIW. Image B shows NAu-1 in suspension with DIW after reaction with $\text{Fe(II)}_{\text{aq}}$ and subsequent oxidation with H_2O_2 . Comparison of two images depicts the change in colour after a reduction oxidation cycle with $\text{Fe(II)}_{\text{aq}}$.

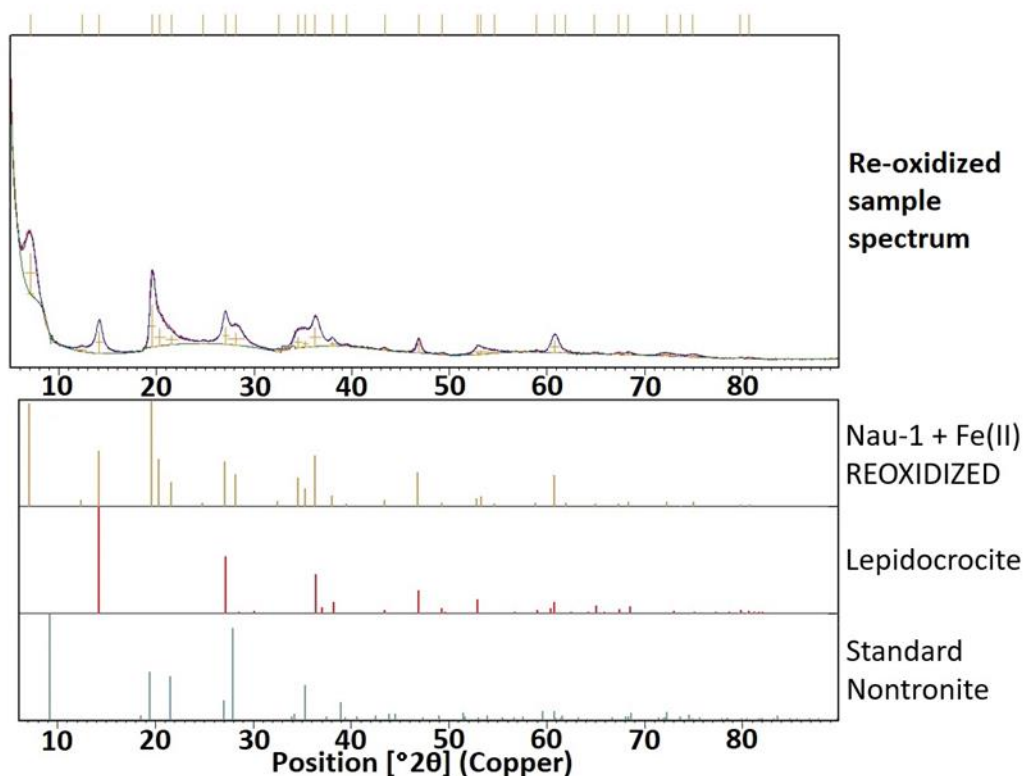


Figure SI 5.3: Upper figure shows the measured XRD spectrum for NAu-1 reduced with $\text{Fe(II)}_{\text{aq}}$ and reoxidised with H_2O_2 . Lower figure shows the location and magnitude of the peaks observed in the reoxidised NAu-1 spectrum, as well as the standard expected peaks for Nontronite and Lepidocrocite for comparison.

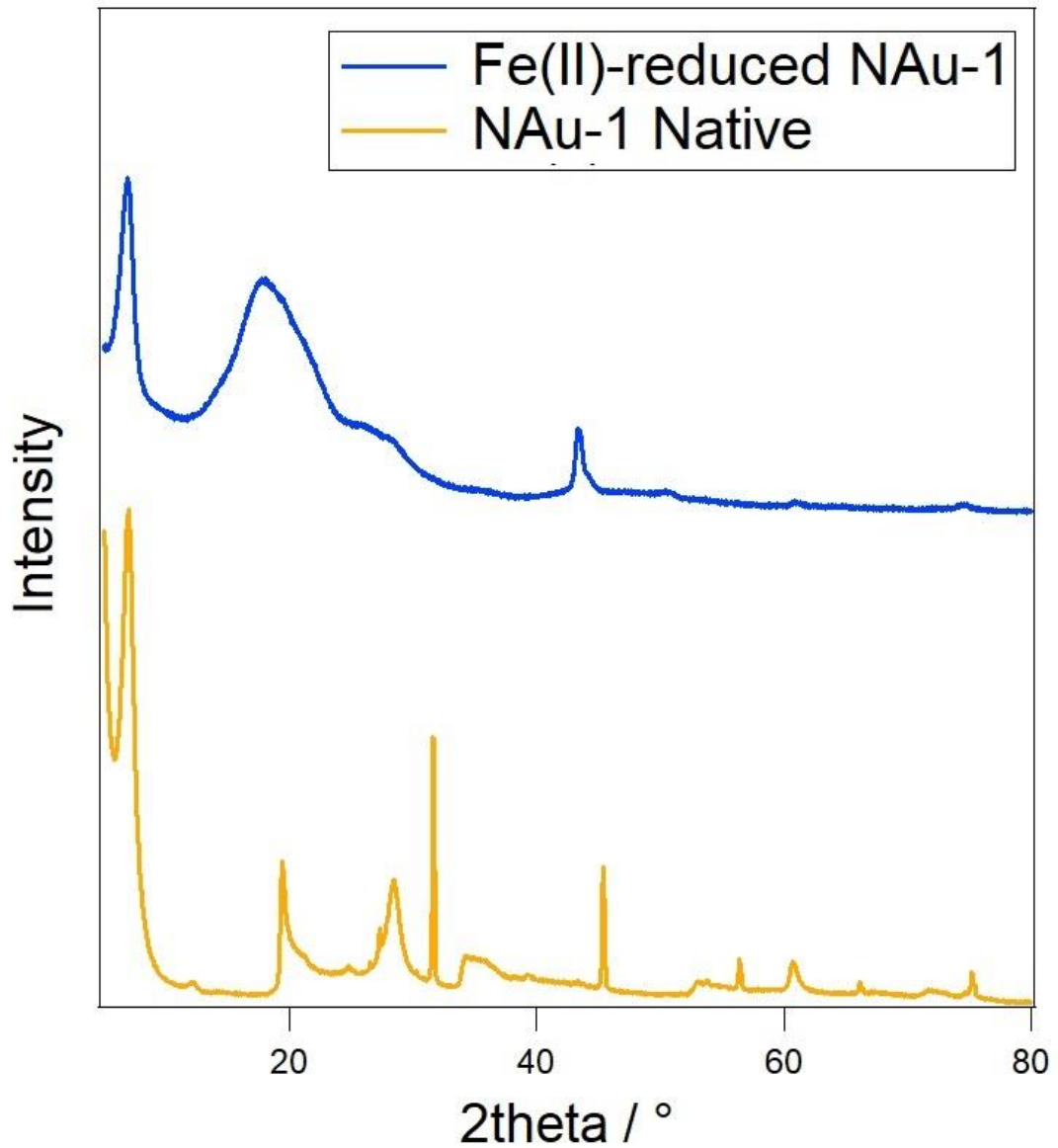


Figure SI 5.4: The measured spectra for native, unaltered N Au-1 (orange) and for N Au-1 after reaction with Fe(II)_{aq}. The Fe(II)-reduced N Au-1 sample was measured using a sealed anoxic dome to prevent oxidation, however the dome caused interference with the reading making analysis difficult.

Table SI 5.1: Hypofine parameters derived from spectra fitting of Mössbauer spectra of dithionite-reduced NAu-1 exhibiting high and low Fe reduction extents. Spectra were measured at 4 K temperature. Centre shift (CS) relative to α -Fe(0). Variable line width fitting technique (Full Static Hamiltonian) was used to establish the Mössbauer parameters. Fe species are colour coded to match the spectra of Figure 5.5.

		CS (mm/s)	H (T)	$e^2qQ/2$ (mm/s)	η (-)	w (mm/s)	θ (-)	% Area
^{56}Fe -reduced	Sextet	0.49	50.33	-0.14	0	0.40	0	5.35
	Fe(II) doublet	1.16	0	3.07	0	0.37	0	6.48
	Fe(III) doublet	0.50	0	0.42	0	0.46	0	57.7
	Lump	0.57	21.25	0.22	0	1.55	0	30.48
		CS (mm/s)	H (T)	$e^2qQ/2$ (mm/s)	η (-)	w (mm/s)	θ (-)	% Area
^{56}Fe -reduced, reoxidised	Sextet	0.51	49.98	-0.15	0	0.20	0	6.18
	Fe(III) doublet	0.49	0	0.44	0	0.36	0	83.32
	Poorly-ordered	0.48	13.88	0.24	0	2.12	0	10.50
		CS (mm/s)	H (T)	$e^2qQ/2$ (mm/s)	η (-)	w (mm/s)	θ (-)	% Area
^{56}Fe -reduced, reoxidised, ^{56}Fe -reduced	Sextet 1	0.45	50.32	-0.14	0	0.39	0	12.40
	Sextet 2	0.43	45.50	0.44	0	0.28	0	4.90
	Sextet 3	0.31	40.62	0.47	0	0.30	0	4.00
	Fe(II) doublet	1.27	0	3.13	0	0.30	0	6.29
	Fe(III) doublet	0.48	0	0.52	0	0.40	0	15.12
	Fe(III) 'other'	0.48	7.17	0.02	0	0.79	0	16.86
	Collapsed	0.87	24.46	0.01	0	1.50	0	40.45
		CS (mm/s)	H (T)	$e^2qQ/2$ (mm/s)	η (-)	w (mm/s)	θ (-)	% Area
^{56}Fe -reduced, reoxidised,	Sextet 1	0.47	50.02	-0.14	0	0.44	0	10.22
	Sextet 2	0.50	45.31	0.40	0	0.40	0	11.03
^{56}Fe -reduced, reoxidised	Fe(III) doublet	0.48	0	0.45	0	0.38	0	65.65
	Poorly-ordered	0.37	18.00	-0.64	0	1.35	0	13.10

Table SI 5.2: Hypofine parameters derived from spectra fitting of Mössbauer spectra of dithionite-reduced N_{Au}-1 exhibiting high and low Fe reduction extents. Spectra were measured at 77 K. Centre shift (CS) relative to α -Fe(0). Voigt-based fitting was used to establish the Mössbauer parameters. Species are colour-coded to match the spectra of Figure 5.8

		P	CS (mm/s)	H (T)	QS (mm/s)	σ (mm/s)	% Area
⁵⁷ Fe-reduced	Fe(III) doublet 1	100 %	0.47	0	0.44	0.15	14.90
	Fe(II) doublet 1	component 1 (50 %)	1.29	0	2.75	0.30	60.85
			component 2 (50 %)	2.87			
	Fe(II) doublet	100 %	1.40	0	3.40	0.16	9.75
	Fe 'other'	100 %	0.67	0	0.30	0.38	14.50
⁵⁷ Fe-reduced, reoxidised	Fe(III) doublet 1	100 %	0.49	0	0.55	0.31	45.10
	Fe(III) doublet 2	100 %	0.46	0	0.98	0.45	38.20
	Fe(II) doublet	100 %	1.40	0	3.33	0.29	6.72
	Fe 'other'	100 %	0.95	0	2.31	2.90	9.98
⁵⁷ Fe-reduced, reoxidised, ⁵⁶ Fe-reduced	Fe(III) doublet 1	100 %	0.48	0	0.56	0.24	46.23
	Fe(II) doublet 1	component 1 (50 %)	1.25	0	2.85	0.22	35.30
			component 2 (50 %)	2.86			
	Fe(II) doublet	100 %	1.49	0	3.24	0.15	3.87
	Fe 'other'	100 %	0.75	0	0.66	0.78	14.60
⁵⁷ Fe-reduced, reoxidised, ⁵⁶ Fe-reduced, reoxidised	Fe(III) doublet 1	100 %	0.49	0	0.53	0.23	67.90
	Fe(III) doublet 2	100 %	0.45	0	0.98	0.37	27.10
	Poorly resolved	100 %	0.55	0	0	2.51	5.00
⁵⁶ Fe-reduced, reoxidised, ⁵⁷ Fe-reduced	Fe(III) doublet 1	100 %	0.48	0	0.54	0.26	40.00
	Fe(II) doublet 1	component 1 (50 %)	1.27	0	2.80	0.20	42.12
			component 2 (50 %)	2.81			
	Fe(II) doublet	100 %	1.36	0	3.34	0.21	4.75
	Fe 'other'	100 %	0.76	0	0.52	0.59	13.13
⁵⁶ Fe-reduced, reoxidised, ⁵⁷ Fe-reduced, reoxidised	Fe(III) doublet 1	100 %	0.48	0	0.52	0.31	45.00
	Fe(III) doublet 2	100 %	0.47	0	1.02	0.43	30.70
	Poorly resolved	100 %	0.55	0	0	3.00	14.00
	Fe(III) sextet	100 %	0.50	45.24	0.21	2.96	10.30

Table SI 5.3: Hypfine parameters derived from spectra fitting of Mössbauer spectra of dithionite-reduced NAu-1 exhibiting high and low Fe reduction extents. Spectra were measured at 4 K temperature. Centre shift (CS) relative to α -Fe(0). Variable line width fitting technique (Full Static Hamiltonian) was used to establish the Mössbauer parameters. Fe species are colour coded to match the spectra of Figure 5.9.

		CS (mm/s)	H (T)	$e^2qQ/2$ (mm/s)	η (-)	w (mm/s)	θ (-)	% Area
⁵⁷ Fe-reduced	Sextet 1	0.46	54.02	-0.20	0	0.25	0	7.41
	Sextet 2	0.45	50.12	-0.05	0	0.30	0	4.63
	Sextet 3	0.47	46.00	-0.12	0	0.30	0	2.04
	Fe(II) doublet	1.35	0	-3.25	0	0.40	0	29.06
	Fe(III) doublet	0.48	0	0.49	0	0.40	0	6.36
	Octet	1.30	12.42	-2.97	0	0.46	90	35.93
	Collapsed	0.67	26.18	0.60	0	1.26	0	14.58
⁵⁷ Fe-reduced, reoxidised		CS (mm/s)	H (T)	$e^2qQ/2$ (mm/s)	η (-)	w (mm/s)	θ (-)	% Area
	Sextet 1	0.5	49.75	-0.08	0	0.28	0	14.41
	Sextet 2	0.49	47.48	-0.09	0	0.23	0	12.94
	Sextet 3	0.486	45.60	-0.03	0	0.21	0	20.54
	Sextet 4	0.49	43.81	-0.03	0	0.22	0	13.94
	Sextet 5	0.49	40.87	0	0	0.39	0	14.09
	Fe(II) doublet	1.41	0	3.34	0	0.25	0	10.30
Fe(III) doublet	0.51	0	0.54	0	0.41	0	13.77	
⁵⁷ Fe-reduced, reoxidised, ⁵⁶ Fe-reduced		CS (mm/s)	H (T)	$e^2qQ/2$ (mm/s)	η (-)	w (mm/s)	θ (-)	% Area
	Sextet 1	0.54	54.06	-0.32	0	0.18	0	2.31
	Sextet 2	0.53	49.97	-0.16	0	0.35	0	12.45
	Sextet 3	0.49	45.53	0.01	0	0.24	0	19.72
	Sextet 4	0.49	43.41	0.08	0	0.22	0	13.73
	Sextet 5	0.46	40.42	0.20	0	0.33	0	9.60
	Fe(II) doublet	1.35	0	3.22	0	0.34	0	11.55
	Fe(III) doublet	0.40	0	0.38	0	0.67	0	3.66
Octet	1.37	12.85	-2.92	0	0.52	90	26.46	
⁵⁷ Fe-reduced, reoxidised, ⁵⁶ Fe-reduced, reoxidised		CS (mm/s)	H (T)	$e^2qQ/2$ (mm/s)	η (-)	w (mm/s)	θ (-)	% Area
	Sextet 1	0.49	49.53	-0.09	0	0.28	0	19.75
	Sextet 2	0.49	47.46	-0.06	0	0.19	0	11.54
	Sextet 3	0.49	45.48	0.01	0	0.18	0	22.76
	Sextet 4	0.49	43.61	0.05	0	0.20	0	21.70
Sextet 5	0.49	40.83	0.1	0	0.31	0	18.33	
Fe(III) doublet	0.48	0	0.33	0	0.56	0	10.10	
⁵⁶ Fe-reduced, reoxidised, ⁵⁷ Fe-reduced		CS (mm/s)	H (T)	$e^2qQ/2$ (mm/s)	η (-)	w (mm/s)	θ (-)	% Area
	Sextet 1	0.49	53.92	-0.20	0	0.29	0	4.44
	Sextet 2	0.48	49.64	-0.16	0	0.41	0	10.32
	Sextet 3	0.49	45.51	0.02	0	0.21	0	19.42
	Sextet 4	0.48	43.60	0.07	0	0.22	0	12.88
	Sextet 5	0.46	40.452	0.15	0	0.33	0	9.34
	Fe(II) doublet	1.34	0	3.19	0	0.38	0	15.34
	Fe(III) doublet	0.48	0	0.50	0	0.40	0	4.35
Octet	1.34	12.57	-2.99	0	0.53	90	23.92	
⁵⁶ Fe-reduced, reoxidised, ⁵⁷ Fe-reduced, reoxidised		CS (mm/s)	H (T)	$e^2qQ/2$ (mm/s)	η (-)	w (mm/s)	θ (-)	% Area
	Sextet 1	0.48	50.03	-0.11	0	0.279289	0	18.51
	Sextet 2	0.48	47.33	-0.09	0	0.224028	0	14.48
	Sextet 3	0.49	45.44	0.01	0	0.19239	0	23.94
	Sextet 4	0.48	43.16	0.05	0	0.203098	0	17.43
Sextet 5	0.48	40.30	0.11	0	0.338719	0	17.28	
Fe(III) doublet	0.48	0	0.60	0	0.39	0	8.35	

Chapter 6: Synthesis and Conclusions

6.1 Introduction

The research conducted has highlighted that redox cycling of Fe-bearing clay minerals can be sustainable and that under optimum conditions clay minerals can serve as a renewable source of reduction equivalents. Our data indicate that the degree of sustainability is dependant on the electron transfer pathway and the extent of structural Fe reduction. Based on the knowledge gaps outlined in Chapter 2, the project has:

- Evaluated the impact of chemical redox cycling on Fe-rich smectites, using dithionite to achieve both a high and low extent of structural Fe reduction. The project measured how structure, morphology, and intrinsic reactivity was altered over three successive cycles of dithionite-reduction and oxidation. Results showed that the reactivity of the clay minerals was not significantly impacted by redox cycling, at a high or low extent of reduction. Redox cycling did leave some irreversible changes to the mineral structure, however the process was largely sustainable and effects did not compound with successive cycles. Results highlighted a major shift in Fe-speciation occur for clay minerals redox cycled to a high reduction extent after the third reoxidation. It is unclear whether this would impact the reactivity of the mineral, if redox cycling experiments were to continue.
- Effectively subjected Fe-rich smectites to multiple cycles of reduction and oxidation, using only reduced electron-shuttle AH₂DS as the reducing agent. The experiment demonstrated that reduction of clay mineral Fe by AH₂DS is thermodynamically limited, and reduction extent was consistently capped at ~10%. Results also measured the impact of redox cycling with AH₂DS on reactivity and mineral structure and observed no significant changes over three redox cycles, indicating that redox cycling can be conducted sustainably in this instance.
- Investigated the transformation of 3-chloronitrobenzene in the presence of Fe(II)-reduced smectite. Results showed the changes in clay mineral structural

Fe speciation over multiple reduction-oxidation cycles and found evidence of structural Fe redistribution, suggesting clay mineral structure was significantly and irreversibly altered by Fe(II) redox cycling. The study also examined the impacts of the secondary Fe precipitates on the overall observed reactivity of the system. Precipitate minerals were found to cause a significant increase in reactivity. There was a significant increase to intrinsic reactivity on the second cycle, which coincided with an increased relative percentage of magnetically ordered material. It was theorised that increased magnetic ordering of the Fe material allowed improved electron transfer, leading to greater reactivity towards the contaminant.

The primary research outcomes, significance, and environmental implications are summarised below.

6.1.1 Assessment of dithionite reduction as proxy for reduction in natural sediments

This study has evaluated the impact of chemical redox cycling on Fe-rich smectites, using dithionite to achieve both a high and low extent of structural Fe reduction. The results indicated that dithionite could be used repeatedly and sustainably to reduce clay mineral structural Fe for at least three cycles. Reactivity was not significantly impacted by multiple cycles of reduction and oxidation for either minerals reduced to a high or low extent of Fe(II) content. Structural Fe speciation was most affected at high reductions extents (as measured with Mössbauer spectroscopy), but there was no evidence to indicate that these changes would impact clay mineral efficacy.

The results gathered in Chapter 3 on redox cycling with dithionite provide a basis to understand fundamentally how fluctuating valence state affects clay minerals in a controlled and isolated system. At low reduction extents (i.e. 20%), the results highlight the impact of redox cycling at environmentally relevant levels. The data demonstrates that when extents of structural Fe(II) remain within the ranges expected for natural systems, clay minerals are renewable and sustainable. Neither structure or reactivity is significantly altered, meaning clay minerals could provide a renewable source of reduction equivalents. However, sustainability of redox cycling under laboratory conditions could imply that irreversible changes observed at low reduction

extents in other studies with different reduction pathways (e.g. Yang et al. 2012, Zhao et al. 2015) might be the result of additional system variables. The results of Chapter 5 found that the presence of aqueous Fe(II) led to major structural rearrangements of the clay mineral, and previous work has seen significant atomic Fe exchange between the aqueous and mineral phase (Neumann et al. 2015). Similarly, work involving microbes has described dramatic mineralogical shifts such as dissolution and complete transformation (e.g. Dong et al. 2003, 2009, Kim et al. 2012, Yang et al. 2012, Shi et al. 2021). In natural systems, aqueous ions such as Fe(II) and bacteria are not only abundant, but their interactions with clay minerals would be largely unavoidable. This means that although results demonstrate that redox cycling is sustainable at environmentally relevant reduction extents, this does not imply that clay minerals can be used sustainably in natural systems.

High reduction extent data demonstrates the impact of redox cycling under extreme conditions, and can be used to examine the limits of clay mineral utility and reusability. Using dithionite to achieve unnaturally high reduction extents also provide a means to simulate engineered systems, such as artificial redox manipulation. As with low reduction extent, clay minerals were found to be largely reusable even when reduction extent is significantly increased. Reaction kinetics implied that although reactivity was not impacted by redox cycling, the higher reduction extent caused an increase in intrinsic reactivity as rate constants were increased beyond the scale of increased Fe(II) content. This indicates that clay minerals could be renewably used for contaminant control even at unnaturally high reduction extents.

While there were some structural changes observable in Mössbauer spectroscopy, these changes did not appear to influence the intrinsic reactivity of the clay mineral over multiple redox cycles. Additionally, the spectra of reoxidised samples did not appear to change significantly after the first reduction cycle. In comparison, research by Gorski et al. (2012, 2013) paper highlighted a shift in redox profile after the first reduction, but subsequent cycles were unaffected by reduction. A key difference to the Gorski et al. (2012, 2013) paper however is that our experiment did not reduce the mineral to 100% structural Fe(II) content, and in all cycles some structural Fe(III) remained. There was a significant change to the Mössbauer spectrum after the third

reoxidation for highly reduced samples, but the altered spectrum is similar to those of fully-reduced, reoxidised nontronites (Ribeiro et al. 2009). The structural rearrangement observed in Cycle 3 (reoxidised) Mössbauer spectrum, specifically the departure from a central doublet, might represent the transition to trioctahedral configuration as discussed in previous papers (Manceau et al. 2000a, 2000b, Ribeiro et al. 2009, Tratnyek et al. 2011). This rearrangement might also be what causes the shift in redox profile described by Gorski et al. (2012,2013), and therefore would explain why there is no clear shift in reaction kinetics after the first cycle. This could imply that redox cycling of clay minerals at unnaturally high reduction extents might be sustainable beyond three redox cycles. The transition to trioctahedral configuration might impact transformation kinetics due to a shift in redox profile, but research (Gorski et al. 2013) indicates cycling should be repeatable after the transition. It is unclear whether a transition to trioctahedral configuration would negatively impact structural resilience over time. Further work would be required to investigate this hypothesis further.

6.1.2 Effects of Fe redox cycling by electron shuttles on the reactivity and structure of clay minerals, and suitability as proxy for microbial reduction

The data collected in this chapter indicates that redox cycling of Fe-rich clay minerals in the presence of microbially produced electron-shuttles appears entirely sustainable. Reduction-oxidation cycling of clay minerals with reduced electron-shuttles produced no significant impact on either the structure or the reactivity of the clay mineral. Any effects observed in the reduced state were largely reversible upon reoxidation, indicating that in this instance Fe-rich clay minerals could be used sustainably. The minimal impact of reduction is likely because the achievable reduction extent in the clay mineral is limited to approximately 10% Fe(II), and research has shown that the degree of reversibility decreases with increasing reduction extent. Results also demonstrated that the reaction of AH₂DS and NAu-1 reached equilibrium, which supports previous research suggesting microbial reduction of Fe-rich smectites by microbial reduction is thermodynamically and energetically limited (Jaisi et al. 2007a, Luan et al. 2014).

The lack of irreversible alterations is strong evidence to suggest that irreversible effects of microbial reduction such as dissolution and illitization (e.g. Dong et al. 2003, Kim et al. 2004, Shi et al. 2021), might instead potentially be effects of greater microbial metabolism rather than electron transfer. Previous studies have observed the microbial dissolution of silicate minerals (Vorhies and Gaines 2009, Gilmour et al. 2022) resulting in the release of Al, Si, and Fe. Additionally, studies have observed microbial production of organic ligands and chelating agents by microbes to access mineral-bound (Rogers and Bennett 2004, Kim 2012, Melton et al. 2014). If the reduction of structurally-bound Fe is thermodynamically limited (as results indicate), then microbes may require a means to remove the Fe from said structure to allow respiration to proceed. By exuding organic substances that destabilise and dissolve silicates, it might allow an additional method for bacteria to access Fe for respiration, Fe that was previously inaccessible due to thermodynamic limitations. This would explain why mineral dissolution and transformation occur in tandem with microbial reduction. Microbial reduction however is not a direct causation of mineral dissolution, as the project has demonstrated that the reduction process is sustainable. The results of this experiment suggest that in the absence of living microorganisms, microbial reduction of clay minerals via organic compounds (e.g. humic substances) and exudates is sustainable.

6.2 Effects of redox cycling via biologically-mediated, abiotic reduction – impact on clay mineral structure and the role of secondary precipitates

Results found that the reaction of smectite NAu-1 with aqueous Fe(II) leads to significant increases in system reactivity towards 3-chloronitrobenzene. On the second cycle specifically, rate constant values increased by orders of magnitude, but were largely unchanged on the third cycle. The data confirmed that partial oxidation of the aqueous Fe(II) lead to the formation of secondary, mixed-valent precipitates and that these were dominating the changes in reaction kinetics.

Isotope specific Mössbauer analysis highlighted that the clay mineral was being irreversibly altered by each reduction cycle. The study has observed that the percentage of reduceable structural Fe increased and that structural Fe was being redistributed with each successive cycle. Even though the project could not collect

direct evidence for this hypothesis, our observations can be rationalised by atom exchange during the interaction of clay mineral Fe with aqueous Fe(II), as previously demonstrated (Neumann et al. 2015). This calls the sustainability of the clay minerals into questions as it is not known if these atomic exchanges would lead to a gradual deterioration of the mineral over many successive cycles. After only two redox cycles, approximately 20% of clay mineral structural Fe had been rearranged to species resembling the external Fe-oxyhydroxides. This would indicate that all structural Fe might be reprecipitated as new minerals in only a few cycles of reduction and oxidation. It is possible that this structural Fe is replaced by oxidised Fe(II) during atom exchange, and the interaction follows the conveyor-belt model as described in Neumann et al. (2015), but this cannot be confirmed. If dissolved structural Fe atoms are replaced by oxidised aqueous Fe(II) atoms (as described in the conveyor-belt model), it is unknown whether this would result in a product mineral with equivalent structural integrity.

The data so far could indicate that aqueous Fe(II) could leave a greater impact on clay minerals than microbial reduction. Previous work has found that dissolution due to microbial reduction decreases with each cycle as smaller fragments are preferentially dissolved in favour of larger particles (e.g. Yang et al. 2012). There was no indication in our data to indicate a cease to the redistribution of structural Fe after Fe(II) redox cycling. Similarly, in other circumstances where studies have measured release of structural Fe from clay minerals, such as in response to microbial activity (e.g. Rogers and Bennett 2004, Gilmour et al. 2022), release of silica is also measured. The work conducted in this project did not measure the release of silica, but it is possible it may have occurred in tandem with Fe release. Release of both Fe and Si from clay minerals could indicate destruction of the clay mineral. Aside from dissolution caused by direct contact of microbes and clay minerals, the bioreduction of other Fe minerals leads to the release of Fe(II) (Dong et al. 2003). As both microbes and Fe minerals are abundant in natural systems and both pose a threat to clay mineral sustainability, this may imply that clay minerals are finitely renewable in the environment.

Mössbauer analysis also provided insight into the behaviour of the secondary precipitate minerals over multiple reduction-oxidation cycles. It was found that in the

first cycle the oxidation of aqueous Fe(II) formed a mixed-valent species with some partial magnetic ordering. This species was converted to lepidocrocite upon reoxidation, as confirmed with XRD. For the second cycle, it was demonstrated that there was significant interaction between the new aqueous Fe(II) and the solid lepidocrocite remnant from Cycle 1. Significant electron transfer between the two phases was observed, and the resulting spectra of both pools of Fe were transformed to resemble one another. Although both Cycle 1 and Cycle 2 contained reactive mixed-valent Fe precipitates, the precipitates of Cycle 2 displayed significantly greater reactivity than those of Cycle 1. When examining the Mössbauer spectrum of secondary precipitates in Cycle 2, it was found they displayed similar parameters to the spectrum in Cycle 1. However, Cycle 2 precipitates consisted of a far greater relative percentage of magnetically-ordered material. It was theorised that the increased magnetic ordering present in Cycle 2 allowed improved electron transmission through the secondary precipitate minerals, which caused a greater accessibility of reactive Fe(II) and subsequently led to the observed increases in kinetics.

The results of Chapter 5 indicate that clay minerals may not be sustainable when subjected to redox cycling with aqueous Fe(II). However, the interactions between clay mineral and Fe(II) might lead to the formation of secondary minerals that are far superior in contaminant transformation. The secondary minerals were also either improved, or unchanged by subsequent reduction cycles. This aligns well with previous work (e.g. Entwistle 2021), and demonstrates that clay minerals and Fe(II) could provide an effective measure for the control of land contamination.

6.3 Environmental impacts on the suitability of clay minerals as sustainable materials for remediation of land contamination

In conclusion, the project has demonstrated that the oxidation state of structural Fe in clay minerals can be used sustainably, and that clay minerals can provide a renewable source of reduction equivalents. This means that clay minerals are a potentially highly valuable material for redox-active processes. However, the degree of sustainability might be limited to controlled environments. Results indicate that environmental influences such as microbial activity and dissolved species are likely to be the causes of significant alterations (such as dissolution and mineral transformation) described by previous research (e.g. Kim et al. 2012, Yang et al. 2012, Shi et al. 2021). The project

has found that mineral transformation (as described in literature) is not necessarily the result of redox cycling, but rather a result of interactions with secondary products resulting from bacterial activity. Clay minerals can be directly altered by bacterially-produced organic ligands and chelating agents (Rogers and Bennett 2004, Kim et al. 2012), or indirectly altered by aqueous Fe(II) released by the bioreduction of other Fe-minerals (as demonstrated in Chapter 5). The ubiquitous presence of bacteria in sediments means that structural alterations may be unavoidable, even if the valence state of structural Fe can be effectively cycled. This means that clay minerals will surely play a role in the transformation of land contaminants, but their ability to continue to do so over time may not be indefinite. This research does however open the doors to future innovation, demonstrating that clay minerals do offer substantial utility and promise as chemically resilient redox-active materials.

References

Adamou P., (2020), "Assessing treatment technologies for reducing antibiotic resistant gene abundance and diversity in domestic wastewater treatment effluents", Ph.D Thesis, Newcastle University

Amonette J.E, Templeton J.C., (1998), "Improvements to the quantitative assay of nonrefractory minerals for Fe (ii) and total Fe using 1, 10-phenanthroline" *Clays and Clay Minerals*", Vol. 46(1), P51–62

Amonette J.E., Szecsody J.E., Schaef H.T., Gorby Y.A., Fruchter J.S., Templeton J.C., (1994), "Abiotic reduction of aquifer materials by dithionite: a promising *in-situ* remediation technology", (No. PNL-SA--24505). Pacific Northwest Lab.

Alexandrov V., Neumann A., Scherer M.M., Rosso K.M., (2013), "Electron Exchange and Conduction in Nontronite from First Principles", *The Journal of Physical Chemistry*, Vol. 117, 5, p2032-2040

Arnold R.G., DiChristina T.J., Hoffmann M.R., (1988), "Reductive dissolution of Fe (III) oxides by *Pseudomonas* sp. 200", *Biotechnology and Bioengineering*, Vol. 32, p1081-1096

Baron F., Petit S., Pentrak M., Decarreau A., Stucki J.W., (2017), "Revisiting the Nontronite Mössbauer Spectra"., *American Mineralogist*, Vol. 102, p1501-1515

Barth M.E., McNichols M.F., (1994), "Estimation and market valuation of environmental liabilities relating to superfund sites" *Journal of Accounting Research*, Vol. 32, p177-209

Berquó T.S., Imbernon R.A.L., Blot A., Franco D.R., (2007), "Low Temperature Magnetism and Mössbauer Spectroscopy Study from Natural Goethite", *Physics and Chemistry of Minerals*, Vol. 34, p287-294

Bergaya F., Lagaly G., (2006), "General introduction: clays, clay minerals, and clay science", *Developments in clay science*, Vol. 1, p1-18

Berverskog B., Puigdomenech I., (1996) "Revised pourbaix diagrams for iron at 25–300 C", *Corrosion Science*, Vol. 38, p2121-2135.

Assessing the sustainability of Fe-bearing clay mineral redox reactions

References

- Bishop M.E., Dong H., Kukkadapu R.K., Liu C., Edelman R.E., (2011), "Bioreduction of Fe-bearing Clay Minerals and their Reactivity towards Pertechnate (Tc-99)", *Geochimica et Cosmochimica Acta*, Vol. 75, p5229-5246
- Bishop M.E., Dong H., Glasser P., Briggs B.R., Pentrak M., Stucki J.W., Boyanov M.I., Kemner K.M., Kovarik L., (2019), "Reactivity of redox cycled Fe-bearing subsurface sediments towards hexavalent chromium reduction" *Geochimica et Cosmochimica Acta*, Vol. 252, p88-106
- Bonneville S., Van Cappellen P., Behrends T., (2004), "Microbial reduction of iron (III) oxyhydroxides: effects of mineral solubility and availability", *Chemical Geology*, Vol. 212, p255-268
- Boparai H.K., Comfort S.D., Shea P.J., Szecsody J.E., (2008), "Remediating explosive-contaminated groundwater by in situ redox manipulation (ISRM) of aquifer sediments", *Chemosphere*, Vol. 71, p933-941
- Braunschweig J., Bosch J., Meckenstock R.U., (2013), "Iron oxide nanoparticles in geomicrobiology: from biogeochemistry to bioremediation", *New biotechnology*, Vol. 30(6), p793-802
- Brombal D., Wang H., Pizzol L., Critto A., Giubilato E., Guo G., (2015), "Soil environmental management systems for contaminated sites in China and the EU. Common challenges and perspectives for lesson drawing", *Land Use Policy*, Vol. 48, p286-298
- Burke S.P., Banwart S.A., (2002), "A Geochemical Model for Removal of Iron (II)(aq) from Mine Water Discharges", *Applied Geochemistry*, Vol. 17, p431-443.
- Calabrese S., and Porporato A., (2019), "Impact of ecohydrological fluctuations on iron-redox cycling", *Soil Biology and Biochemistry*, Vol. 133, p188-195.
- Chapman P.M., (2002), "Integrating toxicology and ecology: putting the "eco" into ecotoxicology", *Marine pollution bulletin*, Vol. 44, p7-15.
- Coates J.D., Phillips E.J., Lonergan D.J., Jenter H., Lovley D.R., (1996), "Isolation of Geobacter species from diverse sedimentary environments", *Applied and Environmental Microbiology*, Vol. 62, p1531-1536

Assessing the sustainability of Fe-bearing clay mineral redox reactions

References

Coby A.J., Picardal F., Shelobolina E., Xu H. and Roden E.E., (2011) "Repeated anaerobic microbial redox cycling of iron", *Applied and environmental microbiology*, Vol. 77, p6036-6042.

Colón D., Weber E.J., Anderson J.L., (2006), "QSAR Study of the Reduction of Nitroaromatics by Fe(II) Species", *Environmental Science and Technology*, Vol. 40, p4976-4982

Cooper D.C., Picardal F.F., Coby A.J., (2006), "Interactions between microbial iron reduction and metal geochemistry: effect of redox cycling on transition metal speciation in iron bearing sediments", *Environmental science & technology*, Vol. 40, p1884-1891.

Cornell R.M., Schwertmann U., (2003), "The Iron Oxides: Structure, Properties, Reactions, Occurrences and Uses", *Wiley-VCH Verlag GmbH and Co.*, ISBN: 3-527-30274-3

Cundy A.B., Hopkinson L. and Whitby R.L., (2008), "Use of iron-based technologies in contaminated land and groundwater remediation: A review", *Science of the total environment*, Vol. 400, p42-51.

Curtis G.P., Reinhard M., (1994), "Reductive Dehalogenation of Hexchloroethane, Carbon Tetrachloride, and Bromoform by Anthrahydroquinone Disulfonate and Humic Acid", *Environmental Science and Technology*, Vol. 28, p2393-2401

Dayan A.D., Paine A.J., (2001) "Mechanisms of chromium toxicity, carcinogenicity and allergenicity: review of the literature from 1985 to 2000" *Human & experimental toxicology*, Vol. 20, p439-451.

De Grave E., Persoons R.M., Chambaere D.G., Vandenberghe R.E., Bowen L.H., (1986), "An ⁵⁷Fe Mössbauer Effect Study of Poorly Crystalline γ -FeOOH", *Physics of Chemistry and Minerals*, Vol. 13, p61-67

Deng Y., Li H., Wang Y., Duan Y. and Gan Y., (2014), "Temporal variability of groundwater chemistry and relationship with water-table fluctuation in the Jiangnan Plain, central China", *Procedia Earth and Planetary Science*, Vol. 10, p100-103

Assessing the sustainability of Fe-bearing clay mineral redox reactions

References

- Dong H., Kostka J.E., Kim J., (2003), "Microscopic Evidence for Microbial Dissolution of Smectite", *Clays and Clay Minerals*, Vol. 51, p502-512
- Dong H., Jaisi D.P., Kim J. and Zhang G., (2009) "Microbe-clay mineral interactions", *American Mineralogist*, Vol. 94, p1505-1519
- Drief A., Martinez-Ruiz F., Nieto F., Sanchez N.V., (2002) "Transmission Electron Microscopy evidence for experimental illitization of smectite in K-enriched seawater solution at 50°C and basic pH", *Clays and Clay Minerals*, Vol. 50, p746-756
- Drits V.A., Manceau A., (2000), "A Model for the Mechanism of Fe³⁺ to Fe²⁺ Reduction in Dioctahedral Smectites" *Clays and Clay Minerals*, Vol. 48, p185-195
- Dyar M.D., Agresti D.G., Schaefer M.W., Grant C.A., Sklute E.C., (2006), "Mössbauer spectroscopy of earth and planetary materials", *Annual Review of Earth and Planetary Science*, Vol. 34, p83-125.
- Elsner M., Schwarzenbach R.P., Haderlein S.B., (2004), "Reactivity of Fe(II)-Bearing Minerals Towards Reductive Transformation of Organic Contaminants", *Environmental Science and Technology*, Vol. 38, p799-807
- Entwistle J., Latta D.E., Scherer M.M., Neumann A., (2019), "Abiotic Degradation of Chlorinated Solvents by Clay Minerals and Fe(II): Evidence for Reactive Mineral Intermediates", *Environmental Science and Technology*, Vol. 53, p14308-14318
- Entwistle J., (2021), "Biologically Mediated Abiotic Degradation of Chlorinated Solvents by Fe-Bearing Clay Minerals", Ph.D Thesis, Newcastle University
- Ericsson T., Wäppling R., (1976) "Texture Effects in 3/2-1/2 Mössbauer Spectra", *Journal de Physique Colloques*, Vol. 37, p719-723
- Ernstsen V., Gates W.P., Stucki J.W., (1998), "Microbial reduction of structural iron in clays—a renewable source of reduction capacity" *American Society of Agronomy, Crop Science Society of America, and Soil Science Society of America*, Vol. 27, No. 4, p761-766
- EEA., (2014) "Progress in management of contaminated sites". Report LSI003, IND-10-en, Copenhagen, Denmark: European Environment Agency (updated in Nov. 2021)

Assessing the sustainability of Fe-bearing clay mineral redox reactions

References

- Fialips C.-I., Huo D., Yan L., Wu J., Stucki J.W., (2002), "Effect of Fe Oxidation State on the IR Spectra of Garfield Nontronite", *American Mineralogist*, Vol. 87, p630-641
- Fruchter J.S., Cole C.R., Williams M.D., Vermeul V.R., Amonette J.E., Szecsody J.E., Istok J.D., and Humphrey M.D., (2000), "Creation of a Subsurface Permeable Treatment Zone for Aqueous Chromate Contamination Using In Situ Redox Manipulation", *Groundwater Monitoring & Remediation*, Vol. 20, p.66-77
- Fruchter J., (2002), "Peer reviewed: *In-situ* treatment of chromium-contaminated groundwater", *Environmental science & technology*, Vol. 36, p464A-472A.
- Fu F., Dionysiou D.D., Liu H., (2014) "The use of zero-valent iron for groundwater remediation and wastewater treatment: a review", *Journal of hazardous materials*, Vol. 267, p194-205
- Fysh S.A., Clark P.E., (1982), "Aluminous Goethite: A Mössbauer Study", *Physics and Chemistry of Minerals*, Vol. 8, p180-187
- Gao L., Lu X., Liu H., Li J., Li W., Song R., Wang R., Zhang D., Zhu J., (2019), "Mediation of extracellular polymeric substances in microbial reduction of hematite by *Shewanella oneidensis* MR-1", *Frontiers in microbiology*, Vol. 10, p575
- Gates W.P., Wilkinson H.T., Stucki J.W., (1993), "Swelling properties of microbially reduced ferruginous smectite" *Clays and Clay Minerals*, Vol. 41, p360-364
- Gates W.P., Slade P.G., Manceau A., Lanson B., (2002), "Site occupancies by iron in nontronites", *Clays and Clay Minerals*, Vol. 50, p223-239
- Genin J.M., Bauer P.H., Olowe A.A., Rezel D., (1986), "Mössbauer Study of the Kinetics of Simulated Corrosion Process of Iron in Chlorinated Aqueous Solution Around Room Temperature: The Hyperfine Structure of Ferrous Hydroxide and Green Rust I", *Hyperfine Interactions*, Vol. 29, p1355-1360
- Génin J.M.R., Aïssa R., Géhin A., Abdelmoula M., Benali O., Ernstsén V., Ona-Nguema G., Upadhyay C., Ruby C., (2005), "Fougerite and FeII-III hydroxycarbonate green rust; ordering, deprotonation and/or cation substitution; structure of hydrotalcite-like compounds and mythic ferrosic hydroxide Fe (OH)(2+ x)", *Solid State Sciences*, Vol. 7, p545-572

Assessing the sustainability of Fe-bearing clay mineral redox reactions

References

- Gilmour K.A., Davie C.T., Gray N., (2022), "Survival and activity of an indigenous iron-reducing microbial community from MX80 bentonite in high temperature/low water environments with relevance to a proposed method of nuclear waste disposal", *Science of the Total Environment*, Vol. 814, p152660
- Gorski C.A., Scherer M.M., (2009), "Influence of Magnetite Stoichiometry on Fe(II) Uptake and Nitrobenzene Reduction", *Environmental Science and Technology*, Vol. 43, 3675-3680
- Gorski C.A., Nurmi J.T., Tratnyek P.G., Hofstetter T.B., Scherer M.M., (2010) "Redox Behaviour of Magnetite: Implications for Contaminant Reduction", *Environmental Science and Technology*, Vol. 44, p55-60
- Gorski C.A., Aeschbacher M., Soltermann D., Voegelin A., Baeyens B., Fernandes M.M., Hofstetter T.B., Sander M., (2012), "Redox Properties of Structural Fe in Clay Minerals. 1. Electrochemical Quantification of Electron-Donating and –Accepting Capacities of Smectites", *Environmental Science and Technology*, vol.46, p9360-9368
- Gorski C.A., Klupfel L., Voegelin A., Sander M., Hofstetter T.B., (2012), "Redox Properties of Structural Fe in Clay Minerals. 2. Electrochemical and Spectroscopic Characterisation of Electron Transfer Irreversibility of Ferruginous smectite, SWa-1", *Environmental Science and Technology*, Vol. 46, p9369-9377
- Gorski C.A., Klupfel L., Voegelin A., Sander M., Hofstetter T.B., (2013), "Redox Properties of Structural Fe in Clay Minerals. 3. Relationships between Smectite Redox and Structural Properties", *Environmental Science and Technology*, Vol. 47, p13477-13485
- Greffié C., Amouric M., Parron C., (2001), "HRTEM Study of Freeze-dried and Untreated Synthetic Ferrihydrites: Consequences of Sample Processing", *Clay Minerals*, Vol. 36, p381-387
- Grim R.E., (1962), "Applied clay mineralogy"
- Gütlich P., Eckhard B., Trautwein A.X., (2011), "Mössbauer Spectroscopy and Transition Metal Chemistry", *Springer – Verlag Berlin Heidelberg*, ISBN:978-3-540-88427-9

Guyodo Y., Bonville P., Till J.L., Ona-Nguema G., Lagroix F., Menguy N., (2016)

“Constraining the Origins of the Magnetism of Lepidocrocite (γ -FeOOH): A Mössbauer and Magnetization Study”, *Frontiers in Earth Science*, Vol. 4., Article: 28, doi:

10.3389/feart.2016.00028

Haderlein S.B., and Schwarzenbach R.P., (1993), “Adsorption of substituted nitrobenzenes and nitrophenols to mineral surfaces”, *Environmental Science & Technology*, Vol. 27, p316-326

Haderlein S.B., and Schwarzenbach R.P., (1995), “Environmental processes influencing the rate of abiotic reduction of nitroaromatic compounds in the subsurface”, in *Biodegradation of nitroaromatic compounds*, p199–225. Springer

Handler R.M., Beard B.L., Johnson C.M., Scherer M.M., (2009), “Atom exchange between aqueous Fe (II) and goethite: an Fe isotope tracer study”, *Environmental science & technology*, Vol. 43, p1102-1107

Hartenbach A., Hofstetter T.B., Berg M., Bolotin J., Schwarzenbach R.P., (2006), “Using nitrogen isotope fractionation to assess abiotic reduction of nitroaromatic compounds”, *Environmental science & technology*, Vol. 40, p7710-7716

Hashim M.A., Mukhopadhyay S., Sahu J.N. and Sengupta B., (2011), “Remediation technologies for heavy metal contaminated groundwater”, *Journal of environmental management*, Vol. 92, p2355-2388.

Hofstetter T.B., Heijman C.G., Haderlein S.B., Holliger C., Schwarzenbach R.P., (1999), “Complete Reduction of TNT and Other (Poly)nitroaromatic Compounds under Iron-Reducing Subsurface Conditions”, *Environmental Science and Technology*, Vol. 33, p1479-1487

Hofstetter T.B., Schwarzenbach R.P., Haderlein S.B., (2003), “Reactivity of Fe(II) Species Associated with Clay Minerals”, *Environmental Science and Technology*, Vol. 37, 3, p519-528

Hofstetter T.B., Neumann A., Schwarzenbach R.P., (2006), “Reduction of Nitroaromatic Compounds by Fe(II) Species Associated with Iron-Rich Smectites”, *Environmental Science and Technology*, Vol. 40, 1, p235-242

Assessing the sustainability of Fe-bearing clay mineral redox reactions

References

- Hou D., Al-Tabbaa A., (2014), "Sustainability: A new imperative in contaminated land remediation", *Environmental Science & Policy*, Vol. 39, p25-34
- Huang J., Jones A., Waite T.D., Chen Y., Huang X., Rosso K.M., Kappler A., Mansor M., Tratnyek P.G., Zhang H., (2021) "Fe (II) redox chemistry in the environment", *Chemical Reviews*, Vol. 121, p8161-8233
- Husson O., Husson B., Brunet A., Babre D., Alary K., Sarthou J.P., Charpentier H., Durand M., Benada J., Henry M., (2016), "Practical improvements in soil redox potential (Eh) measurement for characterisation of soil properties. Application for comparison of conventional and conservation agriculture cropping systems", *Analytica Chimica Acta*, Vol. 906, p98-109
- Ilgen A.G., Kruichak J.N., Artyushkova K., Newville M.G., Sun C., (2017), "Redox transformations of As and Se at the surfaces of natural and synthetic ferric nontronites: role of structural and adsorbed Fe (II)", *Environmental Science & Technology*, Vol. 51, p11105-11114
- Iordanova N., Dupuis M., Rosso K.M., (2005), "Charge transport in metal oxides: a theoretical study of hematite α -Fe₂O₃", *The Journal of chemical physics*, Vol. 122, p144305
- Istok J.D., Amonette J.E., Cole C.R., Fruchter J.S., Humphrey M.D., Szecsody J.E., Teel S.S., Vermeul V.R., Williams M.D. and Yabusaki S.B., (1999), "In Situ Redox Manipulation by Dithionite Injection: Intermediate-Scale Laboratory Experiments", *Groundwater*, Vol. 37, p884-889
- Jaisi D.P., Kukkadappu R.K., Eberl D.D., Dong H., (2005), "Control of Fe(III) Site Occupancy on the Rate and Extent of Microbial Reduction of Fe(III) in Nontronite", *Geochimica et Cosmochimica Acta*, Vol. 69, p5429-5440
- Jaisi D.P., Dong H., Liu C., (2007a), "Influence of Biogenic Fe(II) on the Extent of Microbial Reduction of Fe(III) in Clay Minerals Nontronite, Illite and Chlorite", *Geochimica et Cosmochimica Acta*, Vol. 71, p1145-1158

Assessing the sustainability of Fe-bearing clay mineral redox reactions

References

Jaisi D.P., Dong H., Kim J., He Z., Morton J.P., (2007b), "Nontronite Particle Aggregation Induced by Microbial Fe(III) Reduction and Exopolysaccharide Production", *Clays and Clay Minerals*, Vol. 55, p96-107

Jaisi D.P., Liu C., Dong H., Blake R.E., Fein J.B., (2008a), "Fe²⁺ Sorption onto Nontronite (NAu-2)", *Geochimica et Cosmochimica Acta*, Vol. 72, p5361-5371

Jaisi D.P., Dong H., Morton J.P., (2008b), "Partitioning of Fe(II) in Reduced Nontronite (NAu-2) to Reactive Sites: Reactivity in terms of Tc(VII) Reduction", Vol. 56, p175-189

Johnson C.E., (1969), "Antiferromagnetism of γ -FeOOH: a Mössbauer Effect Study", *Journal of Physics C: Solid State Physics*, Vol.2, p1996-2002

Jones A.M., Murphy C.A., Waite T.D., Collins R.N., (2017), "Fe(II) Interactions with Smectites: Temporal Changes in Redox Reactivity and the Formation of Green Rust", *Environmental Science and Technology*, Vol. 51, p12573-12582

Ju K.S., Parales R.E., (2010), "Nitroaromatic compounds, from synthesis to biodegradation", *Microbiology and molecular biology reviews*, Vol. 74, p250-272

Kappler A., Bryce C., Mansor M., Lueder U., Byrne J.M., Swanner E.D., (2021), "An evolving view on biogeochemical cycling of iron", *Nature Reviews Microbiology*, Vol. 19, p360-374.

Keeling J.L., Raven M.D., Gates W.P., (2000), "Geology and Characterization of Two Hydrothermal Nontronites from Weathered Metamorphic Rocks at the Uley Graphite Mine, South Australia", *Clays and Clay Minerals*, Vol. 48, p537-548

Kim J., Dong H., Seabaugh J., Newell S.W., Eberl D.D., (2004), "Role of Microbes in Smectite-to-Illite Reaction", *Science*, Vol. 303, p830-832

Kim J., (2012), "Overviews of biogenic smectite-to-illite reaction", *Clay Science*, Vol. 16, p9-13

Klausen J., Trober S.P., Haderlein S.B., Schwarzenbach R.P., (1995), "Reduction of Substituted Nitrobenzenes by Fe(II) in Aqueous Mineral Suspensions", *Environmental Science and Technology*, Vol. 29, p2396-2404

Assessing the sustainability of Fe-bearing clay mineral redox reactions

References

- Komadel P., Lear P.R., Stucki J.W., (1990), "Reduction and Reoxidation of Nontronite: Extent of Reduction and Reaction Rates", *Clays and Clay Minerals*, Vol. 38, p203-208
- Komadel P., Madejova J., Stucki J.W., (1995), "Reduction and reoxidation of nontronite: Questions of reversibility" *Clays and Clay Minerals*, Vol. 43, p105-110
- Komadel P., Madejová J., Stucki J.W., (2006) "Structural Fe (III) reduction in smectites", *Applied Clay Science*, Vol. 34, p88-94.
- Kome G.K., Enang, R.K. Tabi F.O., Yerima B.P.K., (2019), "Influence of clay minerals on some soil fertility attributes: a review", *Open Journal of Soil Science*, Vol. 9, p155-188.
- Kostka J.E., Haefele E., Viehweger R., Stucki J.W., (1999), "Respiration and Dissolution of Fe(III)-Containing Clay Minerals by Bacteria", *Environmental Science and Technology*, Vol. 33, p3127-3133
- Kostka J.E., Dalton, D.D., Skelton H., Dollhopf S., Stucki J.W., (2002), "Growth of iron (III)-reducing bacteria on clay minerals as the sole electron acceptor and comparison of growth yields on a variety of oxidized iron forms", *Applied and Environmental Microbiology*, Vol. 68, p6256-6262.
- Laird D.A., Fleming P.D., (1999), "Mechanisms for adsorption of organic bases on hydrated smectite surfaces", *Environmental Toxicology and Chemistry: An International Journal*, Vol. 18, p1668-1672
- Latta D.E., Gorski C.A., Scherer M.M., (2012), "Influence of Fe²⁺-catalysed Iron Oxide Recrystallization on Metal Cycling", *Biochemical Society Transactions*, Vol. 40, 6, p1191-1197
- Latta D.E., Neumann A., Premaratne W.A.P.J., Scherer M.M., (2017), "Fe(II)-Fe(III) Electron Transfer in a Clay Mineral with Low Fe Content", *ACS Earth and Space Chemistry*, Vol. 1, p197-208
- Lear P.R., Stucki J.W., (1987), "Intervalence electron transfer and magnetic exchange in reduced nontronite", *Clays and Clay Minerals*, Vol. 35, p373-378
- Lee W., Batchelor B., (2003), "Reductive Capacity of Natural Reductants", *Environmental Science and Technology*, Vol. 37, p535-541

Assessing the sustainability of Fe-bearing clay mineral redox reactions

References

Lee K., Kostka J.E., Stucki J.W., (2006), "Comparisons of Structural Fe in Smectites by Bacteria and Dithionite: an Infrared Spectroscopic Study", *Clays and Clay Minerals*, Vol. 54, p195-208

Lewis T.A., Newcombe D.A. and Crawford R.L., (2004) "Bioremediation of soils contaminated with explosives" *Journal of Environmental Management*, Vol. 70, p291-307.

Liu H., Wei Y., Li P., Zhang Y., Sun Y., (2007), "Catalytic synthesis of nanosized hematite particles in solution", *Materials Chemistry and Physics*, Vol. 102, p1-6

Lovley D.R., Coates J.D., Blunt-Harris E.L., Phillips E.J.P., Woodward J.C., (1996), "Humic Substances as Electron Acceptors for Microbial Respiration", *Nature*, Vol. 382, p445-448

Lovley D.R., Fraga J.L., Blunt-Harris E.L., Hayes L.A., Phillips E.J.P., Coates J.D., (1998), "Humic substances as a mediator for microbially catalyzed metal reduction", *Acta hydrochimica et hydrobiologica*, Vol. 26, p152-157.

Luan F., Gorski C.A., Burgos W.D., (2014), "Thermodynamic Controls on the Microbial Reduction of Iron-Bearing Nontronite and Uranium", *Environmental Science and Technology*, Vol. 48, p2750-2758

Luan F., Liu Y., Griffin A.M., Gorski C.A., Burgos W.D., (2015a) "Iron(III)-Bearing Clay Minerals Enhance Bioreduction of Nitrobenzene by *Shewanella putrefaciens* CN32", *Environmental Science and Technology*, Vol. 49, p1418-1426

Luan F., Gorski C.A., Burgos W.D., (2015b) "Linear Free Energy Relationships for Biotic and Abiotic Reduction of Nitroaromatic Compounds", *Environmental Science and Technology*, Vol. 49, p3557-3565

Manceau A., Lanson B., Drits V.A., Chateigner D., Gates W.P., Wu J., Huo D., Stucki J.W., (2000a), "Oxidation-reduction Mechanism of Iron in Dioctahedral Smectites: I. Crystal Chemistry of Oxidised Reference Nontronites", *American Mineralogist*, Vol. 85, p133-152

Manceau A., Lanson B., Drits V.A., Chateigner D., Gates W.P., Wu J., Huo D., Stucki J.W., (2000b), "Oxidation-reduction Mechanism of Iron in Dioctahedral Smectites: II.

Assessing the sustainability of Fe-bearing clay mineral redox reactions

References

- Crystal Chemistry of Reduced Garfield Nontronites”, *American Mineralogist*, Vol. 85, p153-172
- McCusker L.B., Von Dreele R.B., Cox D.E., Louer D., Scardi P., (1999), “Rietveld Refinement Guidelines”, *Journal of Applied Crystallography*, Vol. 32, p36-50
- Melton E.D., Swanner E.D., Behrens S., Schmidt C., Kappler A., (2014), “Interplay of Microbially Mediated and Abiotic Reactions in the Biogeochemical Fe Cycle”, *Nature Reviews – Microbiology*, Vol. 12, p797-808
- Meng L., Zuo R., Wang J.S., Li Q., Du C., Liu X. and Chen M., (2021), “Response of the redox species and indigenous microbial community to seasonal groundwater fluctuation from a typical riverbank filtration site in Northeast China”, *Ecological Engineering*, Vol. 159, p106099.
- Miot J., Benzerara K., Obst M., Kappler A., Hegler F., Schädler S., Bouchez C., Guyot F., Morin G., (2009) “Extracellular iron biomineralization by photoautotrophic iron-oxidizing bacteria” *Applied and Environmental Microbiology*, Vol. 75, p5586-5591
- Misawa T., Hashimoto K., Shimodaira S., (1974), “The Mechanism of Formation of Iron Oxide and Oxyhydroxides in Aqueous Solution at Room Temperature”, *Corrosion Science*, Vol. 14, p131-149
- Murad E., Schwertmann U., (1984), “The Influence of Crystallinity on the Mössbauer Spectrum of Lepidocrocite”, *Mineralogical Magazine*, Vol. 48, p507-11
- Murad E., Cashion J., (2004), “Mössbauer Spectroscopy of Environmental Materials and their Industrial Utilization”, *Kluwer Academic Publishers*, ISBN: 1402077262
- Murray H.H., (1991), “Overview – Clay Mineral Applications”, *Applied Clay Science*, Vol. 5, p375-395
- Neumann A., Hofstetter T.B., Lussi M., Cirpka O.A., Petit S., Schwarzenbach R.P., (2008), “Assessing the Redox Reactivity of Structural Iron in Smectites using Nitroaromatic Compounds as Kinetic Probes”, *Environmental Science and Technology*, Vol. 42, p8381-8387

Assessing the sustainability of Fe-bearing clay mineral redox reactions

References

Neumann A., Hofstetter T.B., Skarpeli-Liati M., Schwarzenbach R.P., (2009), "Reduction of Polychlorinated Ethanes and Carbon Tetrachloride by Structural Fe(II) in Smectites", *Environmental Science and Technology*, Vol. 43, p4082-4089

Neumann A., Petit S., Hofstetter T.B., (2011), "Evaluation of Redox Active Iron Sites in Smectites using Middle and Near Infrared Spectroscopy", *Geochimica et Cosmochimica Acta*, Vol. 75, p2336-2355

Neumann A., Sander M. Hofstetter T.B., (2011), "Redox Properties of Structural Fe in Smectite Clay Minerals", *Aquatic Redox Chemistry*, Tratnyek P., Chapter 17, p361-379

Neumann A., Olsen T.L., Scherer M.M., (2013), "Spectroscopic Evidence for Fe(II)-Fe(III) Electron Transfer at Clay Mineral Edge and Basal Sites", *Environmental Science and Technology*, Vol. 43, p6969-6977

Neumann A., Wu L., Li W., Beard B.L., Johnson C.M., Rosso K.M., Frierdich A.J., Scherer M.M., (2015), "Atom Exchange between Aqueous Fe(II) and Structural Fe in Clay Minerals", *Environmental Science and Technology*, Vol. 49, p2786-2795

Newman A.C.D., (1984) "The significance of clays in agriculture and soils", *Philosophical Transactions of the Royal Society of London. Series A, Mathematical and Physical Sciences*, Vol. 311, p375-389

Nzengung V.A., Castillo R.M., Gates W.P., Mills G.L., (2001), "Abiotic transformation of perchloroethylene in homogeneous dithionite solution and in suspensions of dithionite-treated clay minerals", *Environmental science & technology*, Vol. 35, p2244-2251.

Ona-Nguema G., Abdelmoula M., Jorand F., Benali O., Gehin A., Block J.C., Genin J.M.R., (2002) "Microbial Reduction of Lepidocrocite γ -FeOOH by *Shewanella putrefaciens*; The Formation of Green Rust", *Hyperfine Interactions*, Vol. 139/140, 231-237

Panagos P., Van Liedekerke M., Yigini Y., Montanarella L., (2013), "Contaminated sites in Europe: review of the current situation based on data collected through a European network", *Journal of Environmental and Public Health*, Vol. 2013

Assessing the sustainability of Fe-bearing clay mineral redox reactions

References

- Parsons C.T., Rezanezhad F., O'Connell D.W., Van Cappellen P., (2017), "Sediment phosphorus speciation and mobility under dynamic redox conditions", *Biogeosciences*, Vol. 14, p3585-3602.
- Pecher K., Haderlein S.B., Schwarzenbach R.P., (2002), "Reduction of Polyhalogenated Methanes by Surface-Bound Fe(II) in Aqueous Suspensions of Iron Oxides", *Environmental Science and Technology*, Vol. 36, p1734-1741
- Pedersen H.D., Postma D., Jakobsen R., Larsen O., (2005), "Fast Transformation of Iron Oxyhydroxides by the Catalytic Action of Aqueous Fe(II)", *Geochimica et Cosmochimica Acta*, Vol. 69, 16, p3967-3977
- Pentakov L., Su K., Pentakov M., Stucki J.W., (2013), "A Review of Microbial Redox Interactions with Structural Fe in Clay Minerals", *Clay Minerals*, Vol. 48, p543-560
- Pfannes H.-D., Gonser U., (1972), "Goldanskii-Karyagin Effect vs Preferred Orientations (Texture)" *Applied Physics*, Vol. 1, p93-102
- Piepenbrock A. and Kappler A., (2013), "Humic substances and extracellular electron transfer" In *Microbial metal respiration* (p107-128). Springer, Berlin, Heidelberg.
- Qafoku O., Pearce C.I., Neumann A., Kovarik L., Zhu M., Ilton E.S., Bowden M.E., Resch C.T., Arey B.W., Arenholz E., Felmy A.R., Rosso K.M., (2017), "Tc(VII) and Cr(VI) Interaction with Naturally Reduced Ferruginous Smectite from a Redox Transition Zone", *Environmental Science and Technology*, Vol. 51, p9042-9052
- Refait P., Rezel D., Olowe A.A., Genin J.-M.R., (1991), "Mössbauer Effect Study and Crystallographic Structure of Chlorinated Green Rust One Compounds", *Hyperfine Interactions*, Vol. 69, p839-842
- Reguera G., Nevin J.P., Nicoll J.S., Covalla S.F., Woodard T.L., Lovley D.R., (2020), "Biofilm and Nanowire Production Leads to Increased Current in *Geobacter sulfurreducens* Fuel Cells", *Applied and Environmental Microbiology*, Vol. 72, p7345-7348
- Ribeiro F.R., Fabris J.D., Kostka J.E., Komadel P., Stucki J.W., (2009), "Comparisons of Structural Iron Reduction in Smectites by Bacteria and Dithionite: II. A Variable-

Assessing the sustainability of Fe-bearing clay mineral redox reactions

References

Temperature Mössbauer Spectroscopic Study of Garfield Nontronite*”, *Pure and Applied Chemistry*, Vol. 81, p1499-1509

Rizzo E., Bardos P., Pizzol L., Critto A., Giubilato E., Marcomini A., Albano C., Darmendrail D., Döberl G., Harclerode M., Harries N., (2016), “Comparison of international approaches to sustainable remediation”, *Journal of Environmental Management*, Vol. 184, p4-17.

Roden E.E., (2012), “Microbial iron-redox cycling in subsurface environments”, *Biochemical Society Transactions*, Vol. 40, p1249-1256

Rogers J.R., Bennett P.C., (2004), “Mineral stimulation of subsurface microorganisms: release of limiting nutrients from silicates”, *Chemical Geology*, Vol. 203, p91-108

Rothwell K.A., (2018), “From the Lab to the Real World: the Redox Reactivity of Fe-Bearing Clay Minerals in Complex Biogeochemical Environments”, Ph.D Thesis, Newcastle University

Rosso K.M., Smith D.M.A., Dupuis M., (2003), “An Ab Initio Model of Electron Transport in Hematite (α -Fe₂O₃) Basal Planes”, *Journal of Chemical Physics*, Vol. 118, p6455-6466

Rozenson I., Heller-Kallai L., (1976a) “Reduction and Oxidation of Fe³⁺ in Dioctahedral Smectites-1: Reduction with Hydrazine and Dithionite”, *Clays and Clay Minerals*, Vol. 24, p271– 282

Rozenson I., Heller-Kallai L. (1976b) “Reduction and oxidation of Fe (Super 3+) in Dioctahedral Smectites; 2, Reduction with Sodium Sulphide Solutions”, *Clays and Clay Minerals*, Vol. 24, p283–288

Ruggè K., Hofstetter T.B., Haderlein S.B., Bjerg P.L., Knudsen S., Zraunig C., Christensen T.H., (1998), “Characterization of Predominant Reductants in an Anaerobic Leachate-Contaminated Aquifer by Nitroaromatic Probe Compounds”, *Environmental Science and Technology*, Vol. 32, p23-31

Russell J.D., Goodman B.A., Fraser A.R., (1979), “Infrared and Mössbauer Studies of Reduced Nontronites”, *Clays and Clay Minerals*, Vol. 27, p63-71

Assessing the sustainability of Fe-bearing clay mineral redox reactions

References

- Sandi G., Carrado K.A., Joachim H., Lu W., Prakash J., (2003), "Polymer Nanocomposites for Lithium Battery Applications", *Journal of Power Sources*, Vol. 119, p492-496
- Schaefer M. V., Gorski C. A., Scherer M. M., (2011) "Spectroscopic Evidence for Interfacial Fe(II)–Fe(III) Electron Transfer in a Clay Mineral", *Environmental Science and Technology*, Vol. 45, p540–545.
- Schilt A.A., (1969), "Analytical Applications of 1,10-Phenanthroline and Related Compounds: International Series of Monographs in Analytical Chemistry", *Pergamon Press*, ISBN: 9781483156569
- Schultz C.A., Grundl T.J., (2000), "pH dependence on reduction rate of 4-Cl-nitrobenzene by Fe (II)/montmorillonite systems", *Environmental science & technology*, Vol. 34, p3641-3648
- Schwertmann U., Murad E., (1983), "Effect of pH on Formation of Goethite and Hematite from Ferrihydrite", *Clays and Clay Minerals*, Vol. 31, p277-284
- Schwertmann U., (2000), "Iron Oxides in the Laboratory : Preparation and Characterization", 2nd Edition, *Weinheim ; New York : Wiley VCH*, ISBN: 9783527296697
- Shi Z., Zachara J.M., Shi L., Wang Z., Moore D.A., Kennedy D.W., Fredrickson J.K., (2012), "Redox Reactions of Reduced Flavin Mononucleotide (FMN), Riboflavin (RBF), and Anthraquinone-2,6-disulfonate (AQDS) with Ferrihydrite and Lepidocrocite", *Environmental Science and Technology*, Vol. 46, p11644-11652
- Shi B., Liu K., Wu L., Smeaton C.M., Beard B.L., Johnson C.M., Roden E.E., Cappellen P.V., (2016), "Iron Isotope Fractionations Reveal a Finite Bioavailable Fe Pool for Structural Fe(III) Reduction in Nontronite", *Environmental Science and Technology*, Vol.50, p8661-8669
- Shi B., Smeaton C.M., Roden E.E., Lee S., Liu K., Xu H., Kendall B., Johnson C.M., Parsons C.T., Van Cappellen P., (2021), "Consecutive Fe Redox Cycles Decrease Bioavailable Fe(III) and Fe Isotope Fractionations by Eliminating Small Clay Particles", *Geochimica et Cosmochimica Acta*, Vol. 308, p118-135

Assessing the sustainability of Fe-bearing clay mineral redox reactions

References

- Silva-Valenzuela M.G., Matos C.M., Shah L.A., Carvalho F.M.S., Sayeg I.J., Valenzuela-Diaz F.R., (2013) "Engineering properties of kaolinitic clay with potential use in drugs and cosmetics", *International Journal of Modern Engineering Research (IJMER)*, Vol. 3, p163-165
- Soltermann D., Marques Fernandes M., Baeyens B., Dähn R., Joshi P.A., Scheinost A.C., Gorski C.A., (2014) "Fe(II) uptake on natural montmorillonites. I. Macroscopic and spectroscopic characterization", *Environmental science & technology*, Vol. 48, p8688-8697
- Sposito G., Skipper N.T., Sutton R., Park S., Soper A.K., Greathouse J.A., (1999), "Surface Geochemistry of the Clay Minerals", *Proceeding of National Academy of Science (PNAS) USA*, Vol. 96, p3358-3364
- Starcher A.N., Li W., Kukkadapu R.K., Elzinga E.J., Sparks D.L., (2016), "Fe(II) Sorption onto Pyrophyllite: Effect of Structural Fe(III) (impurity) in Pyrophyllite on Nature of Layered Double Hydroxide (LDH) Secondary Mineral Formation", *Chemical Geology*, Vol. 439, p152-160
- Stucki J.W., Roth C.B., (1977), "Oxidation-reduction mechanism for structural iron in nontronite", *Soil Science Society of America Journal*, Vol. 41, p808-814.
- Stucki J.W., (1981), "A Quantitative Assay of Minerals for Fe²⁺ and Fe³⁺ using 1,10-Phenanthroline: II. A Photochemical Method", *Soil Science Society of America Journal*, Vol. 45, p638-641
- Stucki J.W., Golden D.C., Roth C.B., (1984a), "Effects of Reduction and Reoxidation of Structural Iron on the Surface Charge and Dissolution of Dioctahedral Smectites", *Clays and Clay Minerals*, Vol. 32, p350-356
- Stuck J.W., Golden D.C., Roth C.B., (1984b), "Preparation and Handling of Dithionite-Reduced Smectite Suspensions", *Clays and Clay Minerals*, Vol.32, p191-197
- Stucki J.W., Komadel P., Wilkinson H.T., (1987), "Microbial reduction of structural iron (III) in smectites", *Soil Science Society of America Journal*, Vol. 51, p1663-1665.

Assessing the sustainability of Fe-bearing clay mineral redox reactions

References

Stucki J.W., Wu J., Gan H., Komadel P., Banin A., (2000), "Effects of iron oxidation state and organic cations on dioctahedral smectite hydration", *Clays and Clay Minerals*, Vol. 48, p290-298.

Stucki J.W., Lee K., Zhang L., Larson R.A., (2002), "Effects of Iron Oxidation State on the Surface and Structural Properties of Smectites", *Pure and Applied Chemistry*, Vol. 74, p2145-2158

Stucki J.W., Kostka J.E., (2006), "Microbial Reduction of Fe in Smectites", *Geomaterials (Mineralogy)*, Vol. 338, p468-475

Stucki J.W., (2011), "A Review of the Effects of Iron Redox Cycles on Smectite Properties", *Comptes Rendus Geoscience*, Vol. 343, p199-209

Szczody J.E., Fruchter J.S., Williams M.D., Vermeul V.R., Sklarew D., (2004), "In Situ Chemical Reduction of Aquifer Sediments : Enhancement of Reactive Phases and TCE Dechlorination", *Environmental Science and Technology*, Vol. 38, p4656-4663

Tamura Y., Saturno M., Yamada k., Katsura T., (1984), "The Transformation of γ - FeOOH to Fe₃O₄ and Green Rust II in an Aqueous Solution", *Bulletin of Chemical Society of Japan*, Vol. 57, p2417-2421

Tiwari J., Tarale P., Sivanesan S., Bafana A., (2019), "Environmental persistence, hazard, and mitigation challenges of nitroaromatic compounds", *Environmental Science and Pollution Research*, Vol. 26, p28650-28667

Townsend M.G., Longworth G., Ross C.A.M., Provencher R., (1987), "Ferromagnetic or Antiferromagnetic Fe III Spin Configurations in Sheet Silicates", *Physics and Chemistry of Minerals*, Vol. 15, p64-70

Trolard F., Genin J.M.R., Abdelmoula M., Bourrie G., Humbert B., Herbillon A., (1996), "Identification of a Green Rust Mineral in a Reductomorphic Soil by Mössbauer and Raman Spectroscopies", *Geochimica et Cosmochimica Acta*, Vol. 61, 5, p1107-1111

Tsarev S., Waite T.D., Collins R.N., (2016), "Uranium reduction by Fe (II) in the presence of montmorillonite and nontronite" *Environmental Science & Technology*, Vol. 50, p8223-8230

Assessing the sustainability of Fe-bearing clay mineral redox reactions

References

- Usman M., Hanna K., Abdelmoula M., Zegeye A., Faura P., Ruby C., (2012), "Formation of Green Rust via Mineralogical Transformation of Ferric Oxides (Ferrihydrite, Goethite, and Hematite)", *Applied Clay Science*, Vol. 64, p38-43
- Usman M., Byrne J.M., Chaudhry A., Orsetti S., Hanna K., Ruby C., Kappler A., Haderlein S.B., (2018), "Magnetite and Green Rust: Synthesis, Properties and Environmental Applications of Mixed Valent Iron Minerals", *Chemical Reviews*, Vol. 118, p3251-3304
- Van Der Zee C., Slomp C.P., Rancourt D.G., De Lange G.J., Van Raaphorst W., (2005), "A Mössbauer Spectroscopic Study of the Iron Redox Transition in Eastern Mediterranean Sediments", *Geochimica et Cosmochimica Acta*, Vol. 69, p441-453
- Vorhies J.S., Gaines R.R., (2009), "Microbial dissolution of clay minerals as a source of iron and silica in marine sediments", *Nature Geoscience*, Vol. 2, p221-225
- Weber K.A., Urrutia M.M., Churchill P.F., Kukkadapu R.K., Roden E.E., (2006), "Anaerobic redox cycling of iron by freshwater sediment microorganisms", *Environmental Microbiology*, Vol. 8, p100-113.
- Williams A.G.B., Scherer M.M., (2004), "Spectroscopic Evidence for Fe(II)-Fe(III) Electron Transfer at the Iron Oxide-water Interface", *Environmental Science and Technology*, Vol. 38, p4872-4790
- Winkler, P., Kaiser K., Thompson A., Kalbitz K., Fiedler S., Jahn R., (2018), "Contrasting evolution of iron phase composition in soils exposed to redox fluctuations", *Geochimica et Cosmochimica Acta*, Vol. 235, p89-102.
- Yang J., Kukkadapu R.K., Dong H., Shelobina E.S., Zhang J., Kim J., (2012), "Effects of Redox Cycling of Iron in Nontronite on Reduction of Technetium", *Chemical Geology*, Vol. 291, p206-216
- Yanina S.V., Rosso K.M., (2008), "Linked reactivity at mineral-water interfaces through bulk crystal conduction", *Science*, Vol. 320, p218-222
- Yu S., Lee P.K., Hwang S.I., (2015), "Groundwater contamination with volatile organic compounds in urban and industrial areas: analysis of co-occurrence and land use effects", *Environmental earth sciences*, Vol. 74, p3661-3677.

Assessing the sustainability of Fe-bearing clay mineral redox reactions

References

Yu G.H., Kuzyakov Y., (2021), "Fenton chemistry and reactive oxygen species in soil: Abiotic mechanisms of biotic processes, controls and consequences for carbon and nutrient cycling", *Earth-Science Reviews*, Vol. 214, p103525

Zachara J.M., Kukkadapu R.K., Fredrickson J.K., Gorby Y.A., Smith S.C., (2002), "Biomining of Poorly Crystalline Fe(III) Oxides by Dissimilatory Metal Reducing Bacteria (DMRB)", *Geomicrobiology*, Vol. 19, p179-207

Zhang G., Dong H., Kim J., Eberl D.D., (2007), "Microbial Reduction of Fe³⁺ in Nontronite by a Thermophilic Bacterium and its Role in Promoting the Smectite to Illite Reaction", *American Mineralogist*, Vol. 92, p1411-1419

Zhao L., Dong H., Kukkadapu R.K., Zeng Q., Edelman R.E., Pentrak M., Agrawal A., (2015), "Biological Redox Cycling of Iron in Nontronite and its Potential Application in Nitrate Removal", *Environmental Science and Technology*, Vol. 49, p5493-5501

Zhu Y., Elzinga E.J., (2014), "Formation of Layered Fe(II)-Hydroxides during Fe(II) Sorption onto Clay and Metal-Oxide Substrates", *Environmental Science and Technology*, Vol. 48, p4937-4945

Zuo H., Kukkadapu R., Zhu Z., Ni S., Huang L., Zeng Q., Liu C., Dong H., (2020), "Role of clay-associated humic substances in catalyzing bioreduction of structural Fe (III) in nontronite by *Shewanella putrefaciens* CN32", *Science of the Total Environment*, Vol. 741, p140213.

